Impact of Legalized 25-kip Axle Loads for Self-Propelled Implements of Husbandry on Iowa Bridges

Final Report
October 2024

BRIDGE ENGINEERING CENTER

IOWA STATE UNIVERSITY
Institute for Transportation

Sponsored by
Iowa Highway Research Board
(IHRB Project TR-798)
Iowa Department of Transportation
(InTrans Project 21-781)
Federal Highway Administration

About the Bridge Engineering Center

The mission of the Bridge Engineering Center (BEC) is to conduct research on bridge technologies to help bridge designers/owners design, build, and maintain long-lasting bridges.

About the Institute for Transportation

The mission of the Institute for Transportation (InTrans) at Iowa State University is to save lives and improve economic vitality through discovery, research innovation, outreach, and the implementation of bold ideas.

Iowa State University Nondiscrimination Statement

Iowa State University does not discriminate on the basis of race, color, age, ethnicity, religion, national origin, pregnancy, sexual orientation, gender identity, genetic information, sex, marital status, disability, or status as a US veteran. Inquiries regarding nondiscrimination policies may be directed to the Office of Equal Opportunity, 3410 Beardshear Hall, 515 Morrill Road, Ames, Iowa 50011, telephone: 515-294-7612, hotline: 515-294-1222, email: eooffice@iastate.edu.

Disclaimer Notice

The contents of this report reflect the views of the authors, who are responsible for the facts and the accuracy of the information presented herein. The opinions, findings and conclusions expressed in this publication are those of the authors and not necessarily those of the sponsors.

The sponsors assume no liability for the contents or use of the information contained in this document. This report does not constitute a standard, specification, or regulation.

The sponsors do not endorse products or manufacturers. Trademarks or manufacturers' names appear in this report only because they are considered essential to the objective of the document.

Quality Assurance Statement

The Federal Highway Administration (FHWA) provides high-quality information to serve Government, industry, and the public in a manner that promotes public understanding. Standards and policies are used to ensure and maximize the quality, objectivity, utility, and integrity of its information. The FHWA periodically reviews quality issues and adjusts its programs and processes to ensure continuous quality improvement.

Iowa DOT Statements

Federal and state laws prohibit employment and/or public accommodation discrimination on the basis of age, color, creed, disability, gender identity, national origin, pregnancy, race, religion, sex, sexual orientation or veteran's status. If you believe you have been discriminated against, please contact the Iowa Civil Rights Commission at 800-457-4416 or the Iowa Department of Transportation affirmative action officer. If you need accommodations because of a disability to access the Iowa Department of Transportation's services, contact the agency's affirmative action officer at 800-262-0003.

The preparation of this report was financed in part through funds provided by the Iowa Department of Transportation through its "Second Revised Agreement for the Management of Research Conducted by Iowa State University for the Iowa Department of Transportation" and its amendments.

The opinions, findings, and conclusions expressed in this publication are those of the authors and not necessarily those of the Iowa Department of Transportation or the U.S. Department of Transportation Federal Highway Administration.

Technical Report Documentation Page

1. Report No.	2. Government Accession No.	3. Recipient's Catalog No.
IHRB Project TR-798		

4. Title and Subtitle	5. Report Date
Impact of Legalized 25-kip Axle Loads for Self-Propelled Implements of Husbandry on Iowa Bridges	October 2024
	6. Performing Organization Code

7. Author(s)	8. Performing Organization Report No.
Justin Dahlberg (orcid.org/0000-0002-6184-4122), Zhengyu Liu (orcid.org/0000-0002-7407-0912), Karthian R. Jadhav (orcid.org/0000-0001-6805-6578), and Brent M. Phares (orcid.org/0000-0001-5894-4774)	InTrans Project 21-781

9. Performing Organization Name and Address	10. Work Unit No. (TRAIS)
Bridge Engineering Center Iowa State University 2711 South Loop Drive, Suite 4700 Ames, IA 50010-8664	**11. Contract or Grant No.**

12. Sponsoring Organization Name and Address		13. Type of Report and Period Covered
Iowa Highway Research Board Iowa Department of Transportation 800 Lincoln Way Ames, IA 50010	Federal Highway Administration U.S. Department of Transportation 1200 New Jersey Avenue SE Washington, DC 20590	Final Report
		14. Sponsoring Agency Code SPR-RE22(009)-8H-00

15. Supplementary Notes

Visit https://bec.iastate.edu for color pdfs of this and other research reports.

16. Abstract

Live load field tests of bridges were carried out using certain implements of husbandry (IoH) to observe the transverse load distribution and the dynamic impacts. A finite element (FE) analysis of the field-tested bridges was performed. The strain data from the FE analysis were validated with the field test data to establish an FE analysis method for a parametric study. This parametric study was performed to observe the influence of various bridge parameters on the load distribution factors. Observation of the load distribution factors from the parametric study shows that the load distribution factor equations prescribed in the AASHTO LRFD (2020) capture the distribution for these IoH loads. Live load factors for this load type for prestressed concrete (PC) bridges and steel girder bridges were found through a calibration process using reliability theory, which involves the selection of a target safety index. The live load factor for each bridge type was calculated for the Strength I and II limit states. An Iowa-specific legally loaded vehicle (Terragator Max) was established using a conservative axle configuration and axle loads of 25 kips. Calibration of the live load factors yielded the following key findings:

- An update to the AASHTO load and resistance factors (LRFs) is not needed for existing terragator loads as long as the axle loads comply with the legal load limit of 25 kips.
- When a target safety index of 3.5 is considered, the current live load factor of 1.75 for Strength I should be increased to 1.90 if husbandry vehicles of a configuration similar to that of Terragator Max are manufactured.
- When a target safety index of 2.0 is considered, the same case does not suggest an update to the AASHTO live load factor.
- An update to the AASHTO Strength II LRFs is not required.
- The dead load factors were found to be lower than the current AASHTO-prescribed values. Therefore an update to the AASHTO LRFs is not required.
- The resistance factors were found to be close to the AASHTO resistance factors for moment and shear.

17. Key Words	18. Distribution Statement
agricultural equipment—axle loads—implements of husbandry—load rating—safety index	No restrictions.

19. Security Classification (of this report)	20. Security Classification (of this page)	21. No. of Pages	22. Price
Unclassified.	Unclassified.	182	NA

Form DOT F 1700.7 (8-72) **Reproduction of completed page authorized**

IMPACT OF LEGALIZED 25-KIP AXLE LOADS FOR SELF-PROPELLED IMPLEMENTS OF HUSBANDRY ON IOWA BRIDGES

Final Report
October 2024

Principal Investigators
Justin Dahlberg, Director
Bridge Engineering Center, Iowa State University

Brent Phares, Research Engineer
Bridge Engineering Center, Iowa State University

Research Assistants
Zhengyu Liu, Karthian R. Jadhav

Authors
Justin Dahlberg, Zhengyu Liu, Karthian R. Jadhav, and Brent Phares

Sponsored by
Iowa Highway Research Board and
Iowa Department of Transportation
(IHRB Project TR-798)

Preparation of this report was financed in part
through funds provided by the Iowa Department of Transportation
through its Research Management Agreement with the
Institute for Transportation
(InTrans Project 21-781)

A report from
Bridge Engineering Center
Institute for Transportation at Iowa State University
2711 South Loop Drive, Suite 4700
Ames, IA 50010-8664
Phone: 515-294-8103 / Fax: 515-294-0467
https://bec.iastate.edu

TABLE OF CONTENTS

LIST OF FIGURES

LIST OF TABLES

ACKNOWLEDGMENTS

The authors would like to acknowledge the Iowa Department of Transportation (DOT) for sponsoring this research and the Federal Highway Administration (FHWA) for state planning and research (SPR) funds used for this project. The authors would also like to thank the members of the technical advisory committee (TAC) for their contributions and direction.

EXECUTIVE SUMMARY

In February 2019, Iowa House Study Bill 218 increased the allowable axle weight of certain implements of husbandry (IoH), commonly referred to as terragators, to 25 kips. This change poses a particular concern to those who oversee and manage the design, rating, and preservation of bridge structures because the resulting structural response of bridges could exceed that which would otherwise be seen from other legal loads. This potential problem was investigated to assess the structural response of bridges subject to these loads and to develop more accurate live load distribution factors (LLDFs), impact factors, and load factors. An Iowa-specific legally loaded vehicle to be used for load rating bridges was also proposed.

To achieve these goals, live load tests of several bridges were conducted using the specific IoH vehicle type that was affected by the state legislation. The field test data were used to observe the transverse load distribution of the bridges and the dynamic impacts of the IoH. A comparison of the field test data results to current design codes published by the American Association of State Highway and Transportation Officials (AASHTO) yielded the following observations:

For prestressed concrete bridges:

- The LLDFs resulting from the field tests for interior girders subject to single-wheel axles were higher than the LLDFs specified in AASHTO (2020), though it was found that these axles typically are lightly loaded relative to the legal allowance and result in relatively low strain magnitudes.
- For exterior girders, the LLDFs calculated using the AASHTO equations were higher than those calculated based on the field tests.

For slab bridges:

- Equivalent strip widths for slab-type bridges calculated from the field test data were larger than those calculated using AASHTO, indicating a greater distribution of the live load than what is calculated in design.
- Thicker slabs reduced the load intensity on a unit strip width and distributed the load more evenly across a larger strip width.

Dynamic impact factor:

- The calculated dynamic impact factor (DIF) was influenced by vehicle speed. For the tested bridges, terragators were operated at three speeds: pseudo-static, 10 mph, and 35 mph. The DIF incrementally increased as speeds increased.
- All but one of the experimentally determined DIF values calculated in this work were less than 1.33, which is the AASHTO-prescribed DIF. The single exception to this was for an empty terragator on a skewed bridge.

Finite element (FE) models were developed for the field-tested bridges, and model validation was completed using the field test data. This process established a method to create numerous FE models of other existing bridges to be used in a parametric study.

The parametric study was performed to observe the influence of various bridge parameters on the load distribution factors. A database of currently used terragator-type vehicles was developed to use for live load input data. The results indicate that the load distribution factors resulting from the parametric study are captured by the load distribution factor equations prescribed in the AASHTO Load and Resistance Factor Design (LRFD) Bridge Design Specifciations (2020). The key findings from the parametric study are summarized as follows:

- The interior girder and exterior girder LLDFs for prestressed concrete (PC) bridges and steel girder bridges were less than the LLDFs calculated from the AASHTO-prescribed equations.
- It was observed that the calculated equivalent strip width for slab bridges was larger than the strip width calculated using the AASHTO-prescribed equation.
- The parametric study results suggest that the bridge parameters that primarily influence the LLDFs of the interior girders are skew angle, girder spacing, and total number of girders. This is true for both PC and steel girder bridges.
- The ratio of girder spacing to span length showed the greatest effect on the LLDFs of PC and steel girder bridges.
- For slab bridges, the parameters that were found to have the greatest influence on the equivalent strip width were skew angle, slab thickness, and span length.

Following the analysis of the distribution factors, the live load factors for PC bridges and steel girder bridges were found using a calibration process based on the reliability theory summarized by Barker and Puckett (2007). Twenty-three bridges for each bridge type were selected and used for calibration. The maximum moment and shear resulting from live load were calculated. The dead loads of bridge components were also calculated to find the dead load factors. The moment and shear capacity of the bridge components were calculated and used as resistance data for the calibration process.

The live load factor for each bridge type was calculated using three cases: Case I, Case II, and Case III. Case I calibrated the load and resistance factors (LRFs) for the identified terragators in the Strength I limit state. For the Strength I limit state, HS-20 loads were used to calculate the nominal load effects. Axle loads at or below 25 kips (legally loaded) from the available terragator loads were used to calculate bending moment and shear due to live loads.

Case II calibrated the LRFs for a hypothetical terragator model in the Strength I limit state. The hypothetical model, or the Iowa-specific legally loaded vehicle, developed for Case II and Case III was named Terragator Max. Here, the coefficient of variation for the live load data was taken from Case I.

Case III calibrated the LRFs for Terragator Max in the Strength II limit state. The coefficient of variation for the live load data was taken from Case I. Terragator Max was treated as an “owner-

specified or evaluation permit vehicle." Therefore, the Terragator Max load was the nominal load for Case III.

The calibration of live load factors using reliability theory includes the selection of a target safety index and reiteration of the process to reach a safety index close to the selected target safety index. For this project, two target safety indices were chosen. A target safety index of 3.5 was chosen following the procedure summarized by Barker and Puckett (2007); this value is consistent with the LRFD philosophy. Another safety index of 2.0 was chosen to reflect the less conservative approach used for load rating, since overly conservative methods can be prohibitive with respect to load restrictions, rehabilition, and replacement. The AASHTO Manual for Bridge Evaluation (MBE) (2018) recommends selection of a lower safety index for bridges with low annual daily truck traffic (ADTT) values. The frequency of IoH vehicle crossings is typically very low relative to ADTT values.

The calibration of live load factors yielded the following key findings:

- A comparison of the Case I LRFs with the Strength I AASHTO LRFs suggests that an update to the AASHTO LRFs is not needed for existing terragator loads as long as the axle loads comply with the legal load limit of 25 kips.
- When a target safety index of 3.5 is considered, a comparison of the Case II LRFs with the Strength I AASHTO LRFs suggests that the current live load factor of 1.75 for Strength I should be increased to 1.90 if husbandry vehicles of a configuration similar to that of Terragator Max are manufactured.
- When a target safety index of 2.0 is considered, the same case does not suggest an update to the AASHTO live load factor.
- A comparison of the Case III LRFs with the Strength II AASHTO LRFs suggests that an update to the AASHTO Strength II LRFs is not required.
- The dead load factors were found to be lower than the current AASHTO-recommended values. Therefore an update to the AASHTO LRFs is not required.
- The resistance factors were found to be close to the AASHTO resistance factors for moment and shear.

These findings suggest that the live load factors in the current AASHTO LRFD do not require an update because an IoH with a vehicle configuration similar to that of Terragator Max is unlikely to be produced. This assumption was made because Terragator Max was developed by considering a conservative and hypothetical vehicle configuration.

1 INTRODUCTION

1.1 Background and Problem Statement

Agricultural equipment, commonly known as implements of husbandry (IoH), has changed and continues to change to adapt to the needs of the industry it serves. As a result, the size and weight of the equipment have steadily increased while most existing roads and bridges were not designed specifically for these loads. The stresses imposed on roads and bridges can exceed the design level stresses, possibly leading to premature degradation or even failure.

In February 2019, Iowa House Study Bill 218 was introduced by the Committee on Agriculture relating to the weight limitations for certain implements of husbandry. Section 321.463, subsection 4, previously prescribed the weight limits of "self-propelled implements of husbandry used exclusively for the application of organic or inorganic plant food materials, agricultural limestone, or agricultural chemicals, unless traveling under a permit […] to 24,000 lb from February 1 through May 31 or 28,000 lb from June 1 through January 31, provided, however, that the maximum gross vehicle weight […] shall not exceed 96,000 lb." This section was amended to prescribe that the weight limits "on any one axle of a self-propelled implement of husbandry used exclusively for the application of organic or inorganic plant food materials, agricultural limestone, or agricultural chemicals operated on highways of this state shall not exceed 25,000 lb." Furthermore, with respect to bridges, the section was amended as follows: "a self-propelled implement of husbandry used exclusively for the application of organic or inorganic plant food materials, agricultural limestone, or agricultural chemicals shall comply with the other provisions of this section and chapter when operated over a bridge in this state, *other than any provision limiting the weight on any one axle to less than 25,000 lb*" (emphasis added). The amended bill effectively codified the allowable axle weight limit to 25,000 lb. This was the first time Section 321.463 permitted axles loads above those calculated using the Federal Bridge Formula.

Without a doubt, an increased allowable weight limit on single axles increases the likelihood that the maximum structural response (stress, deflection) of bridges will become greater as vehicle operators begin taking advantage of the increased load limits. Subjecting bridges to increased loads over both the short and long term has potentially damaging effects. Premature degradation or even failure may result. Hence, it is important to fully understand the load response of bridges to these unique vehicles to understand how it compares to more common vehicle configurations. Such an understanding will allow bridge owners to take appropriate action if/when needed and/or necessary.

1.2 Objectives

The introduction of increased axle weight limits for certain specific vehicle types introduces load limits and vehicle configuration types that were not previously considered for Iowa's bridges, and these changes are of immediate concern and worth engineering examination. Consequently, to gain the knowledge necessary to more accurately assess bridge behavior under these increased loads, seven major objectives were targeted in this project:

1. Identify current in-service terragator-type legal vehicles per Iowa Code 321.463.a(1)(2).
2. Perform live load tests of bridges using terragator vehicles to determine actual live load distribution and dynamic impact factors and to calibrate bridge models.
3. Develop bridge models using finite element numerical analysis and simulate the load effects due to terragator-type vehicle crossings.
4. Compare live load distribution results to current codified live load distribution factors (LLDFs) used for typical vehicle types.
5. Compare dynamic impact factors to codified dynamic load factors.
6. Calibrate live load factors for load and resistance factor design (LRFD) and load and resistance factor rating (LRFR).
7. Develop a legally loaded terragator-type vehicle model for Iowa.

1.3 Research Plan and Report Outline

To achieve the goals of the project, work in three principal areas was conducted: (1) load testing and evaluation of approximately 10 bridges in Iowa, (2) development of engineering/code-based comparisons, and (3) development of recommendations based upon testing, analytical modeling, and advanced data analytics. More specifically, the research project was conducted in five tasks, as follows:

- Task 1: Kickoff Meeting
- Task 2: Literature Review and Information Collection
- Task 3: Live Load Field Test and Analysis of 25 Kip/Axle Implements of Husbandry
- Task 4: Develop Analytical Models (Live Load Distribution Factors, Impact Factors, and Live Load Factors)
- Task 5: Preparation of Final Report

In this report, the results from the literature review are documented in Chapter 2. Information on those vehicles most likely to be used in the state of Iowa and those that can currently be operated legally in Iowa were collected and are documented in Chapter 3. Field work and the results of live load testing on eight in-service bridges subject to selected husbandry vehicles are presented in Chapter 4. The data collected from the field testing were analyzed and used to help create finite element (FE) models of the field-tested bridges. The field data and analytical models were used to investigate the bridges' responses subject to husbandry vehicles with respect to dynamic impact and live load distribution. The results of these analyses are presented in Chapters 5, 6, and 7. A summary and applicable conclusions are presented in Chapter 8.

2 LITERATURE REVIEW

In this project, a comprehensive literature review was conducted with respect to four major topics: (1) the impacts of implements of husbandry vehicles on bridge structures, (2) determination of bridge dynamic responses, (3) determination of bridge load distribution factors, and (4) calibration of live load factors. These four topics are presented in Sections 2.1, 2.2, 2.3, and 2.4, respectively.

2.1 Implements of Husbandry on Bridge Structures

With respect to the impacts of implements of husbandry vehicles on bridge structures, two recently completed research projects that studied the effects of numerous types of husbandry vehicles are notable. These two projects are National Cooperative Highway Research Program (NCHRP) Project 12-110, Proposed New AASHTO Load Rating Provisions for Implements of Husbandry (Wang et al. 2020), and Iowa Highway Research Board (IHRB) Project TR-613, Study of Impacts of Implements of Husbandry on Iowa Bridges (Phares et al. 2017, Greimann et al. 2017, and Freeseman et al. 2017). In this section, a brief summary of these two projects is presented, followed by a discussion of a few other related projects.

TR-613 (Phares et al. 2017, Greimann et al. 2017, and Freeseman et al. 2017) developed guidance to help engineers understand how implements of husbandry loads are resisted by common bridge types. The focus of this study was on bridges having steel girders with concrete and timber decks and bridges having timber girders with timber decks. Field tests of 19 bridges were completed using several types of husbandry vehicles. The tests included both static and dynamic loads with a focus on developing equations and limits for dynamic load allowances and live load distribution factors. Finite element models were created for the 19 bridges and calibrated with the field-collected data. These models served as guidelines to create additional models of other inventory bridges.

An extensive data collection effort was undertaken to identify implements of husbandry combinations, axle spacings, and axle weights to ensure that most, if not all, implements of husbandry would be considered in the study. Moment envelopes were generated for each vehicle crossing. As a result, three generic agricultural notional rating vehicles were developed to envelop the structural response of the numerous single-span to four-span bridges included in the computational and analytical modeling from the loading of 121 real implements of husbandry combinations. The notional rating vehicles were then compared to existing rating and posting vehicles, and it was determined that rating vehicles do not always capture the effects of implements of husbandry. Therefore, it was concluded that a need exists for notional agricultural vehicles in addition to the existing notional rating vehicles. It should be noted that the generic agricultural rating vehicles have individual axle weights that exceed the Iowa legal limit. However, like the HS-20 or other notional models, this model should not be construed as an actual vehicle but rather a model to envelop all agricultural vehicle combinations.

American Association of State Highway and Transportation Officials (AASHTO) load distribution factors were found to be conservative with respect to husbandry vehicles. Empirical

equations were developed for load distribution that provide a good estimation for husbandry vehicles for various bridge types, specifically those within the scope of the project. The empirical equations may prove to be the same or similar for other bridge types, but this conclusion could not be made with certainty because other bridge types were not included in the field tests and analytical modeling.

However, in project TR-613 (Phares et al. 2017, Greimann et al. 2017, and Freeseman et al. 2017), a limited investigation into the impact factors from implements of husbandry was made. The primary effort was a part of the field testing, where it was found that the dynamic strain response exceeded the static strain response by no greater than 12%. The total amount of data collected was minimal in comparison to that collected in other studies for standard gauge-width highway vehicles. Accordingly, further investigation into impact factors was recommended.

NCHRP 12-110 (Wang et al. 2020) developed a notional load to represent a large grouping of, but not all, implements of husbandry. The intent of this notional load, like other notional loads used in design and load rating, was to envelop the maximum load effects of likely vehicles so as to avoid the need to individually assess their load effects, which can become a significant consumption of time and money. Using data from several sources and previous research studies, the researchers compiled a group of husbandry vehicles whose axle weights and configurations, when calculated, did not exceed the Federal Bridge Formula by more than 15%. The implements used in the study included tractors, grain wagons, liquid manure spreaders, fertilizer spreaders, and others.

The notional load model may very well sufficiently capture the load effects of a large percentage of implements of husbandry; however, it is noteworthy that the single axle weight limit is 23 kips and the maximum gross vehicle weight is 92 kips. Both are less than the limits most recently defined in Iowa Code 321.463.a(1)(2). The researchers indicated that implements of husbandry whose weight and configurations exceed the 15% threshold would be individually assessed and be subject to the permitting requirements of the jurisdiction. Though the intent of the research was to capture most implements of husbandry, the notional model does not encompass all implements of husbandry currently in use, which leaves bridge structures to be individually assessed when certain other implements are known to cross.

The project indicated that the load distribution from implements of husbandry is known to be different than that from standard vehicle configurations, including in terms of gauge widths, number of wheels per axle, and tire size, which are all variables that affect final load distribution. The amount of data that quantifies this is limited, and additional effort is needed to fully understand load distribution characteristics. However, in an effort to simplify the load distribution factors that best apply to implements of husbandry, the researchers developed FE models representative of a wide-ranging bridge population and compared the load effects of the HL-93 notional model to those of the implements of husbandry notional model (115% of the Federal Bridge Formula) with a standard gauge width of 6 ft. It was found that the load distribution was similar. As a result, it was concluded that a modifier could be applied to the current AASHTO LRFD Bridge Design Specifications and the AASHTO Standard Specifications for Highway Bridges when the gauge width deviates from 6 ft.

The current live load factor (for LRFR) applied to load rating equations was developed using a statistical reliability analysis. The data set for implements of husbandry used in NCHRP 12-110 was limited in comparison to the data set used to develop the current live load factor but was used nonetheless to develop live load factors. The approach was the same as that used for standard vehicle calibration and would benefit from a greater set of data. The researchers proposed an impact factor no greater than 20% of the static load. This is based on the extensive data set offered by Freeseman (2017), which found the strain response of numerous bridges subjected to various implements of husbandry to be within a range of 0% to 12% of the static strain regardless of bridge type, span, vehicle, and speed.

The effects of the implements of husbandry on bridge superstructures were studied by various other researchers. These studies were conducted on different types of bridge structures. One such study was conducted by Seo et al. (2013) on simply supported steel girder bridges. The goal of this research was to investigate the load distribution characteristics of steel girder bridges on rural roadways in the United States subjected to four agricultural live loads and one highway-type truck. The vehicles were categorized as normal and special loads. The agricultural vehicle with a single-wheel front axle was considered special, while the rest were considered normal vehicles. Load distribution factors were found using field test data, finite element analysis, and statistical analysis. These distribution factors were compared with AASHTO-codified values. The results showed that the distribution factors from the field test and analytical data were lower than the AASHTO values in the case of normal vehicles. For special vehicles, the distribution factors for central girders were higher than the AASHTO values. This was due to the presence of a single wheel on the front axle. In the case of exterior girders, bridges with concrete exterior girders showed a higher distribution factor than the AASHTO value for both kinds of vehicles. This is due to the increased girder stiffness. In the case of a bridge with steel exterior girders, the distribution factor was lower than the AASHTO value for both types of vehicles. The statistical analysis resulted in distribution factors that were lower than the AASHTO values for steel interior and exterior girders but not for concrete exterior girders. To summarize the comparison of results, the AASHTO equations provide design values that are not predictive in nature because they are empirical code equations specifically used for design purposes.

As a continuation of this work, Seo et al. (2015) investigated the LLDFs for a short-span timber bridge subject to heavy agricultural vehicles. The LLDFs were determined from field test data, finite element analysis, and statistical analysis. These LLDFs were compared with the results from AASHTO-codified methods. The FE model was validated with the field test data. A large number of agricultural vehicles with different characteristics were used as input load models to account for uncertainties in the vehicle configuration. The statistical LLDF limits of the bridge were determined by using LLDFs calculated from the analytical results. The results indicated that both the analytical and field-collected LLDFs were higher than the AASHTO specification values for both interior and exterior girders. The statistical interior and exterior girder LLDF limits showed 95% confidence thresholds. This shows that the AASHTO equations were unsatisfactory in determining the LLDFs under agricultural vehicles in some cases.

2.2 Dynamic Impact Factor

Vehicles traveling over bridges induce a dynamic response in the bridge superstructure, which can produce greater live load moment and shear values than a static response. The factor used to account for this response is called the dynamic impact factor, abbreviated as IM or DIF. This factor is calculated utilizing Equation 1 based on the dynamic and static responses (Deng et al. 2014).

$$IM = \frac{R_{dyn} - R_{sta}}{R_{sta}} \quad (1)$$

where R_{dyn} and R_{sta} are the maximum dynamic and static responses, respectively, regardless of whether the two responses occur with a truck at the same longitudinal position.

The IM is often referred to as the dynamic load allowance (DLA). According to the AASHTO LRFD Bridge Design Specifications, the DLA (or IM) is applied to the static design load to account for the dynamic response generated by moving vehicles. For the strength design of most bridge components (except for deck joints), a DLA of 0.33 should be applied (AASHTO 2020).

In some research, the bridge dynamic impact factor is abbreviated as DIF and defined as shown in Equation 2 (Deng and Phares 2016). In the present research, the DIF is used to refer to the live load on the bridge plus the induced dynamic response of that load.

$$DIF = 1 + \frac{R_{dyn} - R_{sta}}{R_{sta}} \quad (2)$$

There are many parameters that could influence the bridge DIF. These parameters include bridge length, bridge width, deck thickness and surface roughness, vehicle speed and weight, etc. These parameters have been researched for many years. Since the goal of the present project was to investigate the effects of husbandry vehicles on bridge structures, the parameters related to vehicles, that is, truck speed and truck weight, were explored. The following paragraphs only present studies that include these two parameters.

Chang and Lee (1994) studied the dynamic behavior of simple-span bridges with rough surfaces under heavy truck loads. The causes of vibration and the dynamic behavior of the bridges were investigated in both the time and frequency domains. Dynamic responses from four different vehicle models were compared to find an appropriate vehicle model for vibrational analysis. The suggested vehicle model was used to calculate impact factors for different vehicle speeds, deck roughnesses, and span lengths. The data obtained from the study were used to derive empirical formulas for impact factors represented in terms of span length, vehicle speed, and surface roughness using multiple linear regression. The results showed that the DIF varies significantly with vehicle speed.

Schwarz and Laman (2001) conducted field tests on three prestressed concrete (PC) I-girder bridges to obtain the DLA, girder distribution factors (GDFs), and service level stress. Bridge response was measured at each girder as test trucks and normal traffic passed over the bridges. Numerical models (grillage) were then developed for each of the three tested bridges and validated against the field-collected data. The results showed that DLA decreases as static live load stress increases. This means that the DLA decreases with an increase in truck weight. The other notable finding was that the DLA increases as the vehicle speed increases. The number of axles did not show a significant effect on DLA.

Li (2005) investigated the dynamic response of bridges due to bridge-vehicle interaction. The evaluation was conducted on multi-girder highway bridges with medium span lengths (50 to 100 ft) that were subjected to overweight, oversized vehicles. The effects of various bridge parameters, including road roughness, bridge length, vehicle weight, vehicle speed, and vehicle/bridge frequency ratio, on bridge response were investigated. Static and dynamic responses from a selected three-span bridge with simply supported prestressed concrete girders were collected and analyzed. The field test results showed that the dynamic impact factor increased with an increase in truck speed. An FE model was developed based on a field-monitored bridge and validated against the field test data. Truckloads and speeds were simulated for the FE analysis. One of the simulated trucks was given a bouncing (hammering) effect. The results indicated that the impact factor increases linearly with an increase in truck speed for trucks with no bouncing effect. For trucks with a bouncing effect, the impact factor increases rapidly, showing a nonlinear relationship. Additionally, the impact factor decreases with an increase in truck weight for all trucks.

Deng and Cai (2010) developed a three-dimensional (3D) vehicle-bridge coupled model to simulate the interaction between bridges and vehicles in order to investigate the impact factor on multi-girder concrete bridges. An HS-20-44 truckload was simulated to interact with the deck surface of the FE model. Based on the results, the researchers found that the impact factor was highest at a truck speed of 18.64 mph (30 km/h) and then dropped as speed increased. This drop in the impact factor was seen from 18.64 mph (30 km/h) to 46.6 mph (75 km/h) and then increased thereafter.

Deng et al. (2014) reviewed and summarized the findings of studies from 1994 to 2014 regarding the parameters that may affect the bridge DIF. These parameters included the span length of the bridge, the fundamental frequency of the bridge, vehicle speed, vehicle weight, vehicle loading position, International Roughness Index (IRI) or road condition, the entrance condition of the bridge, and bridge material. It was found that, in general, the DIF is large in the case of lighter vehicles, since the corresponding static response is small compared to the dynamic response. Although lighter vehicles produce higher DIFs, the practical significance of these DIFs is low due to the small static load effects. The review found that vehicle speed is an important influencing parameter, but establishing a relationship between vehicle speed and DIF is complicated. This is because other parameters, including vehicle weight, road surface conditions, and span lengths, may affect the bridge response.

Deng and Phares (2016) collected DIF data when empty dump trucks, full dump trucks, and semi-trucks passed over five different bridges. The following entrance roughness conditions were evaluated: as-is, Level 1, and Level 2. Level 1 was simulated by placing a ramp at a distance of 10 ft from the bridge deck approach joint. Level 2 was simulated by placing a ramp directly over the joint. The results indicated that the DIFs increase as the static strain decreases and that the DIFs are sensitive to low strains. This means that low truck weights give high DIFs. Accordingly, the DIFs related to greater strains were deemed more reliable. The results also showed that, in all bridges, the DIFs were high for vehicles at high speeds. The DIF ranged from 1 to 1.1 at crawl speed and 1.3 to 2 at 50 mph.

Mohseni et al. (2018) presented a method for determining the DIFs for skewed, composite, slab-on-girder bridges under AASHTO LRFD truck loading. An extensive parametric study of 125 bridges with different key parameters, including skew angle, was conducted. The research showed that truck speed had a significant effect on bridge dynamic response. An increase in truck speed increased the DIF linearly.

2.3 Live Load Distribution Factor

The AASHTO LRFD Bridge Design Specifications provide different equations for the determination of the LLDF for slab-type and girder-deck bridges. AASHTO (2020) provides equivalent strip width equations for slab-type bridges based on lane loads or full axle loads. Equations 5 and 6 are used to calculate the equivalent strip width for a slab bridge with one lane loaded and two lanes loaded, respectively. These equations are applicable for moment as well as shear.

$$E = 10.0 + 5.0\sqrt{(L_1)(W_1)} \tag{5}$$

$$E = 84.0 + 1.44\sqrt{(L_1)(W_1)} \leq \frac{12.0\,W}{N_L} \tag{6}$$

where E is the equivalent width (in.); L_1 is the modified span length taken to be the lesser of the actual span or 60.0 ft; W_1 is the modified width of the bridge taken to be the lesser of the actual width, 60.0 ft for multi-lane loading, or 30.0 ft for single-lane loading; W is the physical edge-to-edge width of the bridge (ft); and N_L is the number of design lanes. To consider the effects (reduction) of bridge skew, Equation 7 is used to calculate the skew correction factor.

$$r = 1.05\text{-}0.25\tan\theta \leq 1 \tag{7}$$

where θ is the skew angle.

For girder-deck bridges, including commonly used prestressed concrete girder bridges and steel girder bridges, the AASHTO LRFD (2020) specifies a series of equations for the determination of the LLDF. For these equations, the LLDF is calculated based on various bridge parameters, such as the type of girders, the type of deck material, and geometric considerations. Different

equations are provided for single and multiple lane loads. The LLDF used to determine the live load flexural moment distribution for an interior girder on a PC bridge is a function of girder spacing and the span length of the bridge. According to the AASHTO LRFD (2020), the LLDF for the moment in an interior girder subject to a single lane load can be calculated using Equation 8. Equation 9 can be used to calculate the LLDF for the moment in an interior girder subject to two or more design lanes loads.

$$\text{LLDF} = \left[0.06 + \left(\frac{S}{14}\right)^{0.4} * \left(\frac{S}{L}\right)^{0.3} * \left(\frac{K_g}{12*L*t_s^3}\right)^{0.1}\right] * r_{moment} \quad (8)$$

$$\text{LLDF} = \left[0.075 + \left(\frac{S}{9.5}\right)^{0.6} * \left(\frac{S}{L}\right)^{0.2} * \left(\frac{K_g}{12*L*t_s^3}\right)^{0.1}\right] * r_{moment} \quad (9)$$

where $\left(\frac{K_g}{12*L*t_s^3}\right)^{0.1}$ can be assumed as 1.09 for prestressed concrete I girders and 1.02 for steel beams, S is the girder spacing, and L is the span length (Tables 4.6.2.2.1-1 and 4.6.2.2.1-3 in the AASHTO LRFD [2020]). To consider the reduction in LLDF due to bridge skew, the LLDF calculated is multiplied by the skew reduction factor. The skew reduction factor can be calculated using Equation 10.

$$r_{moment} = 1 - c_1(\tan\theta)^{1.5} \quad (10)$$

where $c_1 = 0.25(\frac{K_g}{12.0Lt_s^3})^{0.25}(\frac{S}{L})^{0.5}$; $c_1 = 0$ for $\theta < 30^{\circ}$, $\left(\frac{K_g}{12.0Lt_s^3}\right)^{0.25} = 1.15$ for PC girders and $\left(\frac{K_g}{12.0Lt_s^3}\right)^{0.25} = 1.03$ for steel girders.

The LLDF for shear in an interior girder subject to a single design lane load and two or more design lane loads can be calculated by Equation 11 and Equation 12, respectively (Table 4.6.2.2.3a-1 in the AASHTO LRFD [2020]).

$$LLDF = \left[0.36 + \left(\frac{S}{25}\right)\right] * r_{shear} \quad (11)$$

$$LLDF = \left[0.2 + \left(\frac{S}{12}\right) - \left(\frac{S}{35}\right)^{2.0}\right] * r_{shear} \quad (12)$$

To consider the skew-related reduction in LLDF for shear, Equation 13 is used.

$$r_{shear} = [1 + 0.2\left(\frac{12.0Lt_s^3}{K_g}\right)^{0.3}] \quad (13)$$

where and $\left(\frac{12.0Lt_s^3}{K_g}\right)^{0.3} = 0.85$ for PC girders and $\left(\frac{12.0Lt_s^3}{K_g}\right)^{0.3} = 0.97$ for steel girders.

For the exterior girders, the lever rule is specified for the calculation of the LLDFs.

Over the last decade, research has been conducted to evaluate the efficacy of the AASHTO LLDFs for different types of bridges subject to various load scenarios. For example, Yousif and Hindi (2007) conducted a finite element analysis (FEA) involving simple span slab-on-girder concrete bridges to calculate live load distribution factors and compare them with the predictions made by the AASHTO LRFD Bridge Design Specifications. A few linear elastic bridge models were built and analyzed using SAP2000. The live load was positioned at the longitudinal location, which produced the maximum load effects. To calculate the girder distribution factor, the total moment carried by the girder composite section obtained from the FEA was divided by the moment obtained from a single-beam analysis. To compare this girder distribution factor with the AASHTO LRFD prediction, the girder distribution based on the AASHTO LRFD method was divided by the FEA girder distribution factor. The results showed that the AASHTO LRFD overestimated the live load distribution compared to the analytical results.

Conner and Huo (2006) investigated the effects of parapets and bridge aspect ratio on the live load distribution of girders. This study conducted finite element analysis on 34 two-span continuous bridges with varied bridge geometry parameters. To determine the distribution factor, the maximum girder moments were divided by the maximum moment calculated for a single beam. These distribution factors were compared with the AASHTO LRFD predictions. The results suggested that the AASHTO LRFD results were conservative for the model with parapets. The distribution factors for the model with parapets were 36% lower than the AASHTO LRFD predictions for the exterior girders and 13% lower than the AASHTO LRFD predictions for the interior girders.

In addition to finite element simulation, field tests of bridges subjected to controlled vehicle weights is another commonly used approach to investigate the LLDFs of highway bridge structures. For example, Christopher et al. (2016) tested two similar bridges for live load distribution. To calculate the girder distribution factors, the maximum moment on each girder was divided by the sum of moments on all girders. The girder distribution factors of the field-tested bridges were compared with the AASHTO LRFD distribution factors. The comparison showed that for positive moments on all girders, the AASHTO LRFD girder distribution factors were generally found to be conservative.

An AASHTO manual proposed under NCHRP 12-110 (Fu et al. 2020) is specifically intended to evaluate bridges for their capacity to carry implements of husbandry. Per this manual, a state may define two or three tiers of IoH. Tier 1 is equivalent to the state legal load, with consideration given to the wider gauge widths of IoH. Tier 2 includes vehicles that are heavier and travel much less frequent than vehicles in Tier 1, and Tier 3 includes vehicles that are heavier and travel even less frequently than vehicles in Tier 2. Tier 1 vehicles, due to their wider gauge widths, distribute the vehicular load to a wider deck area and to more beams.

2.4 Live Load Factor Calibration

The current AASHTO LRFD (2020) determines live load factors based on probabilistic analysis and reliability theory. The first use of this approach to determine load factors for bridge structures can be traced back to the 1980s. The first well-established research to calculate load factors based on this approach, which involved the development of load and resistance models, selection of the reliability analysis method, and calculation of the reliability index (also known as the safety index), was conducted under NCHRP 12-33. The research details are documented in Nowak (1999).

In this approach, the load and resistance data generally give distributions, as shown in Figure 1. In the figure, the probability density function of the load data is denoted by Q, and that of the resistance data is denoted by R. Q' and R' represent the increase in load and decrease in resistance over time. To ensure a reliable structure, the resistance should be higher than the load effects on the key bridge components. The Q and R curves in Figure 1 do not overlap, while the Q' and R' curves do show an overlap. This overlap denotes the probability of failure. The probability of failure is dependent on the safety index, β, where a higher safety index indicates a low probability of failure and vice-versa.

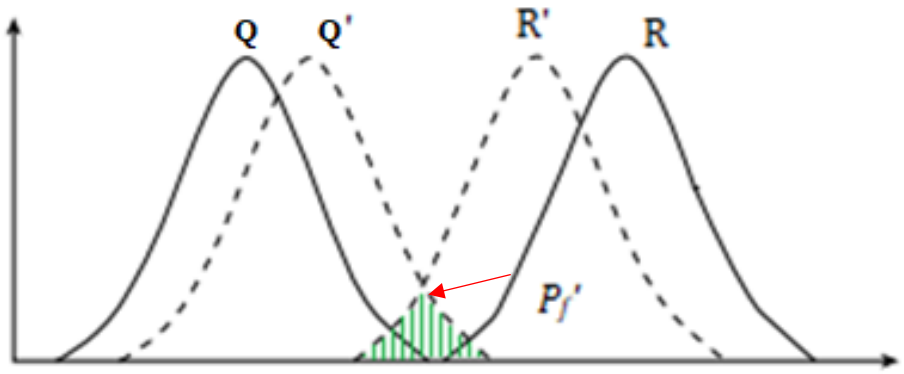

Figure 1. Basic reliability model and failure probability

Nowak (1999) described the calculation of load and resistance factors (LRFs) for the AASHTO LRFD Bridge Design Specifications. The project consisted of the selection of a reliability analysis method, calculation of reliability indices, and development of load and resistance models. Bridges with steel, reinforced concrete, and prestressed concrete girders were selected for the project. The resistance models developed for the selected bridges included three factors: material (strength), fabrication (dimensions), and professional (actual-to-theoretical behavior). Resistance parameters included the moment and shear capacity of the girders. Statistical parameters, including the bias factor and the coefficient of variation for the resistance models, were derived using a special simulation procedure.

Load models were developed for dead loads, live loads, and dynamic loads. The dynamic and live loads were used to assess the dynamic behavior of the selected bridges. A dynamic load allowance of 0.33 was recommended to apply to the truck effect only. The live load model was

developed using the available truck survey data. The load parameters consisted of the maximum moments and shears calculated for the girder bridges. Statistical parameters such as mean and standard deviation were calculated from the available truck data. The mean of the data, along with a nominal load, were used to find the bias factor. A new design live load was developed, which served as the nominal live load to find the bias factors for the live load parameters.

Reliability theory utilizes load and resistance models to calculate reliability indices. In Nowak (1999), these reliability indices were calculated using an iterative procedure and were found to vary depending on span length and girder spacing. A target reliability index was selected from the calculated reliability indices. The target reliability index selected for the project was 3.5. Load and resistance factors for bridges designed using the new LRFD codes were determined in order to find a reliability index close to the target reliability index. The load factors recommended for dead load, asphalt overlay, and live load (including impact) were 1.25, 1.5, and 1.7, respectively. For steel girders, a resistance factor of 1.0 was recommended for both moment and shear resistance. For prestressed concrete girders, a resistance factor of 1.0 was recommended for moment resistance and a resistance factor of 0.9 was recommended for shear resistance. In the case of reinforced concrete T beams, a resistance factor of 0.9 was recommended for both moment and shear resistance. Reliability indices calculated for bridges designed using the new LRFD code were close to the predetermined reliability index level of 3.5 for all materials and spans. Thus, the final calculated load and resistance factors were included in the AASHTO LRFD Bridge Design Specifications.

Following this work, Barker and Puckett (2007) summarized a five-step procedure to calibrate the load and resistance factors for bridge structures based on the reliability theory recommended by Nowak (1999). The **first step** is to establish a database of load and resistance statistics. Calibration based on reliability theory requires statistical load and resistance data. Mean and standard deviation values are used to represent probability density functions. These two values for a given nominal value are used to calculate the bias factor and coefficient of variation for the load and resistance data. The bias factor and coefficient factor are given in Equations 14 and 15.

$$\lambda_x = \frac{\bar{x}}{x_n} \tag{14}$$

$$V_x = \frac{\sigma_x}{\bar{x}} \tag{15}$$

where λ_x is the bias factor, $\bar{x}$ is the mean, σ_x is the standard deviation, V_x is the coefficient of variance, and x_n is the nominal value. In Barker and Puckett (2007), resistance data were developed for girder-type bridges. Load effects (moment, shear, tension, and compression) were calculated and compared to the resistance provided by the actual cross section of the girders.

The **second step** is to estimate the safety index, also known as the reliability index (β). According to Barker and Puckett (2007), the load data are usually normally distributed, and the resistance data are usually lognormally distributed. Thus, Equation 16 can be used to calculate the safety index.

$$\beta = \frac{R_n \lambda_R (1-kV_R)[1-\ln(1-kV_R)]-\bar{Q}}{\sqrt{[R_n V_R \lambda_R (1-kV_R)]^2+{\sigma_Q}^2}} \quad (16)$$

where R_n is the nominal value, λ_R is the bias factor, V_R is the coefficient of variation of the resistance data, σ_Q is the standard deviation, and $\overline{Q}$ is the mean of the load data.

The **third step** is to establish a safety index distribution plot. Barker and Puckett (2007) calculated the safety indices for bridges with different geometries and plotted them against the span length for each girder spacing. Figure 2 shows the safety indices plotted for moment and shear. The variations of the safety indices along the span length for each girder spacing are then observed.

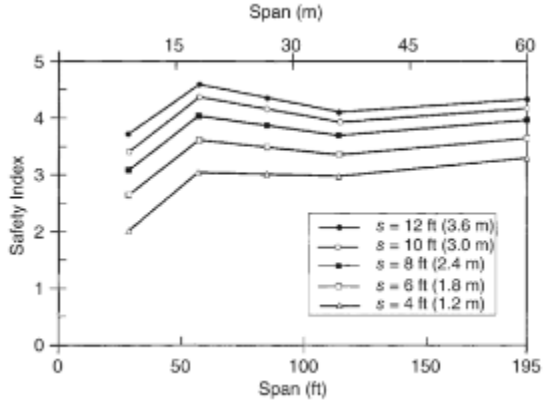

(a) Moment

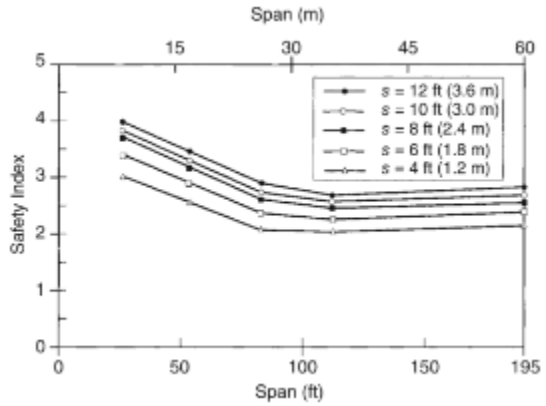

(b) Shear

Barker and Puckett 2007

Figure 2. Safety indices for simple-span prestressed concrete girders

The **fourth step** is to select a target safety index for calibration. Barker and Puckett (2007) evaluated a large range of safety indices for moment and shear design. A uniform safety index was desired in the calibration procedure for all spans and girder spacings. For this reason, a target safety index value was chosen that was used to calculate the trial load and resistance

factors. These trial load and resistance factors were used to find safety index values close to the target safety index in the fifth step. A target safety index of 3.5 was chosen.

The **fifth step** is to calculate the load and resistance factors. For Barker and Puckett (2007), this was done to achieve the target safety index of 3.5. The variation in safety index values observed in step three was due to different ratios of dead load to live load. Since load factors must be common for all bridge types, the variation was minimized by the proper selection of load factors for dead and live loads. The resistance factors that would account for the differences in the reliability of the various limit states were selected. It was observed that achieving the target safety index for all bridge types was not possible. Therefore, calibration of the safety index gave values close to the target safety index, which was considered acceptable.

Barker and Puckett (2007) determined the final load and resistance factors from the calibration procedure. The calibration procedure is tested based on whether the selected load and resistance factors result in safety indices that are clustered around the target safety index and are uniform with span length and girder spacing.

In the work conducted by Nowak (1999), a target safety index of $\beta_T = 3.5$ was used. The final load factors determined for the Strength I limit state were as follows:

Factory made:	$\gamma_{DC1} = 1.25$
Cast in place:	$\gamma_{DC2} = 1.25$
Asphalt overlay:	$\gamma_{DC3} = 1.50$
Live load:	$\gamma_{LL} = 1.75$

The current load factors in AASHTO (2020) were calibrated for an annual daily truck traffic (ADTT) of 5,000 with a safety index of 3.5. The AASHTO Manual for Bridge Evaluation (MBE) (2018) adopted a lower safety index value for LRFR to reflect the reduced exposure period, consideration of site realities, and the economic considerations of rating versus design. For bridges with low ADTT values, a reduced target safety index of 2.5 is used and calibrated to past AASHTO operating level load rating. The ADT for IoH vehicles is quite low in most circumstances; therefore, a low target safety index value for the calibration procedure can be justified.

The selection of a higher-than-calculated resistance factor can be justified for the calibrated safety indices that are close to the target safety index. For example, in the work conducted by Nowak (1999), the calculated resistance factor for moment in prestressed concrete girders was 0.90, while the recommended resistance factor was 1.00. Similarly, the calculated resistance factor for shear was 0.85, and the recommended resistance factor was 0.90.

Moses (2001) defined the safety index as a measure of structural reliability or, conversely, the risk that a component will reach a limit state due to insufficient capacity. A limit state equation to represent the margin of safety of a component for any failure mode was given as g = R-D-L, where R is the random resistance, D is the random dead load effect, and L is the random live

load effect. A component is considered safe if the load and resistance variables lead to a safety margin where g is greater than 0 and fails if g is less than 0. The magnitude of g is random; therefore, the mean and standard deviation of the variable g are used to give a measure of reliability. This measure of reliability or the safety index is expressed as a ratio of the mean of g to the standard deviation of g. When the mean of g is high while the standard deviation is low, the safety index is high, and vice-versa. A high mean of g with a low standard deviation means that the probability that g will fall below 0 is small. This situation shows a low probability of failure or high reliability.

The loading data given by Nowak (1999) were used by Moses (2001) to calibrate live load factors for the *Manual for Condition Evaluation and Load and Resistance Factor Rating of Highway Bridges* prepared under NCHRP Project C12-46. The aim of the calibration was to achieve uniform target reliability indices over a range of applications. These applications included design load rating, legal load rating, posting, and permit vehicle analysis. The calibration process consisted of selecting nominal load and resistance values and corresponding load and resistance factors. The steps generally followed for the calibration process included defining the limit states that were going to be checked, defining the random variables that affect the occurrence of the limit state, and assembling a database for the various random variables.

The database of dead loads, live loads, other environmental loads, and system capacities was generated with random variables. The resulting database was used to calculate the statistical parameters, including the coefficient of variance and bias factors (i.e., the the ratio of the mean to the nominal design value). A deterministic model such as HS-20 or HL-93 was recommended to be used as the nominal value to calculate bias. These data were used to calculate the safety indices as described above. After the calculation of the safety indices, a target safety index needed to be selected for calibration so that the warranted safety level could be achieved for a given component.

The reason to calibrate the load and resistance factors was to calculate a safety index close to the target safety index for any given component. The target safety index values used in formulating the AASHTO LRFD values were stated to be in the range of 2.0 to 4.0. It was explained that due to the higher relative marginal costs for increasing capacity in existing spans than for creating a new design, a lower target safety index could be used in evaluation than in design. Computation of the safety index was recommended to be carried out using assumed load and resistance factors. The best combination of load and resistance factors is produced using an iterative process. An average safety index that falls close to the target safety index with minimum deviation is considered to generate the best combination of load factors.

3 HUSBANDRY VEHICLES

The configuration of IoH vehicles differs from that of traditional trucks observed on public roads. Specific differences between IoH and traditional trucks include wheelbase, wheel track, axle loads, number of axles, and tire thickness. This chapter summarizes information obtained about IoH configurations and related topics.

3.1 IoH Vehicle Identification and Data Enhancement

An extensive database of IoH vehicle information was created using information from various sources. This database included many of the vehicles that could be classified as IoH, with a specific focus on those of interest to this project.

In general, the vehicle configuration information collected included axle load data in the empty and full load conditions, number of axles, wheelbase, and wheel track. In some cases, vehicles were identified but full configuration information could not be found, and therefore these vehicles were eliminated from use in subsequent research tasks. Photographs of typical IoH vehicle are presented in Figure 3, with detailed vehicle information presented in Table 1.

Due to a need for data that covered IoH with various levels of loading, the base IoH data were enhanced to include a larger data sample. The axle loads in partially loaded conditions were estimated using a percentage of the payload capacity. These loads were calculated using interpolation between 0% and 100% of the vehicle's payload capacity, with the axle loads only at 0% and a full payload at 100%. Determinig loads in increments of 20% gave four more axle loads for each vehicle. Thus, each vehicle has six axle loads for different payload conditions. The interpolation, therefore, enlarged the available load data sample. The enhanced axle load data can be found in Table 1.

(a) V 2-1 (7300)

(b) V 2-2 (8400)

(c) V 3-36 (2505)

(d) TG 8400

(e) JDR 4044

(f) JDR 4045

(g) JDR 4060

(h) SP310F

(i) SP370F

(j) SP410F

(k) TG 8300

(l) TG 9300

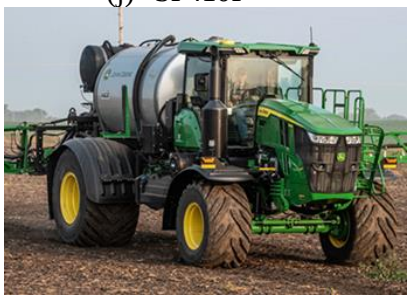

(m) JD 800R

(n) Case IH Patriot 3250

(o) Case IH Patriot 4350

(p) Case IH Patriot 4540

Case IH 4530

Case IH Titan 3540

(s) JD 408R

(t) JD 410R

(u) JD 412R

(v) JD 612R

(w) JD 616R

(x) JD R4023

(y) GVM 380 Prowler

(z) Case IH 3040

(aa) Case IH 4040

(ab) Case IH 3030

Figure 3. IoH vehicles selected

Table 1. Load data of selected IoH vehicles

Vehicle Code	Payload %	Number of axles	Axle 1 weight (kips)	Axle 2 weight (kips)	Axle 3 weight (kips)	Axle 1-2 spacing (ft)	Axle 2-3 spacing (ft)
V2-1 (7300)	0%	2	10.99	17.71	NA	23	NA
	20%	2	11.52	21.18	NA	23	NA
	40%	2	12.04	24.65	NA	23	NA
	60%	2	12.57	28.12*	NA	23	NA
	80%	2	13.09	31.59*	NA	23	NA
	100%	2	13.62	35.06*	NA	23	NA
V2-2 (8400)	0%	2	11.37	17.33	NA	17	NA
	20%	2	12.09	20.61	NA	17	NA
	40%	2	12.80	23.89	NA	17	NA
	60%	2	13.52	27.17*	NA	17	NA
	80%	2	14.23	30.45*	NA	17	NA
	100%	2	14.95	33.73*	NA	17	NA
V3-36 (2505)	0%	3	11.06	16.20	16.20	19	6
	20%	3	10.96	19.69	19.02	19	6
	40%	3	10.87	23.19	21.84	19	6
	60%	3	10.77	26.68*	24.66	19	6
	80%	3	10.67	30.17*	27.48*	19	6
	100%	3	10.58	33.67*	30.30*	19	6
TG 8400	0%	2	11.37	17.33	NA	17	NA
	20%	2	12.09	20.61	NA	17	NA
	40%	2	12.80	23.89	NA	17	NA
	60%	2	13.52	27.17*	NA	17	NA
	80%	2	14.23	30.45*	NA	17	NA
	100%	2	14.95	33.73*	NA	17	NA
JDR4044	0%	2	14.31	17.49	NA	13	NA
	20%	2	14.88	19.59	NA	13	NA
	40%	2	15.44	21.68	NA	13	NA
	60%	2	16.01	23.78	NA	13	NA
	80%	2	16.58	25.88*	NA	13	NA
	100%	2	17.14	27.98*	NA	13	NA
JDR4045	0%	2	16.24	19.84	NA	13	NA
	20%	2	16.80	21.94	NA	13	NA
	40%	2	17.37	24.04	NA	13	NA
	60%	2	17.94	26.14*	NA	13	NA
	80%	2	18.50	28.23*	NA	13	NA
	100%	2	19.07	30.33*	NA	13	NA
JDR4060	0%	2	16.43	20.08	NA	13	NA
	20%	2	17.18	22.87	NA	13	NA
	40%	2	17.94	25.67*	NA	13	NA
	60%	2	18.69	28.47*	NA	13	NA
	80%	2	19.45	31.26*	NA	13	NA
	100%	2	20.21	34.06*	NA	13	NA
SP310F	0%	2	15.32	15.32	NA	13	NA
	20%	2	15.95	17.36	NA	13	NA
	40%	2	16.57	19.39	NA	13	NA
	60%	2	17.20	21.43	NA	13	NA
	80%	2	17.83	23.47	NA	13	NA
	100%	2	18.45	25.51*	NA	13	NA
SP370F	0%	2	17.14	17.14	NA	15	NA
	20%	2	17.86	19.97	NA	15	NA
	40%	2	18.58	22.80	NA	15	NA
	60%	2	19.31	25.63*	NA	15	NA
	80%	2	20.03	28.46*	NA	15	NA
	100%	2	20.75	31.29*	NA	15	NA
SP410F	0%	2	17.48	17.48	NA	15	NA
	20%	2	18.20	20.30	NA	15	NA
	40%	2	18.92	23.13	NA	15	NA
	60%	2	19.64	25.96*	NA	15	NA
	80%	2	20.36	28.79*	NA	15	NA
	100%	2	21.09	31.62*	NA	15	NA

Vehicle Code	Payload %	Number of axles	Axle 1 weight (kips)	Axle 2 weight (kips)	Axle 3 weight (kips)	Axle 1-2 spacing (ft)	Axle 2-3 spacing (ft)
TG8300	0%	2	10.99	17.71	NA	23	NA
	20%	2	11.52	21.18	NA	23	NA
	40%	2	12.04	24.65	NA	23	NA
	60%	2	12.57	28.12*	NA	23	NA
	80%	2	13.09	31.59*	NA	23	NA
	100%	2	13.62	35.06*	NA	23	NA
TG9300	0%	2	13.62	22.94	NA	21	NA
	20%	2	14.39	27.50*	NA	21	NA
	40%	2	15.16	32.06*	NA	21	NA
	60%	2	15.93	36.61*	NA	21	NA
	80%	2	16.70	41.17*	NA	21	NA
	100%	2	17.47	45.73*	NA	21	NA
JD 800R	0%	2	13.95	17.05	NA	13	NA
	20%	2	14.89	20.55	NA	13	NA
	40%	2	15.84	24.04	NA	13	NA
	60%	2	16.78	27.54*	NA	13	NA
	80%	2	17.73	31.03*	NA	13	NA
	100%	2	18.67	34.53*	NA	13	NA
Case IH Patriot 3250	0%	2	13.65	16.69	NA	13	NA
	20%	2	14.19	18.37	NA	13	NA
	40%	2	14.72	20.06	NA	13	NA
	60%	2	15.25	21.75	NA	13	NA
	80%	2	15.78	23.44	NA	13	NA
	100%	2	16.32	25.12*	NA	13	NA
Case IH Patriot 4350	0%	2	14.58	17.82	NA	13	NA
	20%	2	15.18	19.88	NA	13	NA
	40%	2	15.78	21.95	NA	13	NA
	60%	2	16.38	24.01	NA	13	NA
	80%	2	16.98	26.08*	NA	13	NA
	100%	2	17.58	28.14*	NA	13	NA
Case IH Patriot 4540	0%	2	13.75	16.81	NA	15	NA
	20%	2	14.64	20.36	NA	15	NA
	40%	2	15.53	23.91	NA	15	NA
	60%	2	16.42	27.46*	NA	15	NA
	80%	2	17.30	31.02*	NA	15	NA
	100%	2	18.19	34.57*	NA	15	NA
Case IH Patriot 4530	0%	2	13.47	16.46	NA	15	NA
	20%	2	14.27	19.66	NA	15	NA
	40%	2	15.07	22.86	NA	15	NA
	60%	2	15.87	26.05*	NA	15	NA
	80%	2	16.67	29.25*	NA	15	NA
	100%	2	17.46	32.45*	NA	15	NA
Case IH Titan 3540	0%	2	14.23	17.39	NA	23	NA
	20%	2	14.83	21.23	NA	23	NA
	40%	2	15.42	25.08*	NA	23	NA
	60%	2	16.02	28.92*	NA	23	NA
	80%	2	16.62	32.76*	NA	23	NA
	100%	2	17.21	36.61*	NA	23	NA
John Deere 408R	0%	2	13.08	15.99	NA	13	NA
	20%	2	13.46	17.39	NA	13	NA
	40%	2	13.84	18.78	NA	13	NA
	60%	2	14.21	20.18	NA	13	NA
	80%	2	14.59	21.58	NA	13	NA
	100%	2	14.97	22.98	NA	13	NA
John Deere 410R	0%	2	13.70	16.74	NA	13	NA
	20%	2	14.17	18.49	NA	13	NA
	40%	2	14.64	20.24	NA	13	NA
	60%	2	15.11	21.98	NA	13	NA
	80%	2	15.58	23.73	NA	13	NA
	100%	2	16.06	25.48*	NA	13	NA
John Deere 412R	0%	2	14.31	17.49	NA	13	NA
	20%	2	14.88	19.59	NA	13	NA
	40%	2	15.44	21.69	NA	13	NA
	60%	2	16.01	23.78	NA	13	NA
	80%	2	16.58	25.88*	NA	13	NA
	100%	2	17.14	27.98*	NA	13	NA

Vehicle Code	Payload %	Number of axles	Axle 1 weight (kips)	Axle 2 weight (kips)	Axle 3 weight (kips)	Axle 1-2 spacing (ft)	Axle 2-3 spacing (ft)
John Deere 612R	0%	2	15.82	19.33	NA	13	NA
	20%	2	16.38	21.43	NA	13	NA
	40%	2	16.95	23.53	NA	13	NA
	60%	2	17.52	25.63*	NA	13	NA
	80%	2	18.08	27.72*	NA	13	NA
	100%	2	18.65	29.82*	NA	13	NA
John Deere 616R	0%	2	16.42	20.07	NA	13	NA
	20%	2	17.17	22.86	NA	13	NA
	40%	2	17.93	25.66*	NA	13	NA
	60%	2	18.68	28.46*	NA	13	NA
	80%	2	19.44	31.25*	NA	13	NA
	100%	2	20.19	34.05*	NA	13	NA
John Deere R4023	0%	2	8.17	9.99	NA	13	NA
	20%	2	8.49	11.01	NA	13	NA
	40%	2	8.80	12.03	NA	13	NA
	60%	2	9.11	13.05	NA	13	NA
	80%	2	9.43	14.06	NA	13	NA
	100%	2	9.74	15.08	NA	13	NA
GVM 380 Prowler	0%	2	13.59	16.61	NA	15	NA
	20%	2	13.87	20.33	NA	15	NA
	40%	2	14.14	24.05	NA	15	NA
	60%	2	14.42	27.77*	NA	15	NA
	80%	2	14.70	31.49*	NA	15	NA
	100%	2	14.98	35.20*	NA	15	NA
Case IH 3040	0%	2	11.38	19.52	NA	23	NA
	20%	2	11.92	22.98	NA	23	NA
	40%	2	12.45	26.44*	NA	23	NA
	60%	2	12.99	29.90*	NA	23	NA
	80%	2	13.53	33.36*	NA	23	NA
	100%	2	14.06	36.82*	NA	23	NA
Case IH 4040	0%	2	11.77	19.66	NA	15	NA
	20%	2	12.66	23.21	NA	15	NA
	40%	2	13.54	26.77*	NA	15	NA
	60%	2	14.43	30.32*	NA	15	NA
	80%	2	15.32	33.87*	NA	15	NA
	100%	2	16.21	37.42*	NA	15	NA
Case IH 3030	0%	2	11.25	19.36	NA	23	NA
	20%	2	11.79	22.82	NA	23	NA
	40%	2	12.32	26.28*	NA	23	NA
	60%	2	12.86	29.74*	NA	23	NA
	80%	2	13.40	33.20*	NA	23	NA
	100%	2	13.93	36.66*	NA	23	NA

*Axle loads above 25 kips

3.2 Comparison with Permissible Axle Loads

The load data collected from each vehicle shown in Table 1 were compared to the newly legalized axle load of 25 kips. Figure 4 shows a plot that compares the IoH vehicle axle loads with the legalized axle load of 25 kips. The x-axis of the plot shows the vehicle number, which is simply a generic number assigned to each vehicle. The vertically aligned markers at a vehicle number indicate the load data for that vehicle. These axle loads range from 0% to 100% of the vehicle's payload capacity in increments of 10% of the payload.

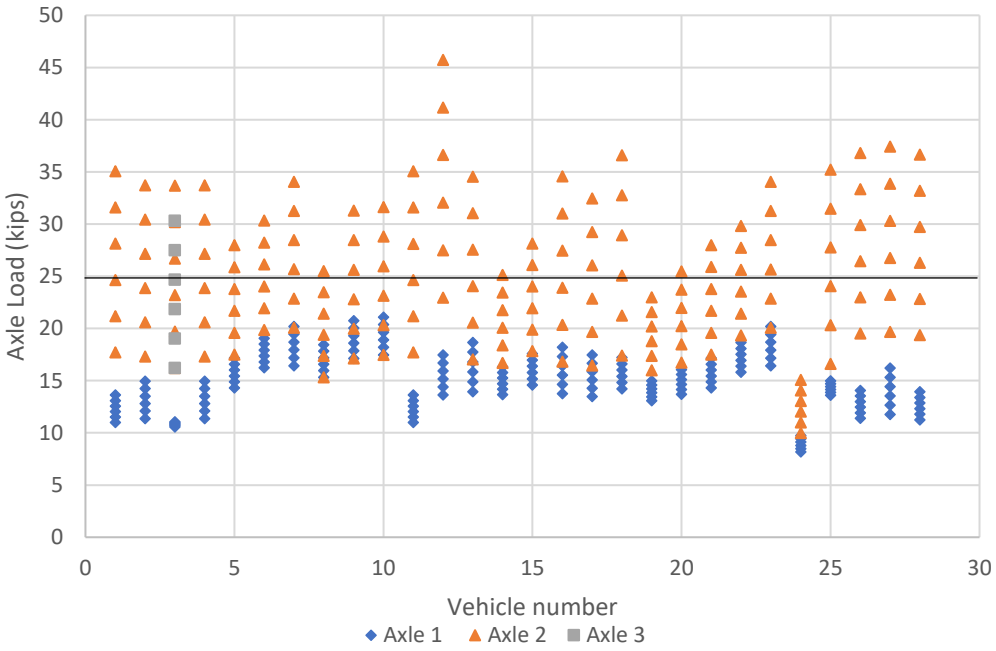

Figure 4. Axle loads of selected IoH vehicles

The results indicated that for most available vehicles the estimated load on the rear axle at full load capacity was higher than 25 kips. The load observed on the front axle of all vehicles was below 25 kips, even at full load capacity. The rear axle loads at empty load capacity were below 25 kips. The rate of increase in load on the rear axle was higher than that of the front axle as the payload increased. The probability that a rear axle load would be more than 25 kips was higher for vehicles loaded to their highest payload capacity.

These observations give a better understanding of the load distributions on the axles of IoH vehicles. The axle load data presented in this chapter were used in the parametric study described in Chapter 6 for the estimation of load distribution and in Chapter 7 for the calibration of load and resistance factors.

4 LIVE LOAD TESTING

Live load testing was conducted to understand the general response of bridges subjected to implements of husbandry vehicles and to collect data that would be used for the calibration of analytical models in subsequent tasks.

Both PC and slab bridges meeting the project criteria were identified in March 2022. An owner/operator that was able to provide numerous terragator types for the project had previously been identified in southeast Iowa, so bridges in this general region were chosen to limit the distance of travel to each bridge.

Following bridge selection, an instrumentation plan that included sensor locations and ideal load path positions was developed for each type of bridge (PC or slab). The field tests were carried out over three days in June and July 2022. On the day of testing for each bridge, strain and deflection transducers were attached to the bridge and then connected to a data acquisition system. During the test, three unique terragator vehicles with controlled and known weights passed over the bridge along each load path. The data were recorded by the data acquisition system and stored for further analysis.

4.1 Bridge Selection

The preliminary task in the selection of bridges was to identify appropriate vehicles for testing in order to limit the distance the vehicles would need to travel to each bridge. This task was intended to increase the efficiency of testing and to reduce the time and expense of the testing process.

Based on input from the project's technical advisory committee, slab bridges and PC bridges were the focus of the field testing. To ensure that the tested bridges represented the target population of bridges in Iowa, the selection process included consideration of a variety of bridge parameters, including skew angle, number of spans, span length, bridge width, number of beams, beam spacing, and slab thickness. In addition, field visits were conducted during the bridge selection process to investigate whether the underside of the bridge was accessible via ladder for the installation of instrumentation. Bridges with limited accessibility were removed from consideration. Five PC bridges and three slab bridges were selected for field testing. Table 2 lists the selected bridges with their key parameters, and Figure 5 shows the location of each bridge.

Table 2. Selected bridges and key parameters

Day	Bridge ID	Bridge type	Span length (ft)					Bridge width (ft)	Number of beams	Beam spacing	Slab Thickness
			Skew	Span 1	Span 2	Span 3	Span 4				
1	9267.1S001	PC	0	80.75	81.5	96.5	85.75	44	7	6 ft 10 in.	NA
	9265.1S001	PC	0	120	NA	NA	NA	44	6	8ft	NA
	9233.9S002	Slab	0	41	53	41	NA	44	NA	NA	20in.
2	337901	PC	15	105.75	111.5	105.75	NA	30	5	7ft	NA
	4811.2S151	Slab	0	45.5	59	45.5	NA	44	NA	NA	24in.
	4802.1S220	Slab	0	39.5	51	39.5	NA	40	NA	NA	20in.
3	9231.5S022	PC	0	43.25	56.5	43.25	NA	44	7	6 ft 11 in.	NA
	9232.8S022	PC	0	95.75	96.5	95.75	NA	44	7	6 ft 9 in.	NA

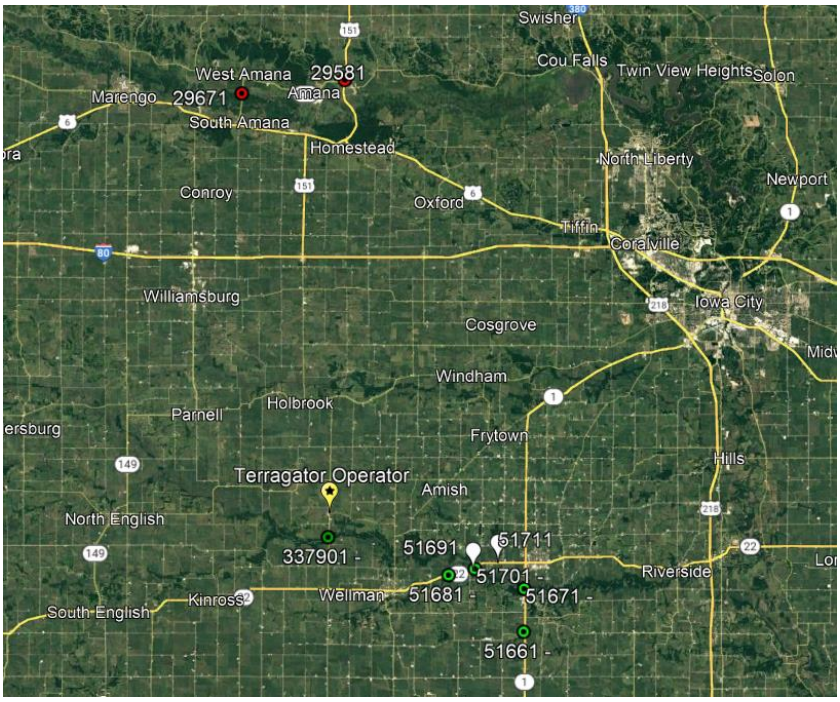

Figure 5. Bridge locations

4.2 Instrumentation Plans

To monitor the response of the selected bridges when subjected to terragator loads, multiple strain and displacement transducers connected to a data acquisition system from Bridge Diagnostics Inc. (BDI) were used for data collection. The system consisted of a BDI STS4 wireless base station to provide a wireless network, BDI STS4-4 wireless intelliducer nodes for data acquisition, BDI ST350 strain transducers, and BDI cable potentiometers. The strain transducers and potentiometers directly connected to the STS4-4 nodes. The STS4-4 nodes connected to the STS4 wireless base station via the base station's wireless network. A laptop was similarly connected to the base station, and the STS-LIVE Windows-based application was launched. The STS-LIVE application received and recorded the data.

Separate instrumention plans were developed for PC and slab bridges.

4.2.1 PC Bridges

Five prestressed concrete girder bridges were instrumented to monitor the induced strain and displacement in the girders under static and dynamic terragator loads. BDI ST350 strain transducers and CPOT-005 cable potentiometers were used to monitor the strain and displacement induced on the bridge girders. Figure 6 shows a typical instrumentation plan for the prestressed concrete girder bridges (Bridge 9267.1S001).

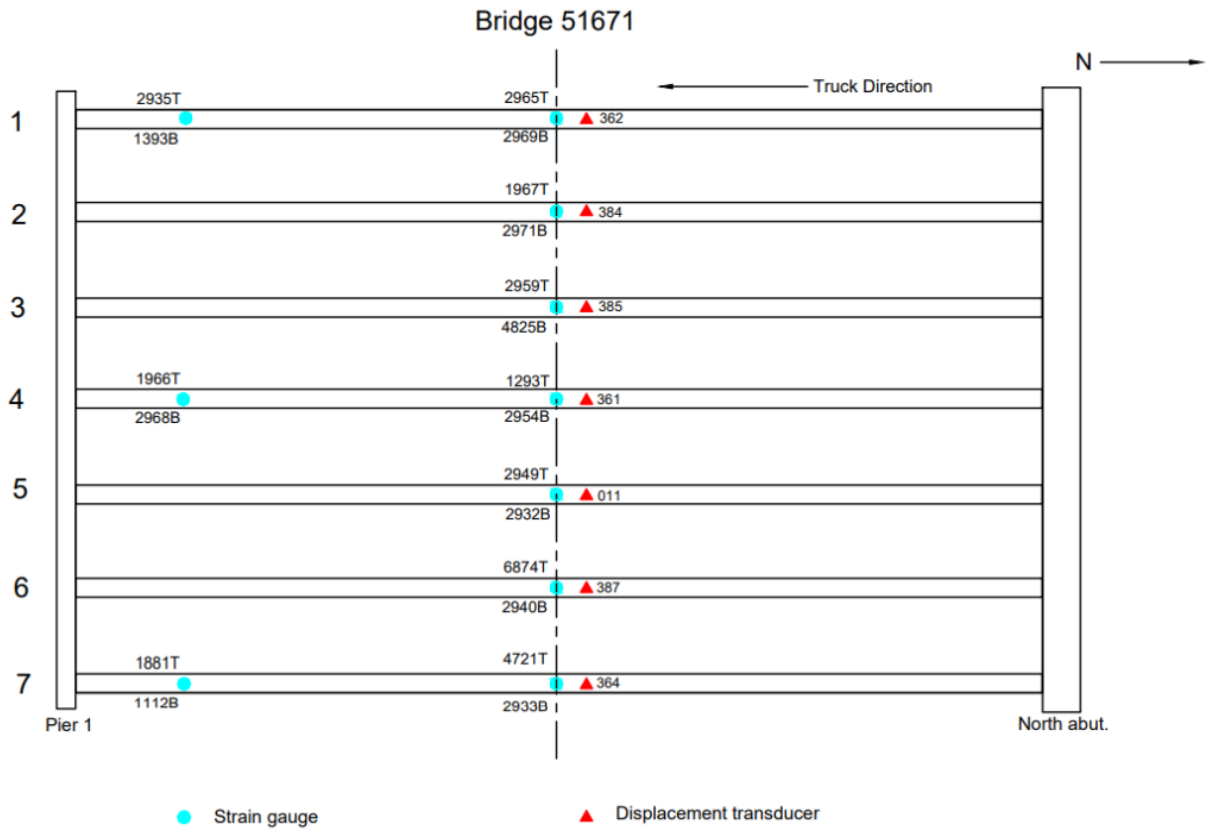

(a) Plan view

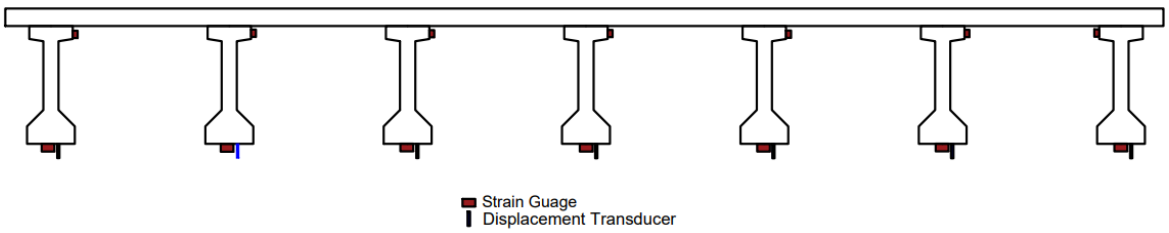

(b) Mid-span section

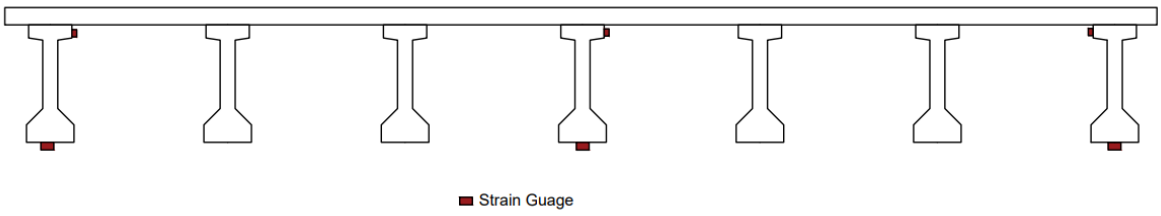

(c) Quarter span section

Figure 6. Instrumentation plan for PC Bridge 9267.1S001

The instrumentation was installed at two sections on each bridge: mid-span and quarter span. At the mid-span section, both strain gauges and displacement transducers were installed on every girder. At the quarter span section, strain gauges alone were installed on the two exterior girders

and on the center girder. Two strain gauges were installed at each instrumentation location, one on the top flange and one on the bottom flange.

Figure 7 shows the strain gauges and cable potentiometers placed at the mid-span section of Bridge 9267.1S001.

(a) Strain gauges on top and bottom flange

(b) Displacement transducer connected to bottom flange

Figure 7. Instrumentation placed on Bridge 9267.1S001

4.2.2 Slab Bridges

Three slab bridges were instrumented and subjected to live terragator loads during the testing phase of the project. Figure 8 shows a typical instrumentation plan for the slab bridges (Bridge 9233.9S002).

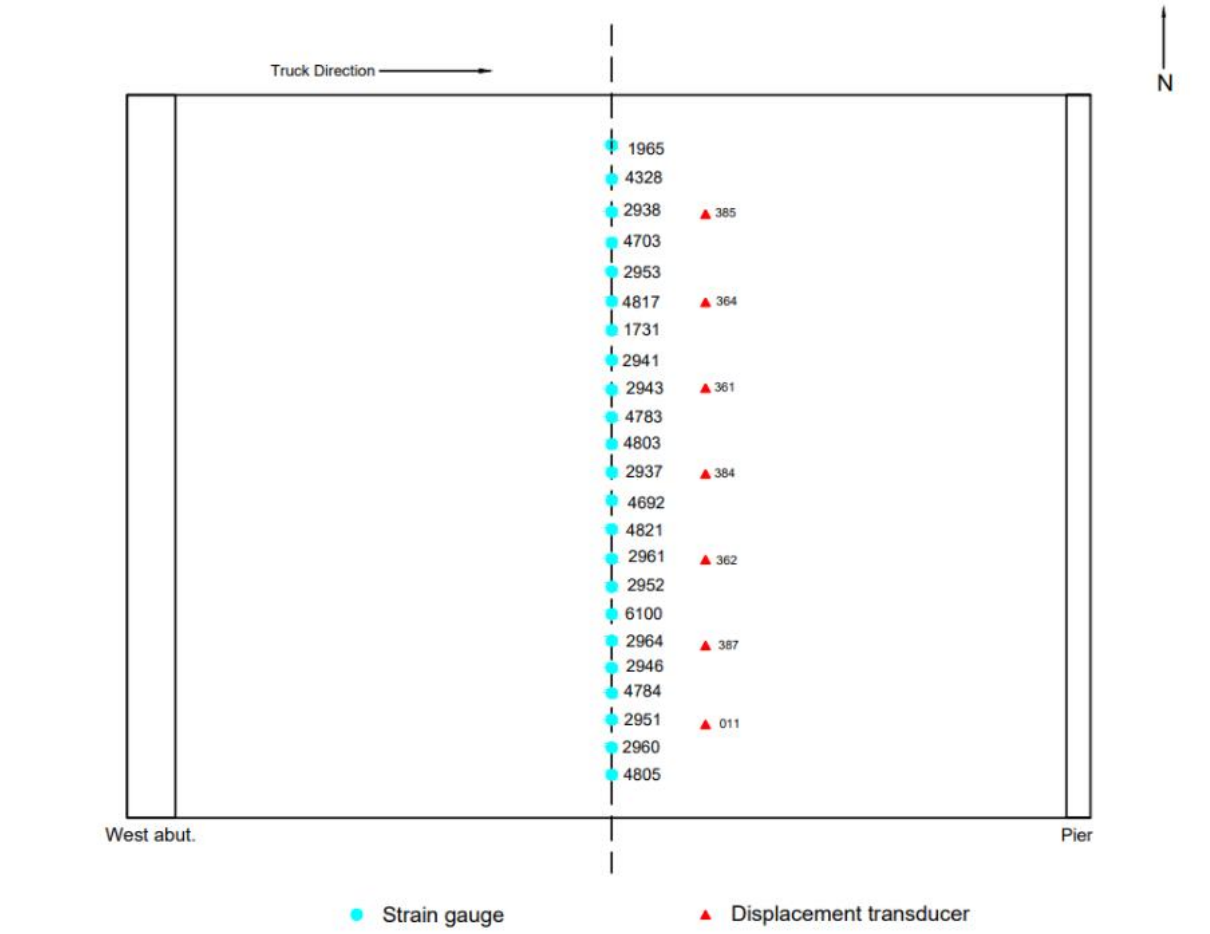

(a) Plan view

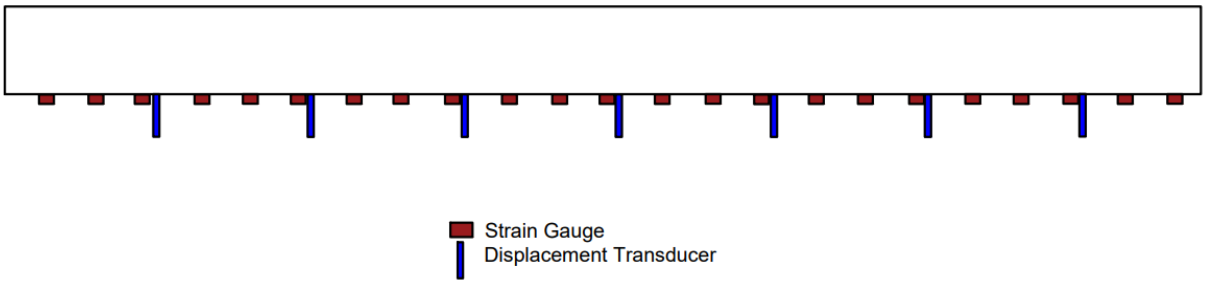

(b) Mid-span section

Figure 8. Instrumentation plan for slab bridges (Bridge 9233.9S002)

On the slab bridges, all instrumentation was installed at mid-span. Seven CPOT-002 cable potentiometers were installed on each bridge to measure the vertical displacement at mid-span. These displacement transducers were placed at equal spacing across the bridge in the transverse direction. Additionally, strain gauges were placed across the bottom of the deck at a spacing of 2 ft.

Strain gauge extensions were used for data collection on the slab bridges. The use of extensions is typical when strain gauges are installed on non-prestressed concrete elements to help negate the effects of localized concrete cracking. The lengths of the extensions were based on the lower and upper limits recommended by Bridge Diagnostics Inc. (2012). The lower limit for the extensions is recommended to be 1.0 x the depth of the slab, and the upper limit is recommended to be the length of the span divided by 20. On Bridges 9233.9S002 and 4802.1S220 extension lengths of 21 in. were used, while on Bridge 4811.2S151 an extension length of 15 in. was used.

Figure 9 shows the displacement transducers and strain gauges with extensions on Bridge 9233.9S002.

Figure 9. Strain gauges and displacement transducers on Bridge 9233.9S002

4.3 Terragator Information

During the field testing for each bridge, three terragators passed over the bridge at different transverse locations. Each terragator had two axles; two terragators had one wheel on the front axle, and one terragtor had two wheels on the front axle. Detailed information for the three terragators used in each load test is presented in Figure 10, Figure 11, and Figure 12.

In each test, the first terragator to cross over the bridge was Terragator TG 7300, shown in Figure 10. During the tests, this terragator was filled with 900 gallons of water, which was 50% of the full payload capacity. This terragator is referred to as T1 throughout this report.

(a) Terragator TG-7300 (T1)

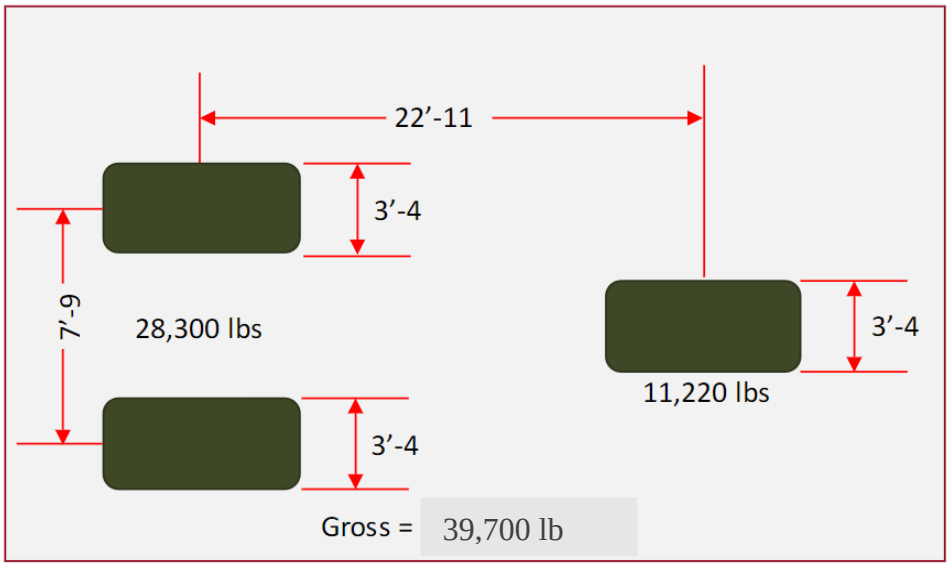

(b) Wheel base, wheel track, and axle loads of T1

Figure 10. Terragator TG-7300 (T1)

The second terragator to cross over the bridge in each test was Terragator TG-8400, shown in Figure 11. During the tests, this terragator had zero payload beyond its own weight. This terragator is referred to as T2 throughout this report. Figure 11 shows the axle weight information for T2.

(a) Terragator TG-8400 (T2)

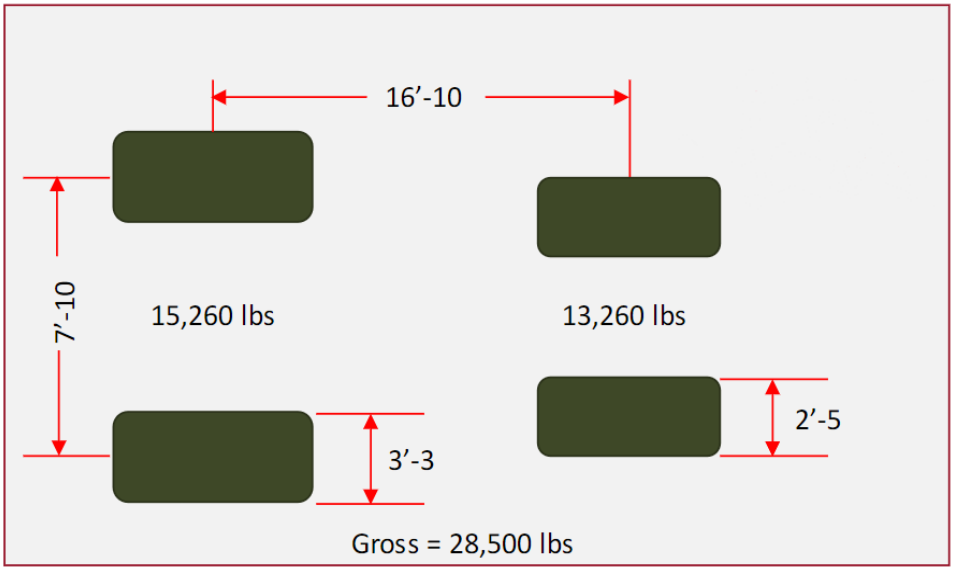

(b) Wheel base, wheel track, and axle weights of T2 on days 1 and 2

Figure 11. Terragator TG-8400 (T2)

The third terragator to cross over the bridge in each test was Terragator TG-8300B, shown in Figure 12. This vehicle was empty, with zero payload beyond its own weight. Terragator TG-8300B is very similar to Terragator TG-7300 and is referred to as T3 throughout this report.

(a) Terragator TG-8300B (T3)

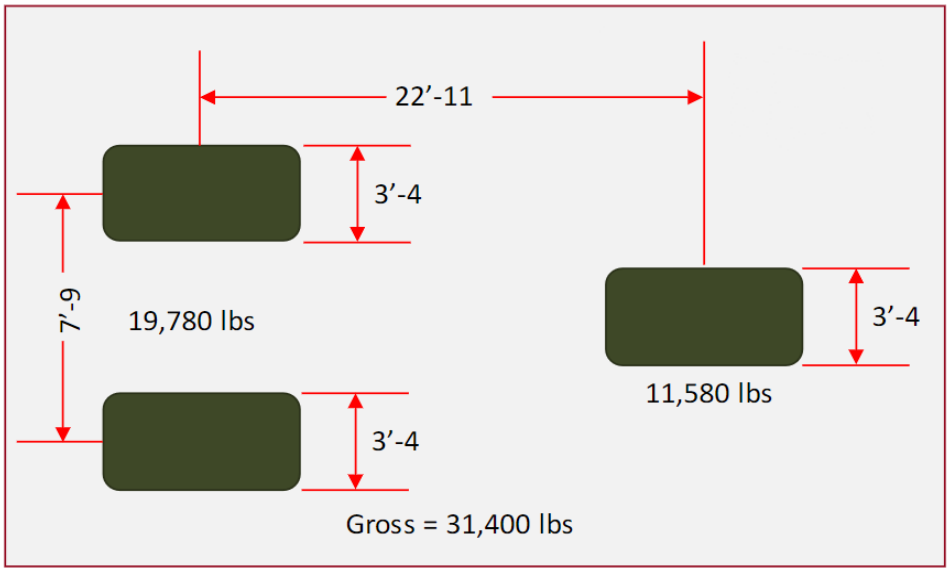

(b) Wheel base, wheel track, and axle weights of T3

Figure 12. Terragator TG-8300B (T3)

4.4 Load Paths and Load Cases

To test the bridges under the terragator loads, three static and two dynamic load cases were utilized. The load cases were applied along three load paths at different transverse locations on the bridges.

For Load Path 1, the passenger’s side wheel was 2 ft from the surface of the right barrier. Similarly for Load Path 3, the driver’s side wheel was 2 ft from the surface of the left barrier. For Load Path 2 the centerline of the terragator was aligned to the centerline of the bridge.

For the three static load cases, the terragators crossed each bridge at approximately a walking pace, thus giving a pseudo-static load effect. The static load cases for Load Paths 1, 2, and 3 were named Load Cases 1, 2, and 3, respectively. These load cases are referred to as LC1, LC2,

and LC3 in this report. To capture the strain and displacement data on each bridge, a sample rate of 20 Hz was used for the static load tests.

For the two dynamic load cases, the terragators were run at a speed of 10 mph and 35 mph over Load Path 2. A sample rate of 100 Hz was used for the dynamic load tests.

Figure 13 shows the transverse locations for Load Path 1 (static load case LC1), Load Path 2 (static load case LC2, dynamic load cases at 10 mph and 35 mph), and Load Path 3 (static load case LC3).

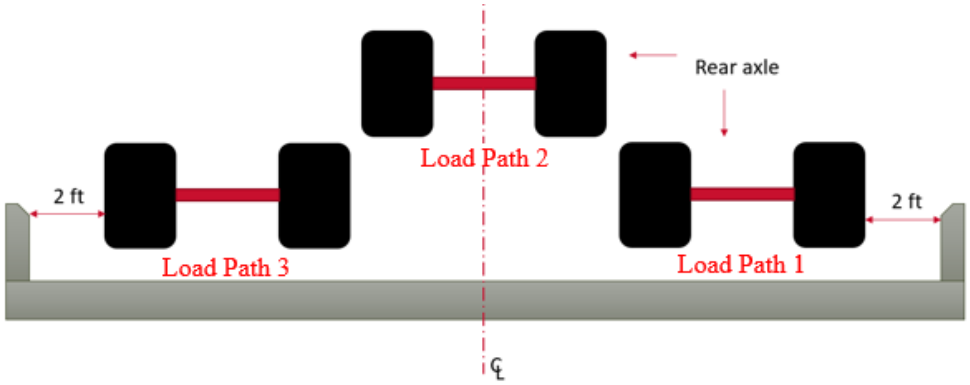

Figure 13. Load path transverse locations

4.5 Field-Collected Data

The data captured by the data acquisition system were used to analyze the behavior of the bridges under the terragator loads. The data had to be zeroed to accommodate drifting and thereby ensure that the captured load effects were induced purely from the load applied. For the static load cases, the data captured were analyzed with respect to the longitudinal location of the terragator's front axle. For the dynamic load cases, the data were analyzed with respect to time.

The static data were used to study the general bridge response and to evaluate the live load distribution factor (for girder bridges) or the equivalent strip width (for slab bridges). The dynamic data were principally used to evaluate the DIF.

4.5.1 PC Bridges

The plots presented in Figure 14 through Figure 18 show the strain data time history for the five PC bridges. For each load case in these figures, the data captured by the mid-span strain gauges on the bottom flanges of the three girders directly under the load path are presented. In each plot, the three curves show the bridge response with respect to the loads from terragators T1, T2, and T3, respectively.

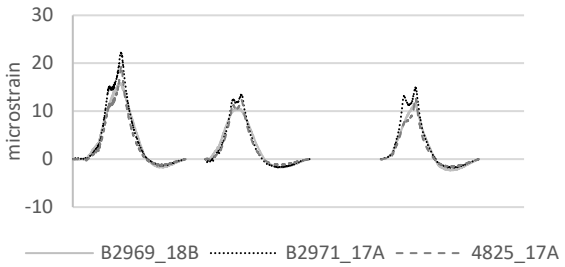

(a) LC1

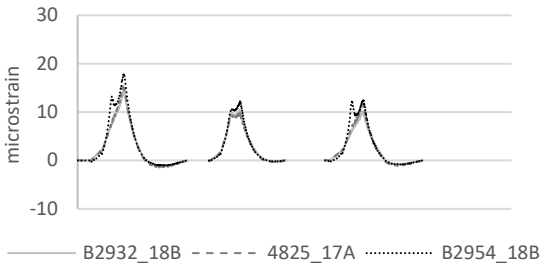

(b) LC2

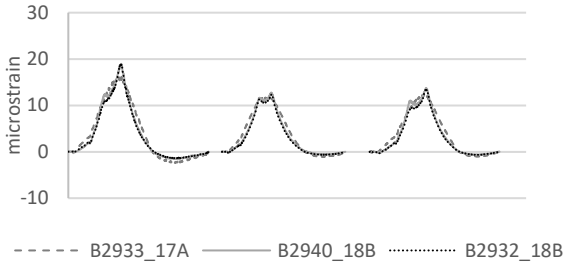

(c) LC3

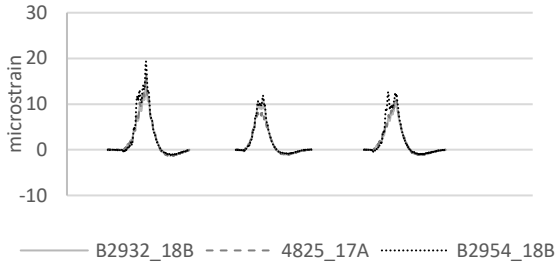

(d) Dynamic 10 mph

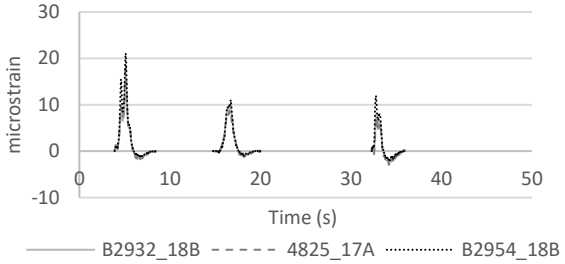

(e) Dynamic 35 mph

Figure 14. Bridge 9267.1S001 strain data

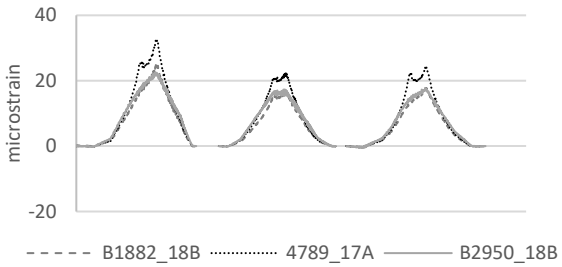

(a) LC1

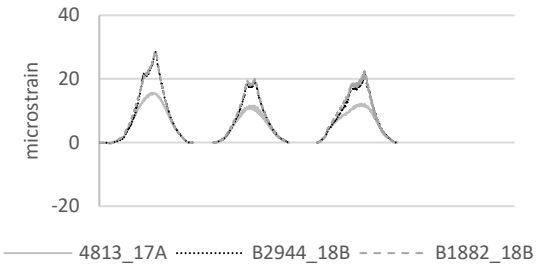

(b) LC2

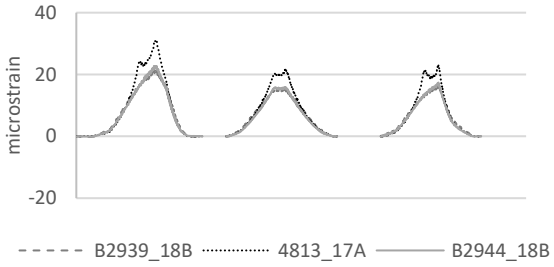

(c) LC3

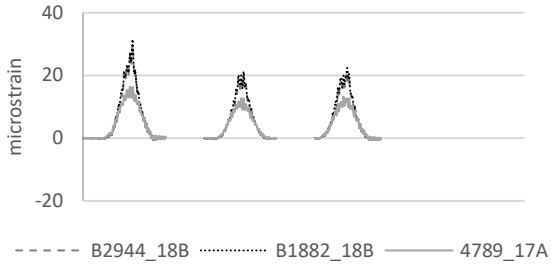

(d) Dynamic 10 mph

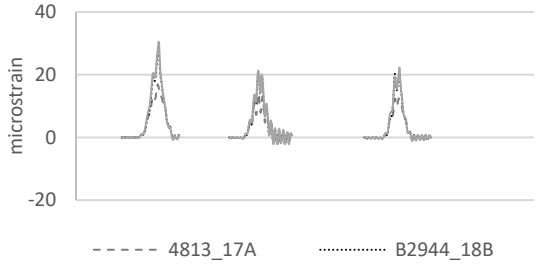

(e) Dynamic 35 mph

Figure 15. Bridge 9265.1S001 strain data

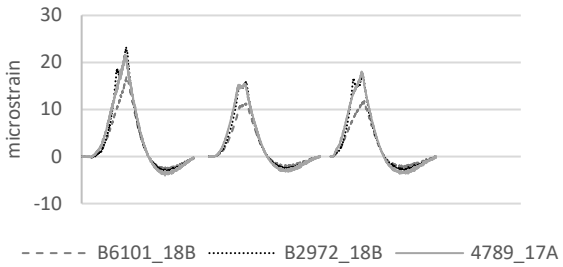

(a) LC1

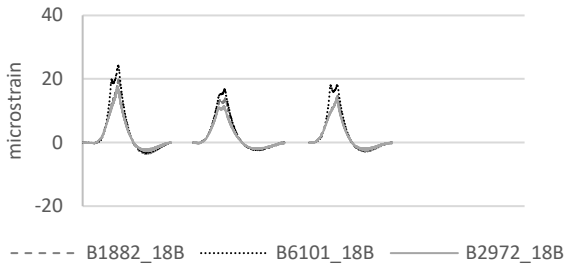

(b) LC2

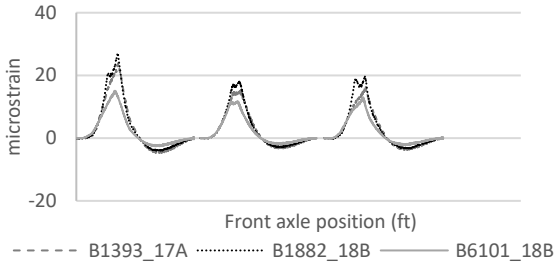

(c) LC3

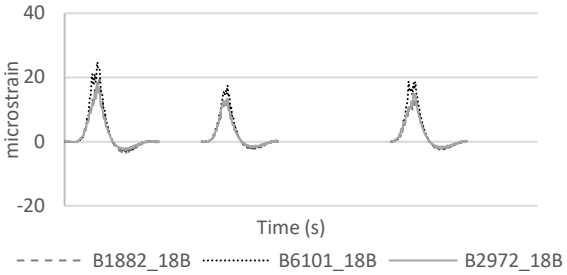

(d) Dynamic 10 mph

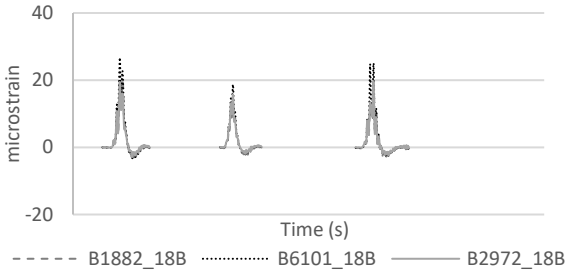

(e) Dynamic 35 mph

Figure 16. Bridge 337901 strain data

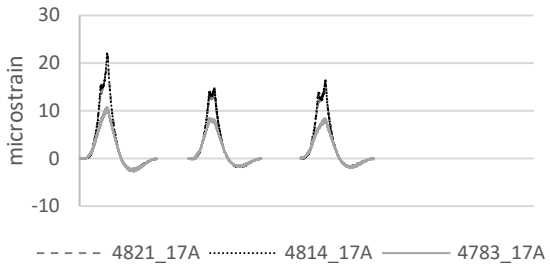

(a) LC1

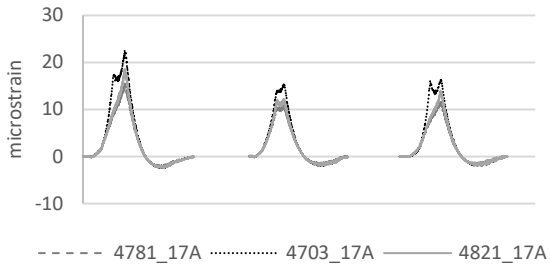

(b) LC2

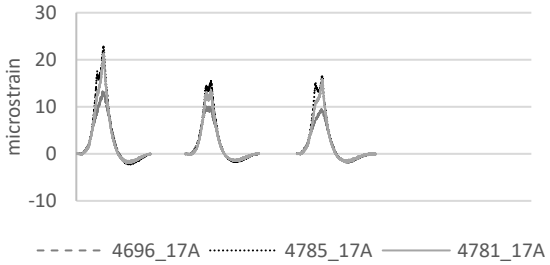

(c) LC3

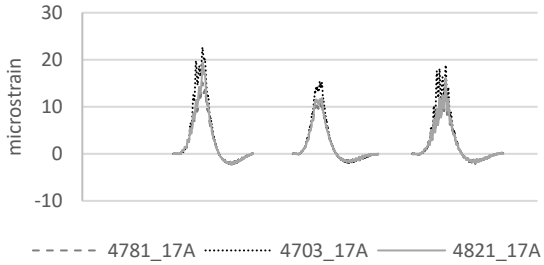

(d) Dynamic 10 mph

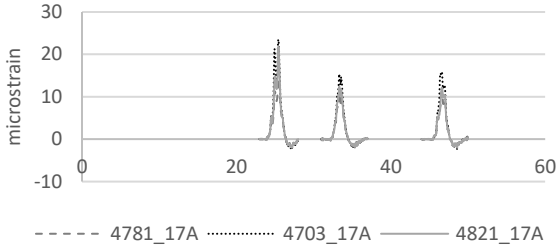

(e) Dynamic 35 mph

Figure 17. Bridge 9232.8S022 strain data

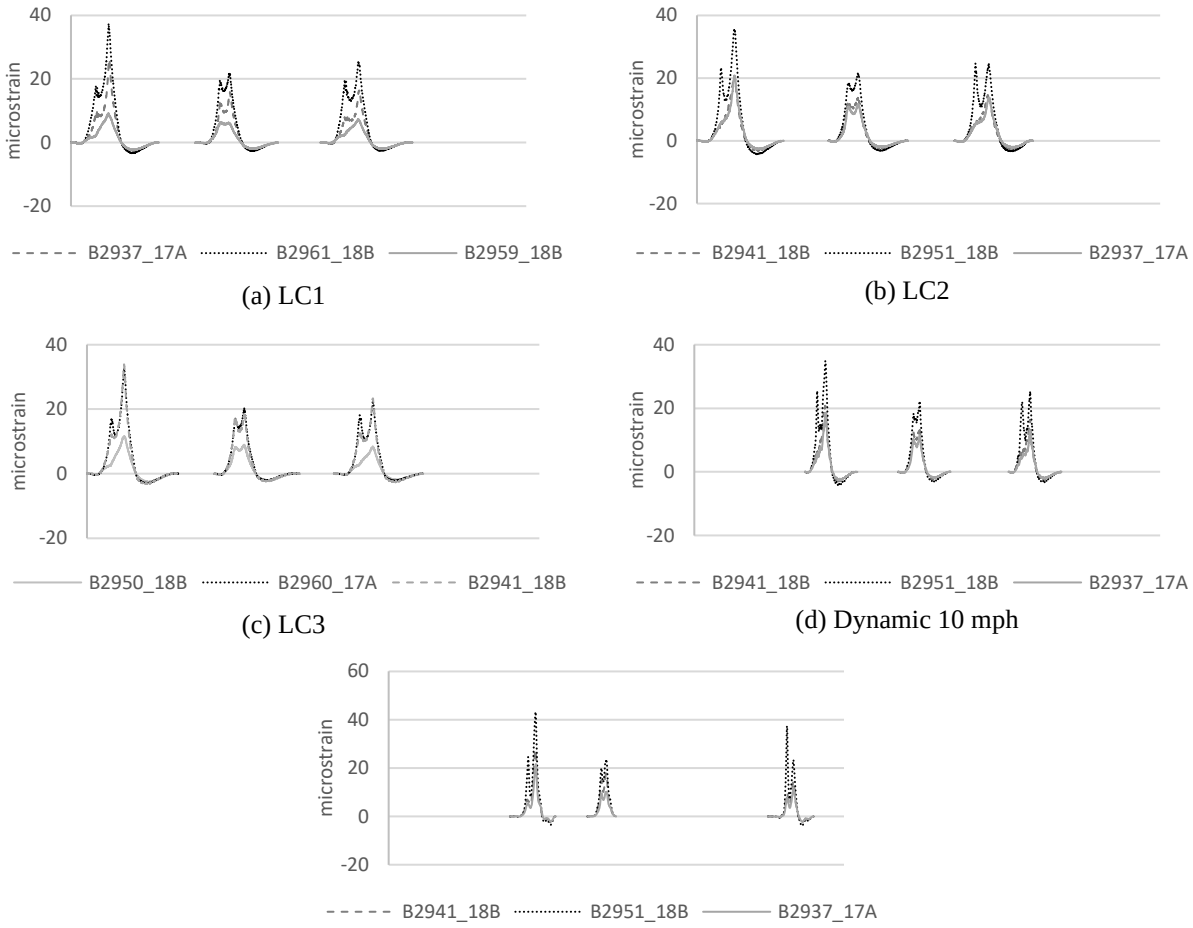

(a) LC1

(b) LC2

(c) LC3

(d) Dynamic 10 mph

(e) Dynamic 35 mph

Figure 18. Bridge 9231.5S022 strain data

In general, all five PC bridges achieved maximum live load-induced strain magnitudes ranging from 20 to 40 microstrain. The greatest strain magnitudes occurred when the back axle of the terragator passed near mid-span. The two peaks evident in the strain plots for each terragator signify the presence of two axles. The higher peak indicates the rear axle, while the lower peak indicates the front axle. In the plots for T2, the two peaks with nearly equal magnitudes for all three gauges indicate nearly equal axle weights.

The plots presented in Figure 19 through Figure 23 show the midspan displacement data for the three girders under the load path for the five PC bridges. In comparison to the strain plots, the displacement plots indicate similar bridge behavior, with the greatest displacements occurring as vehicle T1 crosses the bridge and similar displacement magnitudes evident for vehicles T2 and T3.

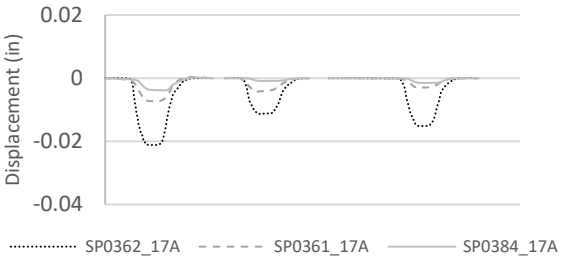

(a) LC1

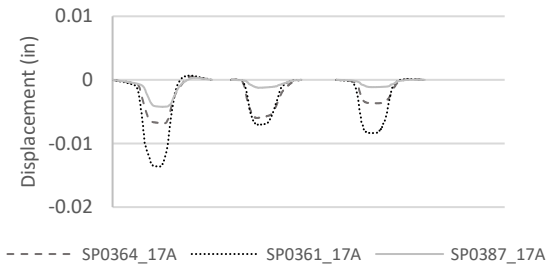

(b) LC2

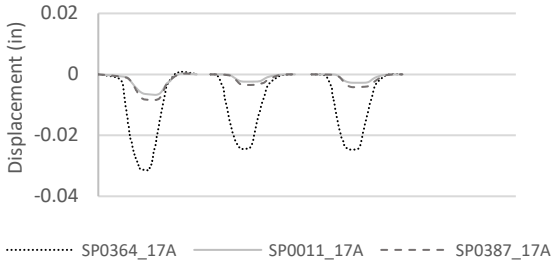

(c) LC3

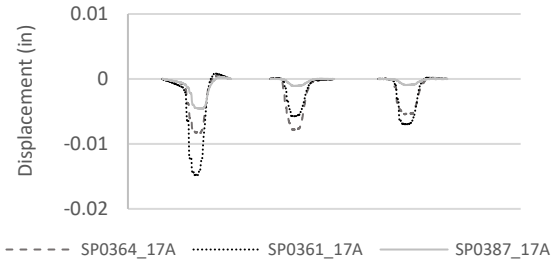

(d) Dynamic 10 mph

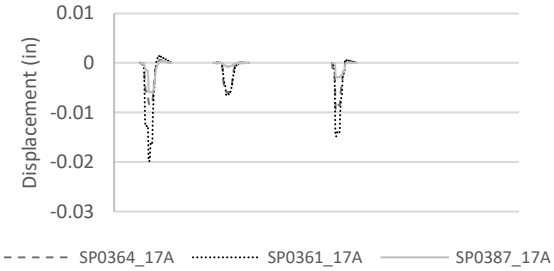

(e) Dynamic 35 mph

Figure 19. Bridge 9267.1S001 displacement data

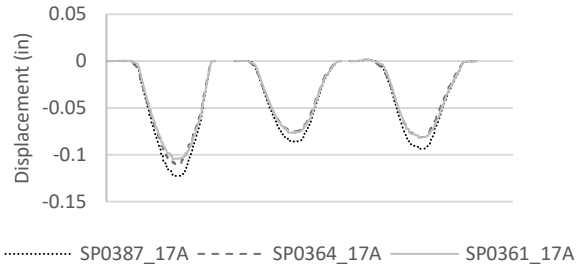

(a) LC1

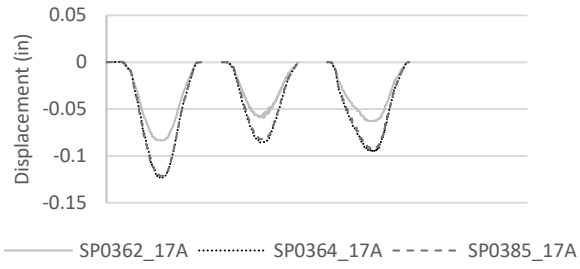

(b) LC2

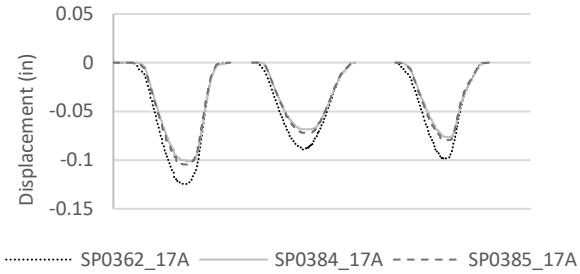

(c) LC3

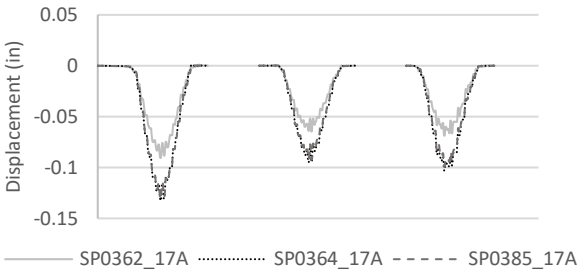

(d) Dynamic 10 mph

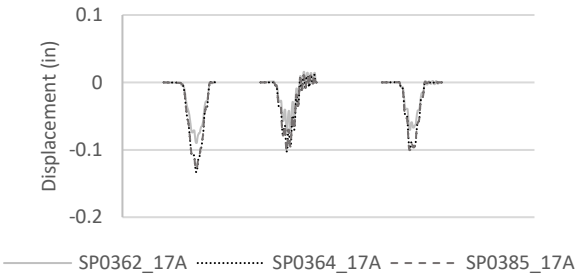

(e) Dynamic 35 mph

Figure 20. Bridge 9265.1S001 displacement data

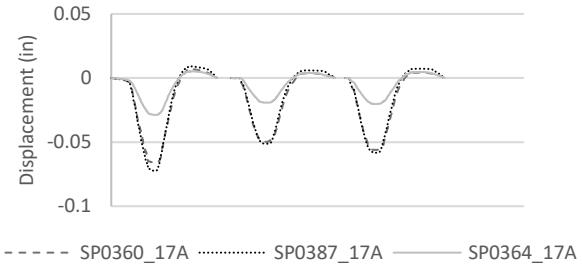

(a) LC1

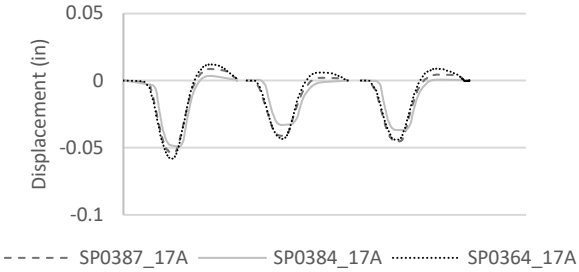

(b) LC2

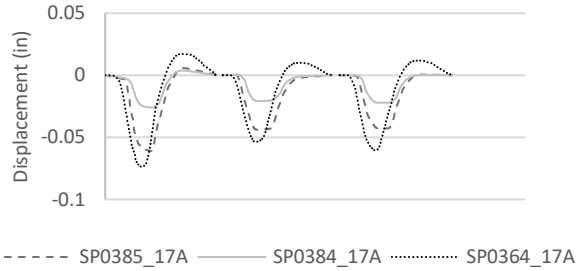

(c) LC3

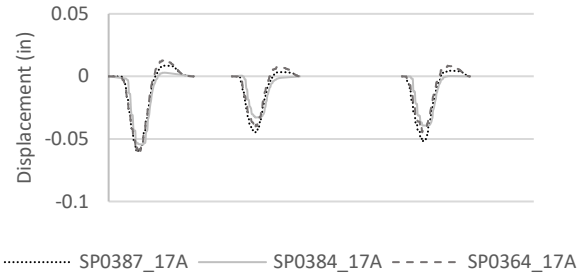

(d) Dynamic 10 mph

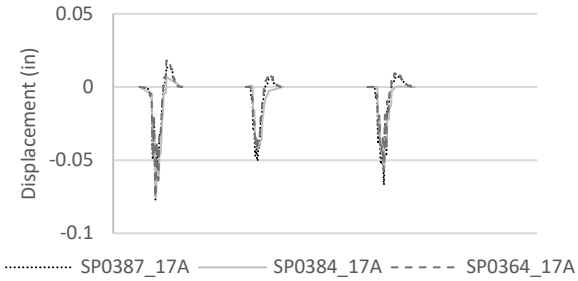

(e) Dynamic 35 mph

Figure 21. Bridge 337901 displacement data

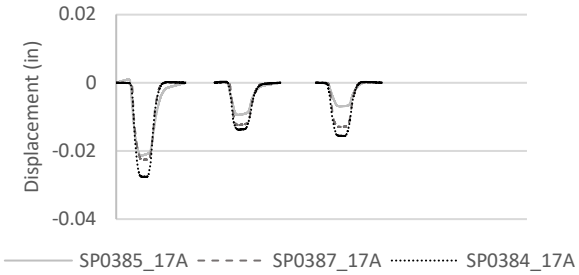

(a) LC1

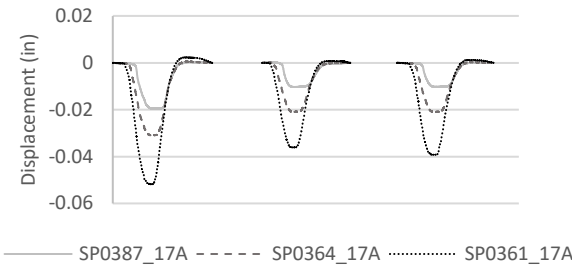

(b) LC2

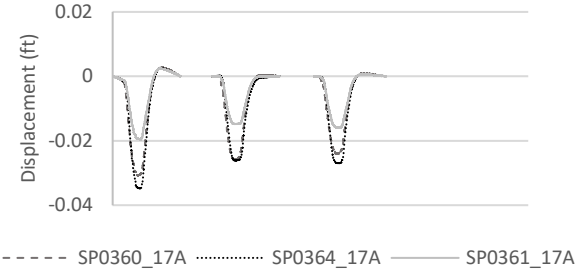

(c) LC3

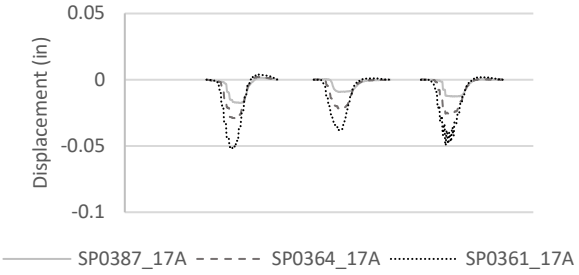

(d) Dynamic 10 mph

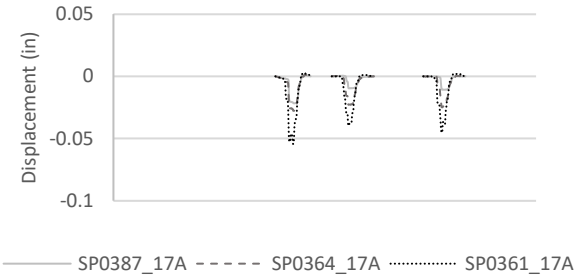

(e) Dynamic 35 mph

Figure 22. Bridge 9232.8S022 displacement data

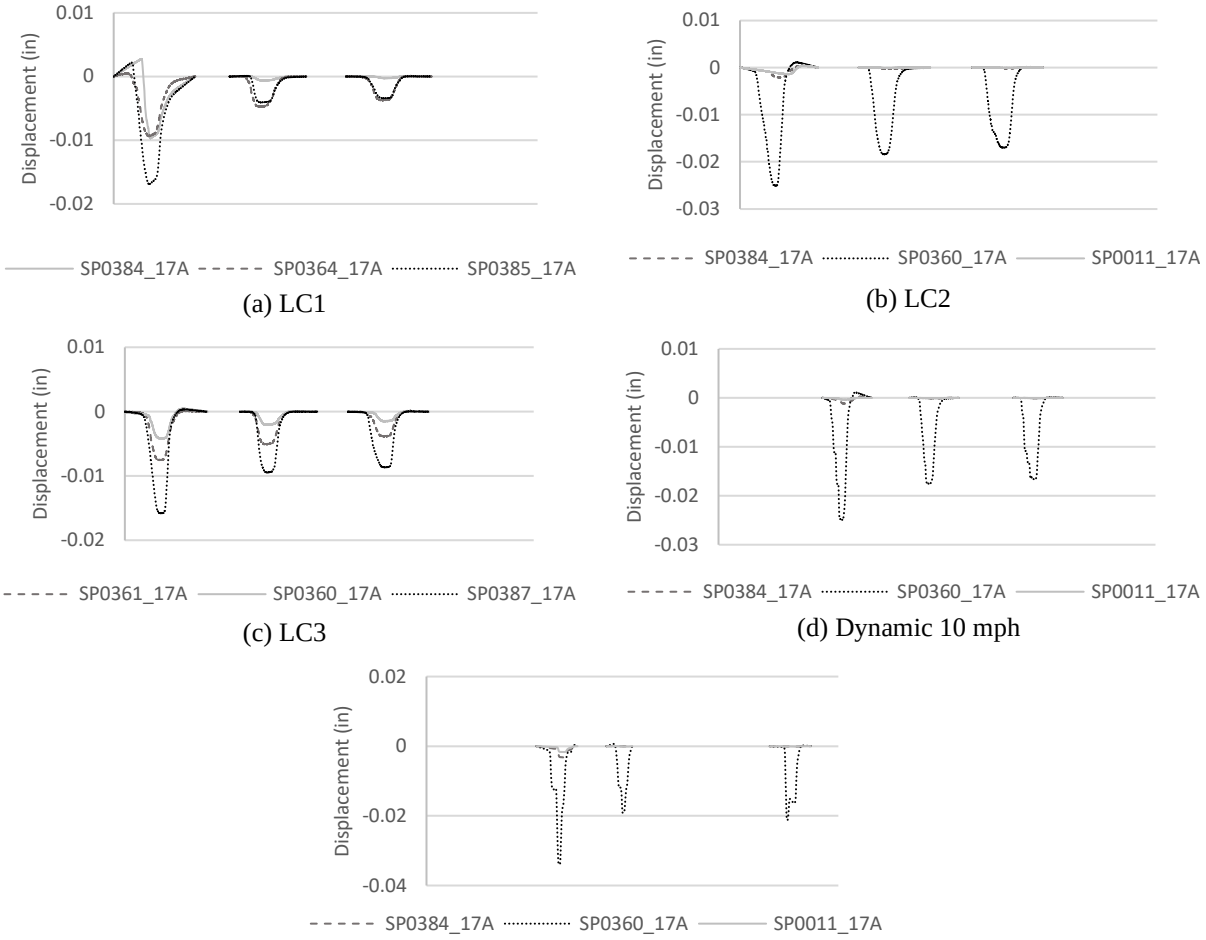

Figure 23. Bridge 9231.5S022 displacement data

4.5.2 Slab Bridges

The strain and displacement data for the slab bridges are presented in a way similar to that used for the PC bridges in Section 4.5.1. The plots presented in Figure 24 to Figure 26 show the strain data for the three slab bridges. For each of the five load cases in these figures, the strain data captured by the three strain gauges directly under the load path are presented. In each plot, the three curves indicate the bridge response with respect to the loads from terragators T1, T2, and T3.

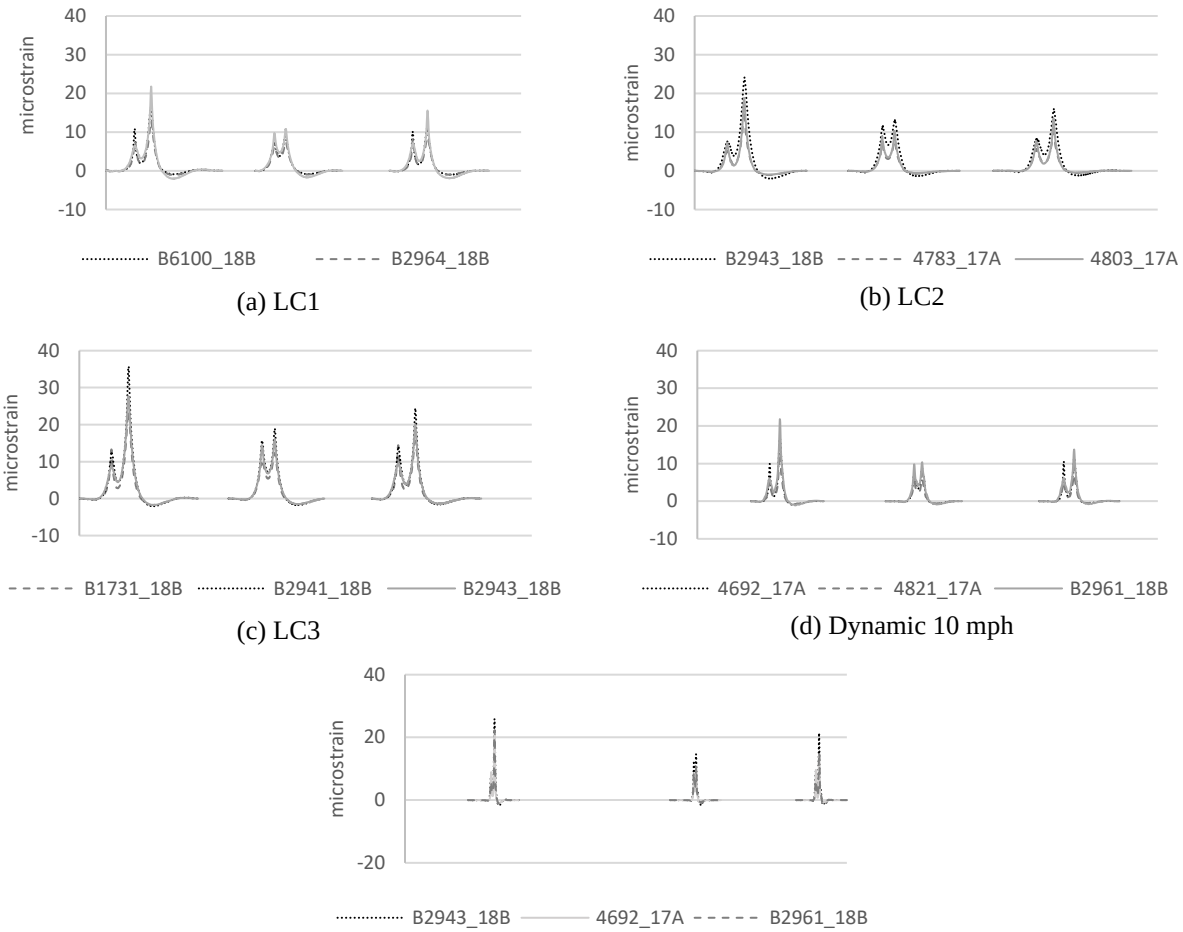

(a) LC1

(b) LC2

(c) LC3

(d) Dynamic 10 mph

(e) Dynamic 35 mph

Figure 24. Bridge 9233.9S002 strain data

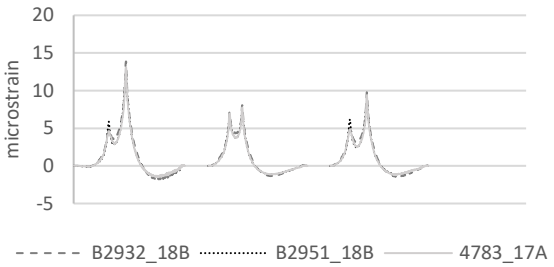

(a) LC1

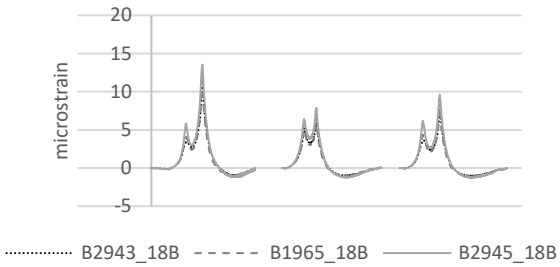

(b) LC2

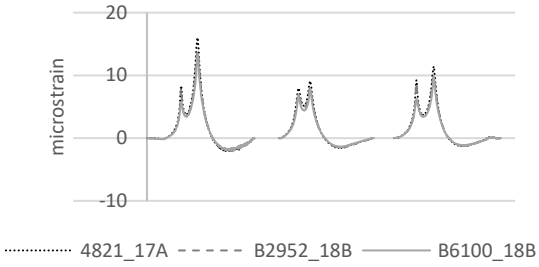

(c) LC3

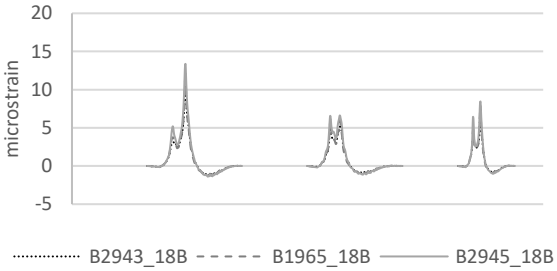

(d) Dynamic 10 mph

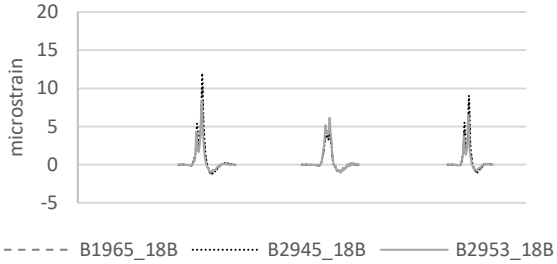

(e) Dynamic 35 mph

Figure 25. Bridge 4811.2S151 strain data

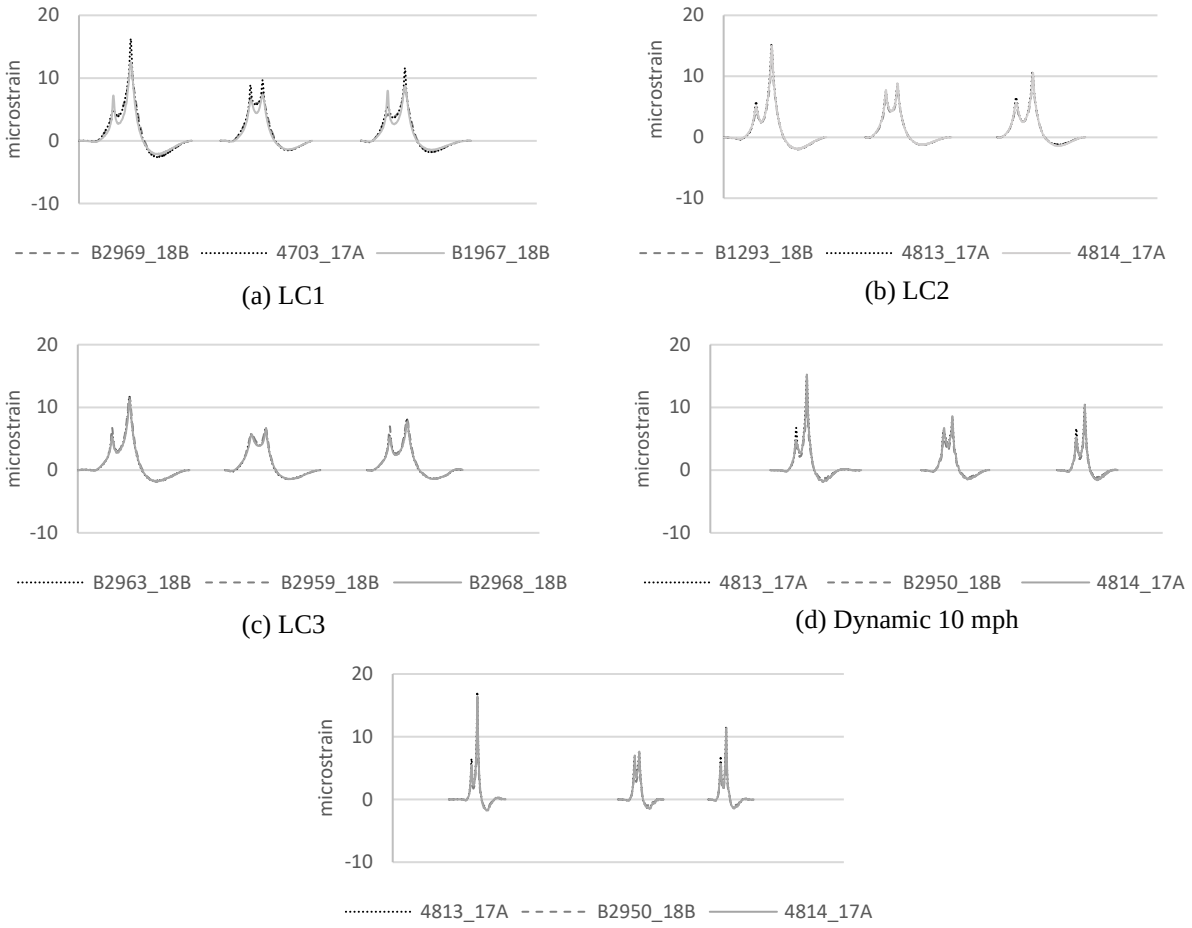

(a) LC1

(b) LC2

(c) LC3

(d) Dynamic 10 mph

(e) Dynamic 35 mph

Figure 26. Bridge 4802.1S220 strain data

Each plot shows two peaks for all three gauges. The first peak indicates the strain due to the front axle, while the second peak indicates the strain due to the rear axle. The peak due to the rear axle is generally higher than the peak due to the front axle in the case of T1 and T3. In the case of T2, both peaks are of almost equal magnitudes, indicating a similar weight on both axles.

The three terragators show different maximum strain peaks. The first (left) plot shows the highest peak level, followed by the third (right) plot and the second (middle) plot. This is because the rear axle weight of T1 is the highest, followed by that of T3 and T2.

The plots presented in Figure 27 through Figure 29 show the displacement data for the three slab bridges. In comparison to the strain plots, the displacement plots indicate similar bridge behavior, with the greatest displacements occurring as vehicle T1 crosses the bridge and similar displacement magnitudes evident for vehicles T2 and T3.

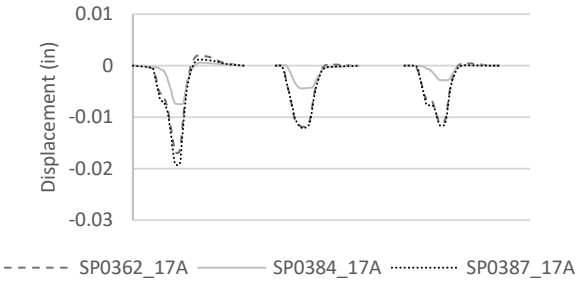

(a) LC1

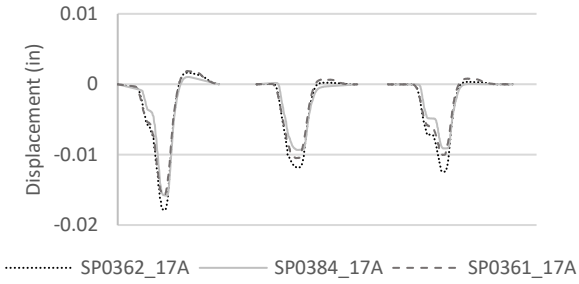

(b) LC2

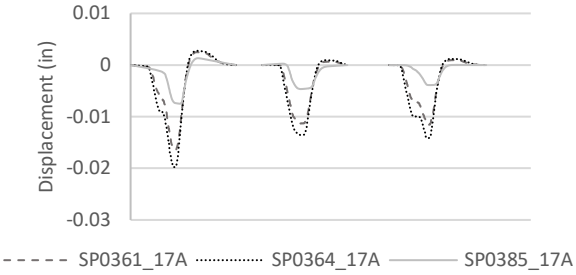

(c) LC3

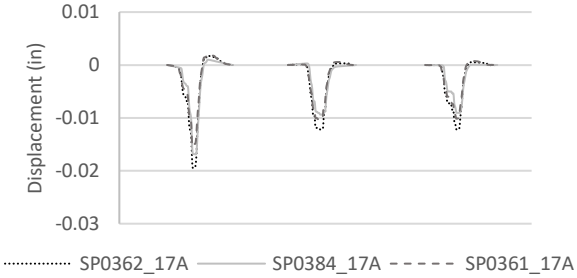

(d) Dynamic 10 mph

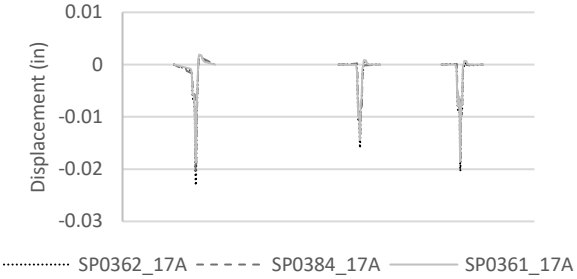

(e) Dynamic 35 mph

Figure 27. Bridge 9233.9S002 displacement data

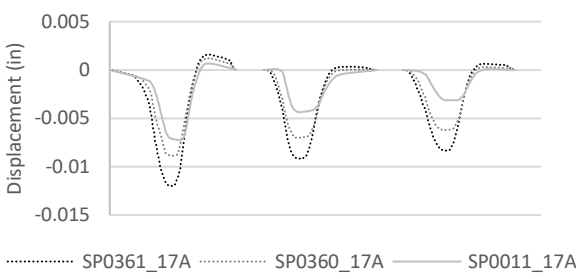

(a) LC1

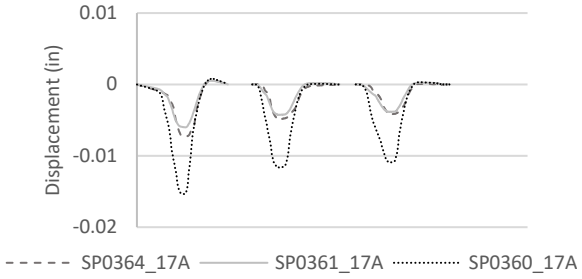

(b) LC2

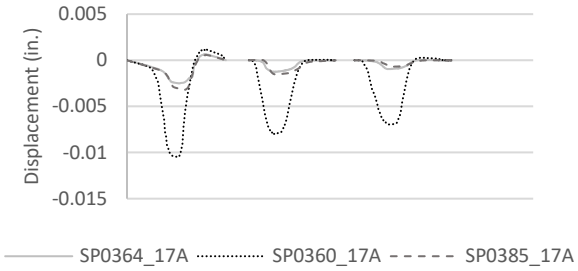

(c) LC3

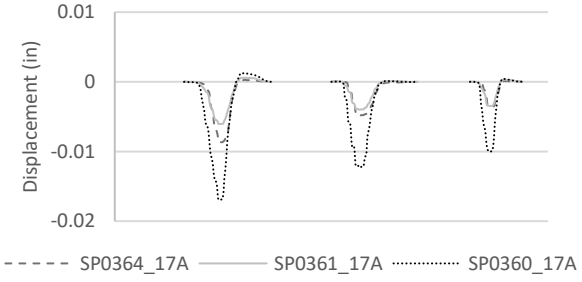

(d) Dynamic 10 mph

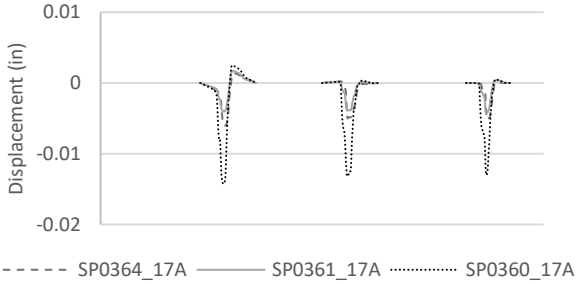

(e) Dynamic 35 mph

Figure 28. Bridge 4811.2S151 displacement data

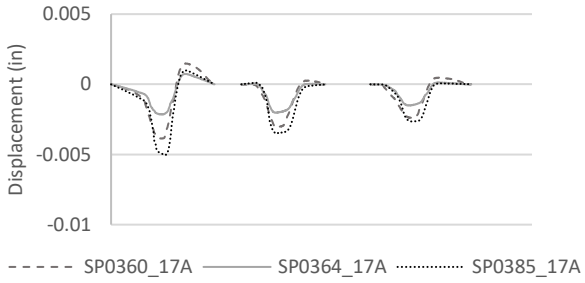

(a) LC1

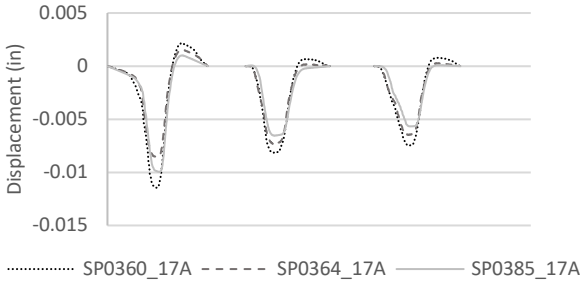

(b) LC2

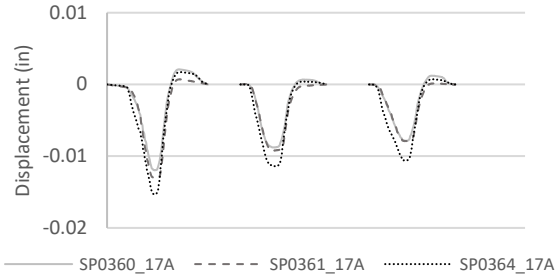

(c) LC3

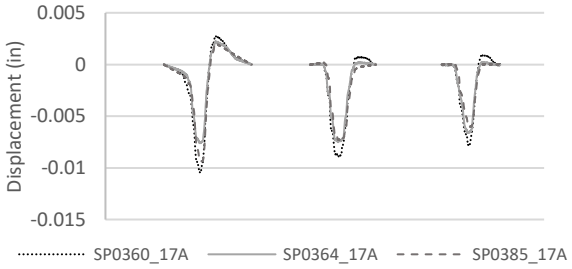

(d) Dynamic 10 mph

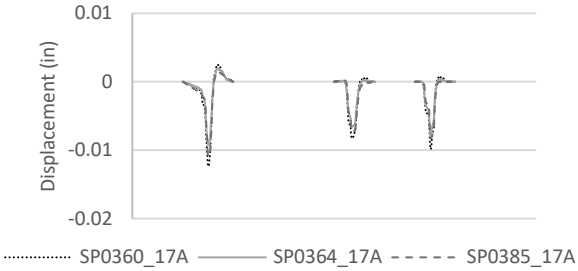

(e) Dynamic 35 mph

Figure 29. Bridge 4811.2S151 displacement data

5 DYNAMIC IMPACT FACTOR

In some cases, vehicles traveling faster than walking speed can induce stresses, strains, or deflections that are higher than those induced at a slower speed. This is generally due to the dynamic interaction between the vehicle and the bridge. In this chapter, the field-collected static and dynamic data are analyzed to evaluate the dynamic load effects of the terragators on the field-tested bridges. The DIF was calculated for each bridge and compared with AASHTO-specified values.

5.1 Determination of DIF Based on Field-Collected Data

In this research, DIF is used to refer to the live load on the bridge plus the induced dynamic response of that load. The DIF is calculated using Equation 22.

$$DIF = 1 + \frac{\varepsilon_{dynamic} - \varepsilon_{static}}{\varepsilon_{static}} \quad (22)$$

where $\varepsilon_{dynamic}$ is the maximum dynamic strain and ε_{static} is the maximum static strain.

To calculate the DIFs for the field-tested bridges, the maximum static strain values were extracted from the LC2 data. The maximum dynamic strain values were obtained from the Dynamic 10 mph and Dynamic 35 mph data.

For the PC bridges, these strain values were obtained from the bottom flange gauges on each girder at mid-span. For the slab bridges, the maximum strain values were extracted from each gauge at mid-span.

The maximum static strain and maximum dynamic strain obtained from each gauge were used to calculate the DIFs for the respective gauges using Equation 22. Figure 30 shows an example of strain data from one gauge on Bridge 9265.1S001. The peak values of both curves were used to calculate the dynamic impact factor.

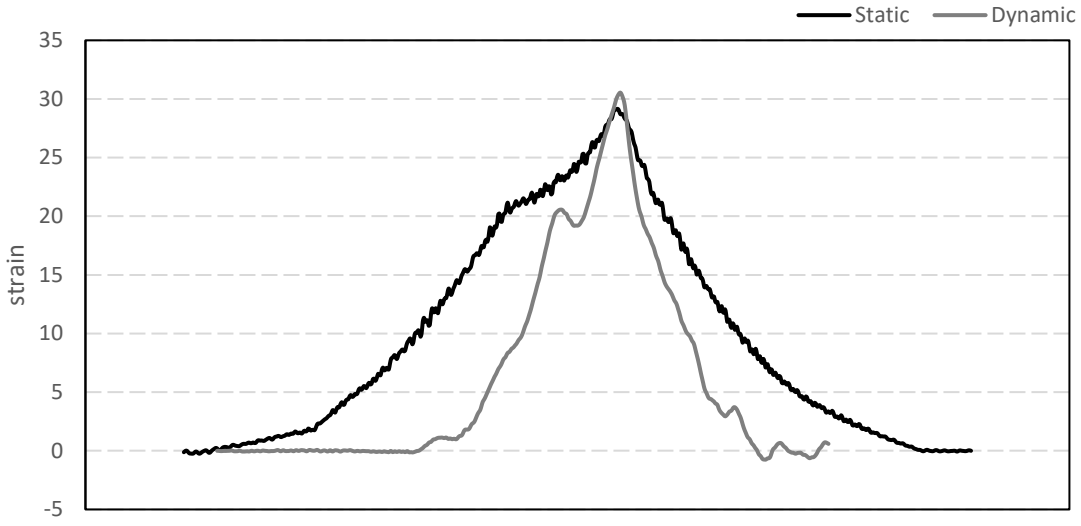

Figure 30. Static and 35 mph dynamic strain data on gauge 1882 of Bridge 9265.1S001

For the slab bridges, only the DIFs for the gauges within the equivalent strip width of each respective bridge were used to calculate the average DIF.

5.2 DIF Results

The DIF values calculated from the field test data are tabulated separately for PC bridges and slab bridges in Table 3 and Table 4, respectively.

Table 3. DIFs of PC bridges

Bridge	DIF at 10 mph					DIF at 35 mph				
	9267.1S001	9265.1S001	337901	9232.8S022	9231.5S022	9267.1S001	9265.1S001	337901	9232.8S022	9231.5S022
T1	1.07	1.08	1.00	1.00	0.97	1.17	1.03	1.07	1.04	1.21
T2	0.97	1.06	1.03	0.99	1.03	0.90	1.04	1.11	1.00	1.10
T3	0.99	1.00	1.02	1.15	1.03	0.94	1.00	1.36	0.97	1.52

Table 4. DIFs of slab bridges

Bridge	DIF at 10 mph			DIF at 35 mph		
	9233.9S002	4811.2S151	4802.1S220	9233.9S002	4811.2S151	4802.1S220
T1	0.99	0.99	1.03	1.13	0.92	1.09
T2	0.96	0.99	0.97	1.13	0.89	0.93
T3	0.94	0.93	0.95	1.25	1.01	1.10

The DIFs for the PC bridges in many cases were near 1.0, indicating that the maximum strain value for the dynamic cases did not vary significantly from that of the static cases. On average, the DIFs calculated for the load cases in which the terragators were traveling at 35 mph were greater than those for the load cases in which the terragators were traveling at 10 mph. Further, when comparing T1 and T3, which had the same configuration but were loaded differently, the unloaded vehicle (T3) had a higher calculated DIF. While the sample size is, relatively, too small to make broad conclusions regarding DIFs for all terragator-type vehicles, it is important to note that, in this study, lightly loaded vehicles moving at a higher rate of speed appear to produce greater dynamic impacts than more heavily loaded vehicles moving at a slower rate of speed. The data-based evidence matches the anecdotal observation of these vehicles traveling at varying rates of speed, which indicates that the rigid suspension required for carrying heavy loads results in a bumpy response when the vehicle is lightly loaded.

The DIFs for the slab bridges similarly were near 1.0, especially when the vehicle was traveling at 10 mph, indicating that the maximum strain value for the dynamic cases did not vary significantly from that for the static load cases. The average DIF for the vehicles traveling at 35 mph was higher than that for the vehicles traveling at 10 mph but only slightly higher than 1.0.

There were two instances when the DIF exceeded the prescribed factor of 1.33 in AASHTO (2020). In both cases, the bridge was a PC girder bridge and the vehicle was the T3 terragator.

5.3 Comparison with the AASHTO Design Value

According to AASHTO (2020), the main source of dynamic effects due to moving vehicles is riding surface discontinuities. The other major source is long, undulating, resonant excitation as a result of similar frequencies of vibration between the bridge and crossing vehicles.

The end result of dynamic effects being introduced into the vehicle-bridge system is that the resulting stresses on the bridge may be higher than those induced by the static effects alone and therefore need to be accommodated in the design and analysis of bridge components. AASHTO recommends that dynamic effects be accommodated in bridge analyses by increasing the static effects by 33% or a factor of 0.33. This factor is applied to the static live load as multiplier with a value of (1+DIF/100). The current codified value was determined using dynamic load data from

common truck types. It is noteworthy that this value was not developed specifically for terragator vehicles.

The DIFs calculated in this research using field test data were compared with the AASHTO value. The DIFs calculated using Equation 22 were plotted for each field-tested bridge and appear as a range of DIFs for each bridge in the plots. The plots for PC and slab bridges are shown in Figure 31.

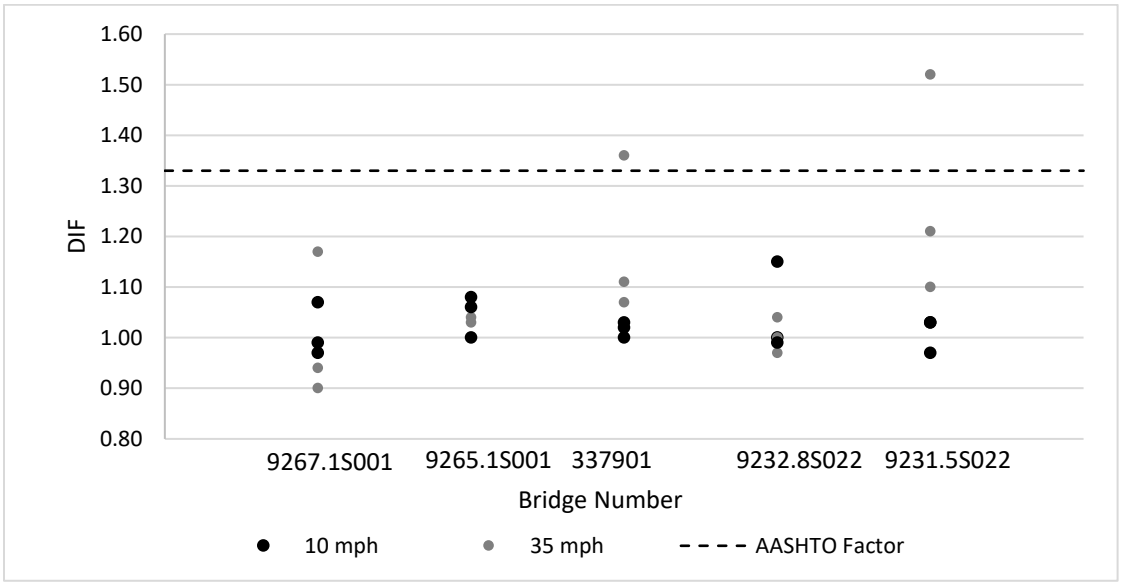

(a) PC bridges

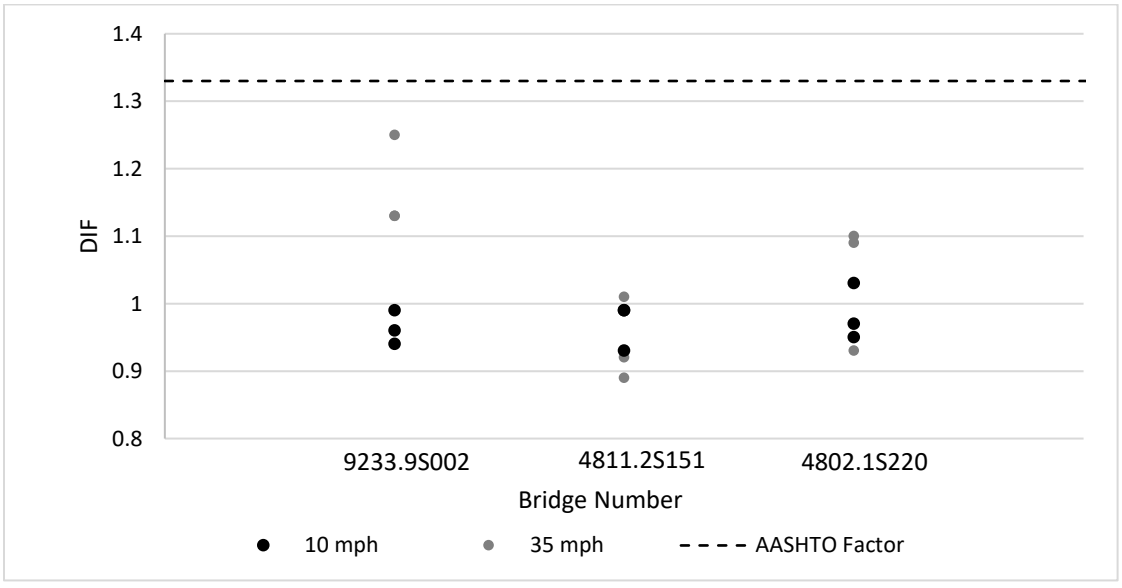

(b) Slab bridges

Figure 31. Field dynamic impact factor compared with AASHTO-specified values

In these plots, the AASHTO-specified DIF, 1.33, is presented as a dashed line. In this way, the experimental data can be easily compared with the DIF specified by AASHTO. The DIF data for

each bridge are differentiated by whether the DIF was calculated for terragators traveling at 35 mph or 10 mph. Experimental DIF values below the dashed line indicate that the AASHTO-recommended DIF value is conservative, and experimental values above the dashed line indicate that the AASHTO-recommended value is non-conservative.

The experimental DIF results for PC bridges indicate that the tested bridge/terragator combinations had values that are conservative with respect to the AASHTO value in all but two cases. The highest DIF for PC bridges was 1.52. Overall, the DIFs resulting from terragators traveling at 35 mph were higher than those resulting from terragators traveling at 10 mph. For slab bridges, all DIF values were below the AASHTO value.

6 CHARACTERIZATION OF HUSBANDARY VEHICLE LOAD DISTRIBUTION

This chapter presents an evaluation of the lateral live load distribution of PC and slab bridges using field-collected performance data. The LLDFs were calculated for the PC bridges, and the equivalent strip widths were calculated for the slab bridges. In addition, to cover a wider variety of bridge types, five steel girder bridges on which Phares et al. (2017) conducted similar live load tests using a few husbandry vehicles were also considered. The data from Phares et al. (2017) were used to calculate the LLDFs for these five steel girder bridges. Once the load distribution results were determined, they were compared with AASHTO-specified load distribution values.

Following the examination of the field-measured lateral live load distributions, the load distribution characteristics of bridges with a range of bridge parameters were evaluated using analytical models. First, FE models were created for all PC, slab, and steel girder bridges that had been field tested in this work and in Phares et al. (2017). The LLDF and equivalent strip width results were used to calibrate and validate the FE models. Following that, a series of FE models with a wide range of parameters were created based upon the calibrated models and used in a parametric study.

6.1 Lateral Live Load Distribution Based on Field-Collected Data

6.1.1 PC Bridges

When a vehicle crosses a PC girder bridge, each girder carries a percentage of the vehicle loading, which results in corresponding stresses, strains, moments, etc., in each girder. If all girders have equal stiffness, the girders directly under the load typically experience higher strains than the girders away from the load. Figure 32 shows typical longitudinal strains over the cross section of a bridge for three different load cases (LC1, LC2, and LC3). The load position in LC1 is centered over girder 5, in LC2 over girders 3 and 4, and LC3 over girder 2.The strain data distributions seem fairly typical, in that the strain magnitudes are highest in the girders nearest to the live load.

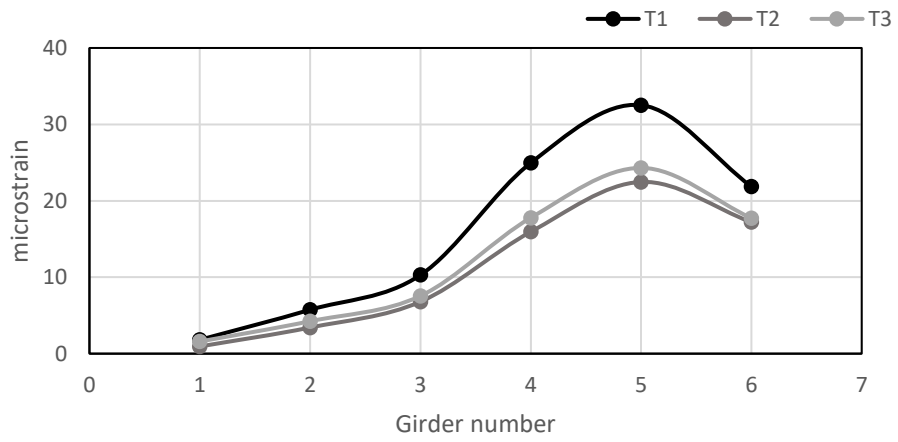

(a) LC1

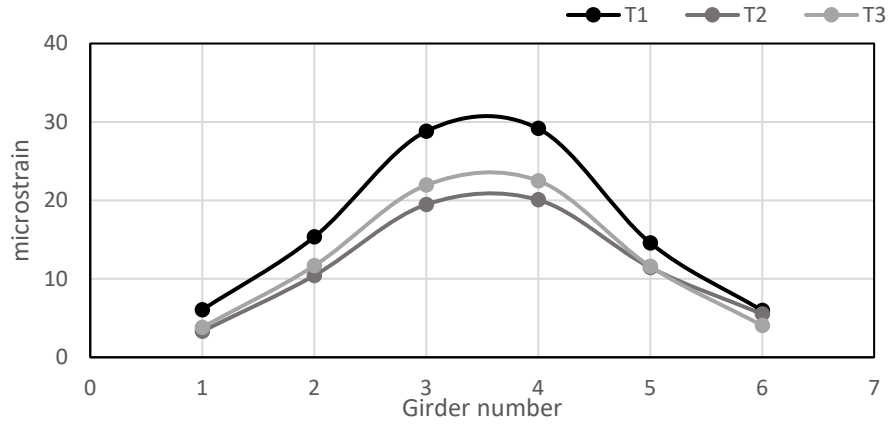

(b) LC2

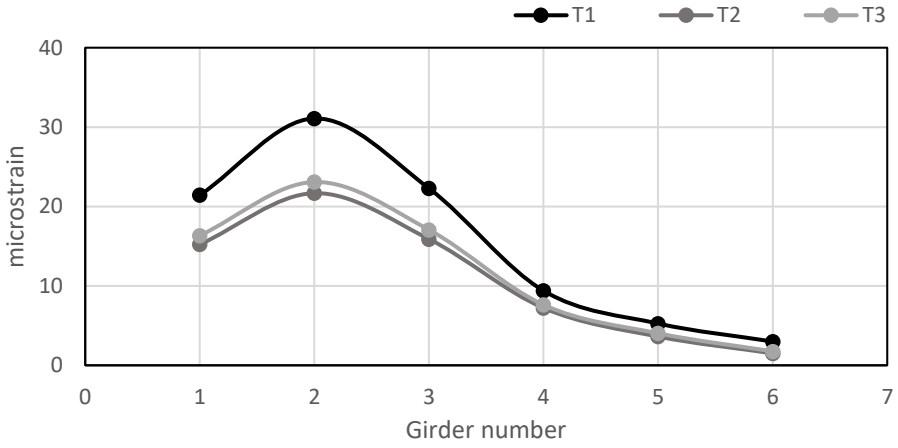

(c) LC3

Figure 32. Strain distribution across a bridge in the transverse direction (Bridge 9265.1S001)

6.1.1.1 Determination of LLDF Based on Field-Collected Data

The portion of live load carried by a girder is frequently represented by the LLDF. The LLDF is basically the percentage of the total load that an individual girder resists.

Strain values collected during live load test are commonly used to calculate the LLDF. Assuming the girder properties and geometry are the same for each of the girders, the strain is directly proportional to the moment and girder stiffness, as shown in Equation 23.

$$\varepsilon_i = \frac{M_i y}{EI} \tag{23}$$

where M_i is the moment carried by the *i*th girder, E is the Young's modulus of the material, I is the moment of inertia, and y is the distance from the neutral axis to the strain measurement location.

In the present study, strain data were collected at the bottom surfaces of the bottom flanges of the girders at mid-span. If each girder is assumed to have the same stiffness, these data can be used to calculate the LLDF on a given girder using Equation 24.

$$LLDF_i = {\varepsilon_i}/{\sum_{i=1}^{n} \varepsilon_i} \tag{24}$$

where ε_i is the strain collected from the *i*th girder and $LLDF_i$ is the LLDF for the *i*th girder.

6.1.1.2 Determination of LLDF Based on AASHTO (2020)

The AASHTO LRFD BDS (2020) provides equations to calculate the LLDFs of girder bridges, with different equations for single and multiple lane loads. Since single lane loads were applied during the field tests, the AASHTO equation for a single lane load was used to compare the AASHTO values with the field test results.

Equation 8, along with a skew reduction factor, is prescribed by AASHTO (2020) to calculate the LLDFs of girder bridges.

6.1.1.3 LLDF Results and Comparison with AASHTO Values

The LLDFs calculated using the AASHTO equation can be used as reference values for comparison with the field-collected behavior information. A comparison of the LLDFs calculated using the field test data and the LLDFs calculated from the AASHTO equation indicates how live loads are being distributed relative to a codified value.

Figure 33 shows the LLDFs calculated from the field test data using Equation 24 and those predicted by the AASHTO (2020) equations for the five field-tested PC bridges.

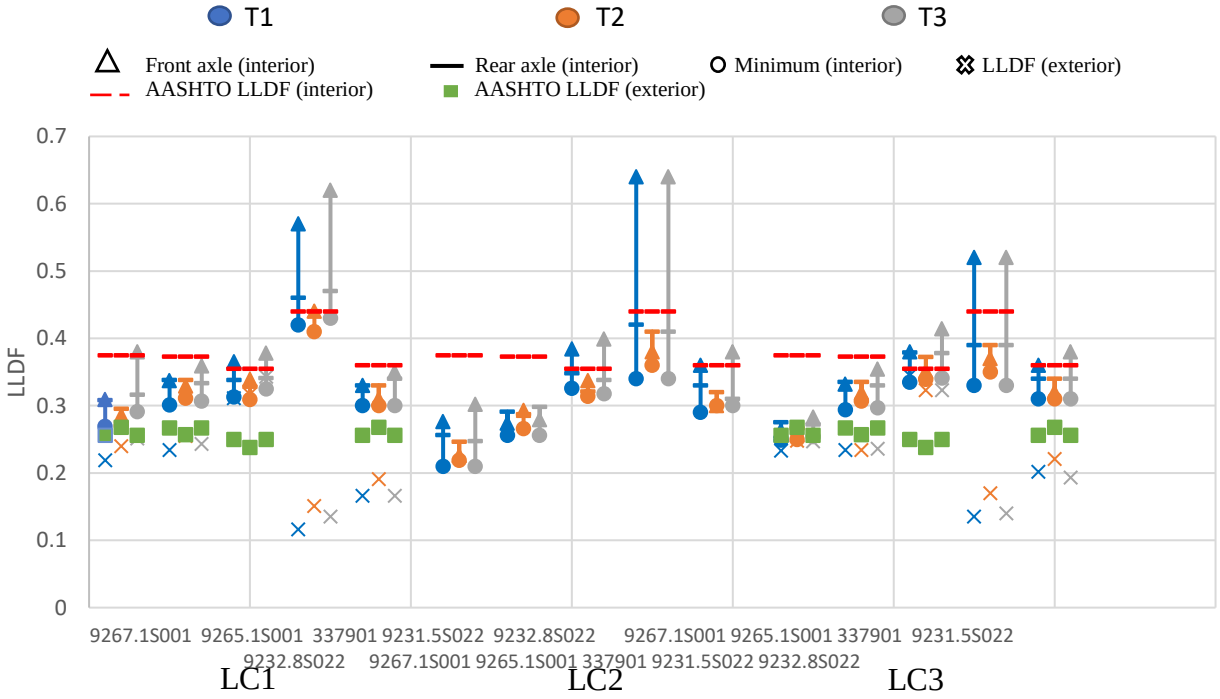

Figure 33. LLDFs of all tested PC bridges

The LLDFs were calculated for the front axle and rear axle separately so that differences in geometry and their impacts on LLDF could be studied. For the interior girders, it was found that the LLDFs for the front axles were much higher than those for the rear axles for terragators T1 and T3 and that those values exceeded the AASHTO-specified values. The LLDFs for the front axles of T1 and T3 were also higher than the LLDF for the front axle of T2 (which had two wheels). The LLDFs for the rear axles were very similar for all terragators.

For the exterior girders, the maximum LLDFs from the field tests were lower than the AASHTO values.

Although the results indicated that the field-captured LLDFs for interior girders subject to single-wheel axles were higher than the LLDFs specified in AASHTO (2020), it was found that these axles were all front axles, which usually carry less vehicle load and result in relatively low strain magnitudes.

6.1.2 Slab Bridges

When a load is applied to a slab bridge, the portion of the slab directly under the axle typically experiences higher strain and displacement than the rest of the bridge. This can be seen in the

strain distribution charts in Figure 34. The strain data in Figure 34 are the longitudinal strains measured by the strain gauges installed at mid-span on the instrumented span.

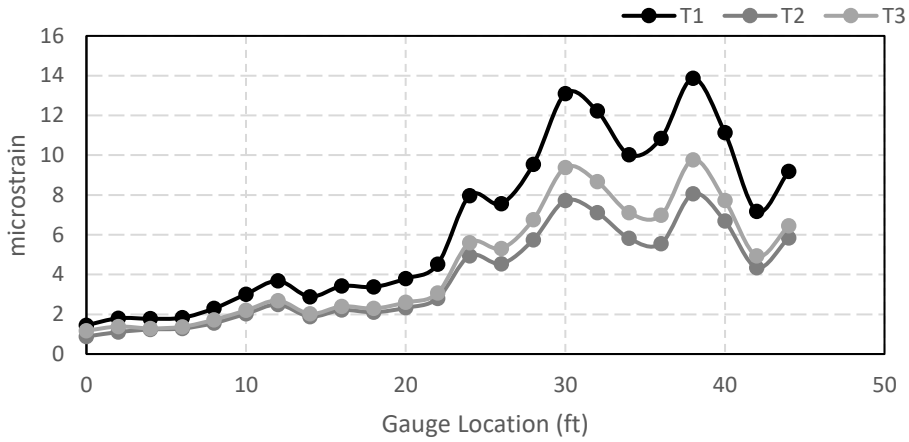

(a) LC1

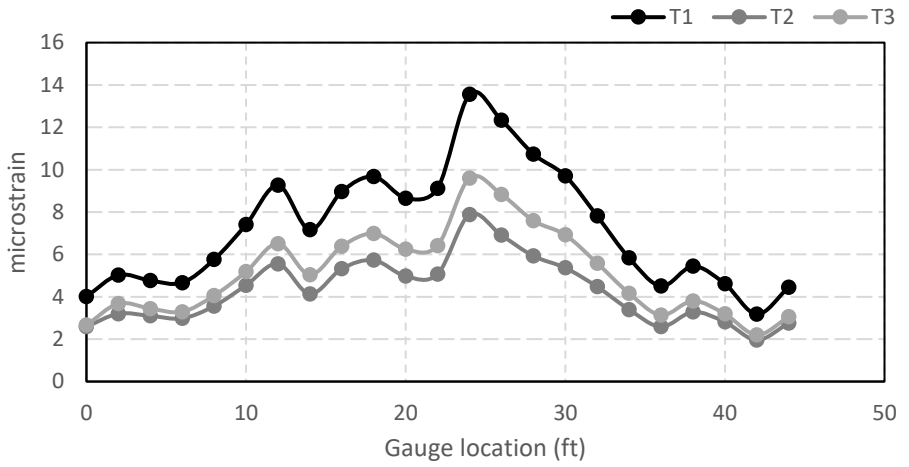

(b) LC2

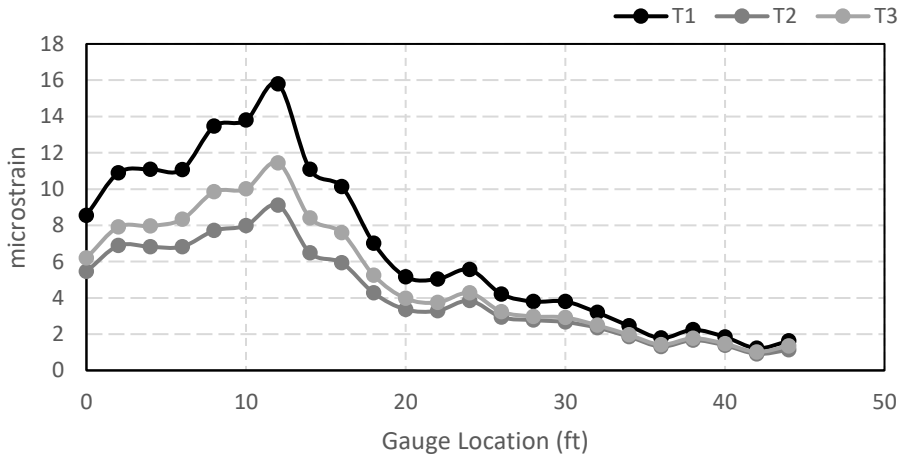

(c) LC3

Figure 34. Load distribution on Bridge 4811.2S151

The strain distribution across the transverse section of a slab bridge generally shows two peaks. These two peaks are not necessarily at the same strain magnitude, but their presence indicates a load from two wheels on the rear axle.

6.1.2.1 Determination of Equivalent Strip Width Based on Field Test Data

The load intensity on slab bridges is not calculated in the same way as it is on PC bridges. In the case of PC bridges, the LLDF gives the load effects on each girder. This method cannot be used on slab bridges. To find the load effects on a unit strip width of a slab bridge, the equivalent strip width (E) is used.

The equivalent strip width is the length in the transverse direction of the bridge deck over which the load is concentrated and is the portion of the bridge's width assumed to resist the load. The strip is generally under the point at which the load is applied. Figure 35 shows a schematic diagram of the equivalent strip width. The hatched region indicates the equivalent strip width.

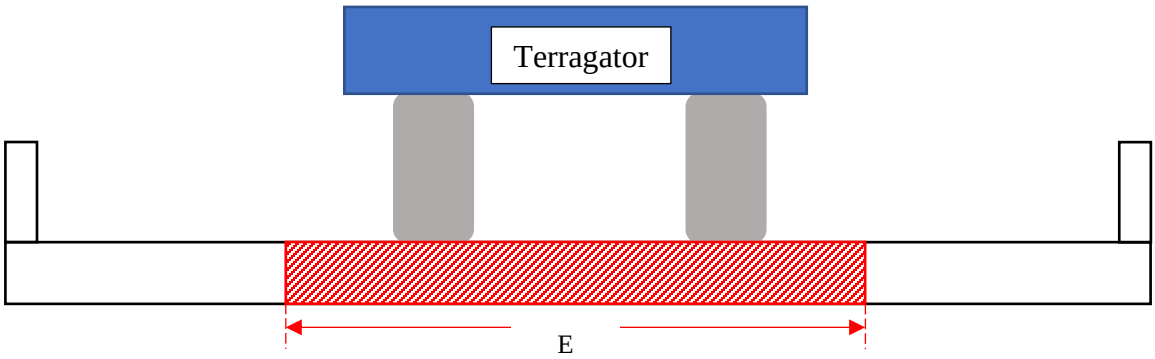

Figure 35. Schematic diagram of equivalent strip width

This unit strip load is used to calculate the live load flexural moment on the slab of the bridge. For simplicity, the flexural moment across the equivalent strip width is considered to be constant.

The equivalent wheel load widths from the field test data were calculated using the following general procedure: (1) numerically integrate the area under the moment distribution curve and (2) divide the summation by the estimated maximum moment.

The field test results provided strain and displacement data instead of moments. However, these strain and displacement values are directly related to the moment. The relationship between strain and moment at the *i*-th measurement location is illustrated in Equation 25.

$$Strain_i = \frac{Moment_i}{ES_i} \quad => \quad Moment_i = Strain_i \times ES_i \tag{25}$$

where E is the Young's modulus and S_i is the section modulus at the location where the i-th sensor is installed.

If the section moduli at all strain measurements are assumed to be equal, the strip width may be calculated as follows:

$$\text{E (Equivalent strip width)} = \frac{\sum_{i=1}^{n}(\text{strain}_i \times d_i)}{\text{strain}_{max}} \tag{26}$$

where n is the total number of strain sensors, $strain_i$ is the strain reading of the i-th sensor, $strain_{max}$ is the maximum strain measured by the sensors, and d_i is the spacing of adjacent strain gauges.

The strain distribution using an equivalent strip width is illustrated in Figure 36. The hatched region indicates the equivalent strip width.

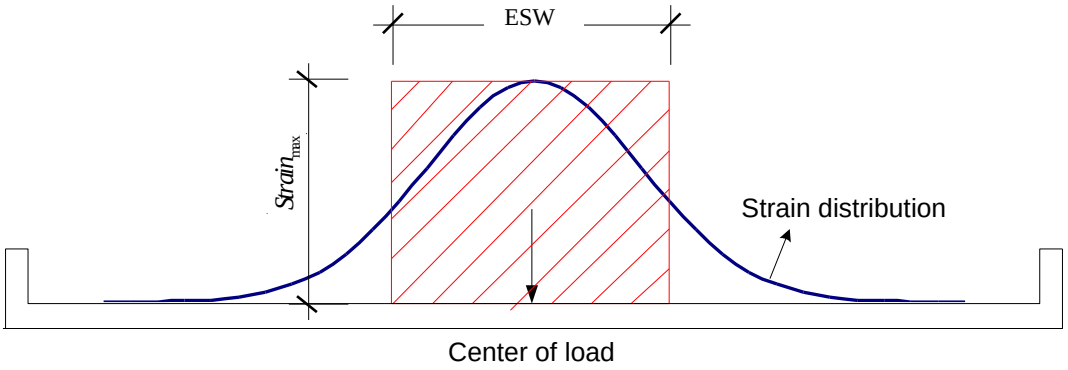

Figure 36. Strain distribution

6.1.2.2 Determination of Equivalent Strip Width Based on AASHTO (2020)

Just as with PC girder bridges, AASHTO (2020) prescribes general equations to calculate the equivalent strip widths of generic concrete slab bridges. Different equations are provided for single and multiple lane loads. Since single lane load cases were applied during the field tests, the AASHTO equation for a single lane load was used to calculate the equivalent strip widths for comparison to the field test data.

Equation 5 is recommended by AASHTO (2020) to calculate E and is based on bridge dimensions. The equivalent strip width calculated using the AASHTO equation can be used as a reference value to compare against the strip widths calculated from the field test data.

6.1.2.3 Equivalent Strip Width Results and Comparison with AASHTO Values

Figure 37 shows the equivalent strip widths calculated from the field-collected performance data as well as from the equation recommended by AASHTO. The equivalent strip widths of the field test data were calculated for the front axles and rear axles separately. The minimum equivalent strip widths for the front axles and rear axles are presented in Figure 37 along with the maximum equivalent strip widths.

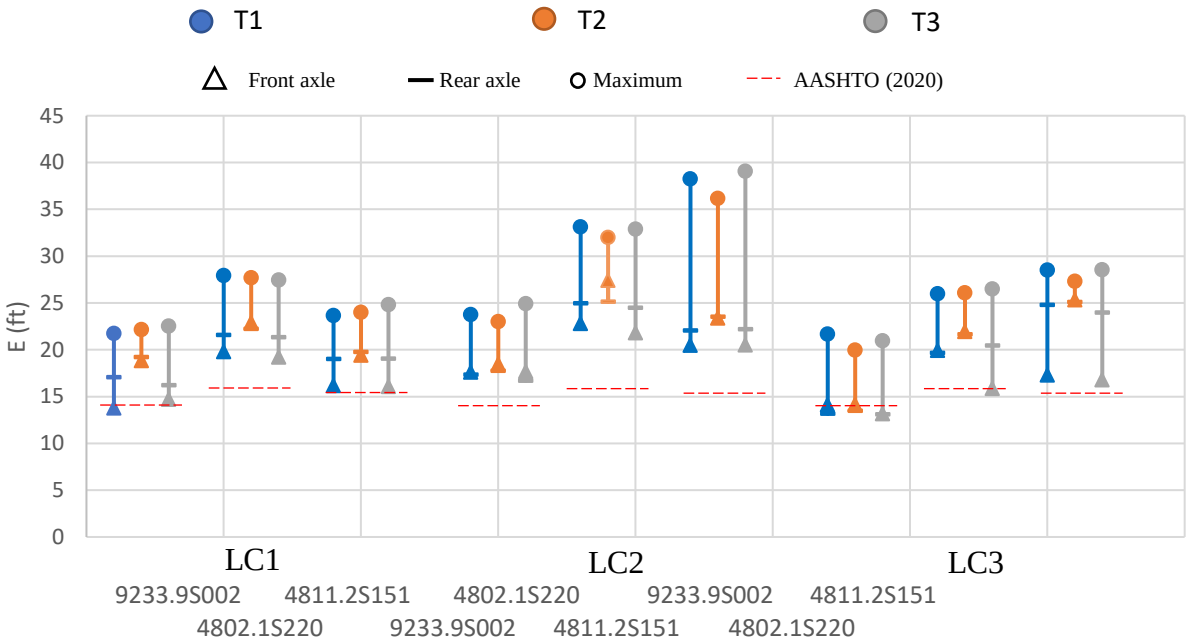

Figure 37. Equivalent strip widths of all slab bridges

The strip widths under the front axles were smaller than the strip widths under the rear axles for the two terragators with one front wheel. This was not the case for the terragator with two front wheels. For this terragator, the strip widths under front and rear axles were almost the same. For Load Case 2, the strip widths seem to be generally larger than for Load Cases 1 and 3. Also, the strip widths under heavy loads—T1 and T3—were generally smaller than those under the lightest terragator, T2. All strip widths calculated from the field test data were larger than those recommended by AASHTO.

The equivalent strip widths on Bridge 4811.2S151 were higher than those on the other bridges. This is because the slab of this bridge is thicker than that of the other two bridges, which suggests that thicker slabs reduce the load intensity on a unit strip width and distribute the load more evenly across a larger strip width.

6.1.3 Steel Girder Bridges

Steel bridges were not included in the field test portion of this research. However, field tests similar to those used in this research were performed on steel bridges by Phares et al. (2017), and the resulting field test data were used in the present research. Phares et al. (2017) conducted research to develop guidance for engineers on how implements of husbandry loads are resisted by traditional bridges, with a specific focus on bridges commonly found on the secondary road system; provide recommendations for accurately analyzing bridges for these loading effects; and make suggestions for the rating and posting of these bridges. To achieve the objectives, the distribution of live load and dynamic impact effects for different types of farm vehicles on three general bridge types—steel-concrete, steel-timber, and timber-timber—were investigated through load testing. The major field test results from five steel-concrete bridges evaluated by Phares et al. (2017) were used in this research, and further research details can be found in Phares et al. (2017).

Table 5 shows the maximum strain experienced by each steel-concrete bridge when the different testing vehicles crossed. It was observed that the semi-truck caused the maximum strain in the girders among all vehicles considered.

Table 5. Maximum static strain experienced by field-tested steel-concrete bridges

	Testing Vehicles				
Bridge	**Tractor with one tank**	**Tractor with two tanks**	**Terragator**	**Tractor Grain Wagon**	**Semi-Truck**
1	76	57	61	54	84
2	101	79	85	73	127
3	73	50	57	48	85
4	74	51	59	52	89
5	60	38	44	39	68

Note: The units of the strain values shown are in microstrain (με).

Figure 38 shows the LLDFs for the implements of husbandry and for a traditional semi-truck for each of the five steel-concrete bridges. Figure 38a for Bridge 1 shows that the interior analytical LLDFs for the implements of husbandry were, in all cases, larger than that of the semi-truck, and the exterior envelopes were also, in all cases, larger than that of the semi-truck. Figure 38a also indicates that the analytical envelopes for the implements of husbandry for all interior girders were lower than the AASHTO LRFD distribution factors, although the envelopes for the central girders, such as G3, G4, G5, G6, and G7, were close to the AASHTO standard values.

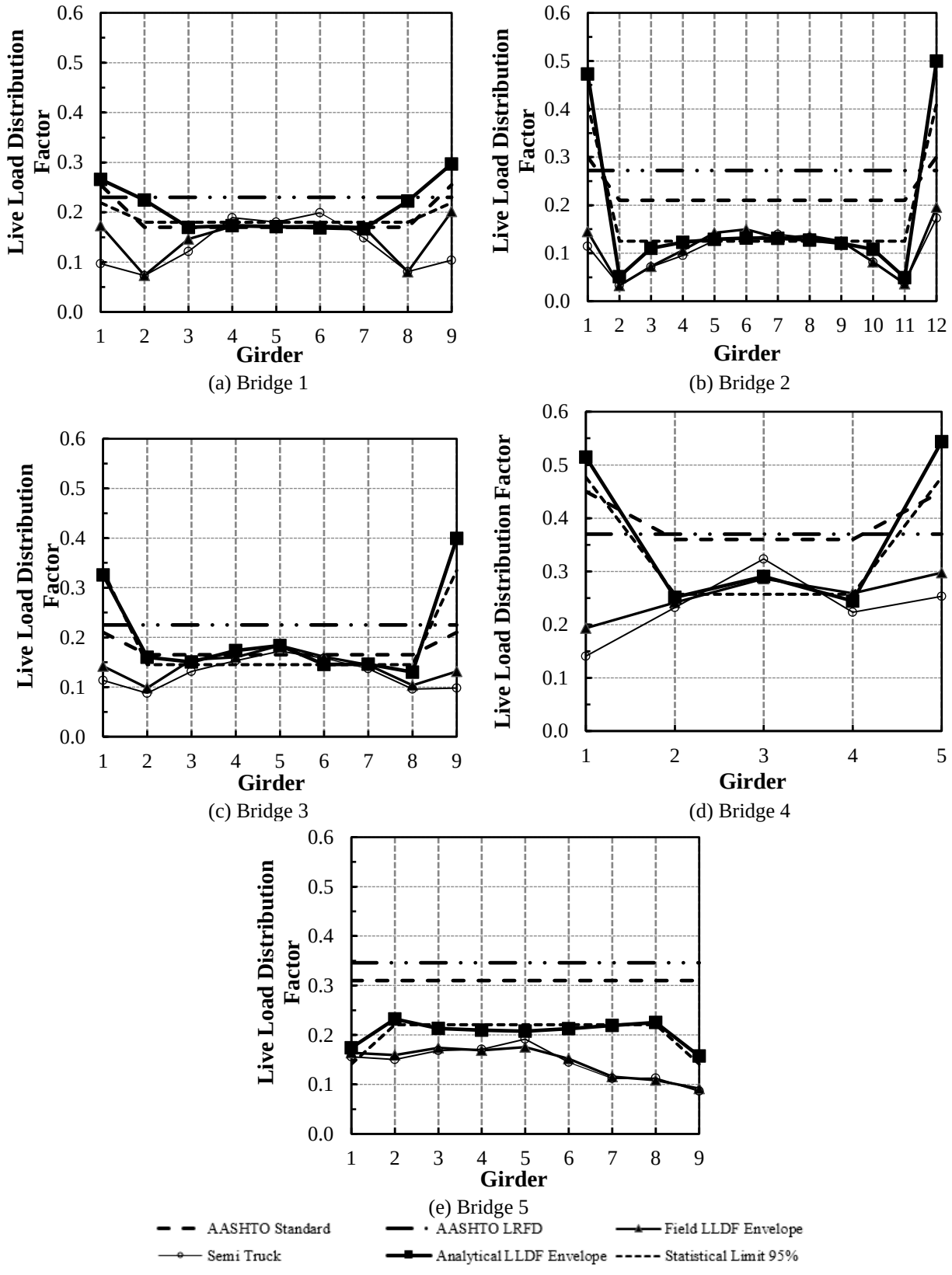

Figure 38. LLDFs for field-tested steel-concrete bridges

Similarly, the semi-truck LLDFs for the central girders, including G4, G5, and G6, were slightly above the AASHTO standard values and lower than the AASHTO LRFD values for all girders. In addition, the analytical LLDFs for the implements of husbandry for the exterior concrete girders were greater than the AASHTO values, probably as a result of the greater stiffness of the exterior girders and curbs. The AASHTO standard and LRFD values were 14% and 5% greater, respectively, than the statistical exterior girder limits and 6% smaller and 22% greater, respectively, than the interior girder limits.

Figure 38b to Figure 38d for Bridges 2 through 4 indicate that the field LLDFs for the implements of husbandry for all interior steel girders were below the AASHTO standard and LRFD values. The analytical LLDFs for the girders of the five steel-concrete bridges are summarized in Table 6, along with both AASHTO values.

The analytical LLDFs for the implements of husbandry for the concrete exterior girders were larger than both the AASHTO standard and LRFD values. The analytical LLDFs for the interior girders, however, were lower than the AASHTO values, probably due to the increased stiffness of the exterior girders. The statistical exterior girder limits for Bridges 2, 3, and 4 exceeded the AASHTO standard values by up to 37%, 60%, and 6%, respectively, and exceeded the AASHTO LRFD values by up to 51%, 50%, and 29%, respectively. The statistical interior girder limits for Bridges 2, 3, and 4 were 41%, 12%, and 29% lower, respectively, than the AASHTO standard values and 54%, 36%, and 31% lower, respectively, than the LRFD values.

In contrast, Figure 38e for Bridge 5, which consists of all steel girders, shows that the field and analytical envelopes for both the exterior and interior girders for the implements of husbandry were smaller than both the AASHTO standard and LRFD values. The statistical limit for the interior girders was 29% and 36% smaller than the AASHTO standard and LRFD values, respectively, and the exterior girder limit was 59% and 55% smaller than the AASHTO standard and LRFD values, respectively.

The percent differences between the AASHTO values and the statistical limits for each bridge are summarized in Table 7.

By comparison, both of the AASHTO values for Bridges 1, 2, 3, and 4, which have exterior girders with significant extra stiffness, when subjected to various normal farm vehicle types and their axle configurations, were, in most cases, acceptable for the interior girders but unsatisfactory for the exterior girders. For Bridge 5, the AASHTO values were suitable, yet conservative, for both the interior and exterior girders.

Table 6. Comparison of analytical and AASHTO-specified LLDFs for field-tested steel-concrete bridges

	Analytical LLDFs												Statistical Limit		AASHTO Values	
Bridge	G1	G2	G3	G4	G5	G6	G7	G8	G9	G10	G11	G12	Interior Girders	Exterior Girders	LRFD	Standard
1	0.27	0.22	0.17	0.17	0.17	0.17	0.17	0.22	**0.30**				0.18	0.22	0.23	0.17
2	**0.47**	0.05	0.11	0.12	0.13	0.13	0.13	0.13	0.12	0.11	0.05	**0.50**	0.13	0.41	0.27	0.21
3	**0.33**	0.16	0.15	0.17	**0.18**	0.15	0.15	0.13	**0.40**				0.15	0.34	0.23	0.17
4	**0.51**	0.25	0.29	0.24	**0.54**								0.26	0.48	0.37	0.36
5	0.17	0.23	0.21	0.21	0.21	0.21	0.22	0.23	0.16				0.22	0.14	0.35	0.31

Note: The highlighted values in the table indicate that the analytical LLDFs were greater than the AASHTO-specified LLDFs.

Table 7. Percent difference between AASHTO-specified LLDFs and statistical limits for field-tested steel-concrete bridges

	Exterior Girder LLDF		Interior Girder LLDF	
Bridge	AASHTO Standard	AASHTO LRFD	AASHTO Standard	AASHTO LRFD
1	29%	-4%	6%	-22%
2	95%	52%	-38%	-52%
3	100%	48%	-12%	-35%
4	33%	30%	-28%	-30%
5	-55%	-60%	-29%	-37%

Note: A negative sign indicates that the analytical LLDF was higher than the AASHTO LLDF.

6.2 Finite Element Model Development and Validation

The live load distribution factors and equivalent strip widths calculated based on the field test data indicate the load distribution characteristics of the bridges subjected to terragator loads. These LLDF and equivalent strip width values, although accurate, may not be 100% representative of the characteristics of all bridges with varied bridge parameters subjected to a variety of husbandry vehicles. To further investigate the load distribution of husbandry vehicles on bridges in Iowa, the load distribution characteristics of additional bridges were needed.

Therefore, FE models were created and validated against the field-collected data. The validated models were then used in a parametric study, which is described in Section 6.3. This method of structural analysis is acceptable and recommended in AASHTO LRFD (2020) Article 4.4, which provides the procedures for FE model validation against field test data.

This section gives a brief description of model development for the PC bridges, slab bridges, and steel girder bridges. All FE models described in this section and Section 6.3 were developed using the commercially available software from Ansys. Once the models were developed and analytically loaded, the strain data were extracted from the models and used to calculate the load distribution values. The results were then compared with the field test results. A calibration of the models was performed when a significant difference was found between the analytical results and field test results.

6.2.1 PC Bridges

FE models were developed for all five field-tested PC bridges. The bridge parameters of the field-tested bridges, including the important bridge component dimensions and material properties, were taken from the original bridge plans.

6.2.1.1 Model Development

The FE models for the PC bridges included the bridge deck, intermediate diaphragms, and the top flange, bottom flange, and web of the girders. All of these components were meshed utilizing Shell 181 elements. To create composite action between the girder and deck, the girder and deck components were connected through sharing of the same nodes. Figure 39 shows an FE model for a typical PC bridge.

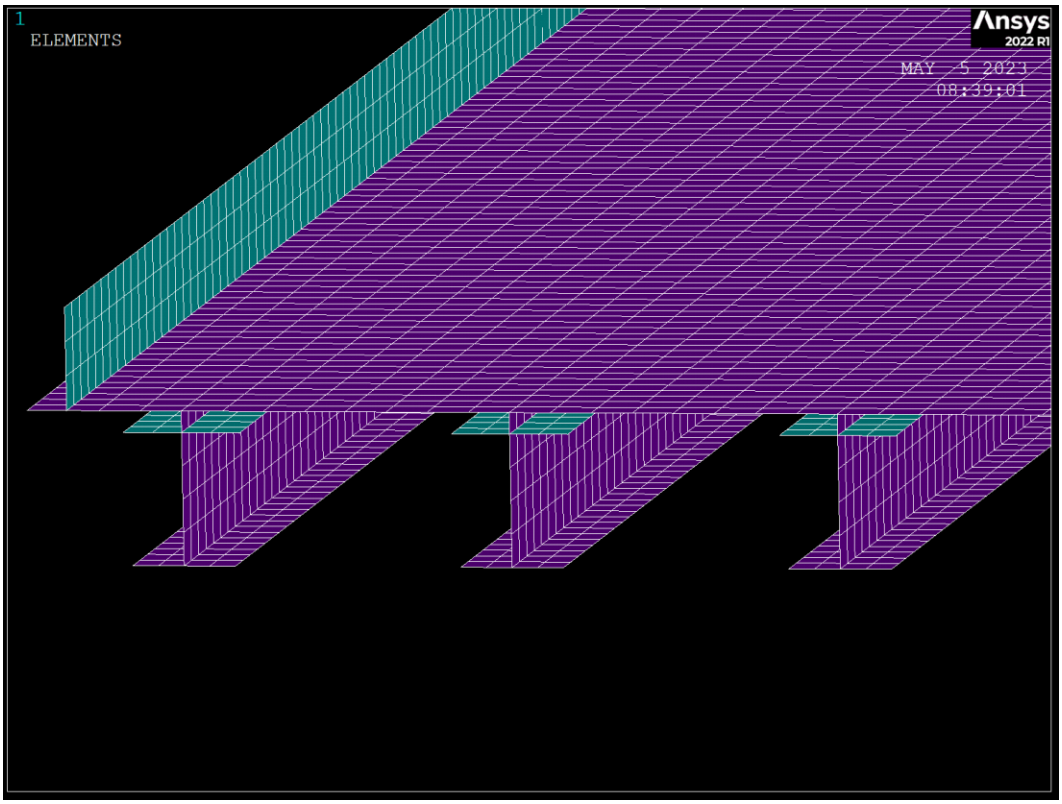

(a) Meshed bridge components

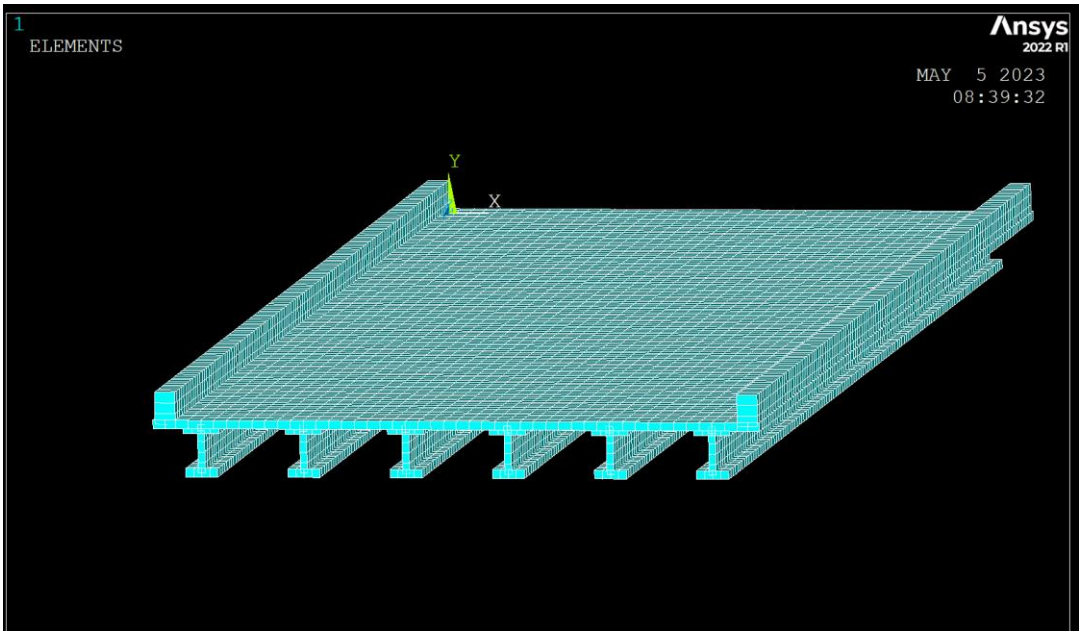

(b) Shape of elements of a PC bridge

Figure 39. Typical FE model for a PC bridge

Table 8 shows a list of the material properties used in the preliminary analysis of the PC bridge models.

Table 8. Material properties of PC bridges

Bridge	Material Property	Barrier	Deck	Intermediate diaphragm	Girder
9265.1S001	**Compressive strength (psi)**	4000	4000	4000	9000
	Poisson's ratio	0.2	0.2	0.2	0.2
9232.8S022	**Compressive strength (psi)**	3500	3500	3500	6000
	Poisson's ratio	0.2	0.2	0.2	0.2
9267.1S001	**Compressive strength (psi)**	3500	3500	3500	5000
	Poisson's ratio	0.2	0.2	0.2	0.2
9231.5S022	**Compressive strength (psi)**	3500	3500	3500	5000
	Poisson's ratio	0.2	0.2	0.2	0.2
337901	**Compressive strength (psi)**	3500	3500	3500	6000
	Poisson's ratio	0.2	0.2	0.2	0.2

In order to represent aging/curing of the concrete material properties, the initial compressive strength of the concrete was increased using Equation 27 to account for strength increases over time.

$$f'c = f'c_{(28)} * \left(\frac{t}{4+0.85*t}\right) \quad (27)$$

where $f'c_{(28)}$ is the 28-day concrete compressive strength taken from the bridge plans and t is the time in days.

For the barrier, deck, intermediate diaphragms, and girder flanges, the effective Young's modulus was calculated and assigned to account for the effect of the reinforcement. The effective Young's modulus was calculated using Equation 28.

$$E_{eff} = \frac{E_c A_c + E_s A_s}{A_c + A_s} \quad (28)$$

where E_c is the Young's modulus of the concrete, A_c is the area of the concrete section, E_s is the Young's modulus of the steel (taken as 29,000 ksi), and A_s is the area of the steel cross section.

The compressive strength of the concrete and tensile strength of the steel was taken from the bridge plans. The compressive strength was then used to calculate the Young's modulus E_c using Equation 29.

$$E_c = 57000 * \sqrt{f'c} \quad (29)$$

where f'c is the compressive strength of the concrete.

Once the material and element properties were defined, they were assigned to the bridge components using a target mesh size of 12 in. Figure 40 shows zoomed-in details for a typical PC bridge model. Restraints were applied at the bottoms of the girder ends and at the pier diaphragm locations. Translations in the vertical direction were restricted. To restrict rotation in the transverse direction, spring elements were placed at the supports at the girder locations.

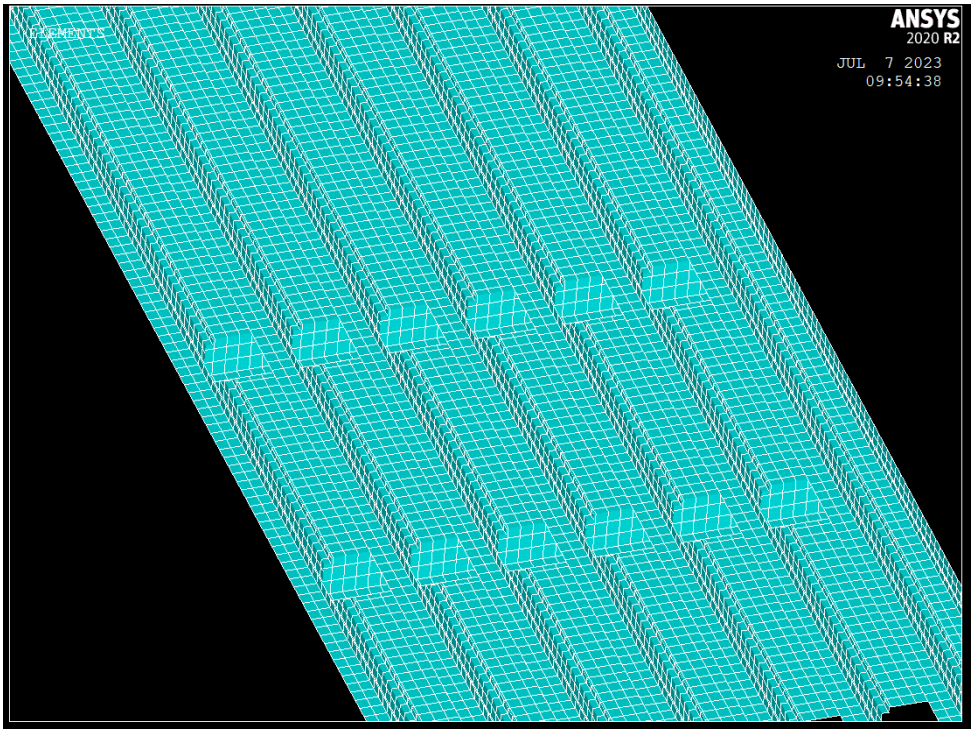

(a) Intermediate diaphragms on PC bridge

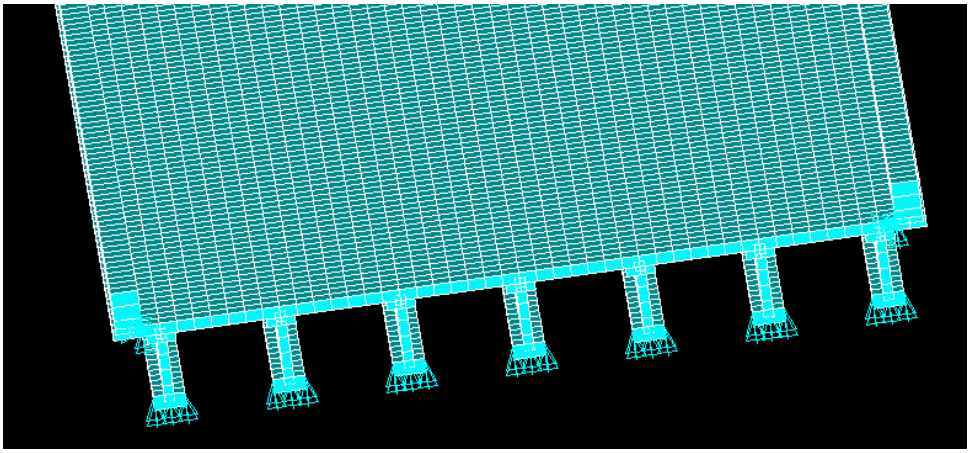

(b) Boundary conditions

Figure 40. PC bridge model details

The girder cross sections utilized in the FE model were simplified for ease of modeling. The idealized girder was configured such that the location of the neutral axis and the moment of inertia were the same as those of the actual girder geometry. Figure 41a shows the cross section

of a girder on Bridge 9265.1S001. Figure 41b shows the modified cross section with the neutral axis location of the same girder on Bridge 9265.1S001.

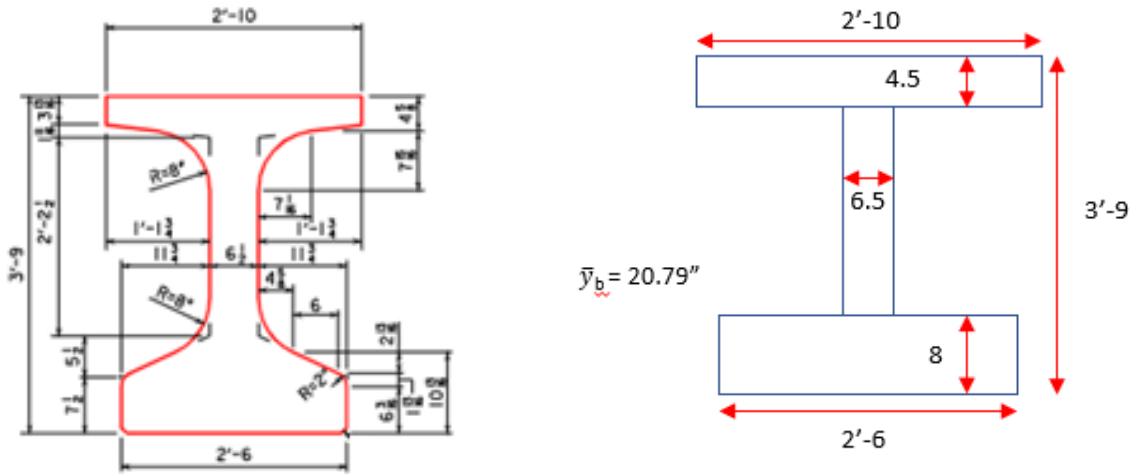

(a) Original girder shape

(b) Idealized girder shape

Figure 41. Girder cross section (Bridge 9265.1S001)

In the field tests, the load applied to the bridge was in the form of a terragator traveling over it. Therefore, a terragator path was replicated to simulate the field testing. For each load case, nodes were selected at each wheel location (Figure 42a).

The axle loads were divided by the number of selected nodes for even distribution of the load over the axle region. For the next load step, nodes were selected at the same transverse location but 2 ft ahead of the previous longitudinal location. The loads applied in the previous load case were deleted to avoid the addition of previous loads along with the current loads (Figure 42b).

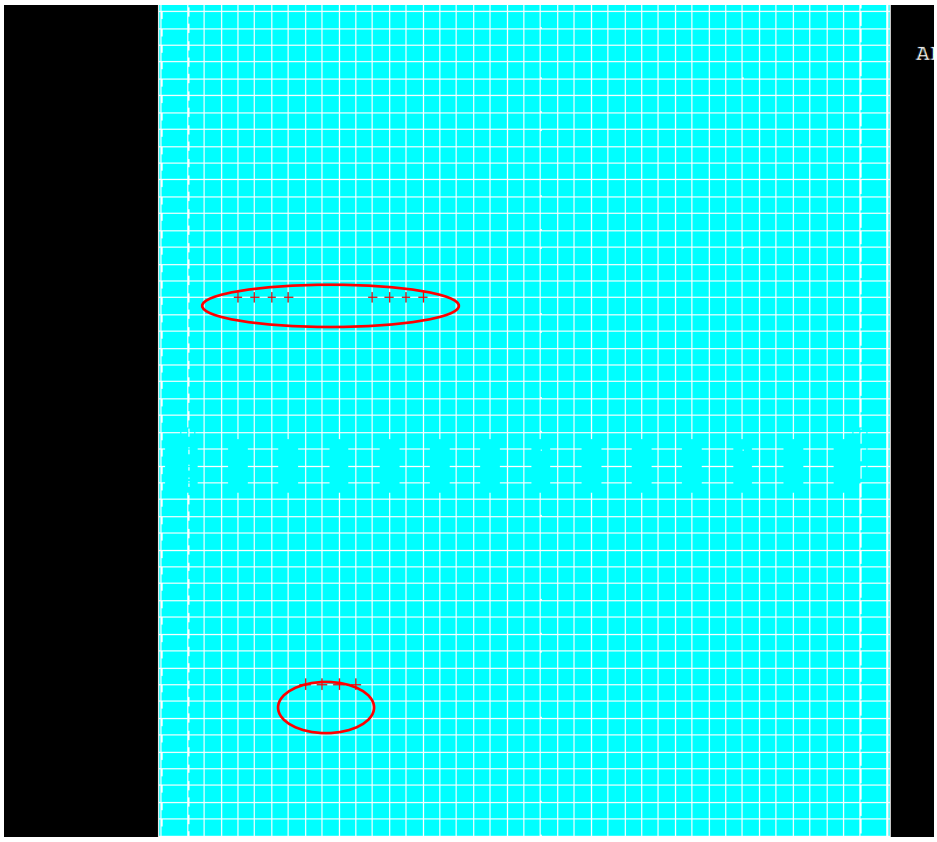

(a) Transverse wheel load location of the terragator

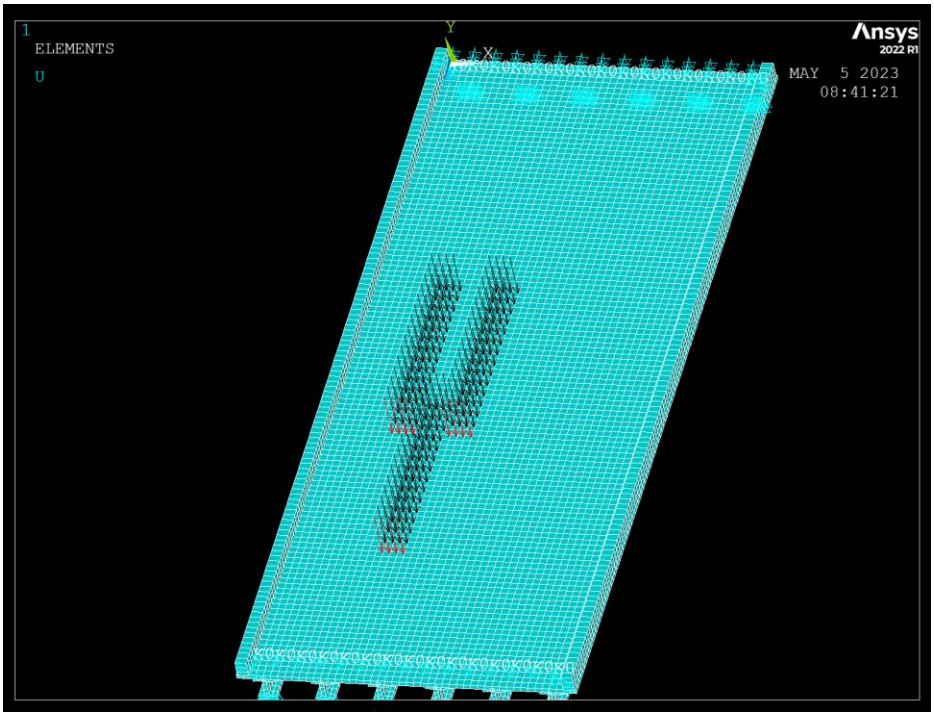

(b) Terragator path

Figure 42. Loading on PC bridge models

6.2.1.2 Model Validation

To check whether these models were a good representation of the field-tested bridges, the LLDFs from the FE models were compared with the LLDFs obtained from the field test data. The load distribution factors for all of the field-tested PC bridges are given in Table 9.

Table 9. Validation of load distribution factors for all PC bridges

			Interior girder LLDF			Exterior girder LLDF		
Bridge	**Terragator**	**Load case**	**Field Test**	**FEA**	**Percent error (%)**	**Field Test**	**FEA**	**Percent error (%)**
9265.1S001	T1	1	0.33	0.33	0	0.22	0.24	9
		2	0.29	0.31	3	NA	NA	NA
		3	0.34	0.33	3	0.23	0.26	13
	T2	1	0.34	0.33	3	0.26	0.26	0
		2	0.29	0.31	7	NA	NA	NA
		3	0.33	0.33	0	0.23	0.26	13
	T3	1	0.33	0.33	0	0.24	0.26	8
		2	0.30	0.31	3	NA	NA	NA
		3	0.33	0.33	0	0.23	0.26	12
9232.8S022	T1	1	0.33	0.33	0	0.17	0.18	6
		2	0.32	0.33	3	NA	NA	NA
		3	0.34	0.33	3	0.19	0.18	5
	T2	1	0.32	0.34	6	0.17	0.21	23
		2	0.31	0.33	6	NA	NA	NA
		3	0.32	0.34	6	0.22	0.21	4
	T3	1	0.33	0.34	3	0.16	0.21	31
		2	0.31	0.32	3	NA	NA	NA
		3	0.33	0.34	3	0.18	0.21	16
9267.1S001	T1	1	0.31	0.30	3	0.22	0.25	14
		2	0.26	0.26	0	NA	NA	NA
		3	0.27	0.30	11	0.23	0.26	13
	T2	1	0.29	0.25	14	0.22	0.24	9
		2	0.24	0.24	0	NA	NA	NA
		3	0.27	0.25	7	0.24	0.24	0
	T3	1	0.32	0.26	25	0.24	0.24	0
		2	0.24	0.24	0	NA	NA	NA
		3	0.27	0.26	4	0.24	0.24	0
9231.5S022	T1	1	0.45	0.40	11	0.13	0.16	23
		2	0.41	0.38	7	NA	NA	NA
		3	0.39	0.40	3	0.11	0.17	54
	T2	1	0.43	0.40	7	0.12	0.16	33
		2	0.40	0.38	5	NA	NA	NA
		3	0.40	0.40	0	0.17	0.16	6
	T3	1	0.46	0.40	13	0.13	0.16	23
		2	0.41	0.38	7	NA	NA	NA
		3	0.40	0.40	0	0.14	0.16	14
337901	T1	1	0.33	0.34	3	0.30	0.30	0
		2	0.34	0.33	3	NA	NA	NA
		3	0.38	0.35	8	0.32	0.31	3
	T2	1	0.33	0.35	6	0.31	0.26	16
		2	0.34	0.34	0	NA	NA	NA
		3	0.37	0.36	3	0.31	0.26	16
	T3	1	0.35	0.35	0	0.33	0.25	24
		2	0.34	0.33	3	NA	NA	NA
		3	0.38	0.36	5	0.29	0.25	14

To validate the finite element results, data from the load case with the maximum strain were considered for each bridge. The strain at the bottom of the shell element representing the bottom flange of the girder was extracted. The field test strain data and the corresponding FEA strain data on each girder were plotted. Figure 43 shows strain plots for all field-tested bridges under the T1 load. Load Cases 1 and 3 were chosen for the exterior girder LLDFs because the load distribution factor is highest on the exterior girders when the load is close to the exterior girders. In nearly every case, the strain distributions for all of the bridge models matched those for the field test data, which indicates that the modeling methodology is valid.

The percent error from the FE results was not very high for the interior girders. The percent error for the exterior girders was higher than that for the interior girders but was still acceptable.

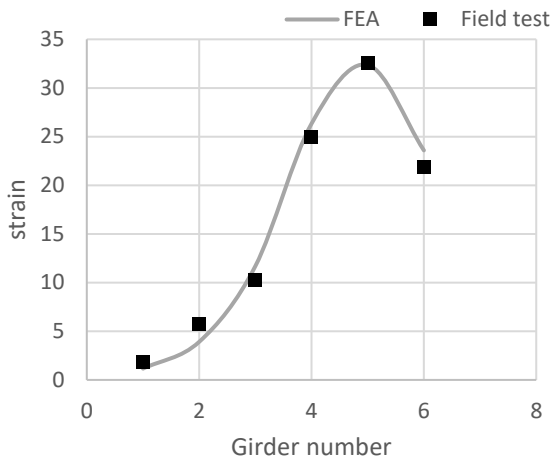

(a) Bridge 9265.1S001 (LC1)

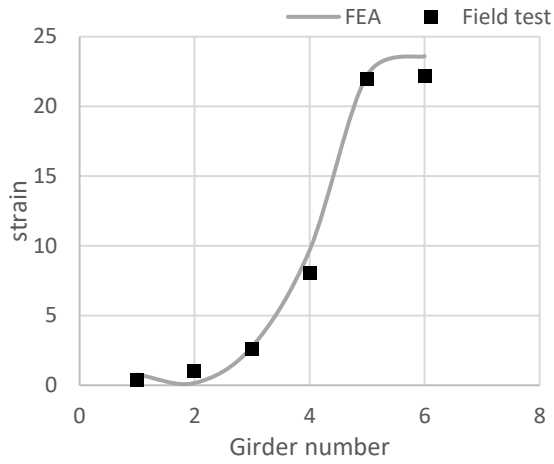

(b) Bridge 9232.8S022(LC1)

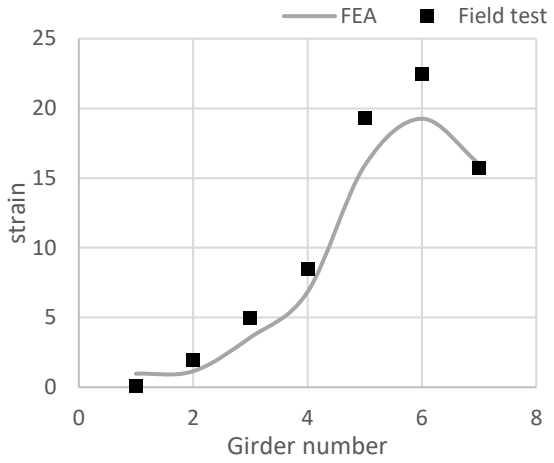

(c) Bridge 9267.1S001(LC1)

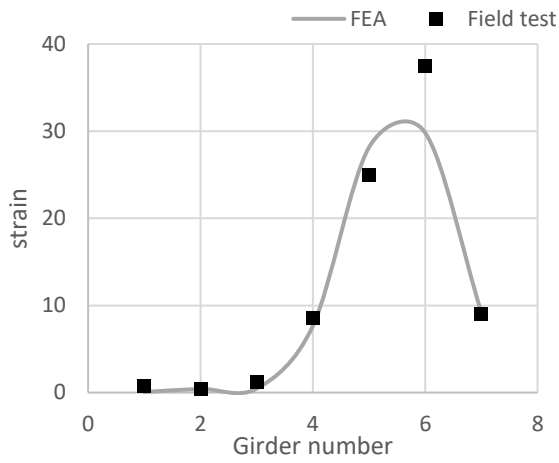

(d) Bridge 9231.5S022(LC1)

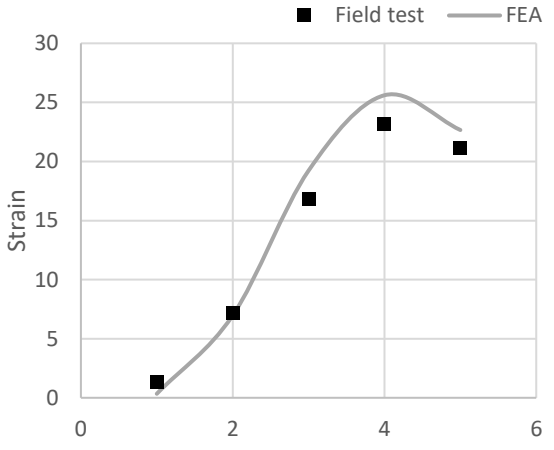

(e) Bridge 337901(LC1)

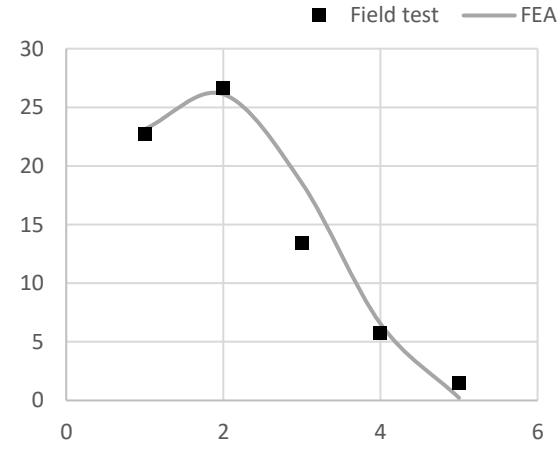

(f) Bridge 337901 (LC3)

Figure 43. Strain distribution in the transverse direction for PC bridges (T1)

6.2.2 Slab Bridges

Pertinent information about the field-tested slab bridges was taken from the bridge plans. Bridge parameters such as bridge width, span length, skew angle, and slab thickness, along with various material properties, were used to create the slab bridge models.

6.2.2.1 Model Development

The FE models for each of the slab bridges included the bridge slab and the barrier. Table 10 lists the material properties used for the preliminary modeling of the slab bridges.

Table 10. Material properties of slab bridges

Bridge	Material Property	Barrier	Slab
9233.9S002	**Compressive strength (psi)**	3500	3500
	Poisson's ratio	0.2	0.2
4811.2S151	**Compressive strength (psi)**	3500	3500
	Poisson's ratio	0.2	0.2
4802.1S220	**Compressive strength (psi)**	4000	4000
	Poisson's ratio	0.2	0.2

Similar to the PC bridges, aging/curing of the concrete material properties was considered. The compressive strength was used to calculate the Young's modulus E_c using Equation 29. The effective Young's modulus was calculated using the same approach as that used for the PC bridges.

Once the material and element properties were defined, they were assigned to the bridge components by meshing the previously generated areas with an element size of 12 in. Figure 44a shows a meshed slab bridge model with the shape of the elements.

The boundary conditions applied to the slab bridges were the same as those used for the PC bridge models. To restrict rotation in the transverse direction, spring elements were placed at the supports, as shown in Figure 44b. A load simulating a terragator path was applied to the bridge using the same approach as that used for the PC bridge models.

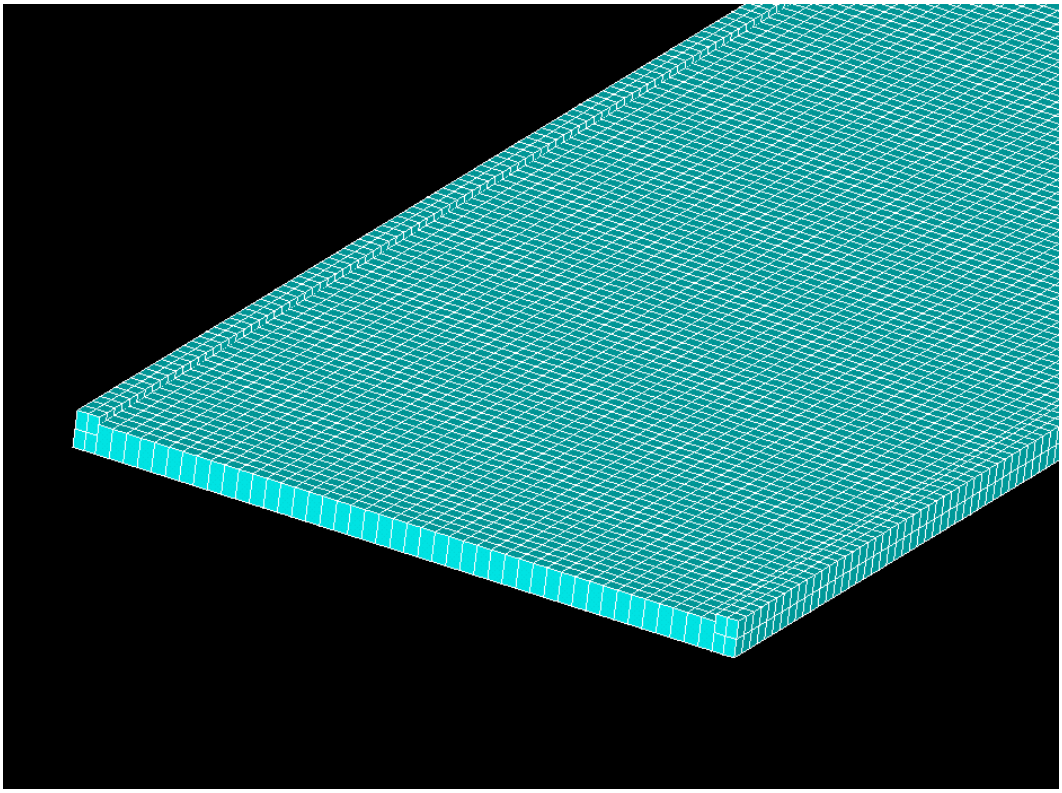

(a) Meshed bridge components

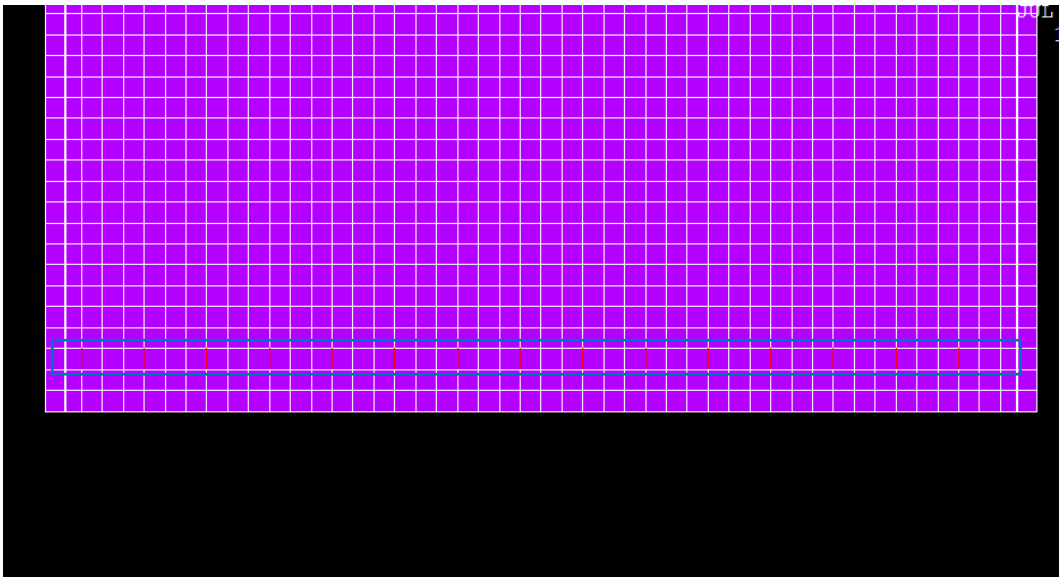

(b) Spring elements at supports

Figure 44. Typical FE model for a slab bridge

6.2.2.2 Model Validation

Table 11 shows the equivalent strip widths calculated from the field test data and the finite element results.

Table 11. Validation of equivalent strip widths for all slab bridges

Bridge	Terragator	Load Case	Field Test E (ft)	FEA E (ft)	Percent error (%)
9233.9S002	T1	1	13.16	20.01	52
		2	18.67	22.57	21
		3	17.22	20.01	16
	T2	1	13.41	20.02	49
		2	19.18	22.60	18
		3	19.74	22.05	11
	T3	1	13.12	20.01	52
		2	19.34	22.57	17
		3	15.97	20.01	25
4811.2S151	T1	1	19.59	22.01	12
		2	24.60	24.08	2
		3	21.13	22.01	4
	T2	1	21.71	22.41	3
		2	25.30	24.44	3
		3	22.40	22.41	0
	T3	1	20.19	22.01	9
		2	24.57	24.08	2
		3	21.06	22.01	5
4802.1S220	T1	1	24.78	21.20	14
		2	22.05	23.34	6
		3	19.06	21.20	11
	T2	1	25.30	21.32	16
		2	23.47	23.42	0
		3	19.78	21.32	8
	T3	1	24.18	21.20	12
		2	22.45	23.34	4
		3	19.04	21.20	11

The strain magnitudes and equivalent strip widths from the FE models showed little deviation from the strain magnitudes and equivalent strip widths from the field test data. For Load Case 1 on Bridge 9233.9S002, the strain magnitudes from the FE model were similar to those from the field test data, yet the FE results showed a large deviation from the field test data in terms of equivalent strip width. Therefore, it was necessary to examine the strain distribution along the transverse section of the bridge. A strain distribution from the FE results that shows consistency with the strain distribution from the field test data can be considered valid.

To validate the finite element results, data from the load case with the maximum strain were considered for each bridge. The strain at the bottom of the shell element representing the slab was extracted. The strain data under the T1 load on each node at mid-span were plotted, as shown in Figure 45. Load Cases 1 and 3 were chosen because the load distribution factor is highest when the load is close to the exterior girders.

Since the equivalent strip widths and strain results from the FE model and the field test data showed good agreement, the modeling approach developed in this section was deemed to be valid for the parametric study of slab bridges described in Section 6.3.

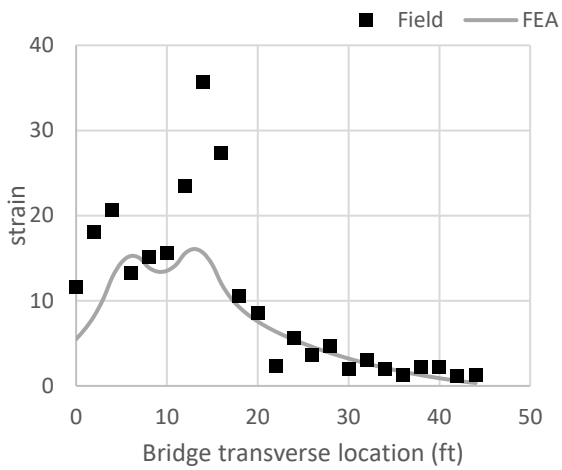

(a) Bridge 9233.9S002 LC1

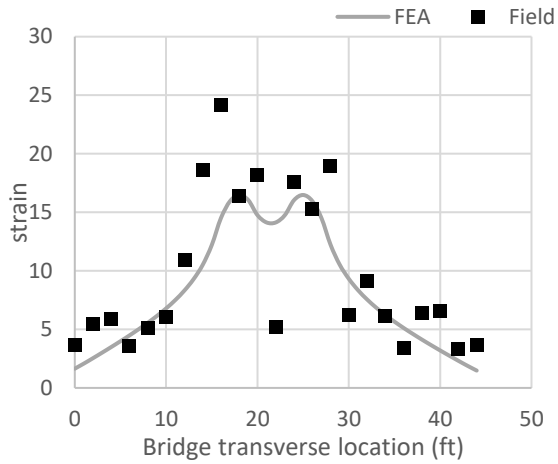

(b) Bridge 9233.9S002 LC2

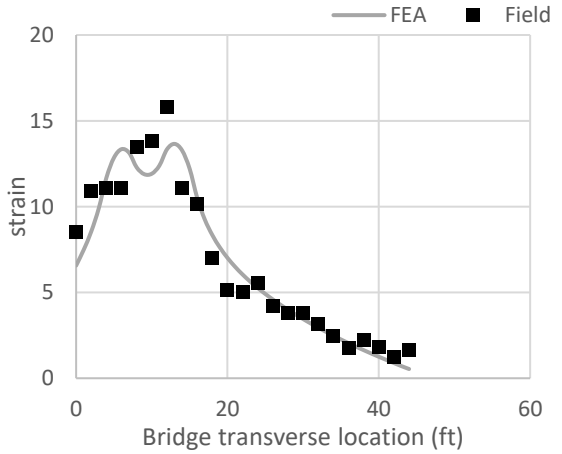

(c) Bridge 4811.2S151 LC1

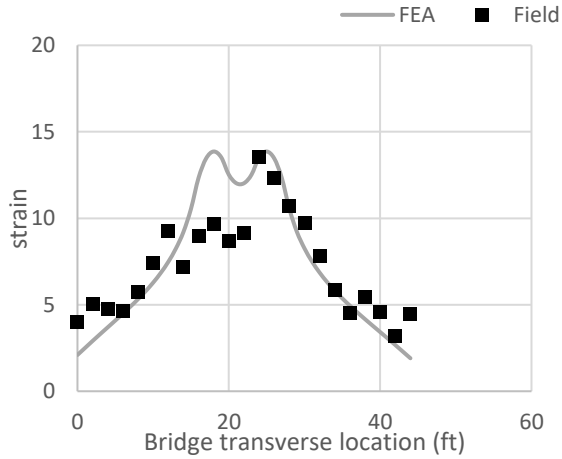

(d) Bridge 4811.2S151 LC2

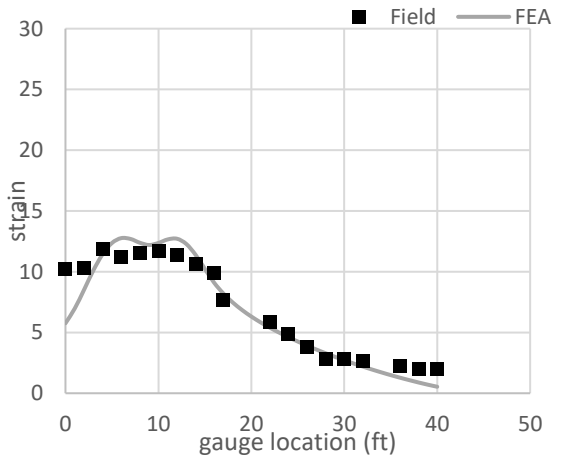

(e) Bridge 4802.1S220 LC1

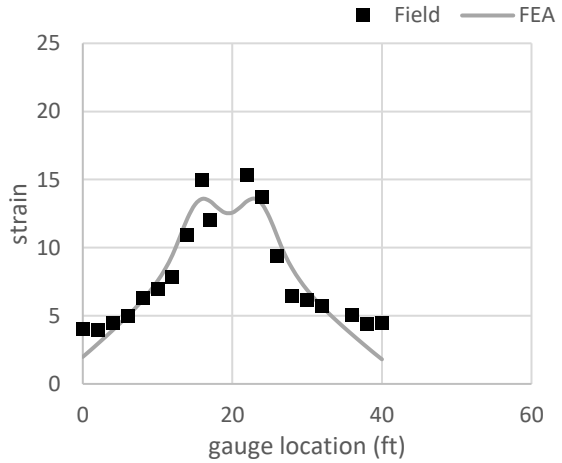

(f) Bridge 4802.1S220 LC2

Figure 45. Strain distribution in the transverse direction for slab bridges (T1)

6.2.3 Steel Girder Bridges

The bridge parameters for the five steel girder bridges evaluated in Phares et al. (2017) were used to create FE models of these bridges. Table 12 lists the key parameters of these bridges.

Table 12. Steel girder bridge parameters

Bridge	Width (ft)	# of girders	Girder spacing (in.)	Span length (ft)
162	27	12	27.6	40
108	18	9	24	30
060	18	9	27.6	36
064	20	5	60	36
162060	24	9	36	42

6.2.3.1 Model Development

The five steel girder bridges evaluated in Phares et al. (2017) were used for FE analysis. Three of these five bridges had concrete exterior girders and steel interior girders. The concrete exterior girders were modeled using the same approach as that used for the PC bridges. For the remaining two bridges, all girders were steel. All steel girders were modeled using Shell 181 elements and were assigned steel material properties.

To generate the FE models for the steel girder bridges, areas were created for the first two girders, the barrier, and the part of the deck over the girders. For the girders, three separate areas were created to model the two flanges and the web. For bridges with concrete exterior girders, the exterior girders were created with a single rectangular area. Figure 46a shows the areas created for Bridge 064.

The areas were meshed using Shell 181 elements, with section properties and material properties taken from the bridge plans. The concrete compressive strength for all bridges was taken as 3,500 psi. A Young's modulus of 29,000 ksi was used for all of the steel girders. An element size of 12 in. was kept consistent for all bridge models. The meshed elements of Bridge 064 are shown in Figure 46b.

To simulate the support conditions, the nodes at the abutment location were given zero displacement in the vertical direction. The rotation about the transverse direction was controlled by generating spring elements at the girder ends.

The terragator loads were applied in the same way as that used for the PC bridge models.

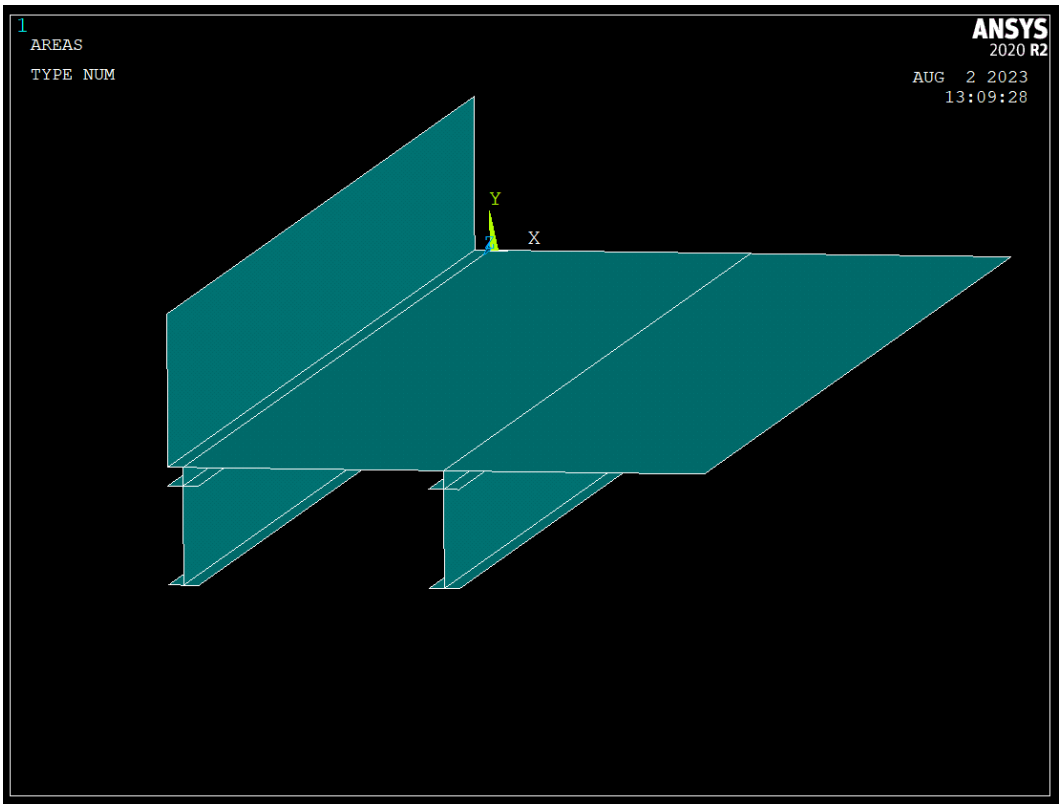

(a) Areas created for Bridge 064 model

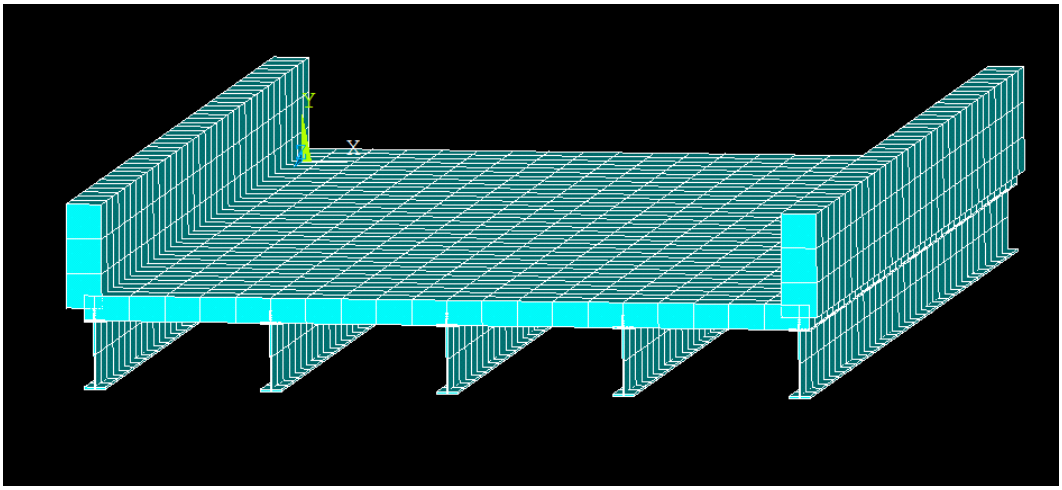

(b) Elements of Bridge 064 model

Figure 46. Typical model for a steel girder bridge

6.2.3.2 Model Validation

The LLDFs from the FE models and the field data were calculated and are presented in Table 13. The results indicate that the FE models are valid, though with some differences of up to 14%.

Table 13. Validation of interior girder LLDFs for steel bridges

	Interior girder			Exterior girder		
Bridge	**Field Test LLDF**	**FEA LLDF**	**Percent error (%)**	**Field Test LLDF**	**FEA LLDF**	**Percent error (%)**
162060	0.16	0.16	0	0.07	0.06	14
060	0.17	0.17	0	0.05	0.05	0
162	0.14	0.13	7	0.02	0.02	0
064	0.33	0.33	0	0.06	0.06	0
108	0.17	0.15	12	0.04	0.04	0

The strains resulting from the steel girder FE models were compared with the field test strain data from Phares et al. (2017) to validate the models. The strain from each girder when the terragator was at mid-span was extracted and plotted. Figure 47 shows the longitudinal strain distribution along the transverse direction for both the FE models and the field test data.

Since the LLDFs and the strain results from the FE models and the field test data showed good agreement, the FE modeling approach was deemed to be valid for use in the parametric study of steel girder bridges described in Section 6.3.

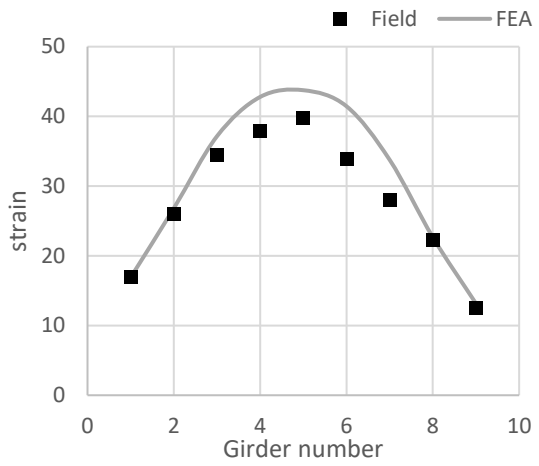

(a) Bridge 162060

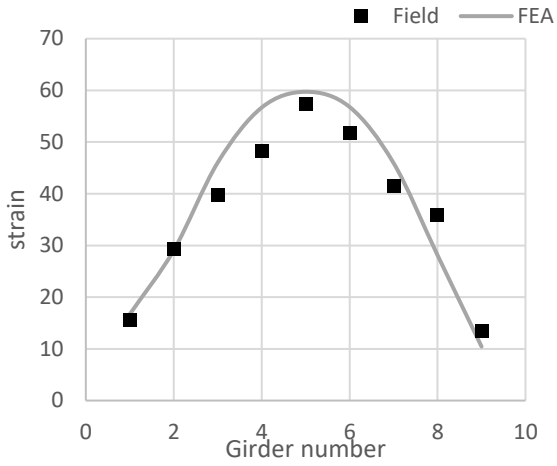

(b) Bridge 060

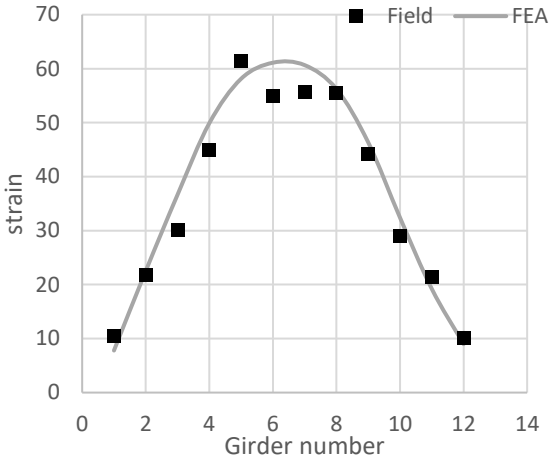

(c) Bridge 162

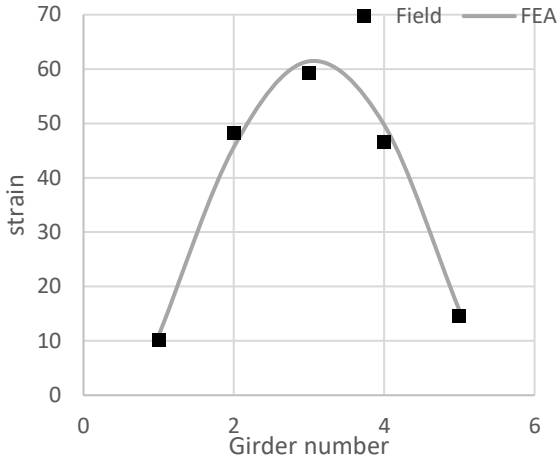

(d) Bridge 064

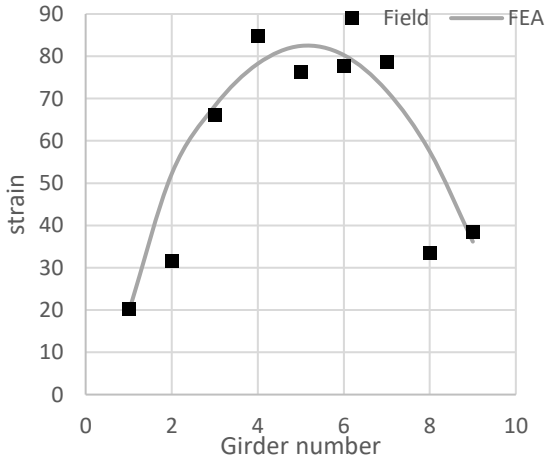

(e) Bridge 108

Figure 47. Strain distribution in the transverse direction for steel girder bridges

6.3 Parametric Study

A parametric study was conducted on a series of finite element models that had various combinations of bridge parameters. The goal of this work was to evaluate the load distribution of IoH vehicles across a transverse section of the modeled bridges and to understand the effects of varying bridge and terragator parameters on the load distribution.

To achieve this goal, 50 slab bridges and 50 PC bridges with various bridge parameters were modeled. The parameters of interest for both types of bridges included span length, bridge width, skew angle, and deck thickness.

For the steel girder bridges, only the five bridge models that were validated in Section 6.2.3 were used for the parametric study. The parametric study for the steel girder bridges was conducted using the same approach as that used for the PC and slab bridges.

In order to cover the various parameters of husbandry vehicles, 28 terragators were identified and modeled in the parametric study with empty and full payloads, resulting in 56 different configurations. Table 14 lists the configurations of the 28 terragators with two payload categories.

FE models were created using the approach described in Section 6.2. To optimize efficiency, a code template was created for each of the three bridge types (PC, slab, and steel girder) that could generate results for all bridge models of that type under each load configuration. Ansys Parametric Design Language (APDL) was used with MATLAB to automatically generate the code for each bridge model with different parameters and loadings.

To do this, a common APDL code template was created for each of the three bridge types (PC, slab, and steel girder). Arrays for bridge and terragator parameters that would be used as inputs for each of the APDL code templates were constructed in MATLAB. Each APDL code template was read using custom-developed MATLAB code. By updating each APDL code template with the bridge and terragator parameter input arrays, MATLAB could generate FE model code and result files and run the Ansys software automatically for each bridge under each terragator load. In total, 5,600 FE analyses were performed.

The strain data yielded from the parametric study were analyzed and used to determine the load distribution factors. The influence of the various bridge parameters on the distribution factors for each bridge type was evaluated.

Table 14. Terragator configurations

Terragator model	Wheel base (in.)	Wheel track (in.)	Rear tire thickness (in.)	Front tire thickness (in.)	Number of wheels on front axle	Empty weight (kips)			Full weight (kips)		
						Front axle	Rear axle	Gross	Front axle	Rear axle	Gross
V2-1 (7300)	276	93	40	40	1	10.99	17.71	28.70	13.62	35.06	48.68
V2-2 (8400)	204	93	40	29	2	11.37	17.33	28.70	14.95	33.73	48.68
V3-36 (2505)	228	93	40	40	1	11.06	16.20	27.26	10.58	33.67	44.24
TG8400	204	93	40	29	2	11.37	17.33	28.70	14.95	33.73	48.68
JDR4044	156	120	16	15	2	14.31	17.49	31.80	17.14	27.98	45.12
JDR4045	156	120	16	15	2	16.24	19.84	36.08	19.07	30.33	49.40
JDR4060	156	120	16	15	2	16.43	20.08	36.51	20.21	34.06	54.27
SP310F	156	120	16	15	2	15.32	15.32	30.64	18.45	25.51	43.96
SP370F	180	120	16	15	2	17.14	17.14	34.28	20.75	31.29	52.04
SP410F	180	120	16	15	2	17.48	17.48	34.95	21.09	31.62	52.71
TG8300	276	93	40	40	1	10.99	17.71	28.70	13.62	35.06	48.68
TG9300	252	93	40	40	1	13.62	22.94	36.56	17.47	45.73	63.20
JD 800R	276	96	40	29	2	13.95	17.05	31.00	18.67	34.53	53.20
Case IH Patriot 3250	156	118	16	15	2	13.65	16.69	30.34	16.32	25.12	41.44
Case IH Patriot 4350	156	118	16	15	2	14.58	17.82	32.40	17.58	28.14	45.72
Case IH Patriot 4540	180	96	40	29	2	13.75	16.81	30.56	18.19	34.57	52.76
Case IH Patriot 4530	180	96	40	29	2	13.47	16.46	29.93	17.46	32.45	49.91
Case IH Titan 3540	276	96	40	40	1	14.23	17.39	31.62	17.21	36.61	53.82
John Deere 408R	156	120	16	15	2	13.08	15.99	29.07	14.97	22.98	37.95
John Deere 410R	156	120	16	15	2	13.70	16.74	30.44	16.06	25.48	41.54
John Deere 412R	156	120	16	15	2	14.31	17.49	31.80	17.14	27.98	45.12
John Deere 612R	156	120	16	15	2	15.82	19.33	35.15	18.65	29.82	48.47
John Deere 616R	156	120	16	15	2	16.42	20.07	36.48	20.19	34.05	54.24
John Deere R4023	156	120	16	15	2	8.17	9.99	18.16	9.74	15.08	24.82
GVM 380 Prowler	180	100	16	15	2	13.59	16.61	30.20	14.98	35.20	50.18
Case IH 3040	276	96	40	29	1	11.38	19.52	30.90	14.06	36.82	50.88
Case IH 4040	180	96	40	29	2	11.77	19.66	31.43	16.21	37.42	53.63
Case IH 3030	276	96	40	40	1	11.25	19.36	30.61	13.93	36.66	50.59

6.3.1 PC Bridges

Table 15 lists the important bridge parameters for the 50 PC bridges used in the parametric study.

Table 15. Bridge parameters of 50 PC bridges

Bridge ID	Skew angle	Span 1 length (ft)	Span 2 length (ft)	Width (ft)	Number of girders	Girder spacing (ft)
0668.7S021	-45	52	82	44	7	7
0669.5S021	0	46	52	44	7	7
0817.2S169	0	46	82	44	7	7
0821.5S169	3	56	64	40	6	7
0827.2S017	0	56	56	44	7	7
0819.7S017	0	56	82	44	7	7
0842.6O030	-22	40	96	32	5	7
1310.6S175	30	30	52	40	7	6
3557.1L035	-24	56	64	40	7	6
3703.2S030	0	90	102	46	8	6
3712.3S004	-15	96	0	40	5	9
4260.5O020	0	40	92	30	5	7
4262.4R020	5	40	92	40	6	7
4263.9L020	-40	68	70	40	6	7
5000.1S117	5	40	112	36	6	7
5015.8L163	0	94	0	40	6	7
5018.3S117	-15	60	86	40	6	7
5019.2L163	1	48	70	40	5	9
5025.8O163	5.5	110	110	32	6	6
5027.3O163	0	110	110	30	5	7
5049.9L080	-2	42	44	42	11	4
5052.4O080	9	42	64	27	6	5
5056.9R080	0	52	52	37	8	5
5057.0S014	-2	112	110	51	8	7
5057.8L080	15	56	70	30	8	4
5058.9O080	4	40	66	32	7	5
5061.0O080	-5.5	42	66	23	4	7
5062.3O080	-2	56	64	23	4	7
5063.9L080	0	48	44	42	11	4
5065.3O080	0	42	66	27	6	5
5068.3R080	3	44	48	42	9	5
5071.3O080	0	48	66	23	4	7
5073.4L080	-5	40	48	42	9	5
5076.6L080	0	56	70	32	7	5
5078.9S014	-35	68	62	44	7	7
5079.1O080	0	42	64	32	6	6
5080.3S014	-15	56	64	37	6	7
5098.3L065	0	72	82	38	5	9
5098.9S065	0	130	130	38	5	9
5099.5S065	0	96	0	42	6	8
5423.3S021	15	40	70	37	6	7
6278.8S063	15	56	82	30	5	7
6279.0S063	0	44	82	37	6	7
6401.9S014	20	78	82	58	9	7
6407.7L330	0	66	72	37	6	7
6411.3L330	-45	66	72	37	6	7
6420.5L330	38	140	130	37	6	7
7774.8R065	7.5	56	70	37	6	7
46071	-5	40	118	65	8	9
49532	30	100	102	37	6	7

6.3.1.1 Maximum Strain Results

The result files generated by the Ansys software for the 2,800 PC bridge models contained strain data from the bottom flanges of the girders at mid-span. These strain data were collected and analyzed. To aid in the analysis, the data were separated into two categories based on the type of terragator. Type I terragators have one wheel on the front axle, whereas Type II terragators have two wheels on the front axle.

Figure 48 shows the maximum strain data from 2,800 PC bridges. The data in blue indicate strain from Type I terragators, and the data in orange indicate strain from Type II terragators.

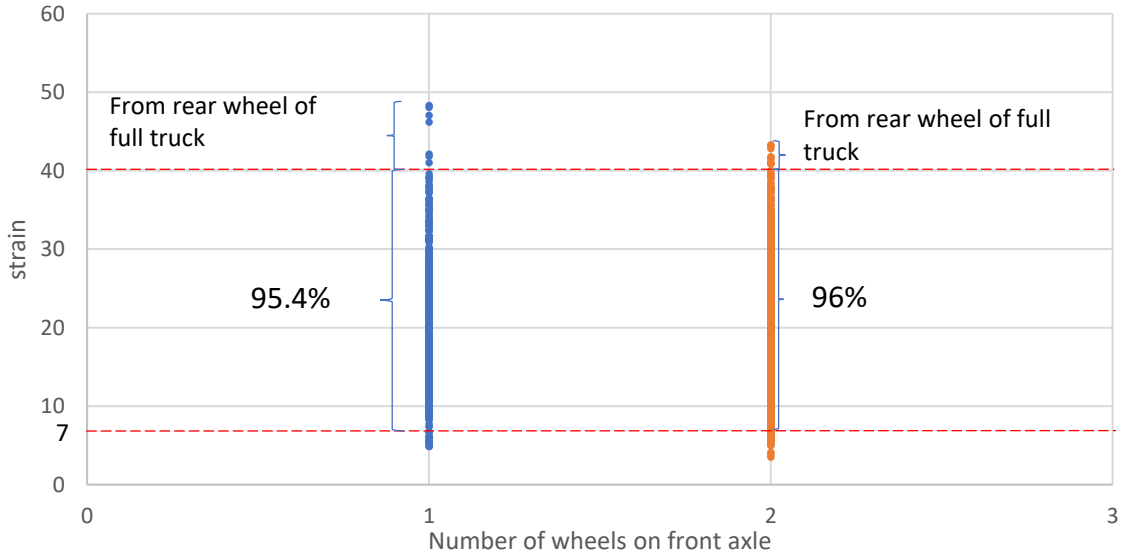

Figure 48. Maximum strain range of PC bridge models

The maximum strain observed was 48 microstrain, which was from the rear axle of a Type I terragator at 100% payload. Based on the strain data collected, most of the maximum strain values for the bridges fell between 7 and 40 microstrain for both types of terragators.

6.3.1.2 Determination of LLDF

The strain data collected were used to calculate the LLDFs of the interior and exterior girders for each FE analysis. The interior girders LLDFs were calculated using Equation 30.

$$LLDF(int) = \frac{\max(\varepsilon)}{\sum_{i=1}^{n} \varepsilon_i} \quad (30)$$

where ε is strain and *n* is the number of girders.

Figure 49 shows the LLDF data for the interior girders. The results indicate that most of the LLDFs were in the range of 0.2 to 0.5. In the case of the Type I terragators, 94.5% of the bridge showed an LLDF of 0.2 to 0.5. The data above 0.5 were from the widest bridge subject to a 0% payload (empty load condition). These LLDFs were calculated from the strain induced by the front axle of a Type I terragator because the maximum strain was observed under the front axle. For the Type II terragators, 98% of the LLDF data were between 0.2 and 0.5. Any data above 0.5 were from the widest bridge specifically under the rear axle load of a Type II terragator.

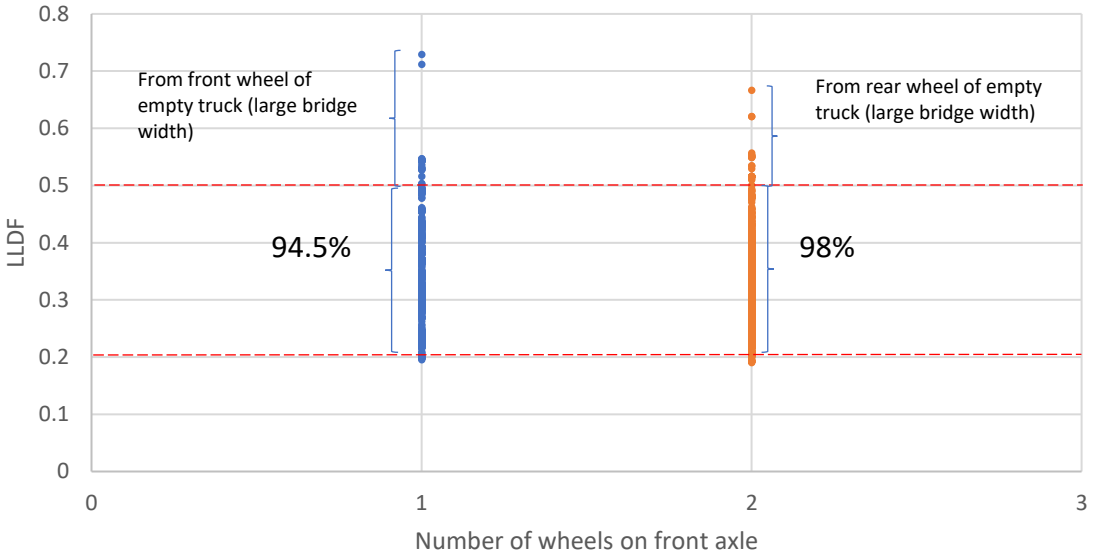

Figure 49. Interior girder $LLDF_{FEA}$ range of PC bridges

The LLDFs on the exterior girders were calculated using Equation 31.

$$LLDF(ext) = \frac{\text{exterior girder}(\varepsilon)}{\sum_{i=1}^{n} \varepsilon_i} \tag{31}$$

where ε is strain and n is the number of girders.

Figure 50 shows the LLDF data for the exterior girders. The majority of the data can be seen fall between 0.1 and 0.35 for both type of terragators.

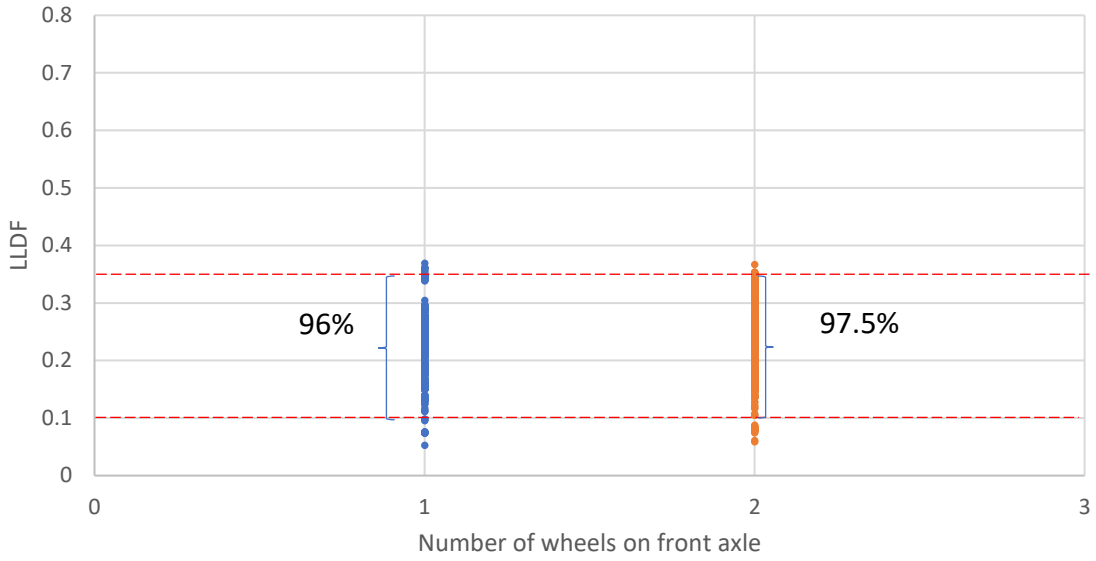

Figure 50. Exterior girder $LLDF_{FEA}$ range of PC bridges

6.3.1.3 Parametric Study Results

To understand the influence of bridge parameters on the LLDFs, the LLDFs for the interior girders and exterior girders were plotted against different bridge parameters, including bridge skew, span length, girder spacing, number of girders, and bridge width.

Figure 51 shows the influence of bridge skew angle on the interior girder LLDFs. The LLDF data for each skew angle seems to have a wide spread. This is due to the high number of bridges with a certain skew angle along with diverse combinations of varying other bridge parameters. In other words, it is possible that the influence of other bridge parameters is greater than that of the skew angle. Due to the spread of the LLDF data for each skew angle, the fit of the trend line generated does not give a high R value. The results indicate that as the bridge skew increases, the LLDF increases by approximately 0.2%.

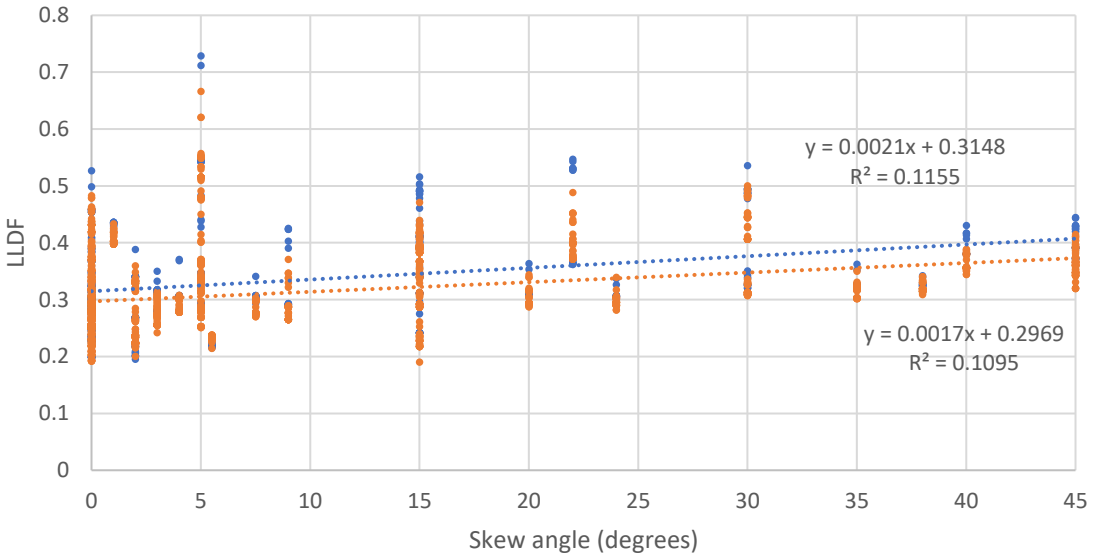

Figure 51. Interior girder LLDF versus skew angle for PC bridges

A similar trend can be observed in the plots for the other bridge parameters. Figure 52 shows the influence of span length on the LLDFs on the interior girders. The trend line suggests that for every foot increase in span length, the LLDF decreases by 0.02% to 0.06%.

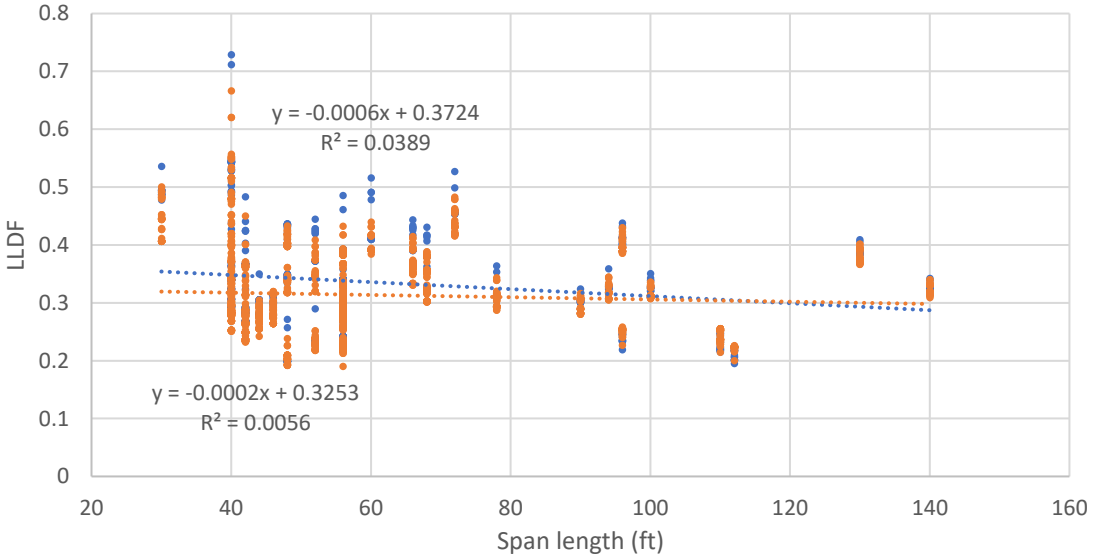

Figure 52. Interior girder LLDF versus span length for PC bridges

The influence of girder spacing on the interior girder LLDFs can be seen in Figure 53. According to the trend line for the data, for every foot increase in girder spacing, the LLDF increases by 3.5%.

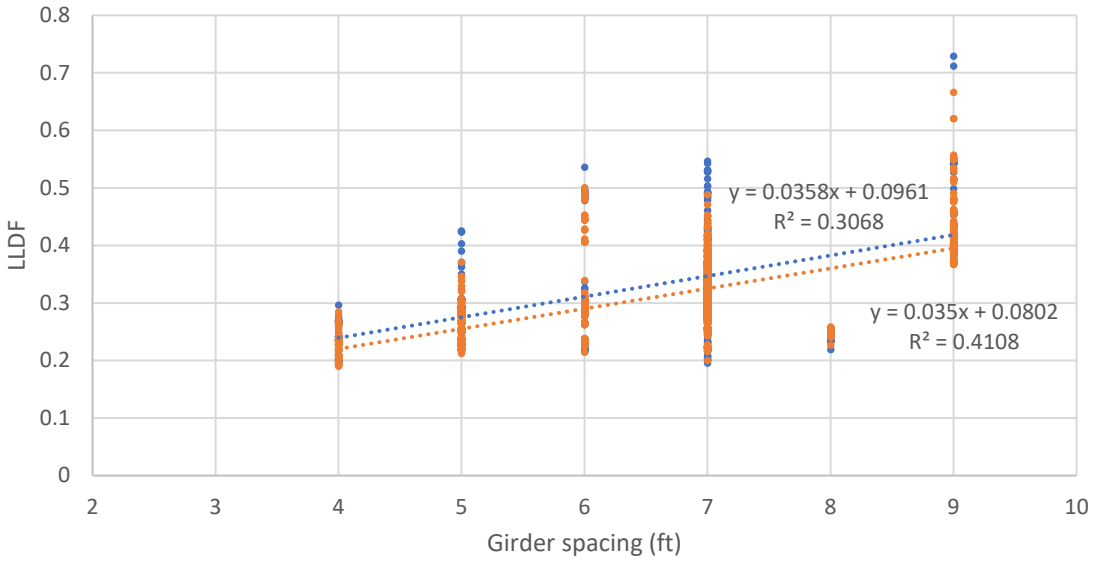

Figure 53. Interior girder LLDF versus girder spacing for PC bridges

Along with girder spacing, the number of girders also plays a role in the interior girders LLDFs, since a higher number of girders demands a greater distribution of load. This decreases the load concentration on any particular girder. As shown in Figure 54, the LLDF decreases by up to 1.8% for each girder added.

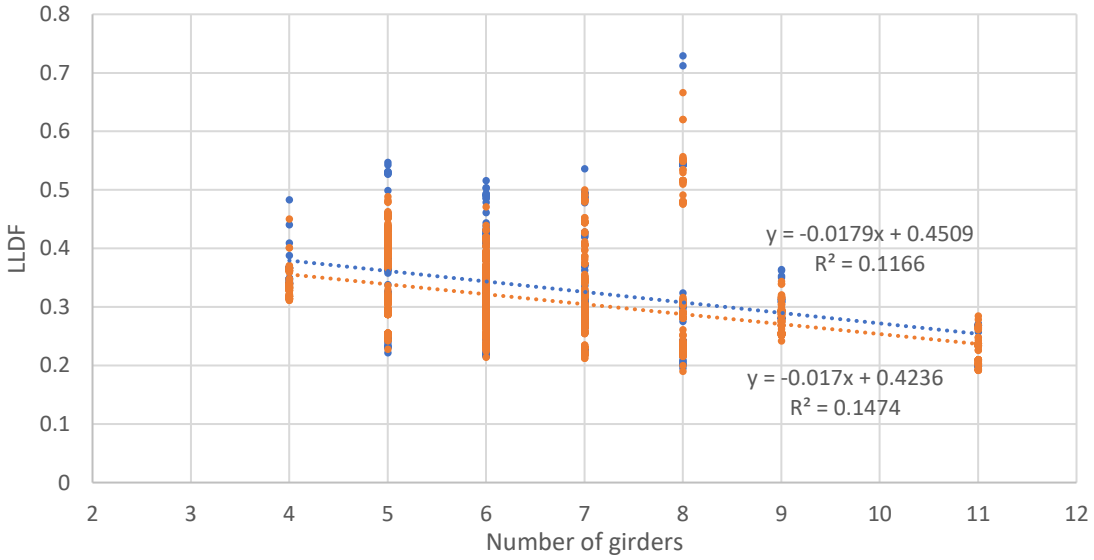

Figure 54. Interior girder LLDF versus number of girders for PC bridges

Figure 55 shows the influence of bridge width on the interior girder LLDFs. In this case, the LLDF increases by 0.16% with every foot increase in the bridge width.

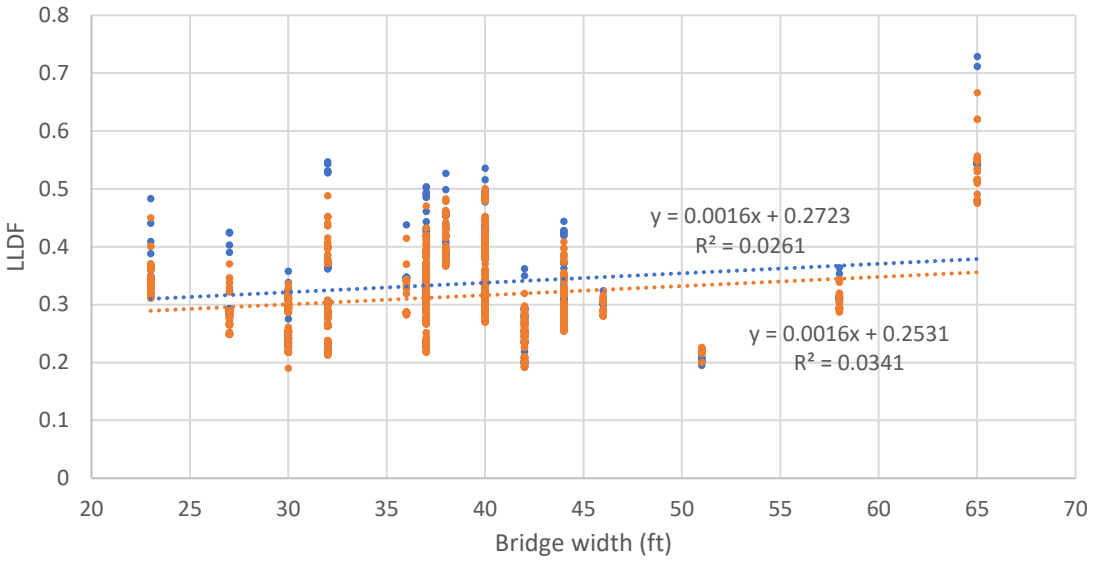

Figure 55. Interior girder LLDF versus bridge width for PC bridges

The AASHTO-recommended LLDF equation uses the ratio of girder spacing to span length. Therefore, to understand the influence of this ratio on the LLDFs in the FE analysis, the LLDF data for each bridge were plotted against the ratio of girder spacing to span length for each respective bridge. This plot can be seen in Figure 56.

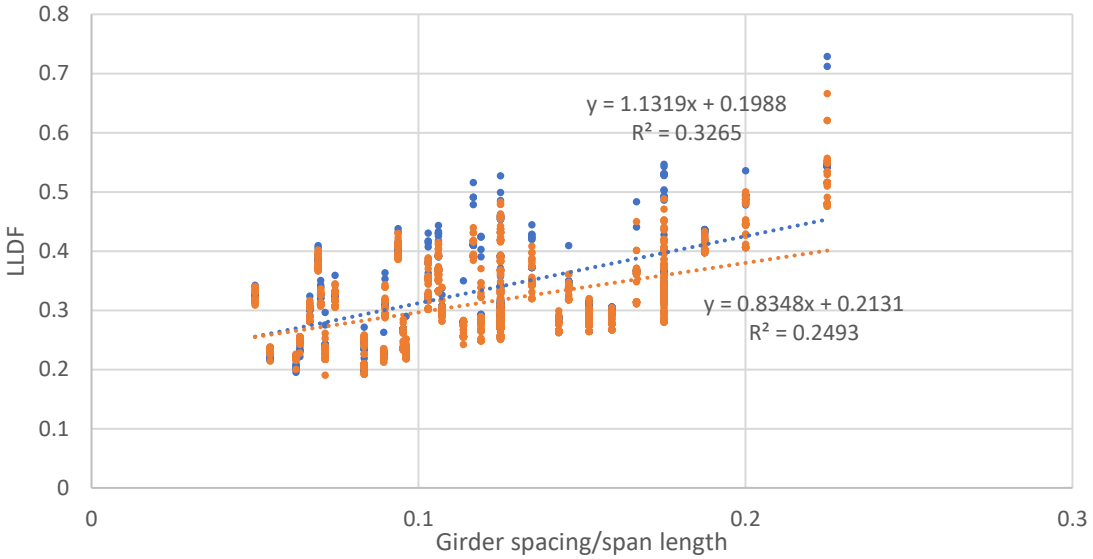

Figure 56. Interior girder LLDF versus ratio of girder spacing to span length for PC bridges

Figure 57 to Figure 61 show the influence of different bridge parameters on the exterior girder LLDFs.

Figure 57 shows that skew angle has a smaller effect on the exterior girder LLDFs than on the interior girder LLDFs, as shown in Figure 51. The LLDF increases by as little as 0.02% to 0.06% for each degree increase in skew angle.

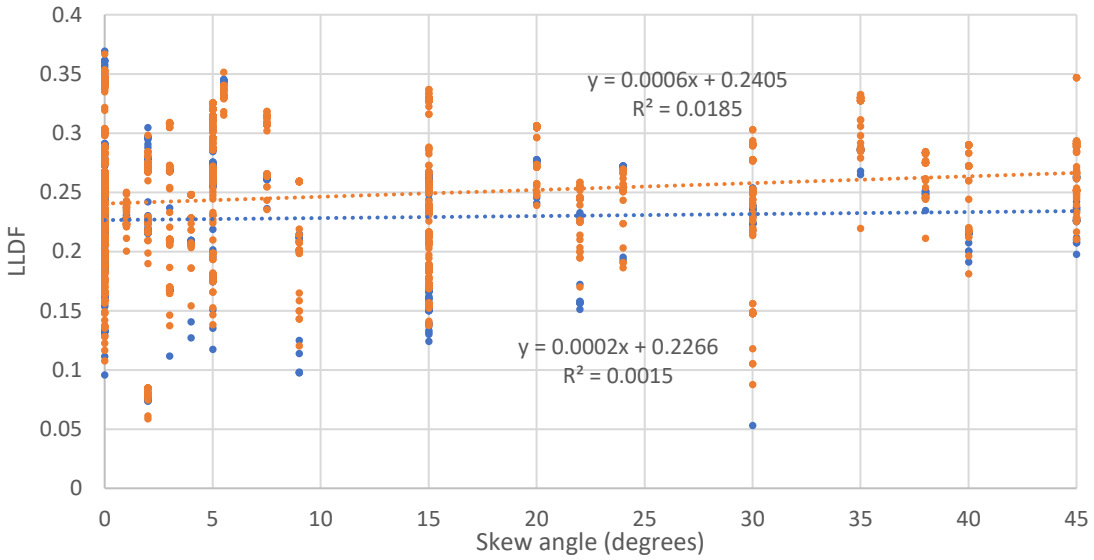

Figure 57. Exterior girder LLDF versus skew angle for PC bridges

Figure 58 indicates that span length has an effect on the exterior girder LLDFs opposite to its effect on the interior girder LLDFs. For each foot increase in span length, the LLDF for the exterior girders increases by 0.08% to 0.1%.

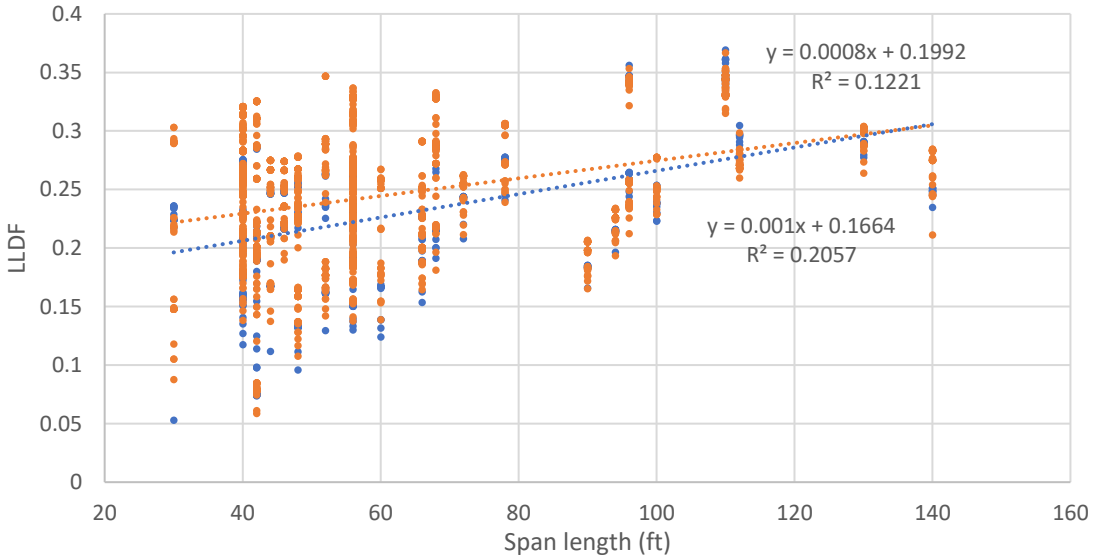

Figure 58. Exterior girder LLDF versus span length for PC bridges

Figure 59 shows that the effect of girder spacing on the exterior girder LLDFs is the same as on the interior girder LLDFs. Although girder spacing has a greater influence on the interior girders, its influence on the exterior girders is also significant. With every foot increase in girder spacing, the exterior girder LLDF increases by approximately 2.6%.

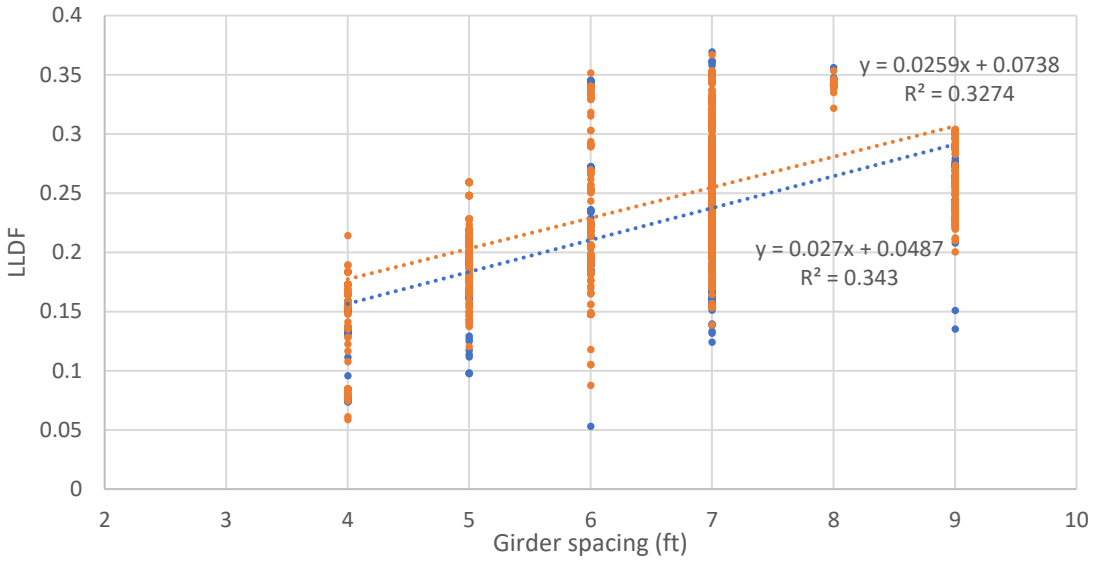

Figure 59. Exterior girder LLDF versus girder spacing for PC bridges

The impact of the number of girders on the exterior girder LLDFs is similar to that on the interior girder LLDFs. The exterior girder LLDF decreases by 1.8% with every additional girder. Figure 60 shows the trend of the exterior girder LLDFs as the number of girders increases.

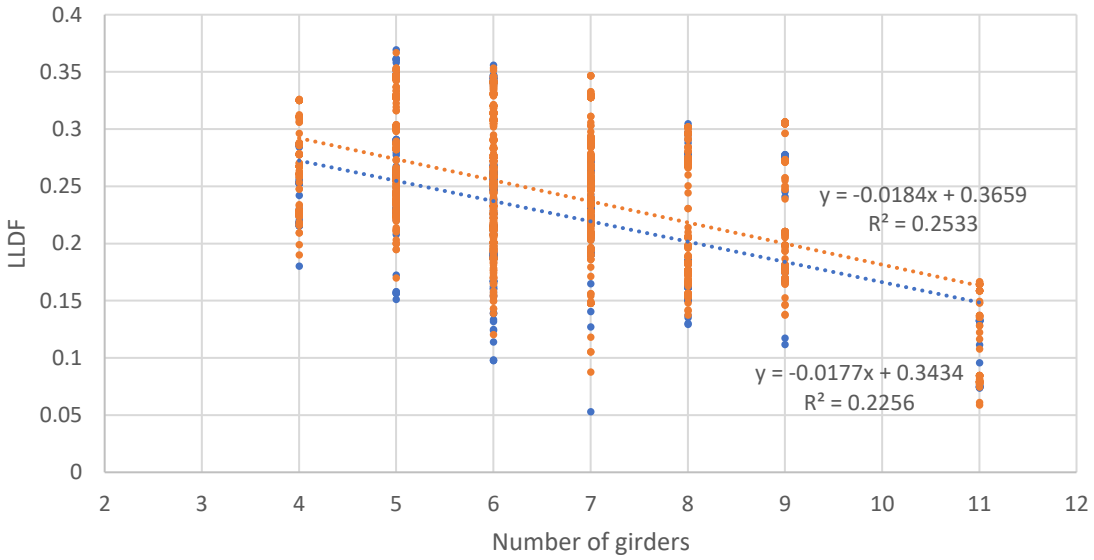

Figure 60. Exterior girder LLDF versus number of girders for PC bridges

Bridge width does not have as much of an effect on the exterior girder LLDFs compared to the other bridge parameters. With every foot increase in bridge width, the exterior girder LLDF increases by 0.02% to 0.04%. This can be seen in the trend line in Figure 61.

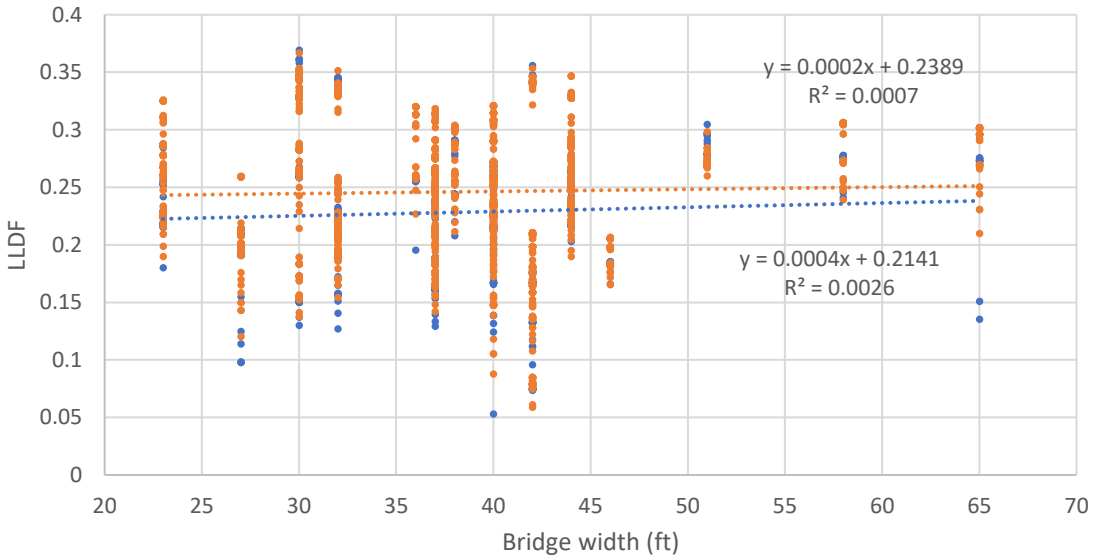

Figure 61. Exterior girder LLDF versus bridge width for PC bridges

Unlike for the interior girder LLDFs, the AASHTO-recommended equation for the exterior girder LLDFs does not include the ratio of girder spacing to span length. Regardless, the ratio was calculated and plotted against the exterior girder LLDFs, as shown in Figure 62, for consistency with the analysis of the interior girder LLDFs.

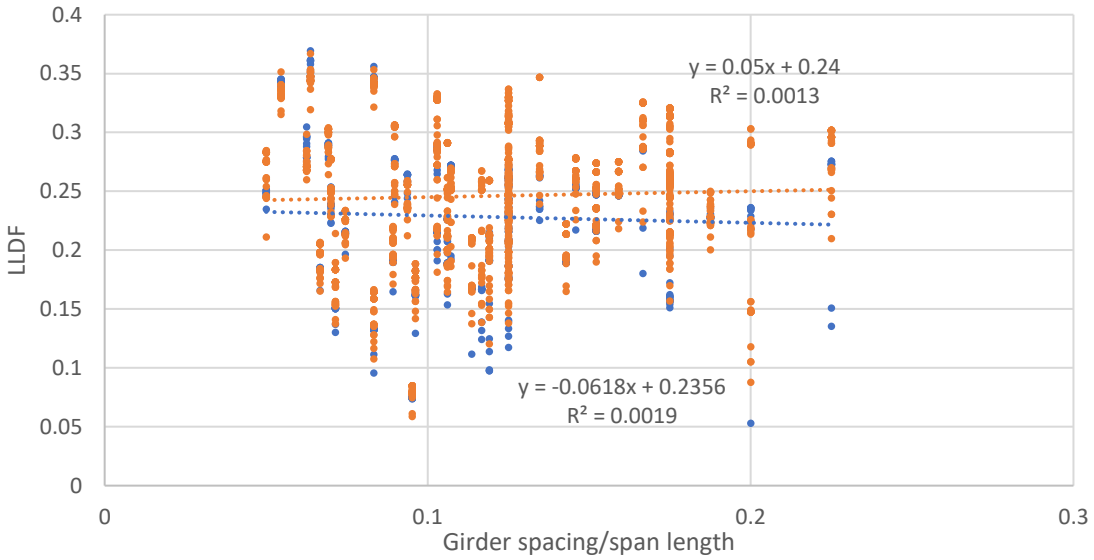

Figure 62. Exterior girder LLDF versus ratio of girder spacing to span length for PC bridges

Table 16 summarizes the impacts of the various bridge parameters on LLDF. The results indicate that girder spacing and number of girders are the most influential bridge parameters for both the interior and exterior girders.

Table 16. Impact of PC bridge parameters on LLDF

Bridge parameters	Interior	Effect	Exterior	Effect
Skew angle (degrees)	0.2% ↑	Notable	0.02%–0.06% ↑	Not Notable
Span length (ft)	0.02%–0.06% ↓	Not Notable	0.08%–0.1% ↑	Notable
Girder spacing (ft)	3.5% ↑	Notable	2.6% ↑	Notable
Number of girders	1.8% ↓	Notable	1.8% ↓	Notable
Bridge width (ft)	0.16% ↑	Notable	0.02%–0.04% ↑	Not Notable
Girder spacing/Span length	83%–113% ↑	Notable	-6.2%–5% ↑	Not Notable

6.3.1.4 Comparison with AASHTO-Specified Values

The LLDFs calculated from the FE models were compared with the AASHTO-specified limits. Equation 8, along with a skew reduction factor (AASHTO 2020), was used to calculate the LLDFs for the interior girders.

Figure 63 shows a plot of the calculated ratio of the FEA LLDFs to the AASHTO LLDFs for all bridges loaded by each terragator. Values above 1 indicate that the LLDFs from the FE analysis were higher than the AASHTO LLDFs.

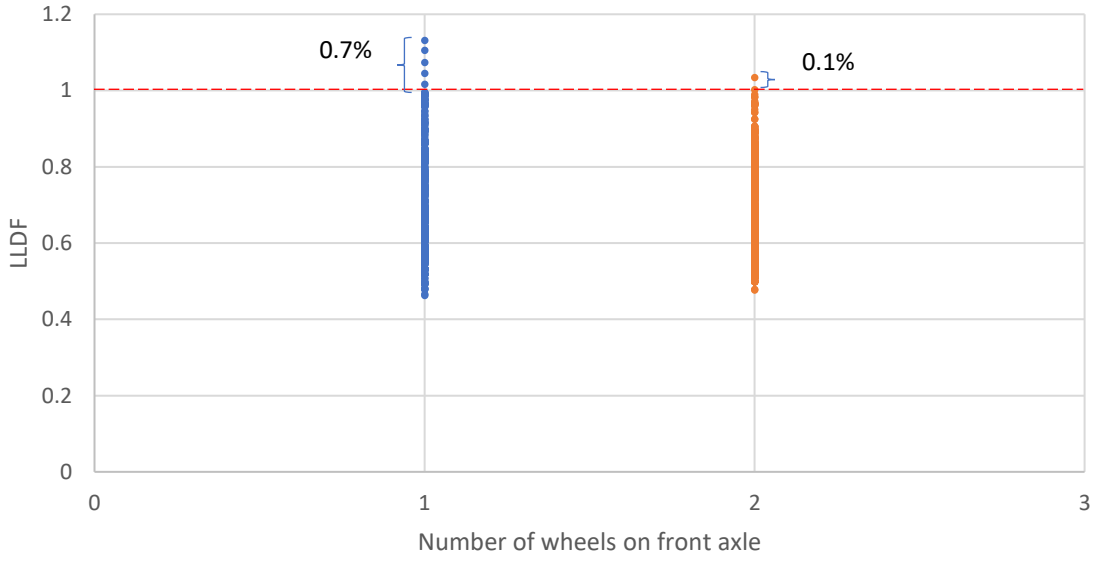

Figure 63. Ratio of $LLDF_{FEA}$ to $LLDF_{AASHTO}$ on interior girders for PC bridges (all terragators)

An analysis of the FEA LLDFs that were higher than the AASHTO LLDFs indicated that the FEA LLDF data were obtained from a few bridges loaded by empty terragators. Since lighter vehicles do not contribute to high strain values, these cases can likely be ignored.

Therefore, a similar plot was created to show the LLDFs calculated only for terragators with a payload of 100%. Figure 64 shows the plot of LLDFs for fully loaded terragators. The results indicate that none of the ratio values are above 1, which shows that the AASHTO equation is adequate for the chosen bridges.

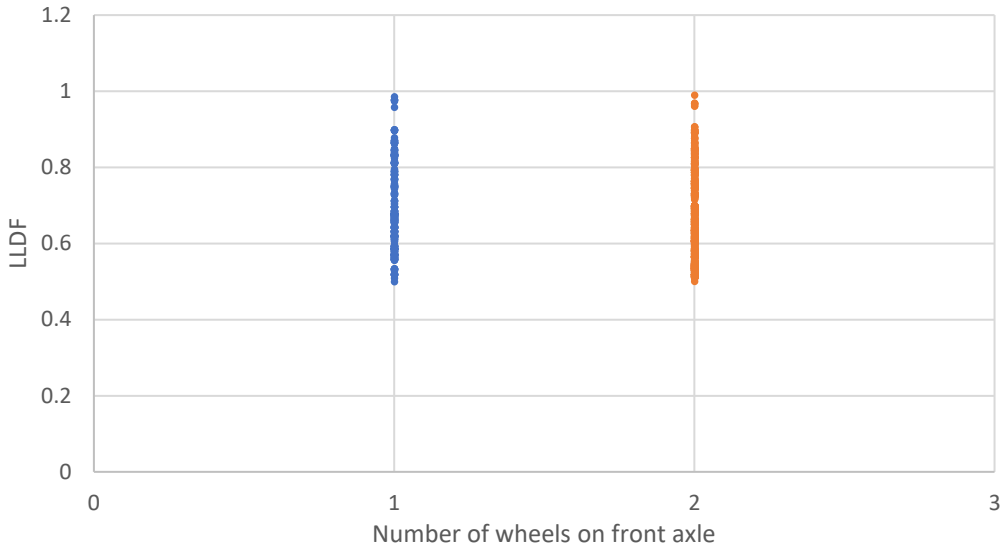

Figure 64. Ratio of $LLDF_{FEA}$ to $LLDF_{AASHTO}$ on interior girders for PC bridges (full terragators only)

AASHTO recommends the lever rule to calculate the exterior girder LLDFs. However, the lever rule cannot be used in the case of terragators because they have a wide axle that places the wheel load beyond the second or even third girder in some instances. This creates a situation where a hinge placed at the second girder will produce reactions at more than one girder, thus resulting in additional unknown variables. In such a situation, Equation 32 is recommended by the AASHTO LRFD (2020) to calculate the LLDFs on exterior girders.

$$R = \frac{N_L}{N_b} + \frac{X_{ext}\sum_1^{N_L} e}{\sum_1^{N_b} x^2} \quad (32)$$

where R is the reaction on an exterior beam in terms of lanes, N_L is the number of loaded lanes under consideration, e is the eccentricity of a design truck or a design lane load from the center of gravity of the pattern of girders (ft), x is the horizontal distance from the center of gravity of the pattern of girders to each girder (ft), X_{ext} is the horizontal distance from the center of gravity of the pattern of girders to the exterior girder (ft), and N_b is the number of beams or girders. R is then multiplied by 1.2 to accommodate the presence of multiple loads in one lane. This multiplier may not be needed for narrow bridges.

Figure 65 shows the ratio of the FEA LLDFs calculated on the exterior girders to the AASHTO LLDFs for all terragators irrespective of their payload condition. All of the ratios fall well below 1.0. Thus, the LLDFs calculated using the AASHTO equation can be said to be adequate for the exterior girders.

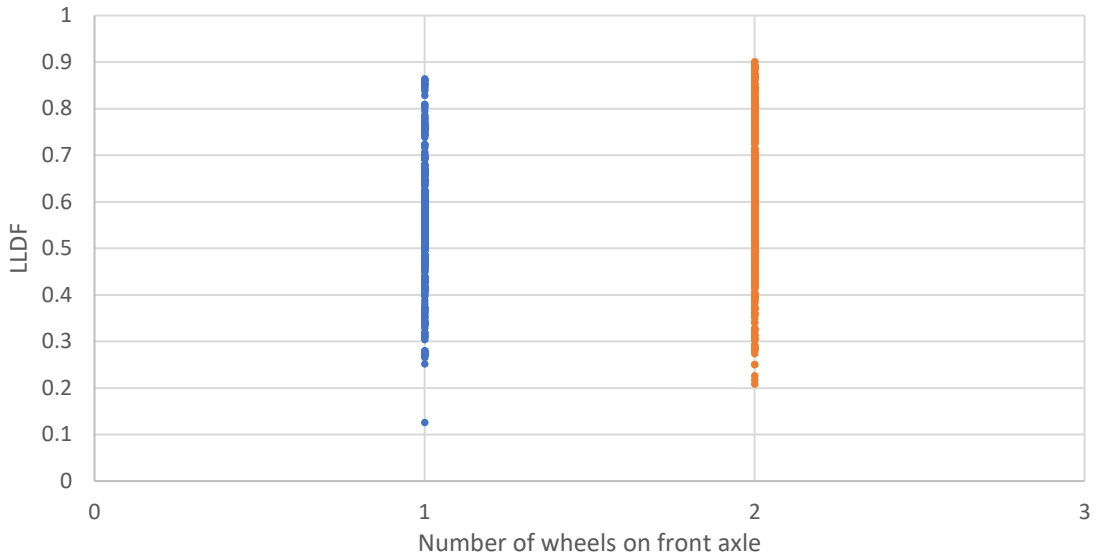

Figure 65. Ratio of $LLDF_{FEA}$ to $LLDF_{AASHTO}$ on exterior girders for PC bridges (all terragators)

Along with the FE analyses of the 50 PC bridges under 56 different terragator loads, an additional FE analysis was performed to determine the strains and LLDFs under HS-20 axle loads. The charts shown in Figure 66 and Figure 67 compare the LLDFs from fully loaded terragators with the LLDFs from the HS-20 load and the LLDFs predicted by the AASHTO equations for interior and exterior girders, respectively. The range of calculated LLDFs attributable to the 56 terragator loads for each bridge is represented by the vertical bar.

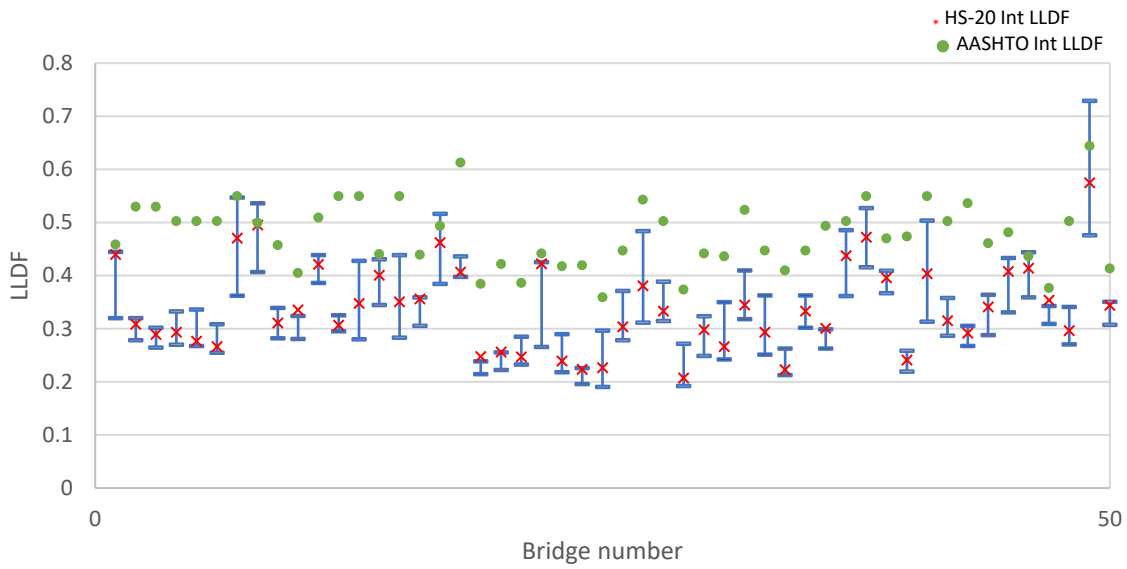

Figure 66. Interior girder LLDF range for PC bridges

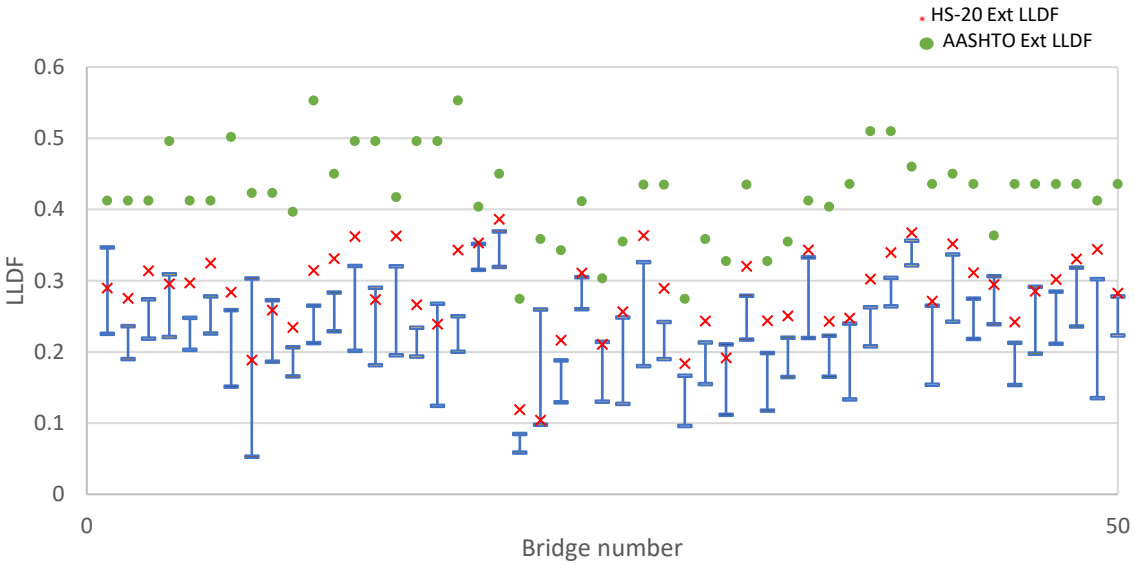

Figure 67. Exterior girder LLDF range for PC bridges

Figure 66 shows the results of the comparison for the interior girders. The results indicate that the LLDFs induced by the terragator loads are higher than those induced by the HS-20 load. This is because the axle loads on some terragators are heavier than the HS-20 load. Some bridges also show higher LLDFs than those calculated from the AASHTO equation.

Figure 67 indicates that the LLDFs induced by the HS-20 load are higher than most of the LLDFs induced by the fully loaded terragators for the exterior girders. This is because the axle width of the HS-20 truck is smaller than that of any of the terragators while the distance of all

vehicles from the barrier is the same. Therefore, the terragator loads tend to spread to the center of the bridges.

Further, to verify whether the strain range for each bridge due to the terragator loads was below the strain due to the HS-20 load, a plot of the maximum strain from each model was created. Figure 68 shows the strain on each bridge under each terragator load along with the HS-20 load.

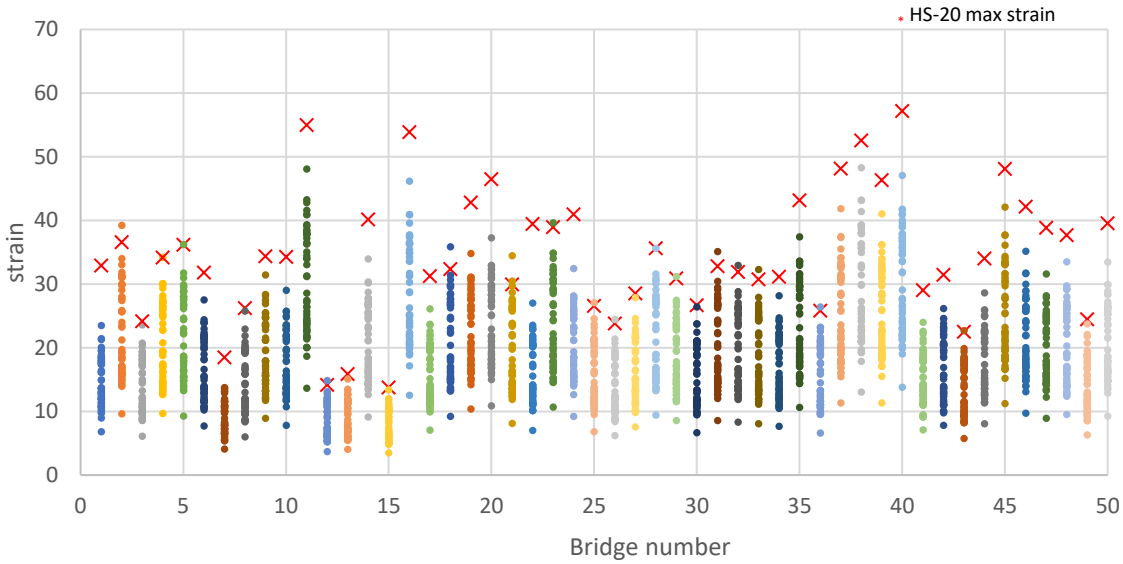

Figure 68. Maximum strain range on each PC bridge

Most bridges show strain data below the strain due to the HS-20 load, including the bridge that showed higher LLDFs than the LLDFs calculated using the AASHTO equations. A few bridges show strains that are above the strain of the HS-20 load (1.8%), but these values represent one data point out of 56 data points on a single bridge. This data point is the result of one terragator (TG 9300) having an axle load of 45 kips, which is higher than the HS-20 axle weight of 32 kips.

6.3.2 Slab Bridges

Table 17 lists the important bridge parameters for the 50 slab bridges used in the parametric study.

Table 17. Bridge parameters of 50 slab bridges

Bridge ID	Skew angle	Span 1 length (ft)	Span 2 length (ft)	Width (ft)	Slab thickness (in.)
0639.2S218	10	27.5	35	44	16.25
0713.9S281	0	36.5	47	40	20
0656.8S218	-30	42.5	55	40	24.5
0661.8S218	0	30.5	39	40	17.5
1009.2S187	-40	36.5	47	36	18.75
0823.2S169	0	30		40	18.5
1341.8S004	-20	24.5	31	30	18.5
3709.8S030	0	34	42	30	20.5
3725.1S004	-30	39.5	51	44	20
3735.3S004	25	36.5	47	40	20
3805.2S175	0	27.5	35	40	15
3808.2S175	-45	30		30	24
3809.2S175	10	21	28	40	15.5
3812.6S175	-30	39.5	51	40	20
3815.1S175	0	28.5	28.5	40	16
3815.4S014	0	30	30	30	17
4033.8S017	-15	39.5	51	44	20
4036.9S069	-39	33.5	43	40	18.5
4044.1L035	0	42	56	40	21.5
4048.9L035	-30	27.5	35	40	15.75
4055.6S175	0	30.5	39	32	16.5
4227.3S065	10	24.5	31	40	15.25
1029.8S281	0	23	29	36	15.75
4239.4S065	0	39.5	51	40	21.25
4242.4S065	0	27.5	35	44	20
5014.6S117	-30	37.25	45.5	30	21.25
5017.5S117	0	30		34	21.25
5054.2R080	-30	30.5	39	40	21.25
5059.1S014	-15	38	49	44	19
5059.5L080	15	30.6	39	30	16
5063.8S014	15	36.5	47	44	18.75
5065.1S014	-15	39.5	51	44	20.5
5079.7S006	0	39.5	51	40	20
5083.2S006	-15	27.5	35	40	16
6410.1S014	0	24.5	31	44	13.75
6417.6L330	45	39.5	51	44	20
6496.5S014	30	36.5	47	44	18.75
6497.7S014	15	41	53	44	22
7900.9S006	0	31	38	28	19
7906.6S006	0	38.5	48	30	22.25
7925.1S021	30	39.5	51	40	21.25
7926.5S021	0	33.5	43	40	18.5
7984.7L080	0	34.25	44	40	16.5
8522.7S065	-15	30.5	39	40	17.5
8527.8S210	45	38.5	48	28	21.25
8554.2L030	0	24.5	31	40	15.25
9164.6L065	-30	26.45	32.33	40	15.75
9430.2R020	0	35	45	40	18.2
9451.2S169	-30	27.5	35	44	15.75

6.3.2.1 Maximum Strain Results

Strain data from the bottom of the slab at mid-span were extracted from the 2,800 slab bridge models and analyzed. As in previous sections, the results are discussed individually for the two different types of terragators identified in Section 6.3.1.1.

Figure 69 shows the maximum strains from the 2,800 slab bridge models. Based on the strain data collected, 95% of the maximum strains on these bridges fell between 7 and 27 microstrain. The data points shown in orange are from the front axle of Type I terragators (those with one wheel on the front axle) in an empty load condition. These data points constituted 4.7% of the data sample (134 models out of 2,800). Since these data were from axles with one wheel, the equivalent strip widths were narrow. Additionaly, since these data were from empty vehicle loads, the maximum strain values were low. Therefore, these data points were eliminated from all further analyses described in Section 6.3.2.

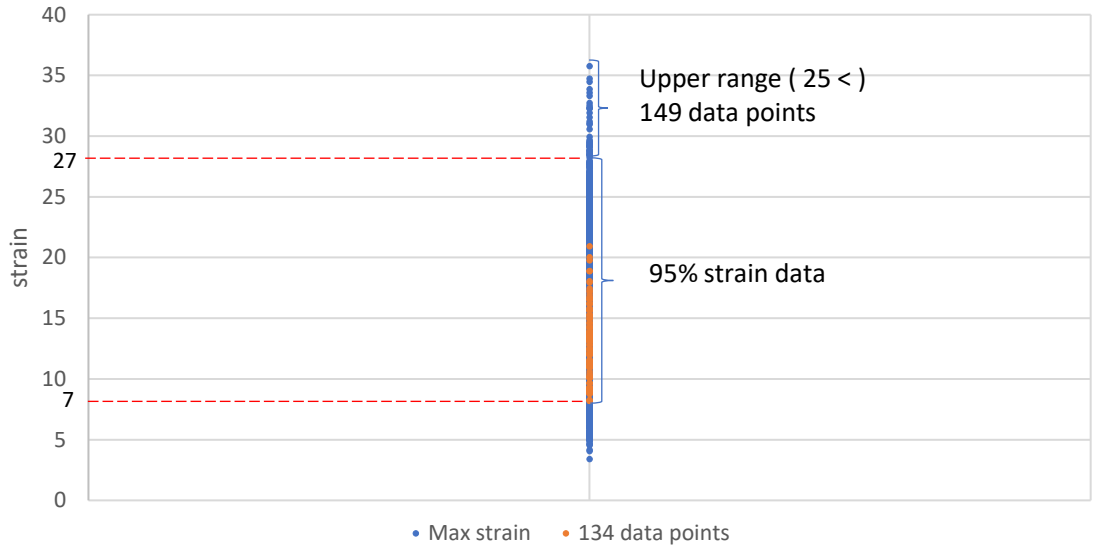

Figure 69. Maximum strain range of slab bridges

6.3.2.2 Determination of E

Equation 26 was used to calculate the equivalent strip widths (E) for the FE models. E was then used in the parametric study to evaluate the influence of various bridge parameters on strip width. These E values were compared with the E values calculated using the relevant AASHTO-recommended equation (Equation 5).

6.3.2.3 Parametric Study Results

In this parametric study, the effect of skew angle, bridge width, slab thickness, and span length on equivalent strip width was investigated. Figure 70 to Figure 73 shows the effects of skew angle, bridge width, slab thickness, and span length, respectively, on E.

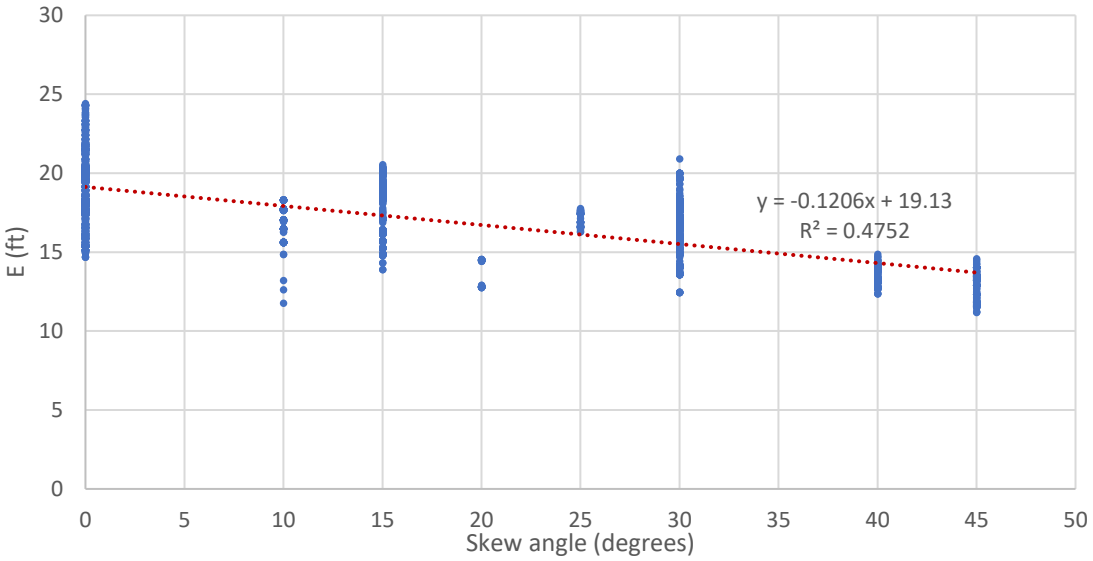

Figure 70. Equivalent strip width versus skew angle for slab bridges

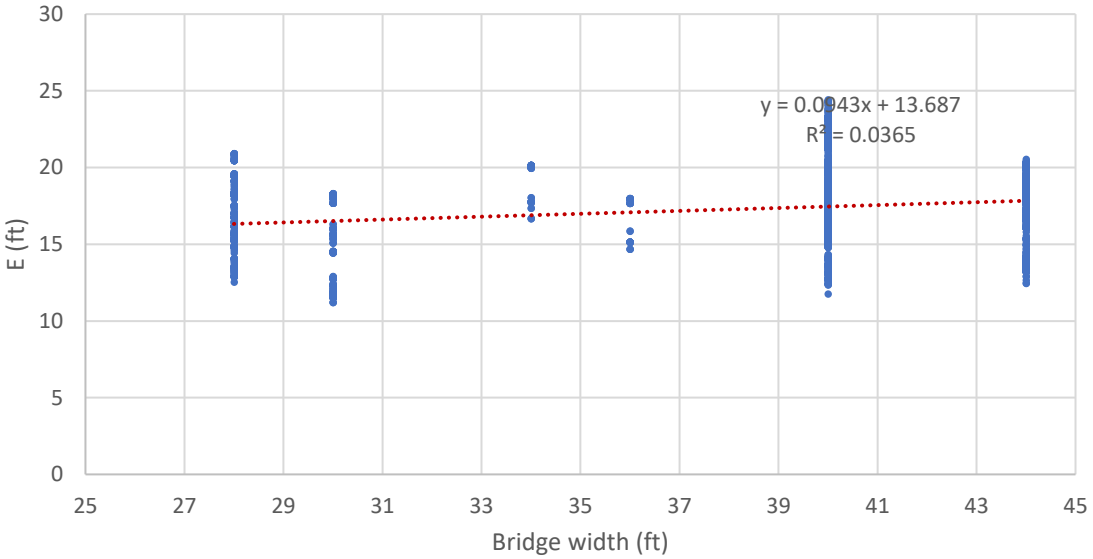

Figure 71. Equivalent strip width versus bridge width for slab bridges

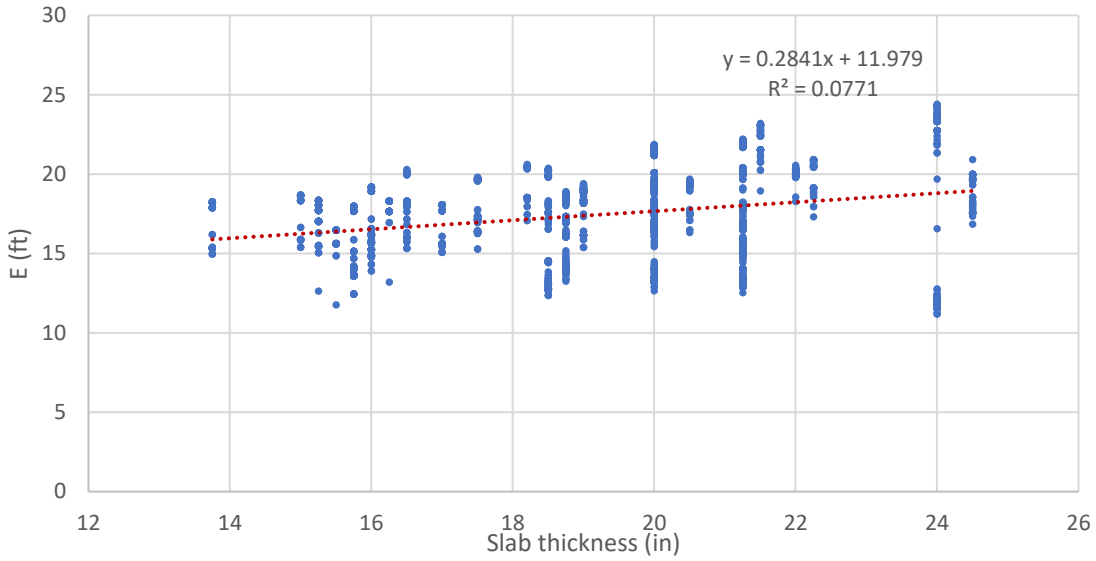

Figure 72. Equivalent strip width versus slab thickness for slab bridges

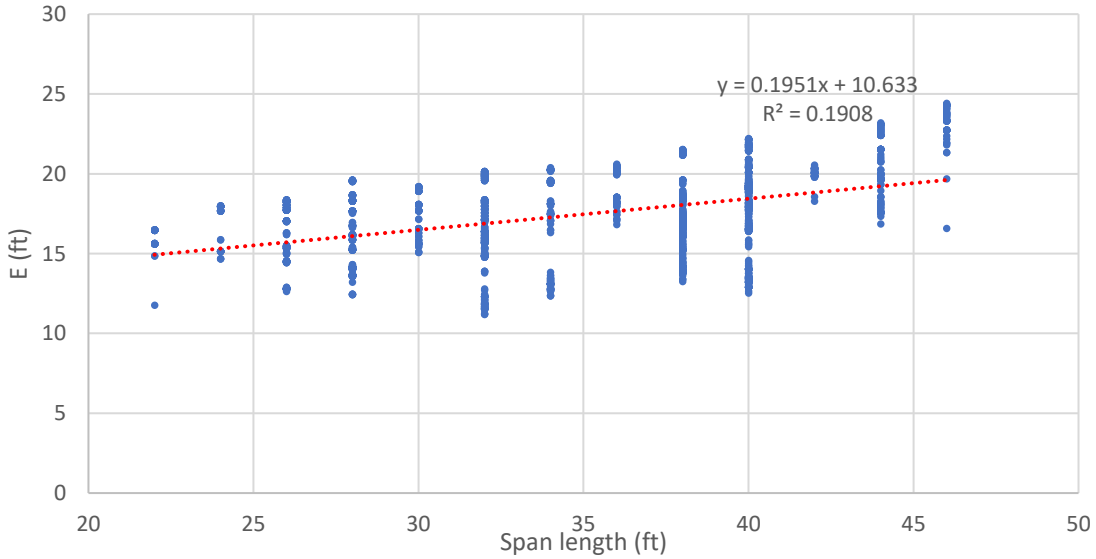

Figure 73. Equivalent strip width versus span length for slab bridges

The results indicate that skew angle, slab thickness, and span length have a notable effect on E. As skew angle increases, E decreases by 0.12 ft per degree increase in skew angle. In the case of bridge width, E increases by 0.09 ft per foot increase in bridge width.

It was found that the parameter that shows the greatest influence on E is slab thickness. The equivalent strip width increases by 0.28 ft per inch increase in slab thickness. Span length also has a notable effect on E; E increases by 0.19 ft per foot increase in span length.

Table 18 summarizes the effects of the various bridge parameters on equivalent strip width.

Table 18. Impact of slab bridge parameters on E

Bridge parameter	E (ft)	Effect
Skew angle (degrees)	0.12 ↓	Notable
Bridge width (ft)	0.09 ↑	Not Notable
Slab thickness (in.)	0.28 ↑	Notable
Span length (ft)	0.19 ↑	Notable

6.3.2.4 Comparison with AASHTO-Specified Values

The AASHTO-recommended equation (Equation 5) was used to calculate E for each of the 50 slab bridges. This was done to understand how the E values calculated from the FE analyses compare with the AASHTO limits. Equation 5 is recommended by AASHTO for calculating equivalent strip width when one lane is loaded

Note that the calculated equivalent strip width was multiplied by a skew reduction factor, r, when applicable.

The ratio of E_{FEA} to E_{AASHTO} was calculated to compare the results from the parametric study with the AASHTO-specified values. The results are presented in Figure 74. The ratios above 1 had parametric study E values that were greater than those predicted by the AASHTO equation. The ratios below 1 had parametric study E values that were narrower than the AASHTO-specified E values. It was found that the ratios below 1 were all from cases in which a Type I terragator was carrying a zero payload.

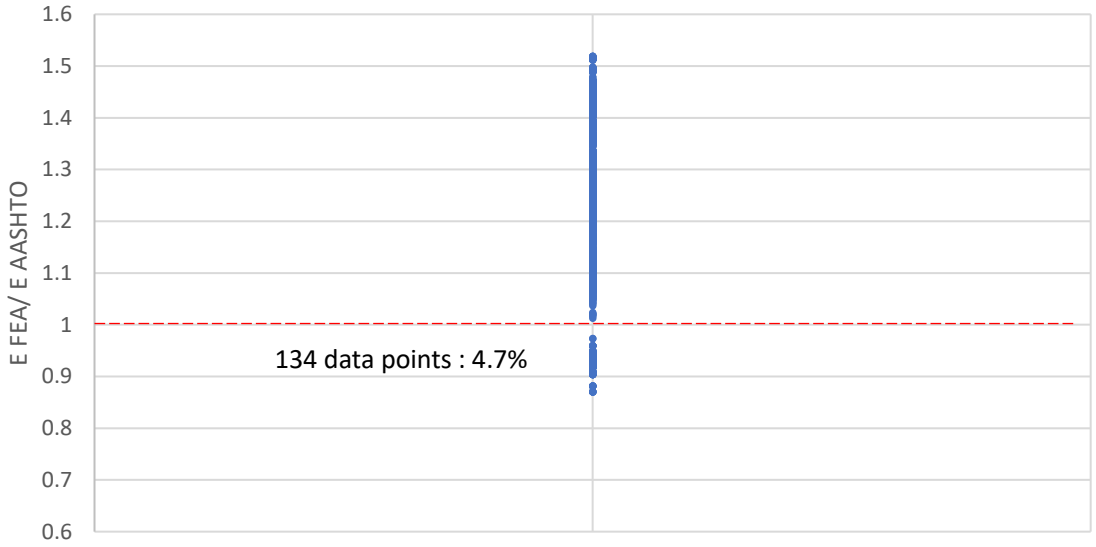

Figure 74. Ratio of E_{FEA} to E_{AASHTO} for slab bridges

Similar to parametric study of PC bridges, an additional FE analysis was completed for the 50 slab bridges to determine the strain and load distributions under the HS-20 axle load. The chart shown in Figure 75 compares the range of E values from the parametric study with the E values from the HS-20 load and the E values calculated using the AASHTO equation for each bridge. The E values from the HS-20 load were found to be in the range of the E values from the FE analysis.

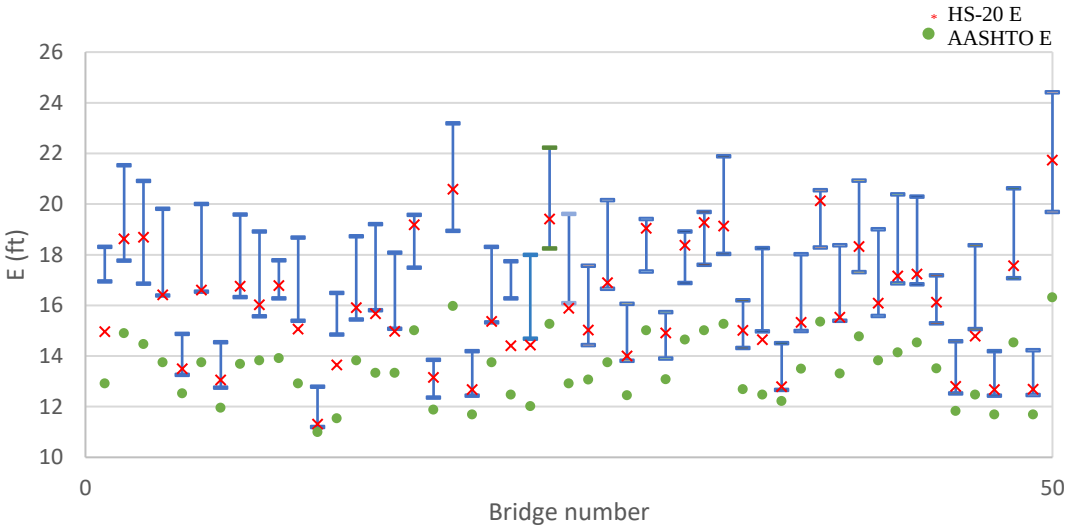

Figure 75. Equivalent strip width range on each slab bridge

Further, the maximum strain range for each bridge under the terragator loads was compared to the strain from the HS-20 load. Figure 76 shows the strain ranges for all of the slab bridges along with the strain from the HS-20 load.

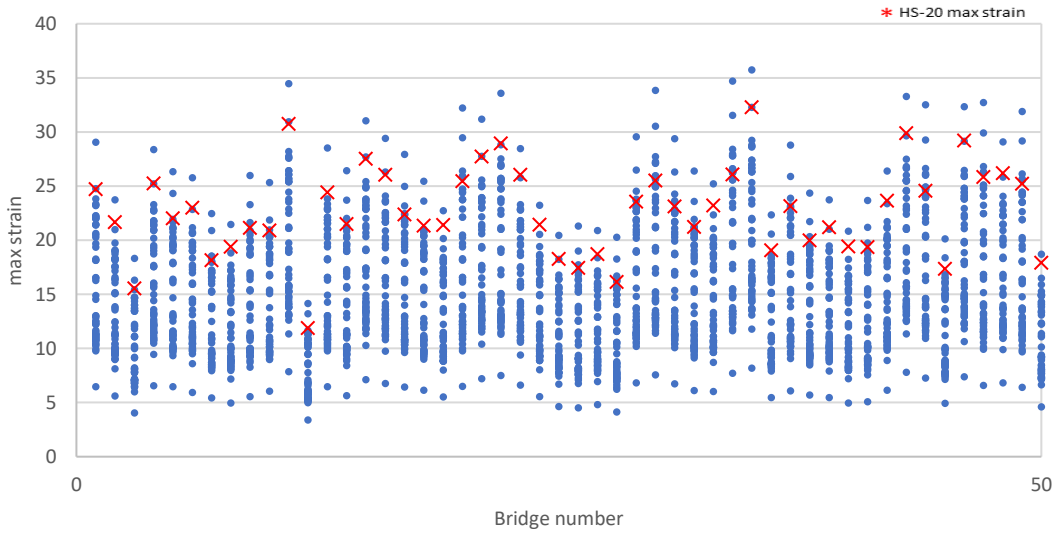

Figure 76. Maximum strain range on each slab bridge

6.3.3 Steel Girder Bridges

For the steel girder bridges, the five calibrated bridge models described in Section 6.2.3 were loaded with the 56 terragator load configurations summarized in Table 14. In total, 280 analyses were performed. The longitudinal strains from the bottom of the steel girders at mid-span of the first span of each bridge were extracted from the analysis results.

6.3.3.1 Maximum Strain Results

The maximum strain from each analysis is plotted in Figure 77 to show the range of maximum strain on the bridges under varying loads. The results indicate that 94% of the strain data fell between 30 and 120 microstrain.

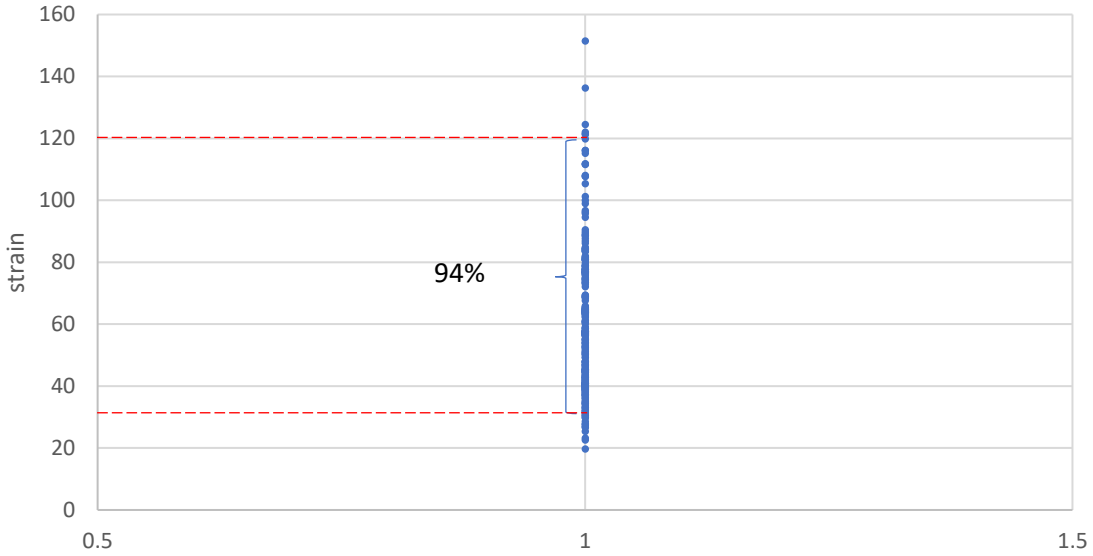

Figure 77. Maximum strain range of steel girder bridges

6.3.3.2 Determination of LLDF

The longitudinal strains from the bottom of the steel girders at mid-span of the first span of each bridge were used to calculate the LLDFs on the interior and exterior girders. The LLDF was calculated for each FE model using the same equation as that used for the PC bridges.

Figure 78 shows the range of interior girder LLDFs. It can be seen that 98.5% of the interior girder LLDF data fell under 0.35. The circled data were extracted from a single bridge. The data from all other bridges were below 0.22. The bridge that showed the highest LLDFs had 5 girders, while the other bridges had 9 to 12 girders. This bridge also had a high girder spacing.

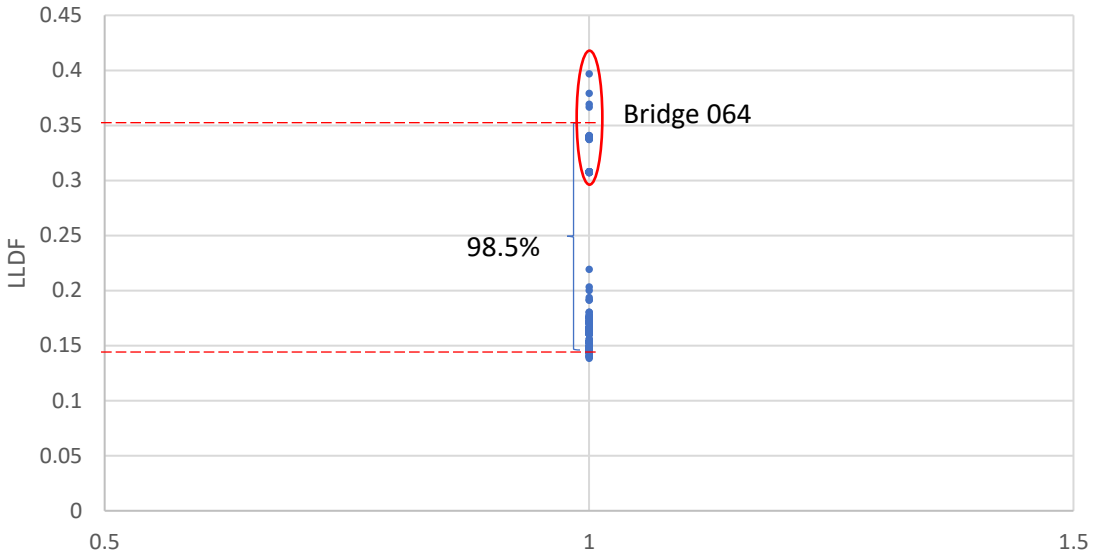

Figure 78. Interior girder LLDF range of steel girder bridges

The exterior girder LLDFs for the steel bridges are shown in Figure 79. All of the exterior girder LLDF data fell under 0.16.

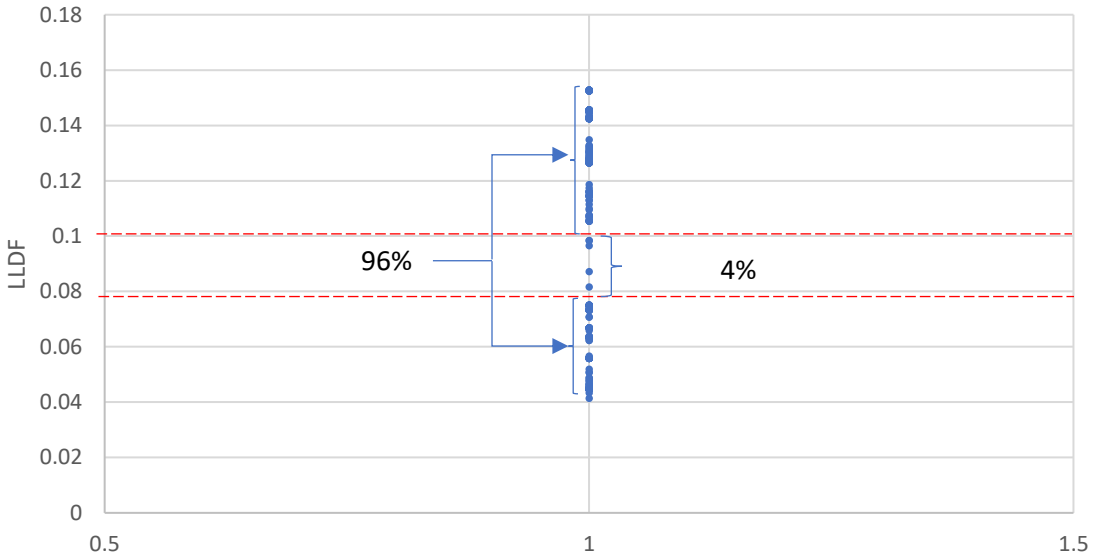

Figure 79. Exterior girder LLDF range of steel girder bridges

6.3.3.3 Parametric Study Results

The LLDFs calculated from the FE analyses were plotted against various bridge parameters to understand the influence of those bridge parameters on the LLDFs. The bridge parameters that were investigated included span length, girder spacing, number of girders, and bridge width. Skew angle was not investigated because none of the bridges were skewed. Additionally, the

ratio of girder spacing to span length was investigated. This was done because the AASHTO-recommended equation for the LLDFs on the interior girders contains the ratio of girder spacing to span length.

Figure 80 to Figure 84 show plots of the interior girder LLDFs against span length, girder spacing, number of girders, bridge width, and the ratio of girder spacing to span length, respectively. The main objective of conducting a parametric study of the steel girder bridges was to understand whether the load distribution behavior of these bridges is similar to that of the PC bridges. Based on the observed influence of the various bridge parameters on the LLDFs, it was found that girder spacing, number of girders, and the ratio of girder spacing to span length show similar trends to those found for the PC bridges. The same was not inferred for span length and bridge width.

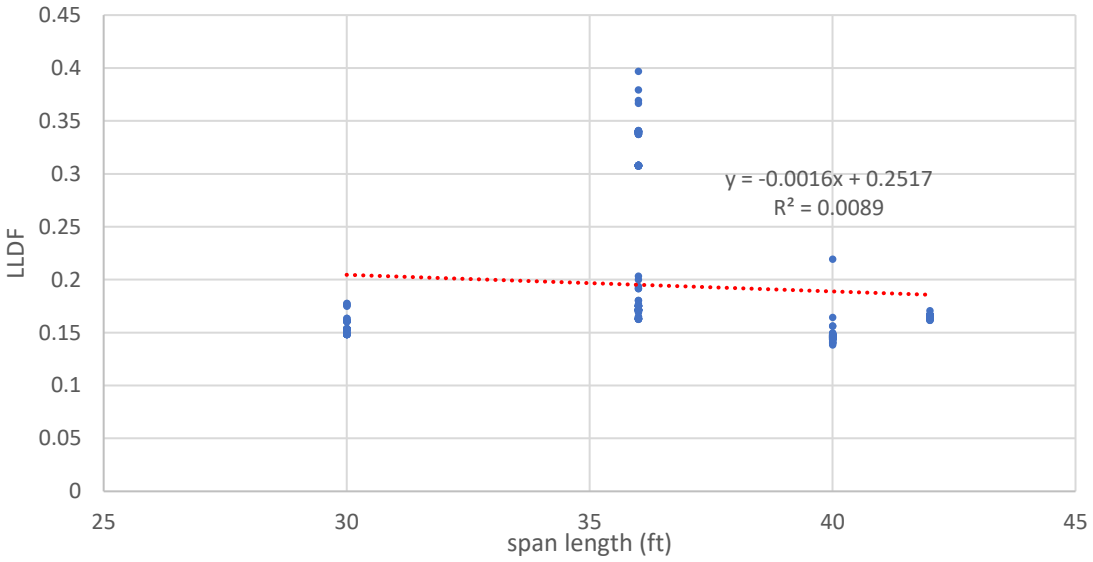

Figure 80. Interior girder LLDF versus span length for steel girder bridges

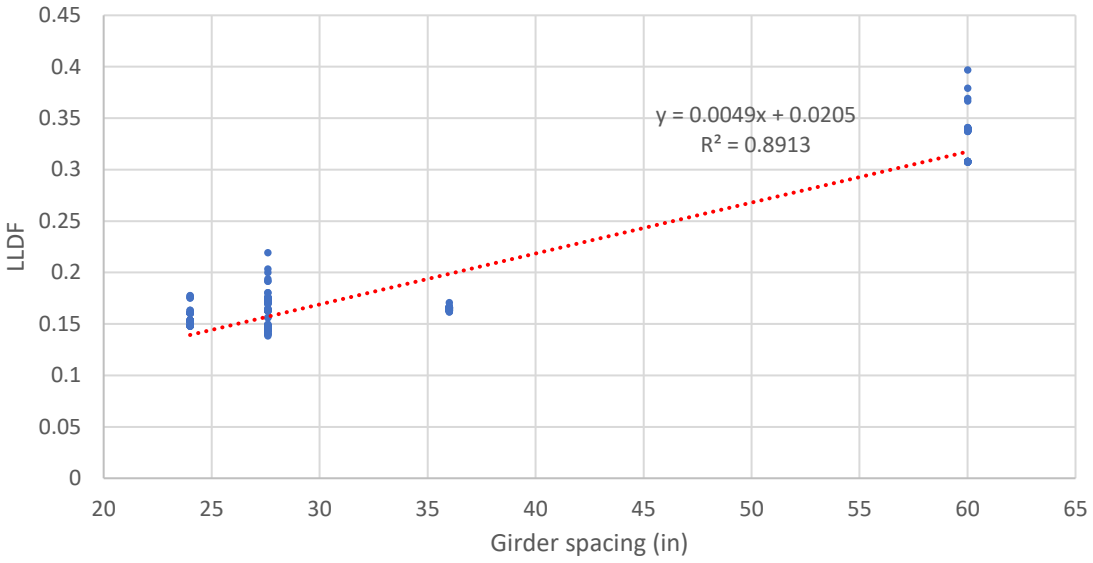

Figure 81. Interior girder LLDF versus girder spacing for steel girder bridges

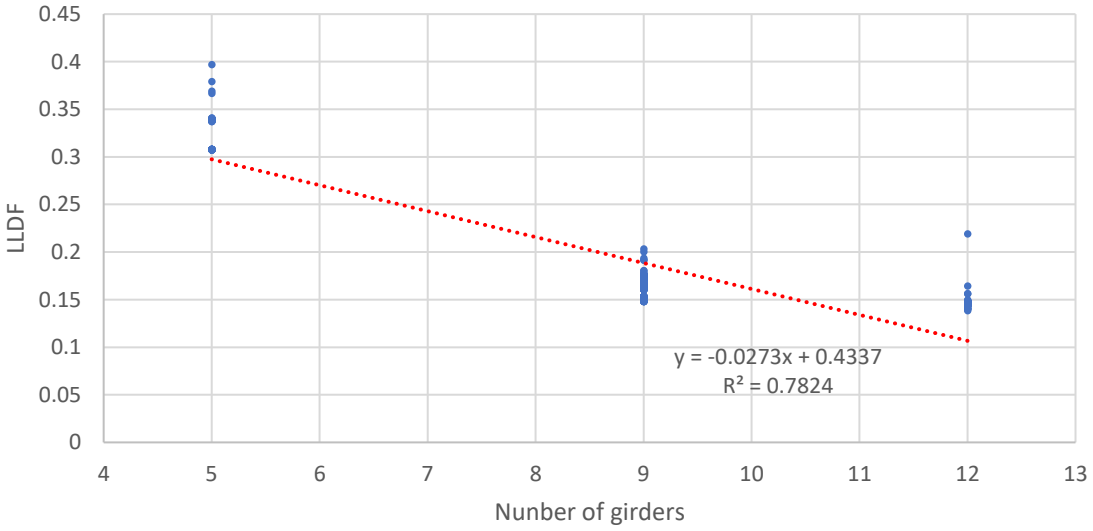

Figure 82. Interior girder LLDF versus number of girders for steel girder bridges

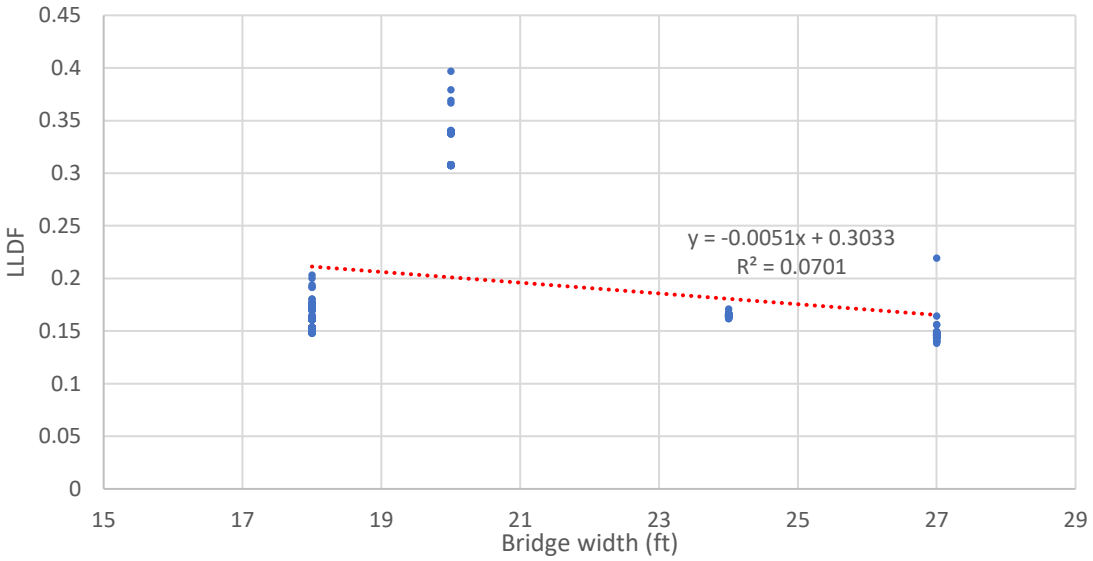

Figure 83. Interior girder LLDF versus bridge width for steel girder bridges

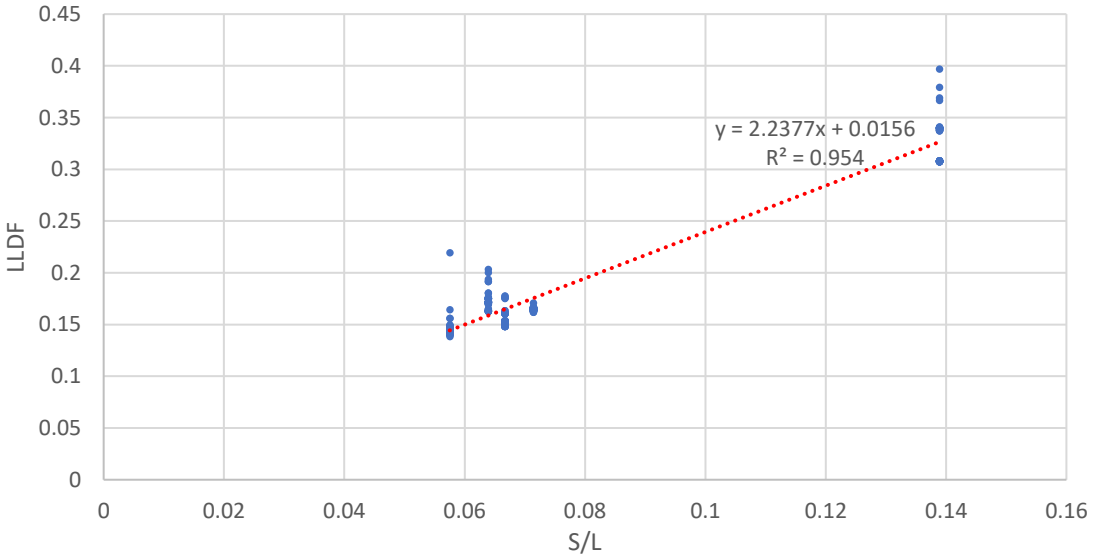

Figure 84. Interior girder LLDF versus ratio of girder spacing to span length for steel girder bridges

The same procedure was used to investigate the effects of the bridge parameters on the exterior girder LLDFs. Figure 85 to Figure 89 show plots of the exterior girder LLDFs versus span length, girder spacing, number of girders, bridge width, and the ratio of girder spacing to span length, respectively. The charts suggest that all of the bridge parameters show effects on the exterior girders of steel girder bridges similar to those on the exterior girders of PC bridges.

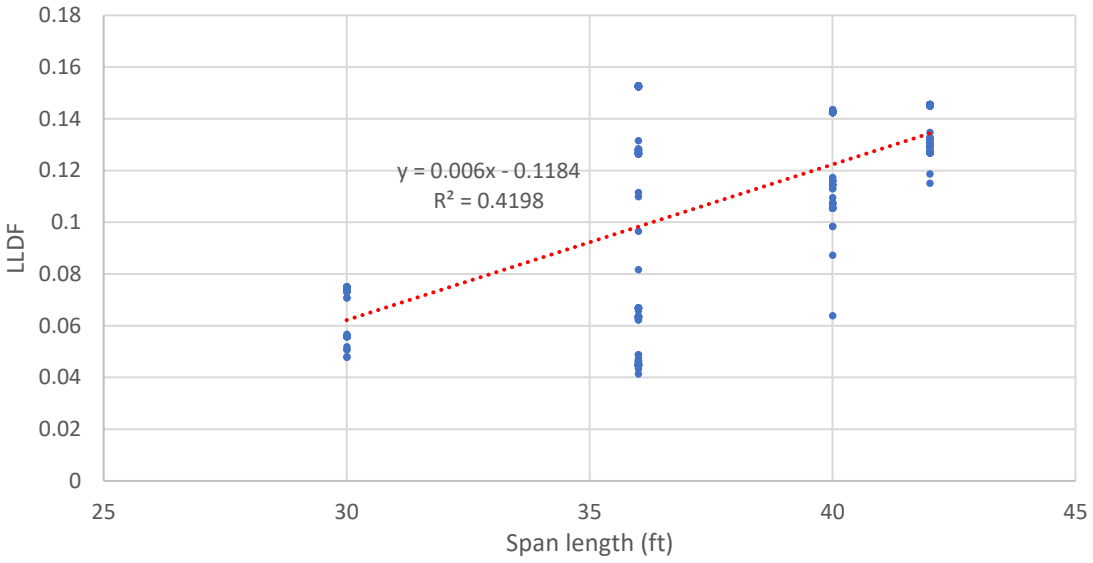

Figure 85. Exterior girder LLDF versus span length for steel girder bridges

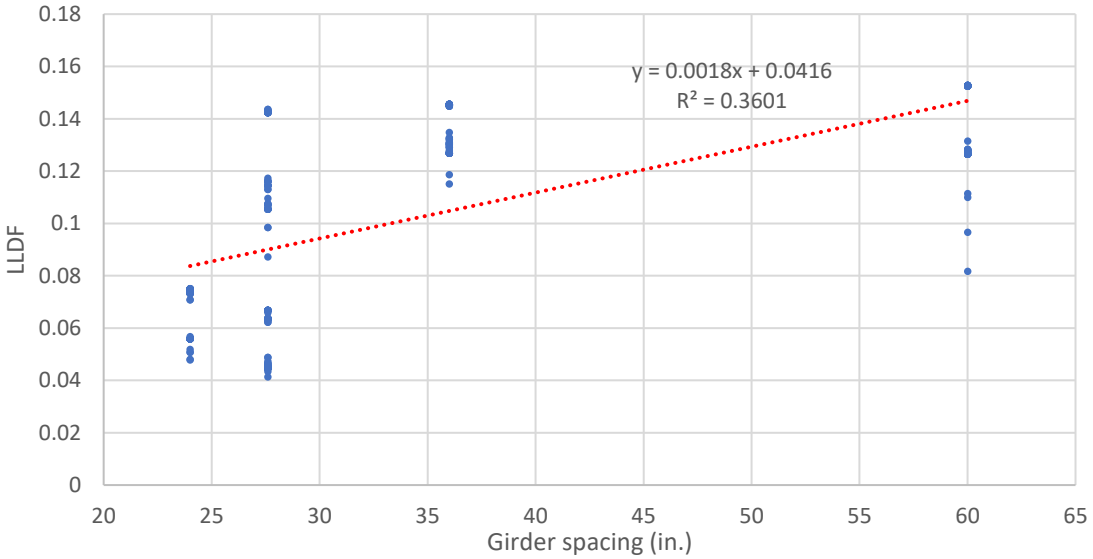

Figure 86. Exterior girder LLDF versus girder spacing for steel girder bridges

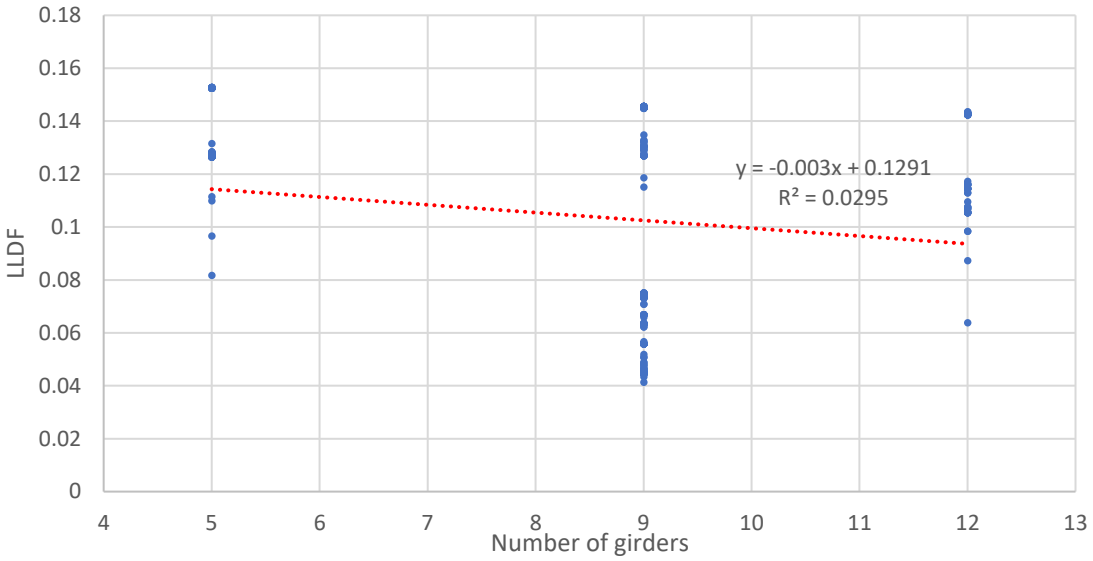

Figure 87. Exterior girder LLDF versus number of girders for steel girder bridges

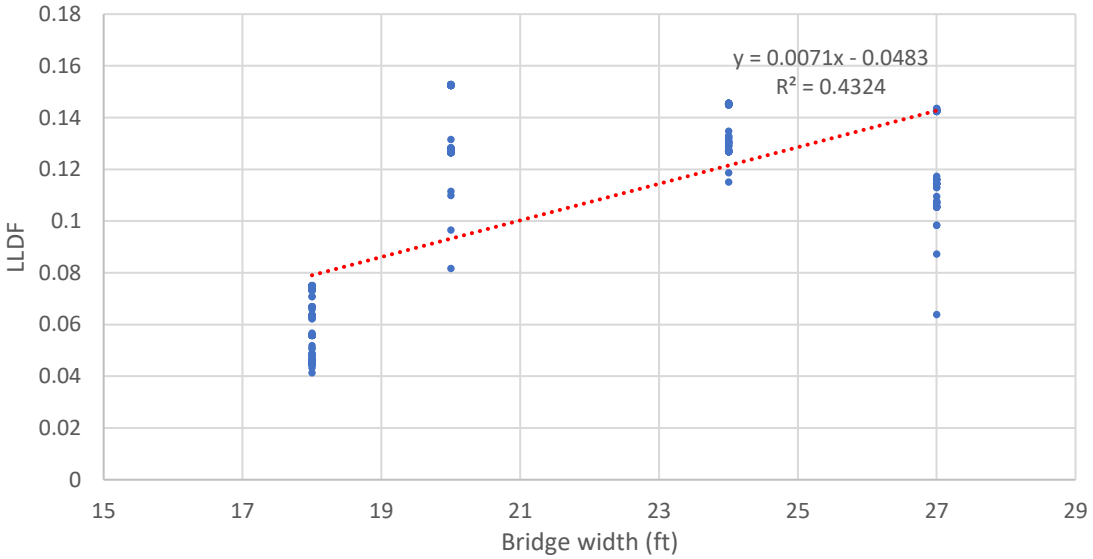

Figure 88. Exterior girder LLDF versus bridge width for steel girder bridges

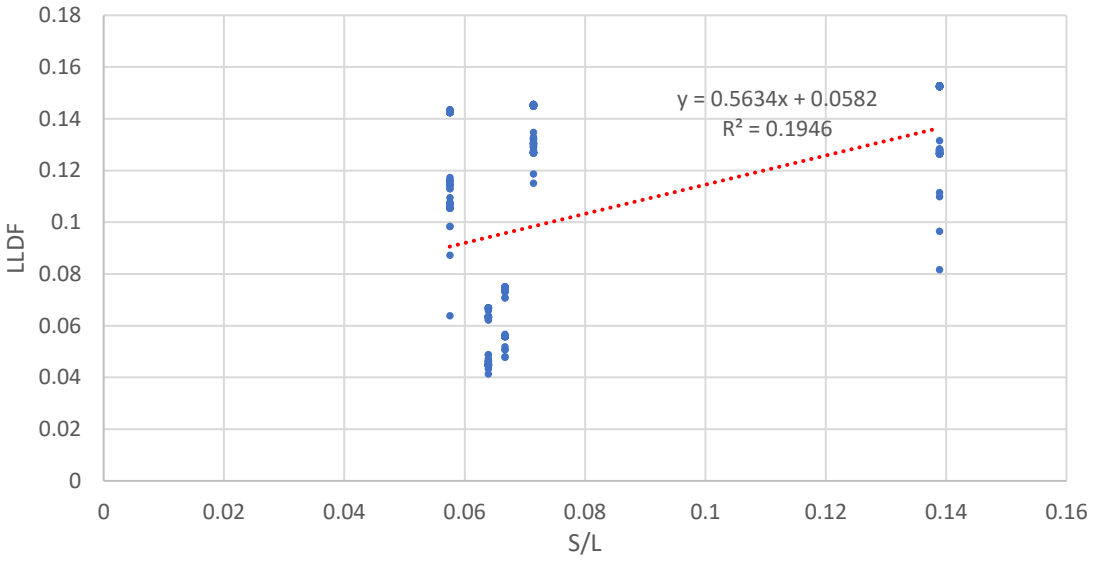

Figure 89. Exterior girder LLDF versus ratio of girder spacing to span length for steel girder bridges

Table 19 shows the general relationship between the various bridge parameters and LLDF for steel girder bridges. The parameters that show notable effects on LLDF are the number of girders and the ratio of girder spacing to span length. Since the parametric study involved fewer steel girder bridges than PC or slab bridges, the LLDF data set for steel girder bridges was comparatively small. Therefore, it was difficult to adequately compare the impact of steel girder bridge parameters and PC bridge parameters on LLDF. However, the available steel girder LLDF data show similarities with the PC LLDF data in terms of the significance of the bridge parameter effects.

Table 19. Impact of steel girder bridge parameters on LLDF

Bridge parameters	Interior	Effect	Exterior	Effect
Span length (ft)	0.16% ↓	Not Notable	0.6% ↑	Notable
Girder spacing (ft)	0.5% ↑	Notable	0.18% ↑	Not Notable
Number of girders	2.7% ↓	Notable	0.3% ↓	Notable
Bridge width (ft)	0.5% ↓	Notable	0.7% ↑	Notable
Girder spacing/Span length	224% ↑	Notable	56% ↑	Notable

6.3.3.4 Comparison with AASHTO-Specified Values

Figure 90 compares the range of interior girder LLDFs from the terragator loads to the LLDFs from the HS-20 load and the LLDFs calculated using the AASHTO-recommended equation for steel girders. Equation 8 was used to calculate the AASHTO LLDFs, where $\left(\frac{K_g}{12*L*t_s^3}\right)^{0.1} = 1.02$ for steel girders. No skew reduction factor was applied.

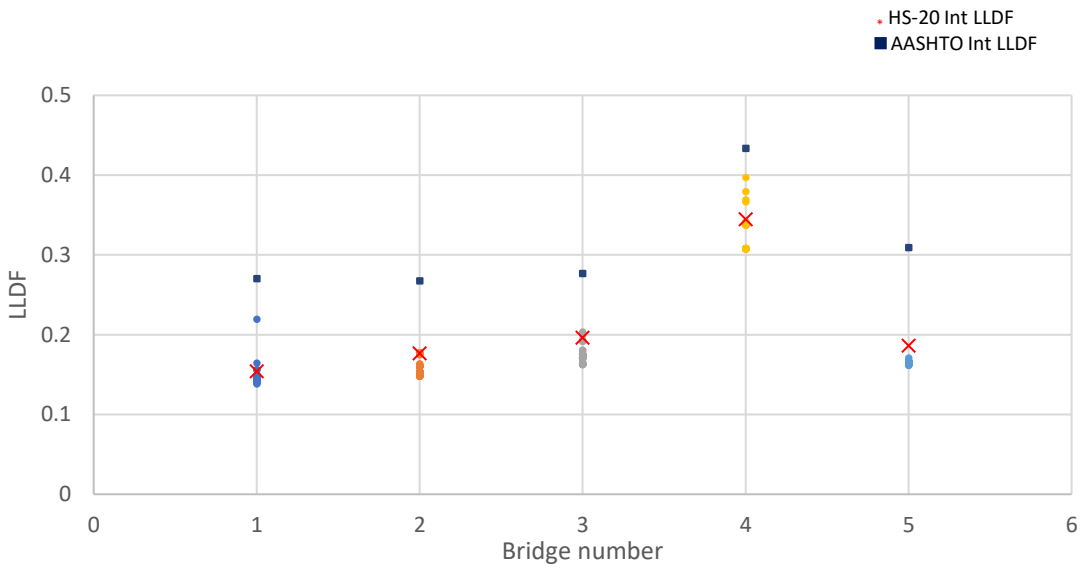

Figure 90. Interior girder LLDF range of each steel bridge

The same AASHTO-recommended equation used to calculate the exterior girder LLDFs for the PC bridges was used to calculate the exterior girder LLDFs for the steel girder bridges. Figure 91 compares the range of exterior girder LLDFs from the terragator loads to the LLDFs from the HS-20 load and the LLDFs from the AASHTO-recommended equation.

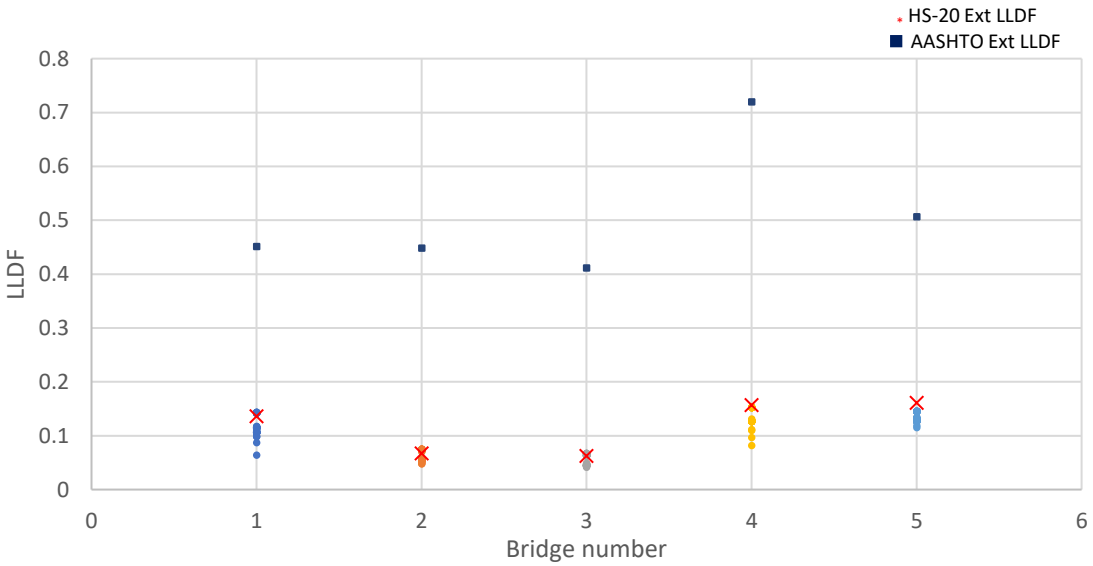

Figure 91. Exterior girder LLDF range of each steel bridge

Figure 90 suggests that the majority of the interior girder LLDFs are below the HS-20 LLDFs. Although Bridge 4 shows interior girder LLDFs that are higher than the HS-20 LLDFs, most data are below the HS-20 LLDFs. The interior girder LLDFs calculated from the AASHTO

equation are higher than all of the LLDFs from the FE analysis. A similar trend is evident in Figure 91 for the exterior girder LLDFs.

Figure 92 shows the range of maximum strain experienced by each bridge under varying terragator loads and the HS-20 load. The results indicate that most of the strain values resulting from the terragator loads were below the strain values resulting from the HS-20 load. The terragator strain data that were higher than the HS-20 strain data were from terragators with heavier axle loads than the HS-20 axle load.

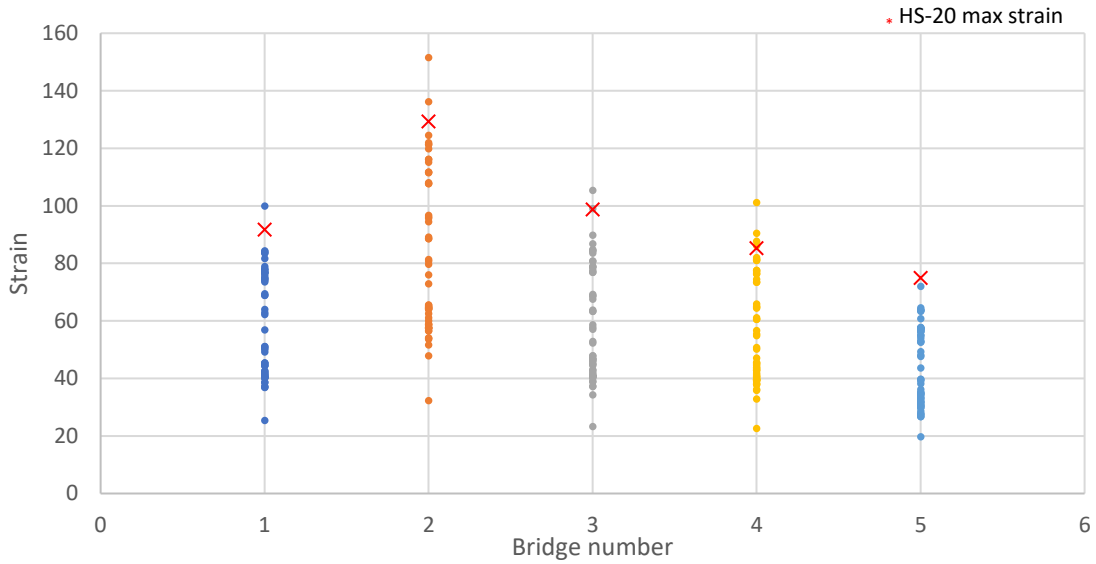

Figure 92. Maximum strain from each steel bridge

6.4 Determination of the Load Distribution of Iowa Husbandry Vehicles

Based on the results from this chapter, the key findings are summarized as follows:

- The interior girder and exterior girder LLDFs of PC bridges and steel girder bridges are small compared to the LLDFs calculated by the AASHTO-recommended equations.
- It was observed that the equivalent strip widths calculated using the field test results for all bridges were larger than the strip widths calculated using the AASHTO equation. The same was observed in the parametric study.
- Observation of the effects of various bridge parameters on LLDF suggests that the bridge parameters that most influence the interior girder LLDFs are skew angle, girder spacing, and number of girders. This is true for both PC and steel girder bridges.
- The ratio of girder spacing to span length showed the greatest effect on the LLDFs of PC and steel girder bridges.
- For slab bridges, the parameters that were found to have greatest influence on equivalent strip width were skew angle, slab thickness, and span length.

7 CALIBRATION OF LOAD AND RESISTANCE FACTORS

The live load factors provided in the AASHTO LRFD Bridge Design Specifications (2020) were derived based on a reliability analysis using extensive amounts of data collected at weigh-in-motion locations. This is an appropriate methodology when determining load factors for standard vehicles (e.g., semi-trucks, dump trucks, etc.), but the application of these load factors to implements of husbandry must be investigated further due in part to the varying axle spacings, weights, and gauge widths and the limited weigh-in-motion data collected for these vehicles. However, the most important factor that must be considered when developing load factors for implements of husbandry is the exposure risk of specific bridges. In this regard, it is necessary to understand the relative occurrence exposure.

This chapter describes an analysis conducted for the newly legalized loads for terragator vehicle types and provides recommendations for load factor modifications based on a statistical reliability evaluation. Fortunately for this analysis, the newly introduced legal axle load limit on self-propelled implements of husbandry used to transport organic or inorganic plant food materials, agricultural limestone, or agricultural chemicals is relatively specific. That is, the implements used for these applications tend to be unique when compared to other implements, but the implements within this subgroup are rather similar to each other. These similarities increase the statistical reliability of any live load factors developed for this vehicle type because widely variable vehicle types and configurations do not have to be accounted for within the analysis. The calculation of the LRFs was carried out for the PC and steel girder bridge types discussed in previous chapters of this report.

7.1 Load and Resistance Factor Calculation Procedures

In this section, the general procedures for the calibration of LRFs are discussed with respect to PC and steel girder bridges. Three cases with different combinations of live load and nominal load were created to calibrate the LRFs under various circumstances. To account for the effects of a potential vehicle with all axles at the 25 kip load level under the new Iowa law, a new terragator model, designated as Terragator Max in this report, was developed. Detailed procedures for determining the load effects for live and dead loads and the nominal capacities of a girder-deck composite section for PC and steel girder bridges are presented.

7.1.1 Calibration Process

LRFs are calculated with a targeted safety index. This safety index is calculated based on resistance and load data. The calculated safety index is different for each bridge, which can give a wide range of site-specific LRFs. To obtain a common LRF for all bridges, the safety index needs to be calibrated for the bridge population or sample. The calibration of the safety index was completed by referring to Nowak (1999). This process was carried out separately for moment and shear depending on the live load effect considered. The following steps were followed to calibrate the safety indices of PC and steel girder bridges.

7.1.1.1 Step 1: Selection of Bridges

In this research, the LRFs were calibrated for PC and steel girder bridges. In total, 23 PC and 23 steel girder bridges were selected from the Iowa Department of Transportation's (DOT's) Structure Inventory and Inspection Management System (SIIMS) (2023). These bridges were categorized based on span lengths of 30 ft, 60 ft, 90 ft, 120 ft, and 150 ft. Each span length was further categorized by 4 ft, 6 ft, 7 ft, 8 ft, and 10 ft girder spacings for PC bridges and 4 ft, 6 ft, 8 ft, 10 ft, and 12 ft girder spacings for steel girder bridges. One bridge was selected for each girder spacing and span length combination.

7.1.1.2 Step 2: Dead Load, Live Load, and Nominal Load Determination

The dead load of each deck in kip/ft was found by multiplying the deck's cross-sectional geometry with an assumed concrete density of 0.15 kip/ft^3. The dead load of an assumed asphalt wearing surface in kip/ft for each bridge was also calculated using cross section and density (0.15 kip/ft^3). The effective deck width was calculated for the cross section of the deck and the asphalt wearing surface. This effective deck width was calculated as the minimum of the girder web thickness plus the clear transverse span, the girder web thickness plus 16 times the deck thickness, or ¼ of the span length. The dead load of each girder was calculated using the girder cross section, the concrete density for PC bridges, and the steel density (0.5 kip/ft^3) for steel girder bridges (Wight and MacGregor 2012, Salmon and Johnson 1996).

The live load data presented in Chapter 3 were used in the calibration of load factors, that is, 6 payload levels for 28 available terragator configurations. These 6 payload categories were 0%, 20%, 40%, 60%, 80%, and 100% of the payload capacity of the terragators. In total, 168 terragator loads were used. The detailed information for these live loads is presented in Table 1.

The design truck load was considered as the nominal value from which the identified terragator loads differ. For the Strength I limit state, design truck loads were considered as the nominal loads. For the Strength II limit state, the loads for an "owner-specified vehicle or evaluation permit vehicle" were considered as the nominal loads. Therefore, the HS-20 model and the newly created Terragator Max model were considered as the nominal vehicles in this study to find the nominal load effects on the bridges. Detailed information about the Terragator Max model is presented in Section 7.1.3.

7.1.1.3 Step 3: Load Effect Determination

To understand the load effects, the bending moment and shear due to the girder, deck, and asphalt wearing surface dead loads for each selected bridge were calculated. It was assumed that the dead load was distributed uniformly. Thus, the moment at mid-span and the shear at the abutment due to the dead load was calculated for a uniformly distributed load on a simply supported beam.

The bending moment and shear due to live loads on a girder-deck composite section were also calculated for terragator live loads. The nominal bending moment and shear were calculated using the nominal vehicle chosen.

7.1.1.4 Step 4: Calculation of Statistical Load Parameters

The load effect data from the terragator live loads and the nominal load effects were used to determine the mean, bias factor, standard deviation, and coefficient of variance of the live load effects. These statistical parameters were calculated using Equations 33, 34, and 35.

$$\lambda_x = \frac{\overline{x_L}}{x_{Ln}} \tag{33}$$

$$\sigma_x = \sqrt{\frac{\sum_{i=1}^{N} \sum (x_{Li} - \bar{x})^2}{N-1}} \tag{34}$$

$$V_x = \frac{\sigma_x}{\bar{x}} \tag{35}$$

where x is the live load effects data for either moment or shear, x_L is the data due to the terragator live load, N is the number of data points, λ_x is the bias factor, $\overline{x_L}$ is the mean of the live load effects data for either moment or shear , σ_x is the standard deviation, V_x is the coefficient of variance, and x_{Ln} is the nominal data.

Bias factors for dead loads λ_{D1}, λ_{D2}, and λ_{D3} and coefficient of variance V_{D1}, V_{D2}, and V_{D3} were taken from Nowak (1999). The bias factors were used to calculate the mean bending moment and shear due to dead loads. Equation 36 was used to calculate the mean.

$$\overline{x_{D_i}} = \lambda_{x_{D_i}} * x_{D_i}; \text{ for i=1,2,3} \tag{36}$$

where x_{D1}, x_{D2}, and x_{D3} are the dead load effect data for either moment or shear due to the girder, deck, and asphalt wearing surface dead loads; λ_{D1}, λ_{D2}, and λ_{D3} are bias factors; and V_{D1}, V_{D2}, and V_{D3} are the coefficients of variance for moment and shear due to the girder, deck and asphalt wearing surface dead loads.

The two main parameters required for load factor calibration are the mean and standard deviation of the overall load effects on each bridge. Data denoted by *Q* represent load effects due to the live loads and dead loads on the girders. To determine the mean $\bar{Q}$ and standard deviation σ_Q, Equations 37 and 38 were used.

$$\bar{Q} = \overline{x_{D_1}} + \overline{x_{D_2}} + \overline{x_{D_3}} + \overline{x_L} \tag{37}$$

$$\sigma_Q = V_Q * \bar{Q} \tag{38}$$

where V_Q is the coefficient of variance of the load effect data, which can be calculated using Equations 39, 40, and 41.

$$V_Q = \sqrt{{V_E}^2 + (V_{D_1+D_2+D_3+x})^2} \tag{39}$$

$$V_{D_1+D_2+D_3+x} = \frac{\sqrt{{\sigma_{D_1}}^2+{\sigma_{D_2}}^2+{\sigma_{D_3}}^2+{\sigma_x}^2}}{\bar{Q}} \tag{40}$$

$$\sigma_{D_i} = V_{D_i} * \overline{x_{D_i}}\text{; for i=1,2,3} \tag{41}$$

where σ_{D_1}, σ_{D_2}, and σ_{D_3} are the standard deviations of the load effect due to the dead load of the girder, deck, and asphalt wearing surface, respectively.

7.1.1.5 Step 5: Resistance Data

The moment and shear capacity x_n of each selected bridge was calculated following codified approaches. Since only one bridge was selected for each girder spacing and span length combination, determination of the statistical factors for the resistance data was not possible. Hence, the bias factor λ_{xn} and the coefficient of variance V_{xn} for the resistance data were taken from Nowak (1999). These factors are presented in Table 20.

Table 20. Resistance data statistical parameters taken from Nowak (1999)

	PC bridges		Steel bridges	
Statistical Parameter	λ	V	λ	V
Moment	1.05	0.075	1.12	0.10
Shear	1.15	0.14	1.14	0.105

7.1.1.6 Step 6: Safety Index

Moses (2001) defines the safety index as a measure of structural reliability or, conversely, the risk that a design component will have insufficient capacity and that some limit state will be reached. A component that gives a higher safety index shows a higher reliability.

Since the resistance data were lognormally distributed and the load data were normally distributed, the safety index of a component, denoted as β, was calculated using Equation 42, as recommended by Barker and Puckett (2007).

$$\beta = \frac{x_n\lambda_{x_n}(1-kV_{x_n})[1-\ln(1-kV_{x_n})]-\bar{Q}}{\sqrt{[x_nV_{x_n}\lambda_{x_n}(1-kV_{x_n})]^2+{\sigma_Q}^2}} \tag{42}$$

where k is comparable to the number of standard deviations from the mean value. As an initial guess, k is often taken as 2 according to Barker and Puckett (2007). Thus, one beta value is obtained per bridge.

7.1.1.7 Step 7: Selection of Target Safety Index β_T

The safety index was calculated for each selected bridge. This resulted in a range of multiple safety index values. To find the common load and resistance factors that could be applied to all bridges, a single safety index value was required. Therefore, a single value in the range of the calculated safety index values was selected as the target beta value. This target value was selected as a reference value for further calibration of the safety index values.

7.1.1.8 Step 8: Load and Resistance Factor Calculation

The selected target safety index was substituted in Equation 43 to calculate the resulting resistance factor and in Equations 44 and 45 to calculate the resulting load factors.

$$\varphi = \lambda_{x_n}(1 - \alpha\beta_T V_{x_n}) \tag{43}$$

where $\alpha = \frac{\sqrt{\sigma_R^2+\sigma_Q^2}}{\sigma_R+\sigma_Q}$

$$\gamma_{D_i} = \lambda_{D_i}(1 + \alpha\beta_T V_{D_i}) \tag{44}$$

$$\gamma_L = \lambda_L(1 + \alpha\beta_T V_L) \tag{45}$$

7.1.1.9 Step 9: Calibration of Beta

The calculated load and resistance factors were used to calculate the new resistance values for each bridge using Equation 46.

$$x_n = \left[\gamma_{D_1}\overline{x_{D_1}} + \gamma_{D_2}\overline{x_{D_2}} + \gamma_{D_3}\overline{x_{D_3}} + \gamma_L\overline{x_L}\right]/\varphi \tag{46}$$

The new x_n values were inserted into Equation 42 to find the new beta values. The new calculated beta values were plotted against span length to check whether the values converged. If the converged beta values clustered near the target beta values, then the calibration process was considered completed.

7.1.2 Three Cases

The LRF evaluation process was carried out for three situations with different combinations of live load and nominal load. All three cases are summarized in Table 21. These three situations were named Case I, Case II, and Case III.

Table 21. Summary of cases considered in LRF evaluation

Limit State	Case	Live Load	Nominal Load
Strength I	I	Identified Terragator population (with axle loads less than 25 kips)	HS – 20 (Truck only)
	II	Terragator Max (with identified live load coefficient of variance)	HS – 20 (Truck only)
Strength II	III	Terragator Max (with identified live load coefficient of variance)	Terragator Max

Case I calibrated the LRFs for the identified terragators in the Strength I limit state. Axle loads 25 kips and below from the available terragator loads were used to calculate the live load bending moment and shear. This was done to understand the load effects of currently available vehicles with legal loads. Since the Strength I limit state consists of a load combination relating to normal vehicular use, the HS-20 load was used to calculate the nominal load effects. Approximately 90 terragator loads were used to characterize the live load effects, and the HS-20 load was used to characterize the nominal load effects.

Case II calibrated the LRFs for a hypothetical terragator model in the Strength I limit state. The hypothetical terragator model developed for Cases II and III was named Terragator Max. Here, the coefficient of variation for the live load data was taken from Case I because there was only a single Terragator Max configuration. Because this case was evaluated for the Strength I limit state, the HS-20 load was utilized to characterize the nominal load effects.

Case III calibrated the LRFs for Terragator Max in the Strength II limit state. Similar to Case II, the coefficient of variation for the live load data was taken from Case I. Terragator Max was treated as an "owner-specified vehicle or evaluation permit vehicle." Therefore, the Terragator Max load was used as the nominal load for Case III.

7.1.3 Development of Terragator Max

The state of Iowa recently passed legislation that increased the permissible axle load to 25 kips. This creates the possibility for manufacturers to produce vehicles that can carry a maximum payload capacity of 25 kips on each axle. To evaluate the effects of the increased legal axle load, a theoretical terragator model was created that, according to the new legislation, can travel without a permit in the state of Iowa. This new terragator model was named Terragator Max.

The terragator configuration data from 28 terragator models were used as a reference to create Terragator Max. The following points were observed regarding the identified terragator population:

- The maximum number of axles observed in the terragator inventory was three axles. This vehicle configuration gives the maximum load effects.
- The minimum axle spacing observed among the identified terragators was 13 ft.
- The largest tire diameter observed was 65 in., and hence the axle spacing between axles 2 and 3 was 6 ft.

Considering these points regarding the geometries of the identified terragators, a husbandry vehicle with likely worst-case load effects was created. The following specifications were assigned to Terragator Max:

- Three axles were included.
- The spacing between axles 1 and 2 was set to 10 ft.
- The spacing between axles 2 and 3 was set to 4 ft. A small axle spacing was used in order to induce higher load effects.
- To maintain consistency with the HS–20 truck, a gauge spacing of 6 ft was used.
- The weight of each axle was set to 25 kips.

A hypothetical schematic diagram of the Terragator Max vehicle configuration is shown in Figure 93.

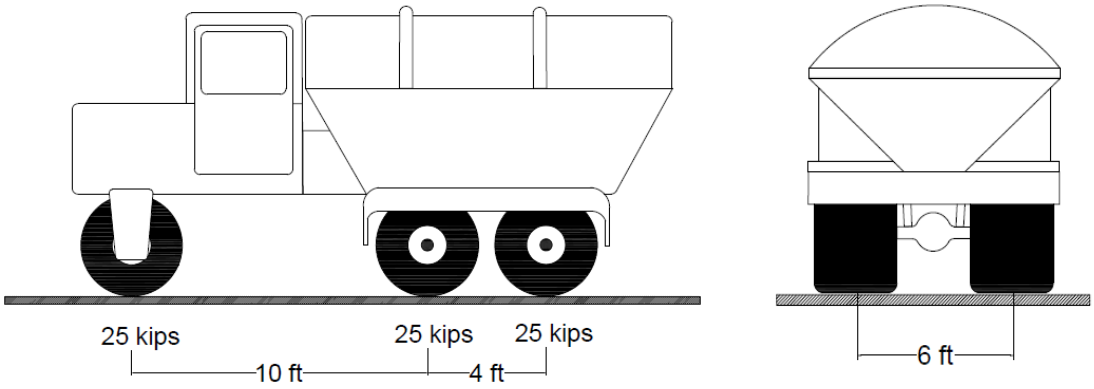

Figure 93. Design vehicle for implements of husbandry (Terragator Max)

7.1.4 Determination of Live Load Effects

A vehicle passing over a bridge induces live load effects on all of the girders on the bridge. Each girder thus resists a part of the vehicle. The girders that are immediately below the vehicle experience higher load effects than the girders farther away from the vehicle. A bridge's load distribution factor describes the fraction of load resisted by each girder. Therefore, to consider

the transverse distribution of load, the load effects on a simplified model must be multiplied by the distribution factor.

For a simply supported beam, it is generally observed that the live load bending moment is at its maximum near mid-span and shear is at its maximum near the beam's supports. These two factors are considered as the live load effects on a bridge.

To understand the impact of terragator loads on the bridges in this study, the live load effects at the mid-span and support locations of the girders were evaluated for various longitudinal positions of the terragators.

In addition to the live load effects from the terragators, the live load effects from Terragator Max and an HS-20 truck were calculated and compared. Figure 93 shows the configuration of Terragator Max, while Figure 94 shows the configuration of an HS-20 truck as described in Section 3.6.1.2.2 of the AASHTO LRFD (2020).

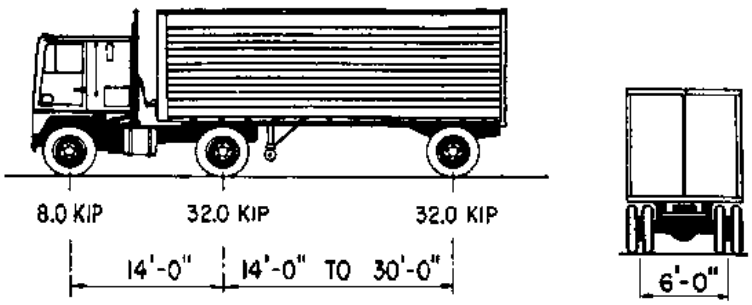

Figure 94. HS-20 design truck

Drawing an influence line for moment and shear at a chosen location on a bridge span provides an extensive understanding of these load effects at that location for various longitudinal positions of a given vehicle. The following sections detail the method used to find the live load effects in this study.

7.1.4.1 Shear

Shear is typically at its maximum in a girder when the heaviest vehicle axle is close to the supports. This assumption was used to calculate the shear values in girders under live loads. The shear due to vehicle loading was calculated using the influence function for shear. Figure 95 shows the influence function for shear at the support of a simply supported beam with a span length of 30 ft.

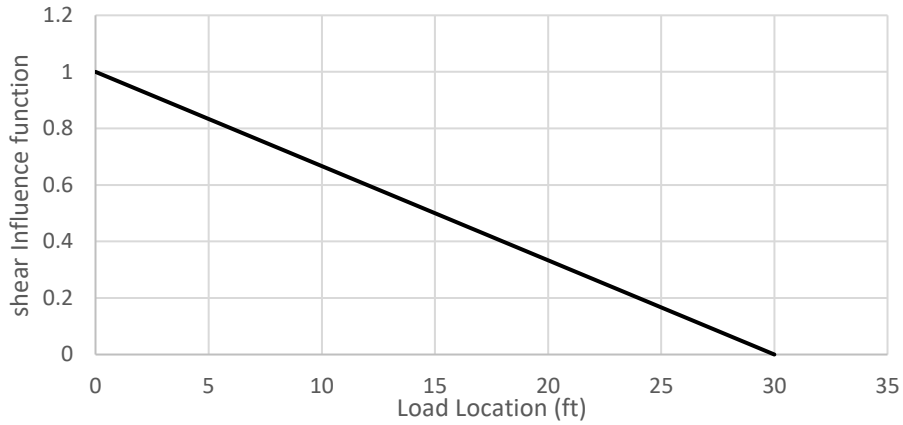

Figure 95. Influence function for shear at a support

Shear was calculated from the influence function using Equation 47, as given by Barker and Puckett (2007).

$$V = \sum_{i=1}^{n} P_i \eta_i \tag{47}$$

where n is the number of axles, P is the corresponding axle weight, and η is the influence function for shear (y-axis value) at the corresponding axle (load) location. Shear at the support of a beam with a span length of 150 ft was calculated using Equation 47 for a two-axle and three-axle vehicle. The results can be seen in Figure 96.

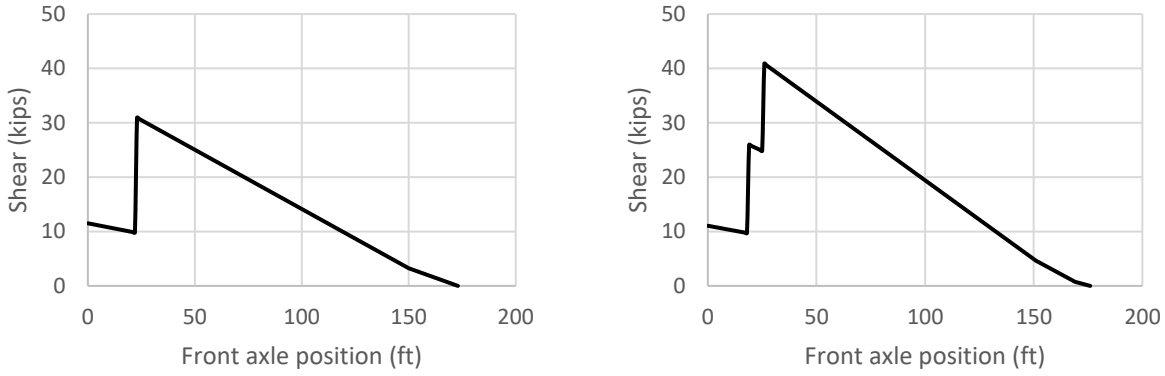

(a) 2 axles

(b) 3 axles

Figure 96. Shear calculated from the shear influence function

The maximum shear values were determined for each bridge under the identified terragator loads, the Terragator Max load, and the HS-20 load. The maximum shear values from the identified terragator loads were compared with the shear values from the Terragator Max and HS-20 loads. Figure 97 shows a comparison of the shear values from the identified terragator loads, the Terragator Max load, and the HS-20 load.

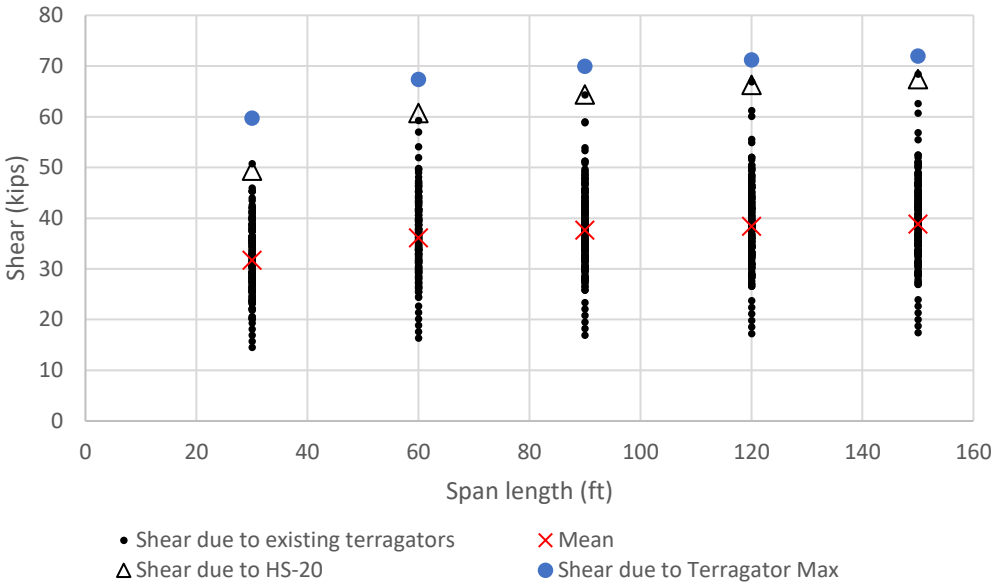

Figure 97. Shear due to live loads

The gross vehicle weight of Terragator Max is 75 kips, which is higher than the HS-20 gross vehicle weight. Figure 98 shows the ratio of the shear induced by Terragator Max to the shear induced by the HS-20 vehicle. A ratio above 1 shows that the shear at the support from Terragator Max is higher than that from the HS-20 vehicle.

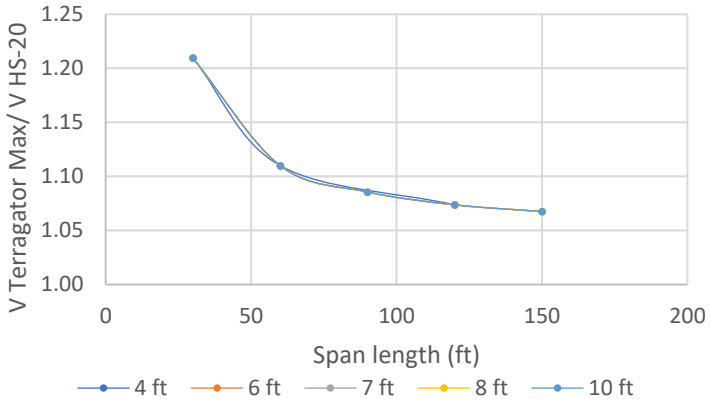

Figure 98. Ratio of shear from Terragator Max to shear from the HS-20 vehicle

7.1.4.2 Bending Moment

The bending moment on a simply supported beam is at its maximum near mid-span. To find the maximum bending moment that occurs at mid-span, the axle loads of the vehicle must be placed at the correct locations. Drawing an influence line of the bending moment at the mid-span of a bridge gives the bending moment at mid-span when a vehicle passes over the bridge. This helps

to evaluate the maximum bending moment at mid-span. The influence function for moment at mid-span of a 30 ft simply supported beam can be seen in Figure 99.

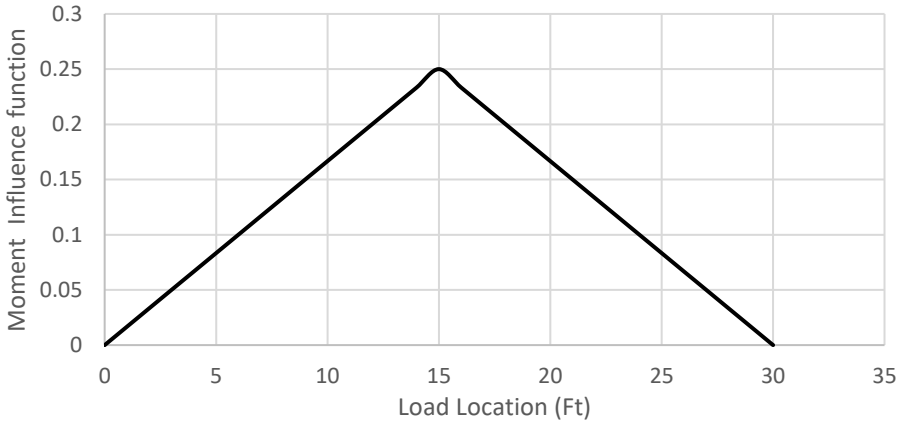

Figure 99. Influence function for bending moment

The bending moment was calculated from the influence function using Equation 48, as given by Barker and Puckett (2007).

$$M = \sum_{i=1}^{n} P_i \eta_i \tag{48}$$

where η is the influence function for bending moment (y-axis value multiplied by the span length L in ft) at the corresponding axle (load) location, n is the number of axles, and P is the corresponding axle weight. The bending moment at mid-span on a beam with a span length of 150 ft was calculated using Equation 48 for a two-axle and three-axle vehicle. The results are shown in Figure 100.

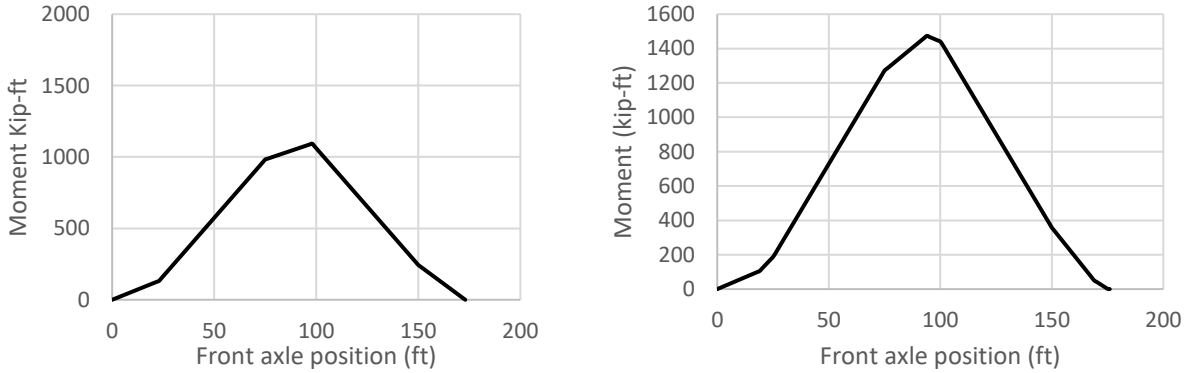

(a) 2 axles

(b) 3 axles

Figure 100. Bending moment calculated from influence function

The maximum bending moments were determined for each span length for all identified terragator loads. The means of these values for each span length were calculated. These bending

moment data were then compared with the bending moment data from the HS-20 and Terragator Max loads. Figure 101 shows the bending moment data from the identified terragator loads compared with the bending moment data from the HS-20 and Terragator Max loads.

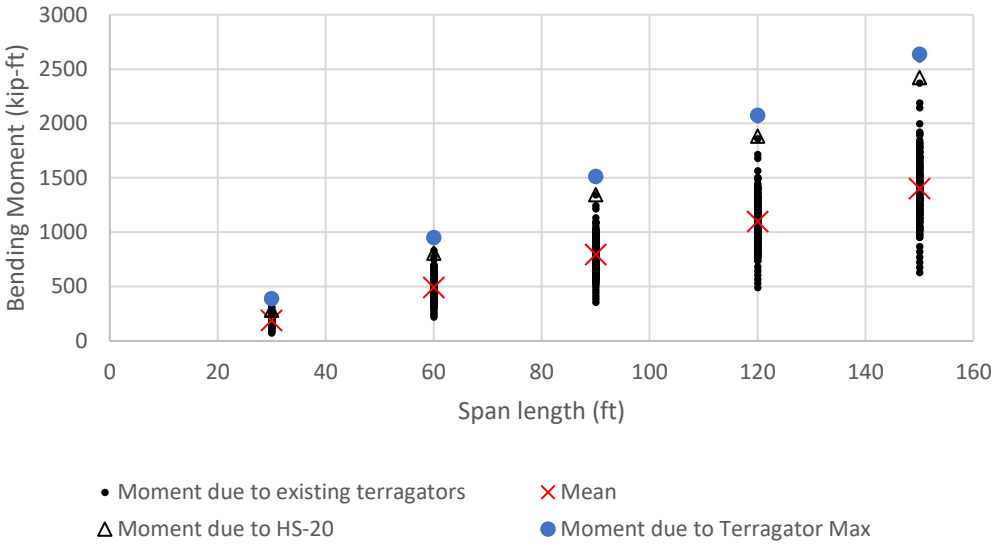

Figure 101. Bending moment due to live loads

Figure 102 shows the ratio of the bending moment from Terragator Max to the bending moment from the HS-20 vehicle. A ratio above 1 shows that the bending moment at mid-span from Terragator Max is higher than that from the HS-20 vehicle.

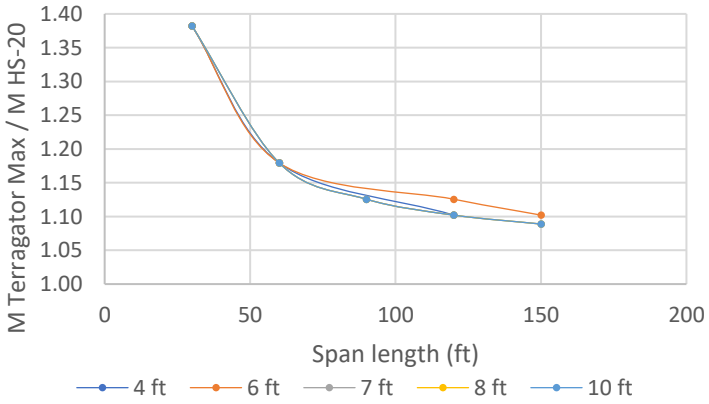

Figure 102. Ratio of bending moment from Terragator Max to bending moment from the HS-20 vehicle

The mean and standard deviation values of the moment and shear data for each span length were then multiplied by the LLDFs calculated from Equation 8 for moment and Equation 11 for shear.

Multiplying the mean and standard deviation values by the LLDFs for a specific type of girder gives the mean and standard deviation values of the load effects data for that type of girder. To accommodate the dynamic impact effects, AASHTO recommends multiplying the load effects by a dynamic impact factor of 1.33.

7.1.5 Resistance Data

The strength required by a bridge component to sustain the live and dead load effects can be considered as the resistance of the bridge component. The strength required can be calculated in terms of moment and shear capacity following codified provisions.

7.1.5.1 PC Bridges

The shear capacity and moment capacity of the PC girders were considered as the resistance data. The shear and moment capacities were calculated using ACI 318-11 (ACI Committee 318 2011). Note that the ACI provisions are nearly the same as the AASHTO provisions. However, using the ACI provisions required fewer unknown variables to be estimated. To calculate the shear capacity, Equation 49 was used.

$$V_n = V_c + V_s \tag{49}$$

$$V_s = \frac{A_v f_y d}{s} \leq 8\sqrt{f'_c} b_w d \tag{50}$$

$$2\sqrt{f'_c} b_w d \leq V_c = \left(0.6\sqrt{f'_c} + 700\frac{(L-2x)d_p}{x(L-x)}\right) * b_w d \leq 5\sqrt{f'_c} b_w d \tag{51}$$

$$x = \frac{b}{2} + \frac{h}{2} \tag{52}$$

where A_v is the area of shear reinforcement at mid-span, f_y is the yield strength of steel, d is the depth of shear reinforcement, s is the spacing of shear reinforcement, $f'c$ is the concrete compressive strength, b_w is the effective width, L is the span length, b is the bearing pad length, and h is the height of the composite girder.

Equation 53 was used to calculate the moment capacity of the girders.

$$M_n = T_p\left(d_p - {}^{a}/_{2}\right) + T_s\left(d - {}^{a}/_{2}\right) + C_s\left(d' - {}^{a}/_{2}\right) \tag{53}$$

$$T_p = A_p f_{ps} \tag{54}$$

$$T_s = A_s f_y \tag{55}$$

$$C_s = A_s' f_y \quad (56)$$

where d_p is the depth of prestressing steel from the top of the deck, a is the depth of the concrete stress block, d is the depth of rebar in the bottom flange of the girder, d' is the depth of rebar in the deck, f_y is the yield strength of steel, f_{ps} is the strength of prestressing steel, and A_p, A_s, and A_s' are the area of the prestressing steel, bottom flange rebar steel, and deck rebar steel, respectively.

7.1.5.2 Steel Girder Bridges

The shear capacity of the steel girders was calculated using Equation 57, which is taken from Section 6.10.9.2 of the AASHTO LRFD (2020).

$$V_n = 0.58 C f_y D t_w \quad (57)$$

where f_y is the yield strength of steel, D is the depth of the girder web, t_w is the web thickness, and C is the web slenderness.

The moment capacity of the steel girders was calculated using Equations 58 and 59, which are taken from Salmon and Johnson (1996).

$$M_n = T_s \left(\frac{d}{2} + t_s - {}^{a}/_{2}\right); \text{ for } a \leq t_s \quad (58)$$

$$M_n = C_c d' + C_s d''; \text{ for } a > t_s \quad (59)$$

$$T_s = A_s f_y \quad (60)$$

$$C_c = 0.85 f'_c b_E t_s \quad (61)$$

$$C_s = (T_s - C_c)/2 \quad (62)$$

where d is the depth of the beam, a is the depth of the concrete stress block, t_s is the deck thickness, b_E is the effective width, A_s is the area of a girder, f_y is the yield strength of steel, $f'c$ is the concrete compressive strength, T_s is the tension in a steel girder, C_c is the compression in the deck concrete, C_s is the compression in the deck rebar, d' is the distance between T_s and C_c, and d″ is the distance between T_s and C_s.

7.2 PC Bridges

Table 22 presents the selected PC bridges according to span length and girder spacing. Table 23 gives the bridge information of the selected PC bridges.

Table 22. PC bridges selected for LRF calculation

Span Length	Girder Spacing				
	4 ft	6 ft	7 ft	8 ft	10 ft
30 ft	0648.4S218	1310.6S175	7696.3S010	2312.0O030	7769.0L035
60 ft	5057.8L080	3557.1L035	0641.9O380	0757.1L380	3913.5S141
90 ft	- -	3703.2S030	0601.5S150	5099.5S065	3712.3S004
120 ft	3813.8O020	7716.9S415	7749.9L141	0634.1S218	7769.0L035
150 ft	- -	8937.5S002	7732.5O080	1783.8S065	7733.8O080

Table 23. Bridge information of selected PC girder bridges

Bridge ID	Original span length (ft)	Original girder spacing (ft)	Idealized span length (ft)	Idealized girder spacing (ft)	Number of girders	Width (ft)	Skew angle (degrees)
0648.4S218	43.5	4.25	30	4	8	30	0
1310.6S175	30.75	6.25	30	6	7	40	30
7696.3S010	30	6.6	30	7	6	36	0
2312.0O030	35	8.5	30	8	4	30	11.5
7769.0L035	36	9	30	10	4	34	13
5057.8L080	68.75	4.25	60	4	8	30	15
3557.1L035	64.8	6.33	60	6	7	40	24
0641.9O380	60.75	6.83	60	7	7	44	25
0757.1L380	64	7.4	60	8	6	40	15
3913.5S141	56	9.25	60	10	5	40	0
3703.2S030	91	6.15	90	6	8	46	0
0601.5S150	96.5	7	90	7	6	32	0
5099.5S065	95	7.5	90	8	6	40	0
3712.3S004	95	9.25	90	10	5	40	15
3813.8O020	120	5.2	120	4	6	30	0
7716.9S415	121.5	6.15	120	6	7	40	0
7749.9L141	116	7.2	120	7	6	40	0
0634.1S218	121	8.03	120	8	6	44	0
7769.0L035	117	9.08	120	10	4	34	13
8937.5S002	141.5	6.5	150	6	7	32	0
7732.5O080	156	7	150	7	7	40	28
1783.8S065	150	8.03	150	8	6	44	5
7733.8O080	151.5	9.25	150	10	5	40	10

PC bridges with span lengths of either 90 ft or 150 ft that also had a girder spacing of 4 ft were not found. Therefore, only 23 PC bridges were finally selected for the LRF calculation. Bridge parameter data were collected from the bridge plans.

The three cases described in Section 7.1.2 were considered for the PC girder bridges. The current load factors in AASHTO (2020) were calibrated using an ADTT of 5,000 with a safety index of 3.5. The AASHTO MBE (2018) suggests that a lower safety index value of 2.5 may be targeted to evaluate bridges at the operating level. An initial completion of the calibration process using a target safety index value of 2.5 resulted in a safety index greater than the target and the need to increase existing load factors and decrease existing resistance factors. IoH vehicles are

considerably few in number, resulting in low ADT values, and therefore a lower target safety index value for the calibration procedure could be justified. A lower target safety index of 2.0 was chosen due to the reduced exposure period, consideration of site realities, and the economic considerations of rating versus design. It is important to consider that a safety index greater than 0.0 implies that the resistance is greater than the load effects.

Hence, in each case, the load and resistance factors were calibrated for both target safety indices of $\beta_T = 2$ and $\beta_T = 3.5$. The following sections give the details of the LRF calculations for all three cases. The details of the resistance data are also mentioned.

7.2.1 Case I

This case was considered to study whether the terragators identified in Chapter 3 give LRFs that are higher or lower than the current AASHTO LRFs. Some of the identified terragators have axle loads that are higher than 25 kips. These loads were eliminated from the calculation of LRF in Case I.

7.2.1.1 Load Data

The dead load data were calculated using the process described in Section 7.1.1. The statistical parameters, including the bias factor and coefficient of variance for dead load data, were taken from Nowak (1999). These parameters, along with the calculated dead load effects, were required to calculate the mean and standard deviation of the dead load data using Equations 36 and 41.

The live load effects on PC girders were calculated according to the procedure described in Section 7.1.4. The empty load and full load data of the 28 available terragators were already known. Using interpolation, loads representing 20%, 40%, 60%, and 80% of the full payload were calculated. This increased the load data population. Only axle loads below 25 kips were used from this population to determine the load effects on the PC girders. The mean, standard deviation, and coefficient of variance of the live load effects data were calculated for each span length category shown in Table 1 using Equations 34 and 35. The mean and standard deviation of the load effects were then multiplied by a DIF of 1.33 and the LLDFs calculated using Equation 8 for moment and Equation 11 for shear. This was done to include the variation in transverse load distribution due to different girder spacings. The statistical parameters for load were then calculated using Equations 36, 37, 38, and 39.

7.2.1.2 Nominal Load

The axle loads of the HS-20 design truck were used to calculate the nominal load effects on the girders. These load effects were calculated for each span length and then multiplied by the DIF and LLDF values given in Equations 8 and 11.

The nominal load effects were used to calculate the live load bias factor using Equation 1. Finding the bias factor allowed the load effects from the identified terragators to be compared with those of the HS-20 design truck. This bias factor was then used in Equation 45 to calculate the live load factor. Since the HS-20 load was considered as the nominal load, the Case I LRF is applicable to to the Strength I limit state.

7.2.1.3 Calculation of Safety Index

The statistical parameters found for the load and resistance data were input into Equation 42 to calculate the safety index for each selected bridge. Figure 103 shows the safety indices calculated from the load and resistance data of all PC bridges for moment and shear.

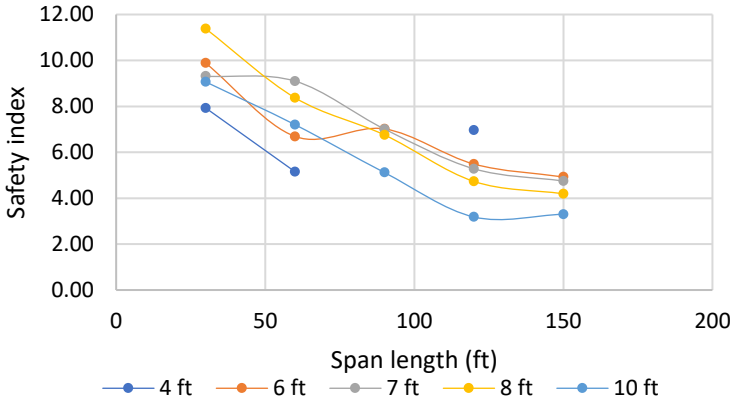

(a) Moment

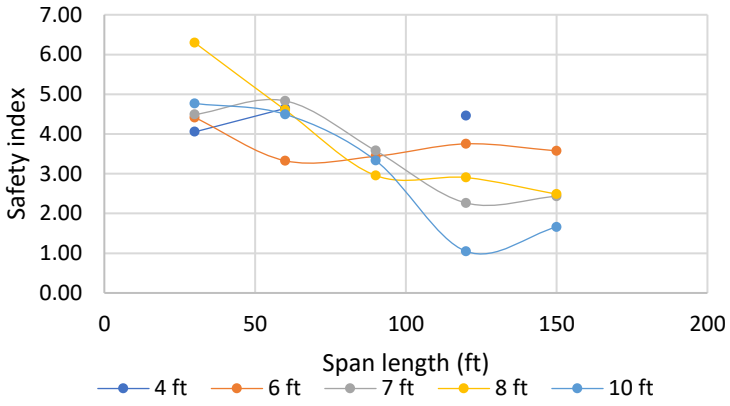

(b) Shear

Figure 103. Safety indices before calibration (Case I - PC girder)

From the safety index plots, it can be observed that the calculated safety indices for a particular span length are scattered. Also, the variation in the safety indices for each girder spacing is high. To find LRFs common to all PC bridges, it was necessary to select a common safety index value. This value was selected from the range of safety indices in Figure 103.

7.2.1.4 Calibration and LRF Calculation Based on β_T =3.5

One safety index value each for moment and shear was selected from the range of calculated safety indices. To maintain consistency with Nowak (1999), a safety index of 3.5 was chosen as the target safety index for the Case I PC bridges. This target safety index was then used to calculate the LRFs using Equations 43, 44, and 45. Determination of a target safety index gives a reference value for calibrating the safety indices. The safety indices found in Section 7.2.1.3 were calibrated using the newly calculated LRFs by substituting the LRFs in Equation 46 and recalculating the safety indices.

After calibration of the safety indices, all values converged closer to the target safety index. This ensured that the common LRFs calculated for the selected PC bridges were applicable to all PC bridges. Figure 104 shows the calibrated safety indices of all selected PC bridges when a target safety index of 3.5 was selected.

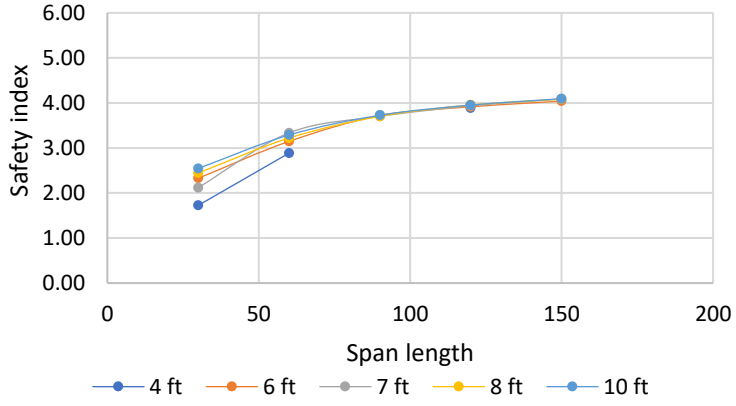

(a) Moment

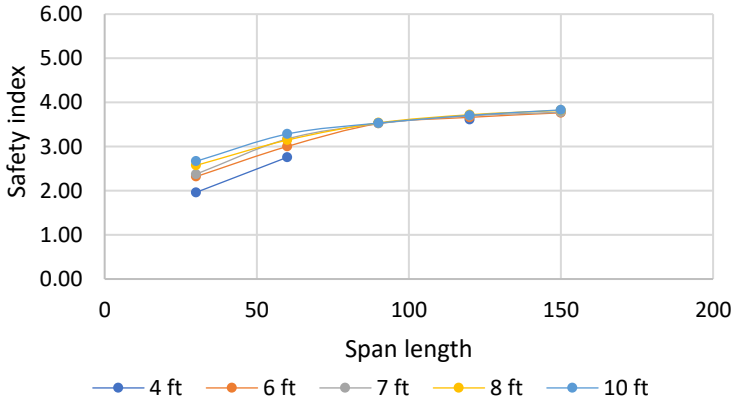

(b) Shear

Figure 104. Calibrated safety indices (Case I - PC girder, β_T=3.5)

To find a live load factor specific to implements of husbandry vehicles, the dead load factors and resistance factors had to be made the same as the current AASHTO LRFs. This was done by

using $k = \alpha\beta = 2$ in Equations 43, 44, and 45. Thus, only the live load factors were different than the current AASHTO LRFs. This made it easy to compare the live load factors. Table 24 shows the final LRFs calculated for the Case I PC bridges along with the calibrated safety index range when $\beta_T = 3.5$.

Table 24. Case I results for PC bridges, $\beta_T = 3.5$

Limit State	Case No.	Live Load	Nominal Load	Load Effects	Factors γ_{LL}	Factors φ	Target Safety index	Calibrated β range	γ_{D1}	γ_{D2}	γ_{D3}
Strength I	I	Identified terragator axle loads below 25 kips	HS – 20 (Truck only)	Moment	0.74	0.9	β_T = 3.5	1.72 – 4.09	1.2	1.26	1.5
				Shear	0.74	0.85		1.96 – 3.83			

7.2.1.5 Calibration and LRF Calculation Based on β_T =2.0

The load and resistance factors from the current AASHTO LRFD were calibrated using a target safety index of 3.5. This index value was chosen to represent severe traffic exposures of 5,000 ADTT. The LRFR procedures use a reduced target safety index of approximately 2.5 on the basis of operating level load rating (AASHTO MBE 2018, Section 6A.1.3).

Moses (2001) states that the marginal cost of increasing the safety index is higher in the evaluation phase than in the design phase. This is because an inadequate load rating for existing bridges may lead to the replacement of components, which is more expensive than increasing the load capacity of those components in the design phase. Thus, the cost of increasing the capacity of an existing structure is higher than that of increasing the capacity in the design phase. Therefore, the target safety index chosen is lower in evaluation than in design.

The overall population of IoH vehicles is not very high, and hence the exposure of bridges to IoH traffic is low. Also, the collected load and resistance data used to calibrate the safety index in this project were at the operating level. Due to these conditions, a lower target safety index was selected to find the LRFs. Figure 105 shows the calibrated safety indices of all selected PC bridges when a target safety index of 2 was selected. Table 25 shows the LRFs calculated for the Case I PC bridges along with the calibrated safety index range when $\beta_T = 2$.

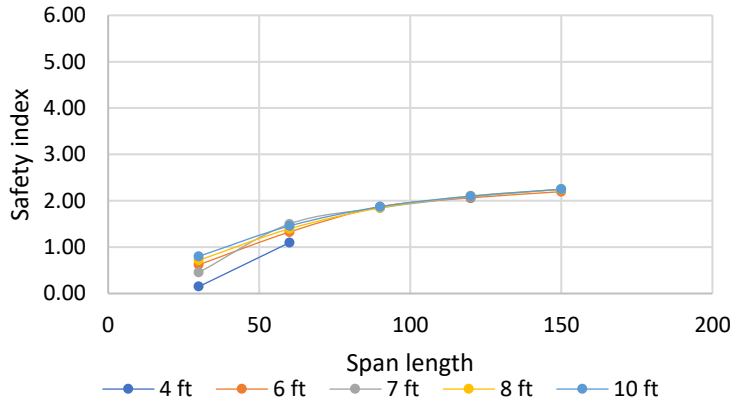

(a) Moment

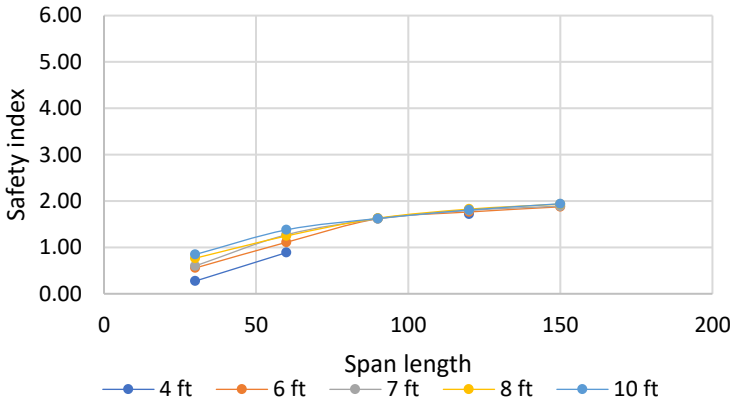

(b) Shear

Figure 105. Calibrated safety indices (Case I - PC girder, β_T=2)

Table 25. Case I results for PC bridges, β_T = 2

Limit State	Case No.	Live Load	Nominal Load	Load Effects	Factors γ_{LL}	Factors φ	Target Safety index	Calibrated β range	γ_{D1}	γ_{D2}	γ_{D3}
Strength I	I	Identified terragator axle loads below 25 kips	HS – 20 (Truck only)	Moment	0.72	0.95	β_T = 2	0.15 – 2.25	1.15	1.20	1.35
				Shear	0.72	0.90		0.27 – 1.94			

7.2.2 Case II

This case was considered to observe the load effects of Terragator Max and the LRFs calculated from this vehicle when the nominal load effects are taken from the HS-20 load.

7.2.2.1 Load Data

The dead load effects for Case II were same as those for Case I. For the live load effects, the axle loads of Terragator Max were considered. The live load effects for each span length category were calculated and then multiplied by the DIF and LLDF values given in Equations 8 and 11 to accommodate different load distributions due to different girder spacings.

Since data for only one vehicle were considered in this case, assumptions were made to find the statistical parameters for a larger population. To consider a population similar to the identified terragators, the coefficient of variance from Case I was applied in Case II. From Equation 41, the standard deviation of the data was then calculated using the coefficient of variance, and the load effects due to Terragator Max were taken as the mean. The statistical parameters for load were then calculated using Equations 36, 37, 38, and 39.

7.2.2.2 Nominal Load

The load effects of the HS-20 vehicle on the girders were taken from the Case I nominal loading data. The bias factor was calculated using the HS-20 vehicle for the nominal load data and Terragator Max for the live load data to find the live load factor. The LRF calculated for Case II is applicable to the Strength I limit state because the HS-20 load was used as the nominal loading.

7.2.2.3 Calculation of Safety Index

Safety indices were calculated for the Case II PC bridges using the statistical parameters for load and resistance found for Case II. These safety indices were plotted against the corresponding span lengths of the bridges. Plots of safety index versus span length are shown in Figure 106 for moment and shear.

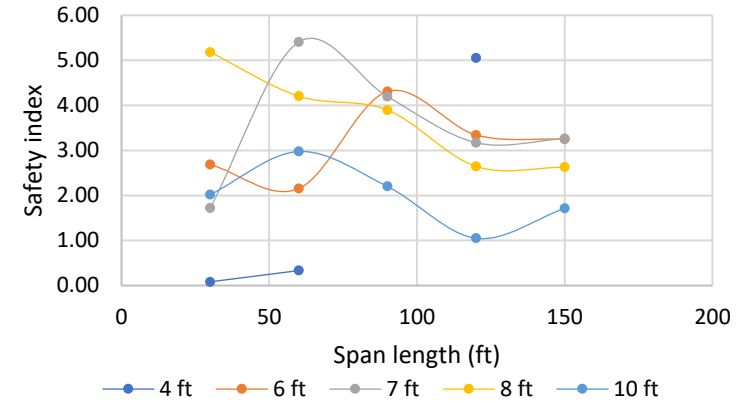

(a) Moment

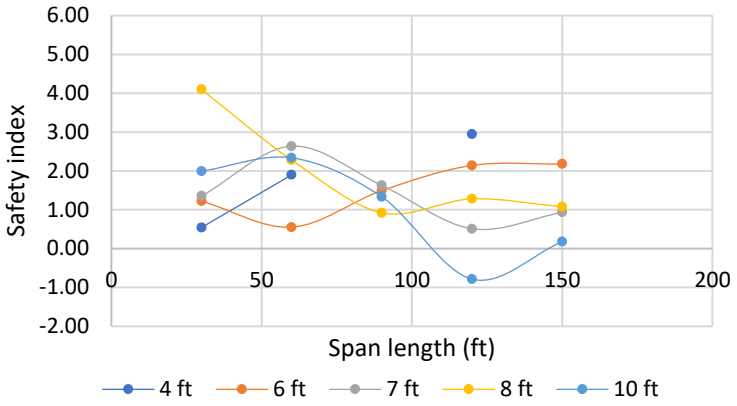

(b) Shear

Figure 106. Safety indices before calibration (Case II - PC girder)

7.2.2.4 Calibration and LRF Calculation Based on β_T =3.5

Figure 107 shows the safety indices after calibration when a target safety index of 3.5 was selected. Table 26 lists the LRFs calculated for the Case II PC bridges when β_T = 3.5.

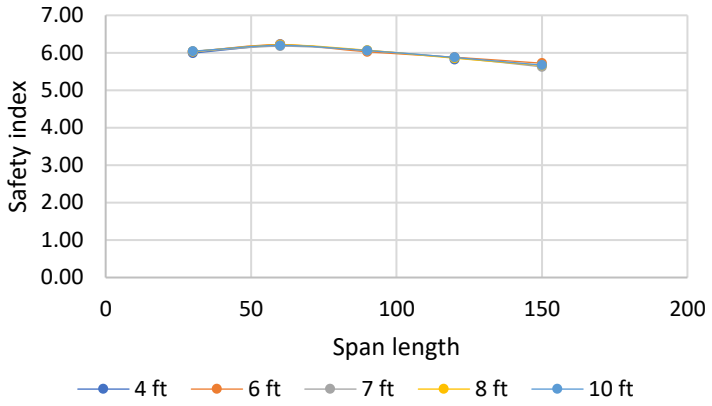

(a) Moment

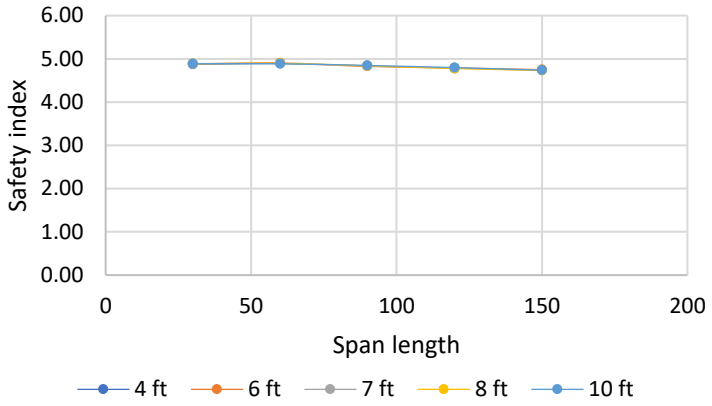

(b) Shear

Figure 107. Calibrated safety indices (Case II - PC girder, β_T=3.5)

Table 26. Case II results for PC bridges, β_T = 3.5

Limit State	Case No.	Live Load	Nominal Load	Load Effects	Factors γ_{LL}	Factors φ	Target Safety index	Calibrated β range	γ_{D1}	γ_{D2}	γ_{D3}
Strength I	II	Terragator Max	HS – 20 (Truck only)	Moment Shear	**1.90** 1.60	0.9 0.85	β_T = 3.5	5.67 – 6.20 4.74 – 4.89	1.2	1.26	1.5

7.2.2.5 Calibration and LRF Calculation Based on β_T =2

A target safety index value of 2 was selected from the range of safety index values calculated for the Case II PC bridges to consider the low exposure of bridges to IoH traffic. This target safety index was used to calculate the LRFs of the bridges. These LRFs were used to calculate the new resistance data, which were used to calculate the new safety indices. The newly calculated safety indices are shown in Figure 108. Table 27 lists the final LRFs calculated for the Case II PC bridges.

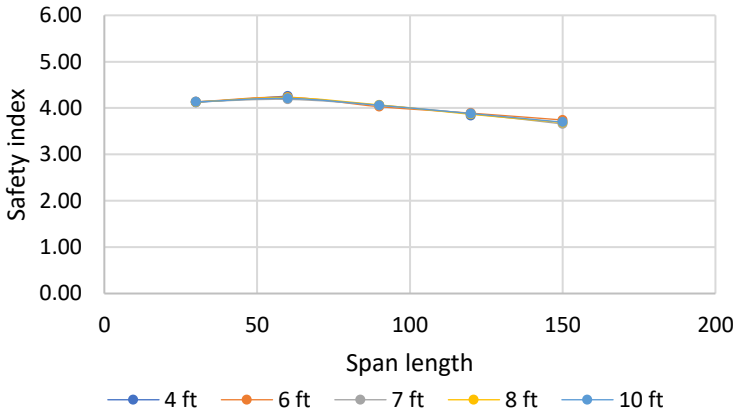

(a) Moment

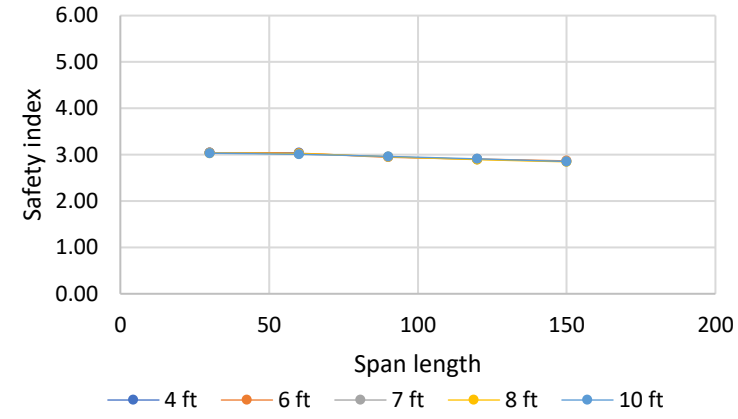

(b) Shear

Figure 108. Calibrated safety indices (Case II - PC girder, β_T=2)

Table 27. Case II results for PC bridges, β_T = 2

Limit State	Case No.	Live Load	Nominal Load	Load Effects	Factors γ_{LL}	Factors φ	Target Safety index	Calibrated β range	γ_{D1}	γ_{D2}	γ_{D3}
Strength I	II	Terragator Max	HS – 20 (Truck only)	Moment	1.75	0.95	β_T = 2	3.70 – 4.21	1.15	1.20	1.35
				Shear	1.50	0.9		2.85 – 3.04			

7.2.3 Case III

Case III was specifically considered to assess the Strength II limit state because the configuration of husbandry vehicles is dissimilar to the more commonly observed truck configuration. Therefore, a husbandry vehicle can be categorized as an "owner-specified vehicle," which is the general criterion for Strength II.

7.2.3.1 Load Data

The dead load effects and statistical parameters for Case III were same as those for Case I. For live load, the load effects and statistical parameters were taken from Case II. Thus, the load data and the statistical parameters for the load data for Case III were the same as those for Case II.

7.2.3.2 Nominal Load

Since Case III was considered for the Strength II limit state, Terragator Max was assumed to be an "owner-specified vehicle." Thus, the load effects due to Terragator Max were taken as the nominal load effects. The load effects were calculated for each span length considered and then multiplied by the DIF and LLDF values given in Equations 8 and 11.

7.2.3.3 Calculation of Safety Index

The statistical parameters for load and resistance found for Case II were used to calculate the safety index of each bridge. These safety indices were plotted against the span lengths of the bridges. The safety indices for moment and shear on the Case III PC bridges can be seen in Figure 109.

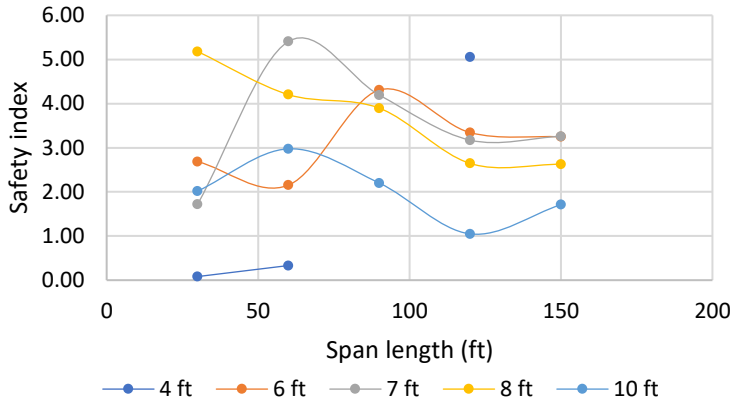

(a) Moment

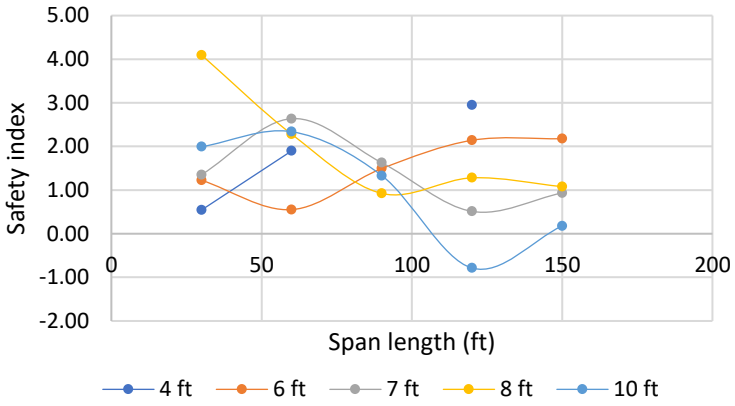

(b) Shear

Figure 109. Safety indices before calibration (Case III - PC girder)

7.2.3.4 Calibration and LRF Calculation Based on β_T =3.5

The LRFs for Case III were calculated by selecting target safety indices of 3.5 and 2. Figure 110 shows the calibrated safety index values for Case III when β_T =3.5. The safety index values, which were scattered in Figure 109, now converged and clustered close to the target safety index, as shown in Figure 110. The final calculated live load factors for Strength II were compared with the current AASHTO live load factors for Strength II. For this reason, the dead load and resistance factors were kept consistent with the AASHTO LRFs. Table 28 shows the LRFs for the Case III PC girder bridges when β_T =3.5.

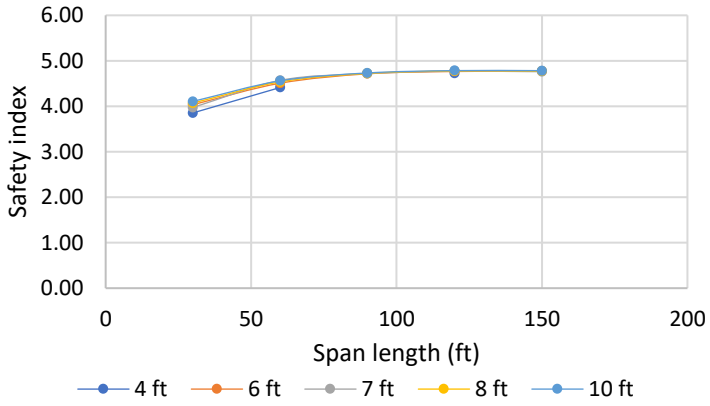

(a) Moment

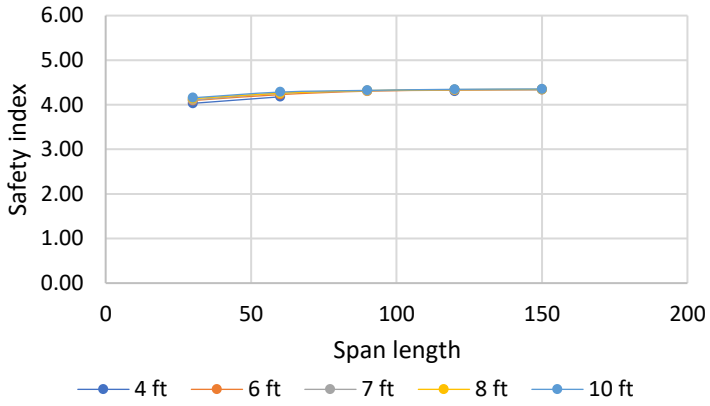

(b) Shear

Figure 110. Calibrated safety indices (Case III - PC girder, β_T=3.5)

Table 28. Case III results for PC bridges, β_T = 3.5

Limit State	Case No.	Live Load	Nominal Load	Load Effects	Factors γ_{LL}	Factors φ	Target Safety index	Calibrated β range	γ_{D1}	γ_{D2}	γ_{D3}
Strength II	III	Terragator	Terragator	Moment	1.35	0.90	β_T = 3.5	3.97 – 4.78	1.2	1.26	1.5
		Max	Max	Shear	1.32	0.85		4.14 – 4.35			

7.2.3.5 Calibration and LRF Calculation Based on β_T =2

A target safety index of 2 was chosen to calculate the LRFs. These LRFs were used to calibrate the safety index values for the Case III PC bridges. The LRFs calculated for the Case III PC bridges were substituted in Equation 46 to calculate the new resistance data. These resistance data, along with the statistical parameters for load and resistance, were used to calculate the new safety index values. The new calculated safety index values were plotted against the corresponding span lengths of the bridges, as shown in Figure 111. Table 29 shows the LRFs for the Case III PC girder bridges when β_T =2.

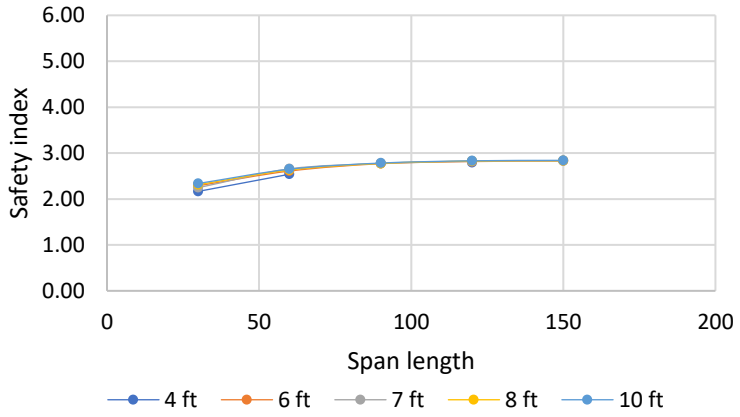

(a) Moment

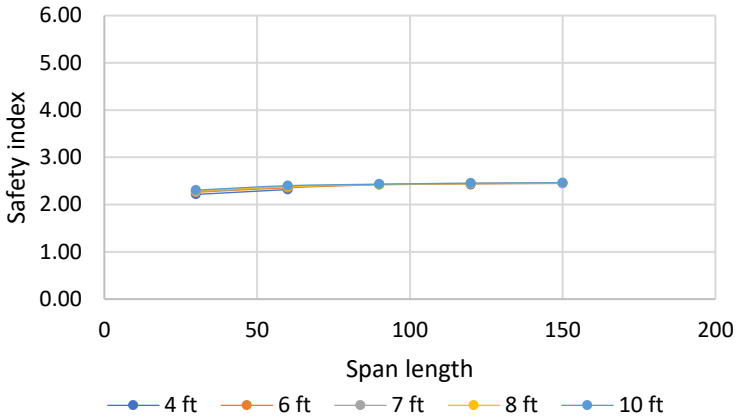

(b) Shear

Figure 111. Calibrated safety indices (Case III - PC girder, β_T=2)

Table 29. Case III results for PC bridges, β_T = 2

Limit State	Case No.	Live Load	Nominal Load	Load Effects	Factors γ_{LL}	Factors φ	Target Safety index	Calibrated β range	γ_{D1}	γ_{D2}	γ_{D3}
Strength II	III	Terragator Max	Terragator Max	Moment	1.25	0.95	β_T = 2	2.17 – 2.84	1.15	1.20	1.35
				Shear	1.23	0.90		2.22 – 2.46			

7.2.4 Discussion

In recognition of the level of detail presented in the preceeding sections, the results from all three cases were gathered and are summarized in this section. Table 30 lists the limit states and loads considered in each case along with the corresponding load factors, resistance factors, and safety index data.

Table 30. Summarized results for PC bridges

Target Safety index	Limit State	Case No.	Live Load	Nominal Load	Load Effects	Factors γ_{LL}	Factors φ	Calibrated β range	γ_{D1}	γ_{D2}	γ_{D3}
$\beta_T = 3.5$	Strength I	I	Identified terragator axle loads below 25 kips	HS – 20 (Truck only)	Moment	0.74	0.9	1.72 – 4.15	1.2	1.26	1.5
					Shear	0.74	0.85	1.96 – 3.83			
		II	Terragator Max	HS – 20 (Truck only)	Moment	**1.90**	0.9	5.67 – 6.20			
					Shear	1.60	0.85	4.74 – 4.89			
	Strength II	III	Terragator Max	Terragator Max	Moment	1.35	0.9	3.97 – 4.78			
					Shear	1.32	0.85	4.14 – 4.35			
$\beta_T = 2$	Strength I	I	Identified terragator axle loads below 25 kips	HS – 20 (Truck only)	Moment	0.72	0.95	0.15 – 2.25	1.15	1.20	1.35
					Shear	0.72	0.90	0.27 – 1.94			
		II	Terragator Max	HS – 20 (Truck only)	Moment	1.75	0.95	3.70 – 4.21			
					Shear	1.50	0.90	2.85 – 3.04			
	Strength II	III	Terragator Max	Terragator Max	Moment	1.25	0.95	2.17 – 2.84			
					Shear	1.23	0.90	2.22 – 2.46			

The calculated LRFs were compared with the LRFs prescribed in the AASHTO design specifications to determine whether updates to the current AASHTO values should be recommended. For reference, Table 31 gives the LRFs recommended by AASHTO for PC girder bridges.

Table 31. Current AASHTO design LRFs for PC bridges

Limit State	γ_{D1}	γ_{D2}	γ_{D3}	γ_{LL}	φ Moment	φ Shear
Strength I	1.25	1.25	1.5	1.75	1.00	0.90
Strength II	1.25	1.25	1.5	1.35	1.00	0.90

A comparison of the Case I LRFs with the Strength I AASHTO LRFs suggests that an update to the AASHTO LRFs is not needed for existing terragator loads as long as the axle loads comply with the legal load limit of 25 kips and they maintain the current geometries, configurations, and weight limits/distributions currently utilized.

A comparison of the Case II LRFs with the Strength I AASHTO LRFs when a target safety index of 3.5 is considered suggests that an update to the AASHTO live load factor is required if husbandry vehicles with a configuration similar to that of Terragator Max are manufactured. When a target safety index of 2 is considered, the same case does not suggest an update to the AASHTO live load factor.

A comparison of the Case III LRFs with the Strength II AASHTO LRFs suggests that an update to the Strength II AASHTO LRFs is not required.

The dead load factors were found to be lower than the current AASHTO-recommended values. Therefore an update to the AASHTO LRFs is not required. The resistance factors were found to be close to the AASHTO resistance factors for moment and shear.

7.3 Steel Girder Bridges

Bridge parameter data for the steel girder bridges were collected from the bridge plans. Table 32 lists the selected steel girder bridges according to span length and girder spacing. Table 33 shows the selected steel girder bridges' original and idealized bridge configurations.

Table 32. Steel girder bridges selected for LRF calculation

	Girder Spacing				
Span Length	**4 ft**	**6 ft**	**8 ft**	**10 ft**	**12 ft**
30 ft	3065.4S009	5286.5S001	4253.5S065	2701.8L035	9866.5S009
60 ft	2459.2S030	0914.5S093	5098.1R065	3559.9O035	0783.4L027
90 ft	7816.6S092	0921.4S003	7703.4L235	4047.1O035	0783.4L027
120 ft	- -	5278.0S001	7723.9A080	1361.9S007	9187.5L005
150 ft	- -	8204.1A074	7708.9O235	5052.7L080	9187.5L005

Table 33. Bridge information of selected steel girder bridges

Bridge ID	Original span length (ft)	Original girder spacing (ft)	Idealized span length (ft)	Idealized girder spacing (ft)	Number of girders	Width (ft)	Skew angle (degrees)
3065.4S009	35.5	4.4	30	4	8	30	0
5286.5S001	60	5.8	30	6	13	79.3	15
4253.5S065	33.5	6	30	8	6	32	0
2701.8L035	41.25	9.75	30	10	5	40	32
9866.5S009	28.5	14.5	30	12	3	30	30
2459.2S030	50	5	60	4	7	30	0
0914.5S093	60	6	60	6	5	24	0
5098.1R065	65.6	8.25	60	8	5	36	0
3559.9O035	56	10	60	10	4	32	25
0783.4L027	60	11	60	12	6	54	45
7816.6S092	91	4.6	90	4	12	47	20
0921.4S003	81	7.4	90	6	9	48	0
7703.4L235	101	8.5	90	8	6	69.5	27
4047.1O035	93.5	10	90	10	4	30	2.5
0783.4L027	99.5	11	90	12	6	54	45
5278.0S001	120	6.8	120	6	7	44	0
7723.9A080	118	7.75	120	8	4	26	41
1361.9S007	119	10	120	10	5	40	45
9187.5L005	113	11.5	120	12	4	34.5	30
8204.1A074	138	6.25	150	6	5	25	16
7708.9O235	162	7.7	150	8	7	41	22
5052.7L080	150	9.75	150	10	5	30	30
9187.5L005	144	11.5	150	12	4	34.5	30

7.3.1 Case I

This case was considered to understand whether the terragators identified in Chapter 3 give LRFs that are higher or lower than the current AASHTO LRFs. Only terragators with axle loads below 25 kips were considered in order to study axle loads below the new legalized load. Terragators with axle loads exceeding this amount were eliminated from the calculation of LRF in Case I.

7.3.1.1 Load Data

The live load effects experienced by a girder depend on the LLDF of the bridge. The mean and standard deviation of the live load effects data calculated for the Case I PC bridges, before these values were multiplied by the LLDFs of the PC bridges, were used to understand the live load effects of the steel girder bridges. Refer to Section 7.2.1.1 for details on the live loads considered for Case I. The mean and standard deviation of the live load effects data from the Case I PC bridges were multiplied by the LLDFs given in Equations 8 and 11.

When multiplied by these LLDFs, the mean and standard deviation gave the load effects data for steel girders. These data were then multiplied by a DIF of 1.33 to accommodate the dynamic load. The statistical parameters for load were then calculated for steel girder bridges using Equations 36, 37, 38, and 39.

7.3.1.2 Nominal Load

The nominal load effects for Case I were calculated using the HS-20 load. The load effects data were then multiplied by the DIF and LLDF values given in Equations 8 and 11. The bias factor for the live load effects data was calculated by substituting the nominal and live load effects data in Equation 33. This bias factor was then used to calculate the live load factor.

7.3.1.3 Calculation of Safety Index

The method used to determine the target safety index for the Case I steel girder bridges was the same as that used for all three cases of PC bridges. The safety indices were calculated using Equation 42. The safety index values for moment and shear on the girders of each bridge were plotted against the span lengths of the bridges. These plots can be seen in Figure 112.

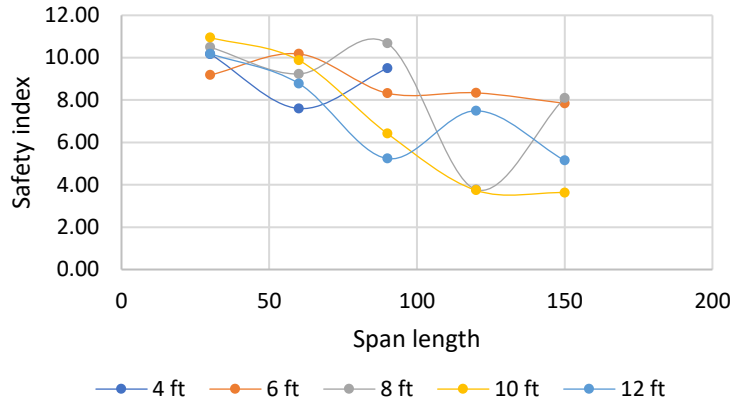

(a) Moment

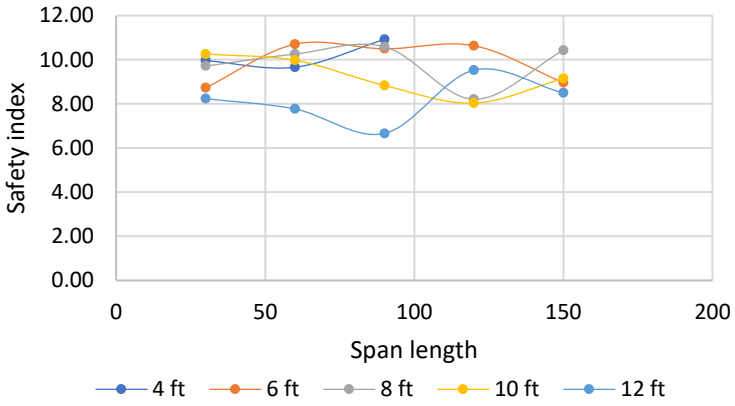

(b) Shear

Figure 112. Safety indices before calibration (Case I - Steel girder)

7.3.1.4 Calibration and LRF Calculation Based on β_T =3.5

Plots of the calibrated safety indices can be seen in Figure 113. The convergence of the safety index values indicates that the calibration was successful. To compare the calculated live load factors with those recommended by the AASHTO LRFD, the dead load factors and resistance factors were kept the same as those of the AASHTO LRFD. Table 34 shows the LRFs calculated for the Case I steel girder bridges when β_T = 3.5.

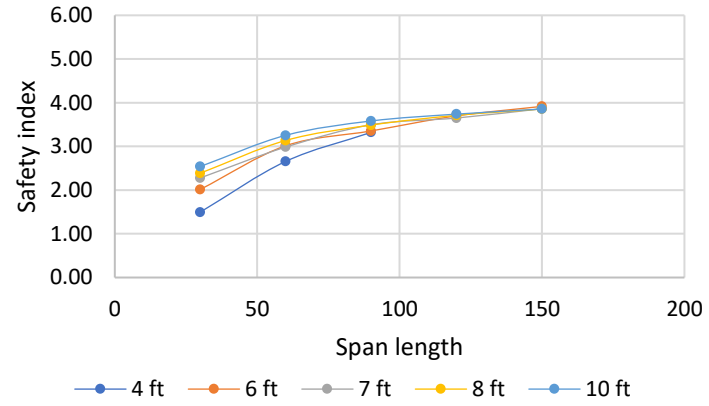

(a) Moment

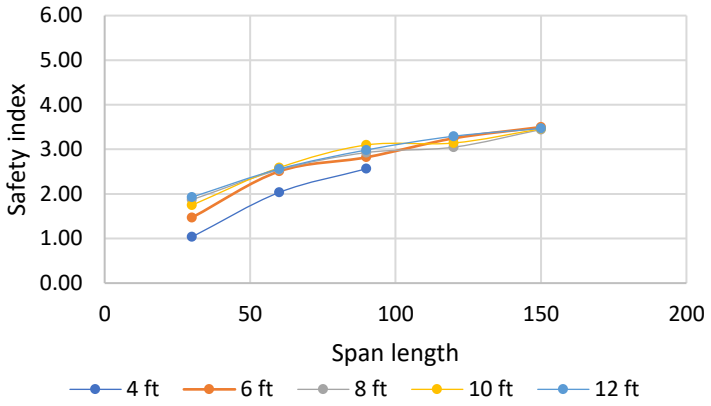

(b) Shear

Figure 113. Calibrated safety indices (Case I - Steel girder, β_T=3.5)

Table 34. Case I results for steel girder bridges, β_T = 3.5

Limit State	Case No.	Live Load	Nominal Load	Load Effects	Factors γ_{LL}	Factors φ	Target Safety index	Calibrated β range	γ_{D1}	γ_{D2}	γ_{D3}
Strength I	I	Identified terragator axle loads below 25 kips	HS – 20 (Truck only)	Moment	0.74	0.9	β_T = 3.5	1.50 – 3.86	1.2	1.26	1.5
				Shear	0.74	0.85		1.04 – 3.47			

7.3.1.5 Calibration and LRF Calculation Based on β_T =2

Figure 114 shows the calibrated safety index values for all selected steel girder bridges in Case I when β_T =2. Table 35 shows the LRFs calculated for the Case I steel girder bridges.

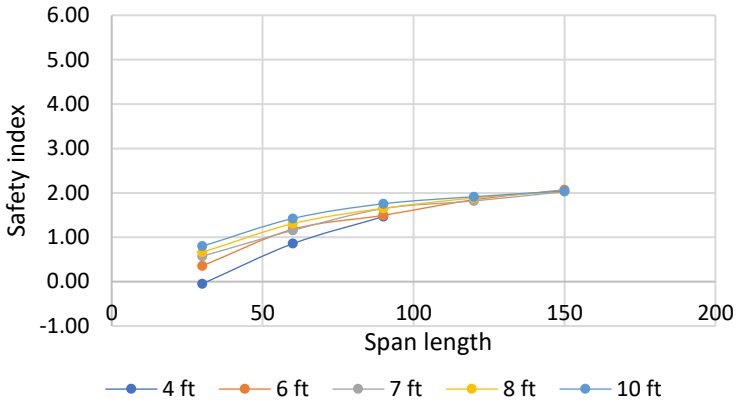

(a) Moment

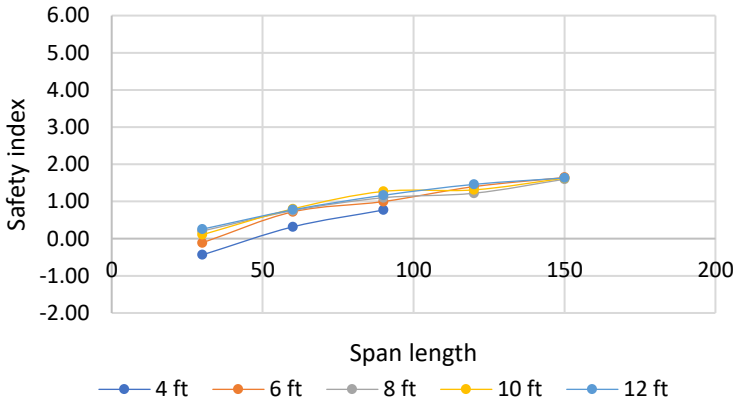

(b) Shear

Figure 114. Calibrated safety indices (Case I - Steel girder, β_T=2)

Table 35. Case I results for steel girder bridges, β_T = 2

Limit State	Case No.	Live Load	Nominal Load	Load Effects	Factors γ_{LL}	Factors φ	Target Safety index	Calibrated β range	γ_{D1}	γ_{D2}	γ_{D3}
Strength I	I	Identified terragator axle loads below 25 kips	HS – 20 (Truck only)	Moment	0.70	0.95	β_T = 2	-0.05 – 2.04	1.15	1.20	1.40
				Shear	0.70	0.95		-0.44 – 1.63			

7.3.2 Case II

The discussion of the Case II PC bridges in Section 7.2.2 can be referred to for a detailed description of the Case II steel girder bridges. The details specific to steel girder bridges are given in the following sections.

7.3.2.1 Load Data

The dead load effects for Case II were the same as those for Case I. The axle loads of Terragator Max were used for the live load effects. The live load effects for each span length category were calculated and then multiplied by the DIF and LLDF values given in Equations 8 and 11. The statistical parameters for the load data for Case II were found using the method described in Section 7.2.2.1.

7.3.2.2 Nominal Load

The HS-20 axle load effects multiplied by the DIF and LLDF values given in Equations 8 and 11 were considered to be the nominal load effects on the steel girders for Case II. Details specific to Case II can be found in Section 7.2.2.2.

7.3.2.3 Calculation of Safety Index

The safety indices of all bridges were calculated and plotted against the span lengths of the bridges. These safety index values were scattered, as shown in Figure 115.

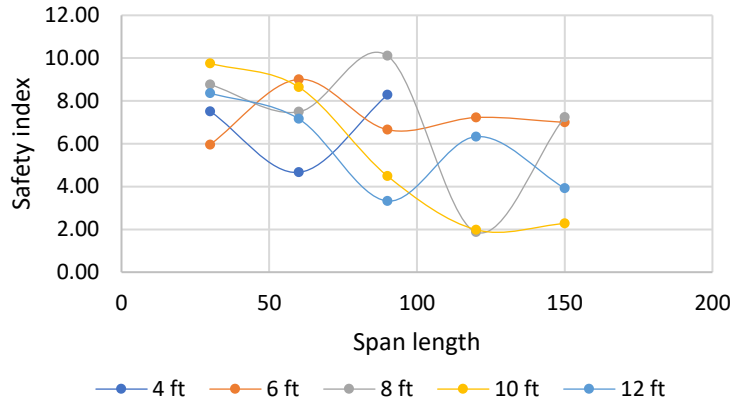

(a) Moment

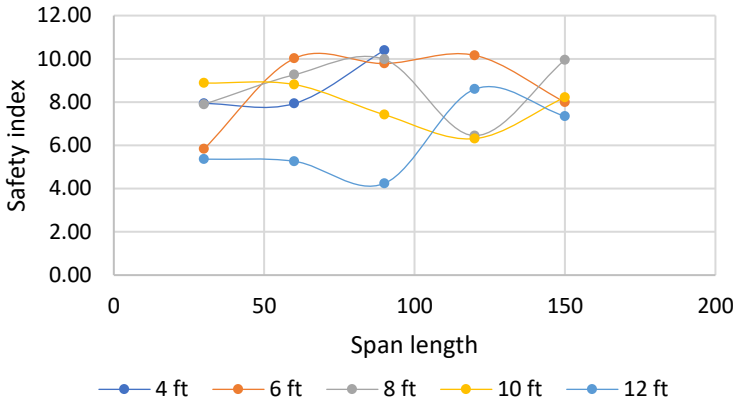

(b) Shear

Figure 115. Safety indices before calibration (Case II - Steel girder)

7.3.2.4 Calibration and LRF Calculation Based on β_T =3.5

The calculated safety index values were calibrated using a target safety index of 3.5. Figure 116 shows the calibrated safety indices. Table 37 shows the final LRFs calculated for the Case II steel girder bridges.

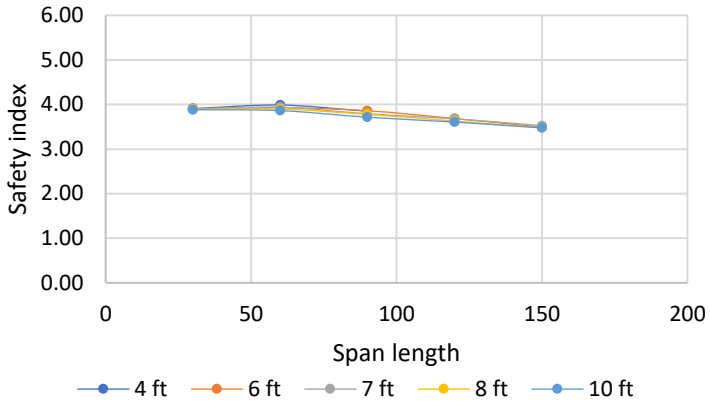

(a) Moment

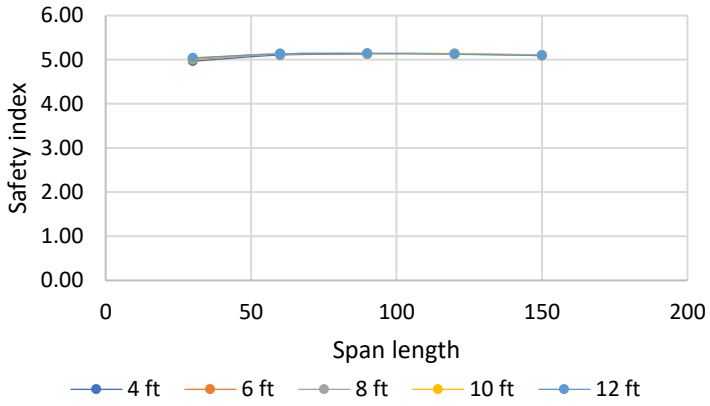

(b) Shear

Figure 116. Calibrated safety indices (Case II - Steel girder, β_T=3.5)

Table 36. Case II results for steel girder bridges, β_T = 3.5

Limit State	Case No.	Live Load	Nominal Load	Load Effects	Factors γ_{LL}	Factors φ	Target Safety index	Calibrated β range	γ_{D1}	γ_{D2}	γ_{D3}
Strength I	II	Terragator Max	HS – 20 (Truck only)	Moment Shear	**1.90** 1.60	0.9 0.85	β_T = 3.5	3.48 – 3.90 4.97 – 5.14	1.2	1.26	1.5

7.3.2.5 Calibration and LRF Calculation Based on β_T =2

A target safety index value of 2 was selected from the range of safety index values calculated for the Case II steel girder bridges. This target safety index was used to calculate the LRFs of the bridges, which were used to calculate the new resistance data. The new resistance data were used to calibrate the safety indices. Figure 117 shows the calibrated safety indices for the Case II steel girder bridges. The convergence of the safety index values close to the target safety index indicates a successful calibration. Table 37 shows the LRFs calculated for the Case II steel girder bridges.

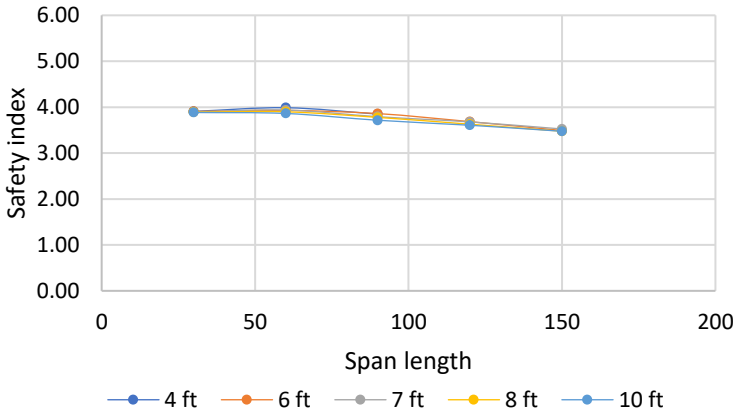

(a) Moment

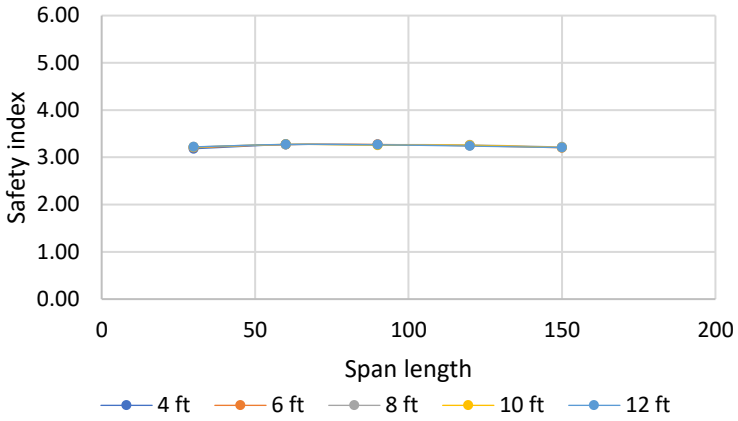

(b) Shear

Figure 117. Calibrated safety indices (Case II - Steel girder, β_T=2)

Table 37. Case II results for steel girder bridges, β_T = 2

Limit State	Case No.	Live Load	Nominal Load	Load Effects	Factors γ_{LL}	Factors φ	Target Safety index	Calibrated β range	γ_{D1}	γ_{D2}	γ_{D3}
Strength I	II	Terragator Max	HS – 20 (Truck only)	Moment Shear	1.75 1.50	0.95 0.95	β_T = 2	3.48 – 3.94 3.18 – 3.27	1.15	1.20	1.40

7.3.3 Case III

Case III was considered to assess the Strength II limit state, in which the nominal load is an "owner-specified vehicle."

7.3.3.1 Load Data

The dead load effects for Case III were the same as those for the Case I steel girder bridges. The load effects data for the Case II steel girder bridges were used for Case III.

7.3.3.2 Nominal Load

Terragator Max axle loads were taken as the Case III nominal load effects. The load effects data were multiplied by the DIF and LLDF values given in Equations 8 and 11. Details about the Case III nominal loads can be found in Section 7.2.3.2.

7.3.3.3 Calculation of Safety Index

The safety index values calculated for the Case III steel girder bridges are plotted in Figure 118.

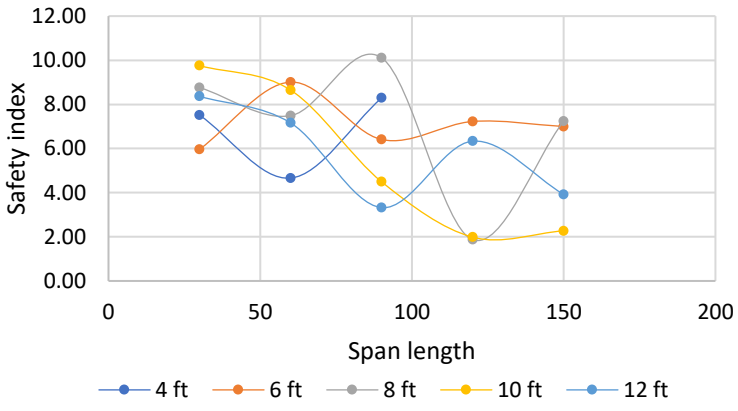

(a) Moment

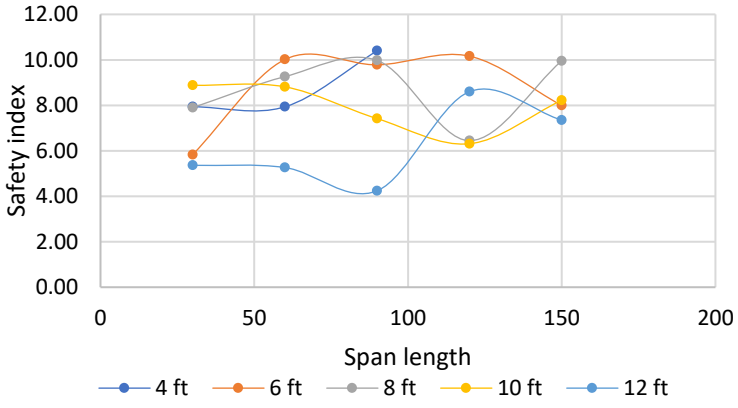

(b) Shear

Figure 118. Safety indices before calibration (Case III - Steel girder)

7.3.3.4 Calibration and LRF Calculation Based on β_T =3.5

The safety index values calculated for the Case III steel girder bridges were calibrated and plotted against the corresponding bridge span lengths. This plot can be seen in Figure 119.

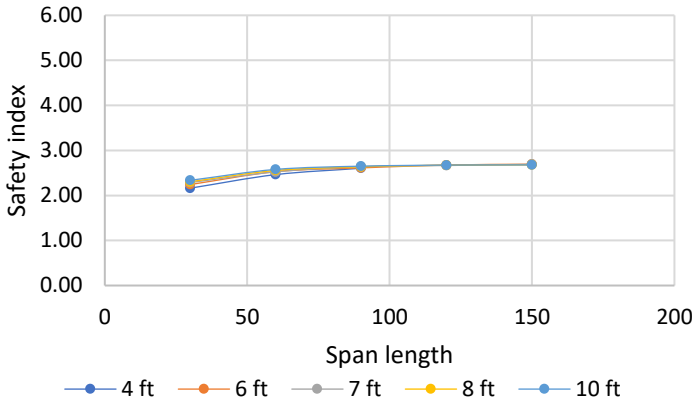

(a) Moment

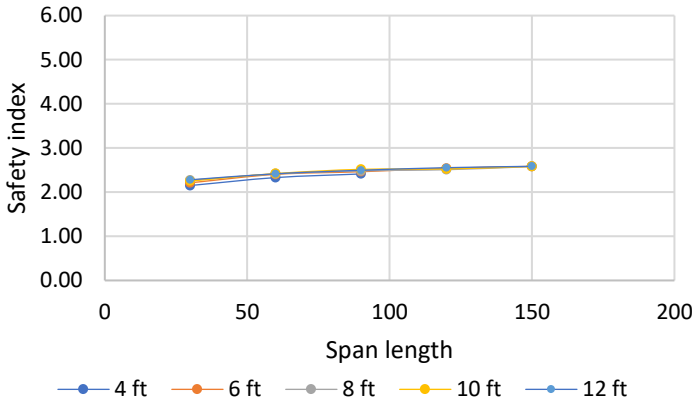

(b) Shear

Figure 119. Calibrated safety indices (Case III - Steel girder, β_T=3.5)

Table 38 shows the calculated load and resistance factors for the Case III steel girder bridges when a target safety index of 3.5 was selected.

Table 38. Case III results for steel girder bridges, β_T = 3.5

Limit State	Case No.	Live Load	Nominal Load	Load Effects	Factors γ_{LL}	Factors φ	Target Safety index	Calibrated β range	γ_{D1}	γ_{D2}	γ_{D3}
Strength II	III	Terragator Max	Terragator Max	Moment Shear	1.35 1.34	0.90 0.90	β_T = 3.5	2.24 – 2.68 2.28 – 2.59	1.2	1.26	1.5

7.3.3.5 Calibration and LRF Calculation Based on β_T =2

A target safety index value of 2 was selected to calibrate the safety index values of the Case III steel girder bridges. This target safety index value was used to calculate the LRFs, which were used to find the new resistance data. The new resistance data were then used to calibrate the

safety index values. Figure 120 shows the calibrated safety indices. The LRFs for the Case III steel girder bridges can be found in Table 39.

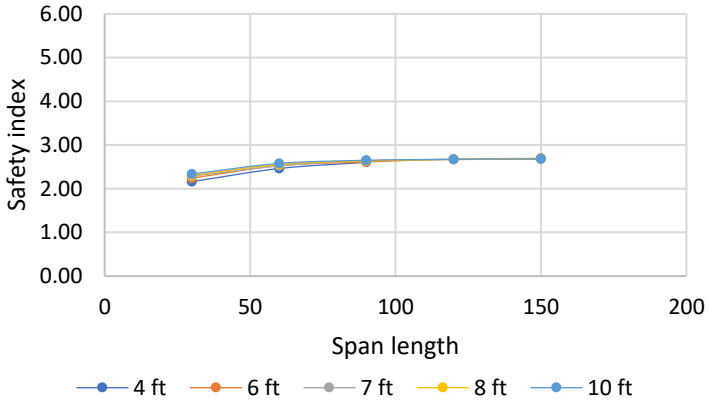

(a) Moment

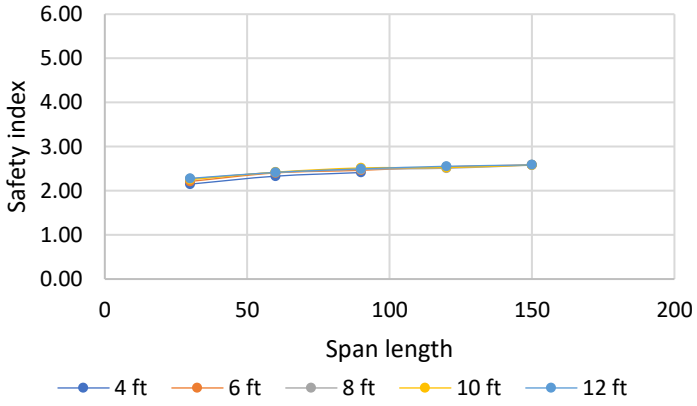

(b) Shear

Figure 120. Calibrated safety indices (Case III - Steel girder, β_T=2)

Table 39. Case III results for steel girder bridges, β_T = 2

Limit State	Case No.	Live Load	Nominal Load	Load Effects	Factors γ_{LL}	Factors φ	Target Safety index	Calibrated β range	γ_{D1}	γ_{D2}	γ_{D3}
Strength II	III	Terragator Max	Terragator Max	Moment Shear	1.30 1.25	0.95 0.95	β_T = 2	2.24 – 2.86 2.25 – 2.59	1.15	1.20	1.40

7.3.4 Discussion

The LRFs calculated for all three cases involving steel girder bridges are summarized in Table 40. For comparison, the current AASHTO LRFs for steel girder bridges are presented in Table 41.

Table 40. Summarized results for steel girder bridges

Target Safety index	Limit State	Case No.	Live Load	Nominal Load	Load Effects	Factors γ_{LL}	Factors φ	Calibrated β range	γ_{D1}	γ_{D2}	γ_{D3}
$\beta_T = 3.5$	Strength I	I	Identified terragator axle loads below 25 kips	HS – 20 (Truck only)	Moment	0.74	0.9	1.50 – 3.86	1.2	1.26	1.5
					Shear	0.74	0.9	1.04 – 3.47			
		II	Terragator Max	HS – 20 (Truck only)	Moment	**1.90**	0.9	3.48 – 3.90			
					Shear	1.60	0.9	4.97 – 5.14			
	Strength II	III	Terragator Max	Terragator Max	Moment	1.35	0.9	2.24 – 2.68			
					Shear	1.34	0.9	2.28 – 2.59			
$\beta_T = 2$	Strength I	I	Identified terragator axle loads below 25 kips	HS – 20 (Truck only)	Moment	0.70	0.95	-0.05 – 2.04	1.15	1.20	1.40
					Shear	0.70	0.95	-0.44 – 1.63			
		II	Terragator Max	HS – 20 (Truck only)	Moment	1.75	0.95	3.48 – 3.94			
					Shear	1.50	0.95	3.18 – 3.27			
	Strength II	III	Terragator Max	Terragator Max	Moment	1.30	0.95	2.24– 2.86			
					Shear	1.25	0.95	2.25 – 2.59			

Table 41. Current AASHTO LRFs for steel girder bridges

Limit State	γ_{D1}	γ_{D2}	γ_{D3}	γ_{LL}	φ Moment	φ Shear
Strength I	1.25	1.25	1.5	1.75	1.00	1.00
Strength II	1.25	1.25	1.5	1.35	1.00	1.00

A comparison of the calculated LRFs with the AASHTO LRFs for steel girder bridges gives the same results as those found for PC bridges. These results are discussed in Section 7.2.4.

Hence, the AASHTO LRFs for Strength I do not require an update as long as the axle loads on existing husbandry vehicles comply with the legal load limit of 25 kips. The AASHTO LRFs for Strength II do not require an update.

8 SUMMARY AND CONCLUSIONS

Recent legislation in the state of Iowa has increased the allowable axle weight of certain implements of husbandry to 25 kips. This change poses a particular concern to those who oversee and manage the construction and preservation of bridge structures because the resulting structural response of bridges could exceed that which would be otherwise seen from current legal loads. This potential problem needed to be investigated and understood to fully assess the structural response of bridges and to develop appropriate live load distribution factors, impact factors, and load factors for implements of husbandry.

The overarching goal of this project was to assess bridge behavior under these increased loads more accurately and to determine whether changes to codified values were warranted. More specifically, seven major objectives were targeted in this project:

1. Identify current in-service terragator-type legal vehicles per Iowa Code 321.463.a(1)(2).
2. Perform live load tests of bridges using terragator vehicles to determine actual live load distribution, dynamic impact factors, and to calibrate bridge models.
3. Develop bridge models using finite element numerical analysis and simulate the load effects due to terragator-type vehicle crossings.
4. Compare live load distribution results to current codified live load distribution factors used for typical vehicle types.
5. Compare dynamic impact factors to codified dynamic load factors.
6. Calibrate live load factors for LRFD and LRFR.
7. Develop a legally loaded terragator-type vehicle model for Iowa.

To achieve these objectives, a literature review was conducted on four major topics: (1) existing research on the impacts of implements of husbandry vehicles on bridge structures, (2) determination of bridge dynamic responses, (3) determination of bridge load distribution factors, and (4) calibration of live load factors.

Further, an extensive database of IoH terragator-type vehicle information was developed using information from various sources. This database included many of the vehicles that could be classified as terragators. The database was used to generate a terragator model for this project—Terragator Max—that was used in load factor calibration. The database of identified terragators was further expanded with different levels of payload for each vehicle. The resulting expanded database was used in the investigation of LLDF and the calibration of LRF.

Live load tests were conducted to characterize the response of bridges subjected to husbandry vehicles and to collect data that would be useful for analytical model calibration. In total, three slab bridges and five PC bridges were selected for testing. These bridges varied in terms of several bridge parameters, including skew angle, number of spans, span length, bridge width, number of beams, beam spacing, and slab thickness. During the bridge tests, the response of each bridge was collected through multiple strain and displacement transducers attached at the bridge's mid-span and quarter-span.

The calculated DIFs resulting from the bridge tests for the PC and slab bridges were near 1.0 in most cases, indicating that the maximum strain values for the dynamic cases did not vary significantly from those for the static cases. While the sample size is, relatively, too small to make broad conclusions regarding DIF for all terragator-type vehicles, it is important to note that, in this study, lightly loaded vehicles moving at a higher rate of speed appear to produce greater dynamic impacts than more heavily loaded vehicles moving at a slower rate of speed. There were two instances when the DIF exceeded the prescribed factor of 1.33 in AASHTO (2020). In both cases, the bridge was a PC girder bridge and the vehicle was the unloaded (T3) terragator.

The parameters of the field-tested bridges were used as a reference to generate finite element models for these bridges. These models were loaded with the terragator axle loads from the field tests. The strain data extracted from the FE models were analyzed and validated against the field test data. After calibration of the models, the validated modeling method was used for a parametric study. Finite element models were created for 50 slab bridges, 50 PC girder bridges, and 5 steel girder bridges with different bridge parameters. In order to cover the various parameters of husbandry vehicles, 28 unique terragators were identified and modeled in the parametric study with empty and full payloads.

Based on the results from the field data and analytical simulations, the following conclusions were reached:

- The results from the parametric analyses of PC and steel girder bridges indicated that girder spacing and the ratio of girder spacing to span length were the most influential bridge parameters on the load distribution factors for both the interior and exterior girders. For slab bridges, span length, skew angle, and slab thickness were the most influential bridge parameters on the equivalent strip width.
- For interior girders, the LLDFs for the front axle were higher than those for the rear axle for terragators with one wheel on the front axle, and those values were slightly higher than the AASHTO-specified values. However, the load on the front axle was less than the load on the rear axle, and the maximum static responses of the respective bridges were a result of the rear axle loads, especially for the half- or full-load scenarios. For exterior girders, the LLDFs calculated based on the AASHTO-prescribed equations gave values higher than those calculated based on the field tests.
- The equivalent strip widths calculated from the field test data were larger than those recommended by AASHTO. Thicker slabs reduce the load intensity on a unit strip width and distribute the load more evenly across a larger strip width.

Once the distribution factors of the bridges were analyzed, the live load factors associated with the terragator-type vehicle loading were investigated for PC and steel girder bridges using a calibration process based on the reliability theory recommended by Barker and Puckett (2007). Twenty-three bridges with different geometries were selected for each type of bridge and used for calibration. The load factor was calibrated for both moment and shear.

The live load factor for each bridge type was calculated for three cases. Case I calibrated LRFs for the identified terragators in the Strength I limit state. Axle loads below 25 kips from the available terragator loads were used to calculate bending moment and shear due to live loads. This was done to understand the load effects of current legal loads. Since the Strength I limit state consists of a load combination relating to normal vehicular use, the HS-20 load was used to calculate the nominal load effects. Approximately 90 terragator loads were used to characterize the live load effects, and the HS-20 load was was used to characterize the nominal load effects.

Case II calibrated the LRFs for a hypothetical terragator model in the Strength I limit state. The hypothetical terragator model developed for Cases II and Case III was named Terragator Max. Here, the coefficient of variation for the live load data was taken from Case I. Because this case was evaluated for the Strength I limit state, the HS-20 load was used to calculate the nominal load effects.

Case III calibrated the LRFs for Terragator Max in the Strength II limit state. The coefficient of variation for the live load data was taken from Case I. Terragator Max was treated as an "owner-specified vehicle or evaluation permit vehicle." Therefore, the Terragator Max load was used as the nominal load for Case III.

The calibration of live load factors using reliability theory includes the selection of a target safety index and reiteration of the process to reach a safety index close to the selected target safety index. For this project, two target safety indices were chosen. A target safety index of 3.5 was chosen following the procedure summarized by Barker and Puckett (2007); this value is consistent with the LRFD philosophy. Another safety index was chosen to reflect the less conservative approach used for load rating, since overly conservative methods can be prohibitive with respect to load restrictions, rehabilition, and replacement. The AASHTO MBE (2018) recommends selection of a lower safety index for bridges with low ADTT values. While the MBE recommends a targeted safety index of 2.5, a targeted safety index of 2.0 was selected for this exercise due to the frequency of IoH vehicle crossings being very low relative to ADTT values.

The calibration of live load factors yielded the following key findings:

- A comparison of the Case I LRFs with the AASHTO LRFs suggests that an update to the AASHTO LRFs is not needed for existing terragator loads as long as the axle loads comply with the legal load limit of 25 kips.
- When a target safety index of 3.5 is considered, a comparison of the Case II LRFs with the AASHTO LRFs suggests that the live load factor for Strength I should increase from 1.75 to 1.90. When a target safety index of 2.0 is considered, the current AASHTO live load factor of 1.75 is sufficient.
- A comparison of the Case III LRFs with the Strength II AASHTO LRFs suggests that an update to the AASHTO Strength II LRFs is not required, even with a high target safety index of 3.5.

- The dead load factors identified through the calibration were found to be lower than the current AASHTO-recommended values. Therefore, an update to the AASHTO LRFs is not required.
- The resistance factors identified through the calibration were found to be close to the AASHTO resistance factors for moment and shear, and no further update to the AASHTO values is needed.

REFERENCES

AASHTO. 2018. *The Manual for Bridge Evaluation*. 3rd Edition. American Association of State Highway and Transportation Officials, Washington, DC.

AASHTO. 2020. *LRFD Bridge Design Specifications*. 9th Edition. American Association of State Highway and Transportation Officials, Washington, DC.

ACI Committee 318. 2011. *Building Code Requirements for Structural Concrete (ACI 318-11).* American Concrete Institute, Farmington Hills, MI.

Barker, R. M., and J. A. Puckett. 2007. *Design of Highway Bridges: An LRFD Approach*. 2nd Edition. John Wiley & Sons, Inc., Hoboken, NJ.

Bridge Diagnostics Inc. 2012. *Operations Manual: ST350 – Strain Transducer*. Bridge Diagnostics Inc., Louisville, CO. https://bditest.com/wp-content/uploads/2022/09/201511-Rev-B-Operations-Manual-Strain-Transducer-ST350-1.pdf

Chang, D., and H. Lee. 1994. Impact Factors for Simple-Span Highway Girder Bridges. *Journal of Structural Engineering*, Vol. 120, No. 3, pp. 704–715.

Christopher, D. E., A. Chehab, and P. Gustavo. 2016. Field tests of two prestressed-concrete girder bridges for live-load distribution and moment continuity. *Journal of Bridge Engineering*, Vol. 21, No. 6.

Conner, S., and X. S. Huo. 2006. Influence of parapets and aspect ratio on live load distribution. *Journal of Bridge Engineering*, Vol. 11, No. 2.

Deng, L., and C. S. Cai. 2010. Development of dynamic impact factor for performance evaluation of existing multi-girder concrete bridges. *Engineering Structures*, Vol. 32, No. 1, pp. 21–31.

Deng, L., Y. Yu, Q. Zou, and C. S. Cai. 2014. State of the art review of dynamic impact factors of highway bridges. *Journal of Bridge Engineering*, Vol. 20, No. 5.

Deng, Y., and B. Phares. 2016. *Investigation of the Effect of Speed on the Dynamic Impact Factor for Bridges with Different Entrance Conditions*. Bridge Engineering Center, Iowa State University, Ames, IA. https://intrans.iastate.edu/app/uploads/2018/03/dynamic_impact_factor_for_bridge_entrances_w_cvr.pdf.

Freeseman, K., B. Phares, L. Greimann, C. Kilaru. 2017. *Study of the Impacts of Implements of Husbandry on Bridges, Volume III: Appendices*. Bridge Engineering Center, Iowa State University, Ames, IA.

Fu, G., Q. Wang, J. Chi, M. Lwin, and R. Corotis. 2020. *NCHRP Report 951: Proposed AASHTO Load Rating Provisions for Implements of Husbandry*. National Cooperative Highway Research Program, Washington, DC.

Greimann, L., B. Phares, P. Liu, and K. Freeseman. 2017. *Study of the Impacts of Implements of Husbandry on Bridges Volume II: Rating and Posting Recommendations*. Bridge Engineering Center, Iowa State University, Ames, IA.

Li, H. 2005. Dynamic Response of Highway Bridges Subjected to Heavy Vehicles. PhD dissertation. Florida A&M University and Florida State University, Tallahassee, FL.

Mohseni, I., A. Ashin, W. Choi, and J. Kang. 2018. Development of dynamic impact factor expressions for skewed composite concrete-steel slab-on-girder bridges. *Advances in Materials Science and Engineering*, Vol. 2018, Article ID 4313671.

Moses, F. 2001. *NCHRP Report 454: Calibration of Load Factor for LRFR Bridge Evaluation*. National Cooperative Highway Research Program, Washington, DC.
Nowak, A. S. 1999. *NCHRP Report 368: Calibration of LRFD Bridge Design Code*. National Cooperative Highway Research Program, Washington, DC.
Phares, B., C. Kilaru, L. Greimann, J. Seo, and K. Freeseman. 2017. *Study of the Impacts of Implements of Husbandry on Bridges Volume I: Live Load Distribution Factors and Dynamic Load Allowances*. Bridge Engineering Center, Iowa State University, Ames, IA.
Salmon, C. G., and J. E. Johnson. 1996. *Steel Structures: Design and Behavior*. 4th Edition. Prentice-Hall Inc., Upper Saddle River, NJ.
Seo, J., B. Phares, and T. Wipf. 2013. Lateral live-load distribution characteristics of simply supported steel girder bridges loaded with implements of husbandry. *Journal of Bridge Engineering*, Vol. 19, No. 4.
Seo, J., C. Kilaru, B. Phares, and P. Lu. 2015. Live load distribution factors for a short span timber bridge under heavy agricultural vehicles. *Structures Congress 2015*. American Association of Civil Engineers, Reston, VA.
Schwarz, M., and J. A. Laman. 2001. Response of prestressed concrete I-girder bridges to live load. *Journal of Bridge Engineering*, Vol. 6, No. 1, pp. 1–8.
SIIMS. 2023. Structure Inventory and Inspection Management System (SIIMS). Iowa Department of Transportation. https://iowadot.gov/siims.
Wight, J. K., and J. G. MacGregor. 2012. *Reinforced Concrete: Mechanics and Design*. 6th Edition. Pearson Education, Inc., Upper Saddle River, NJ.
Yousif, Z., and R. Hindi. 2007. AASHTO LRFD live load distribution for beam-and-slab bridges: Limitations and applicability. *Journal of Bridge Engineering*, Vol. 12, No. 6.

THE INSTITUTE FOR TRANSPORTATION IS THE FOCAL POINT FOR TRANSPORTATION AT IOWA STATE UNIVERSITY.

InTrans centers and programs perform transportation research and provide technology transfer services for government agencies and private companies;

InTrans contributes to Iowa State University and the College of Engineering's educational programs for transportation students and provides K–12 outreach; and

InTrans conducts local, regional, and national transportation services and continuing education programs.

IOWA STATE UNIVERSITY

Visit **InTrans.iastate.edu** for color pdfs of this and other research reports.